

Alberta Recycling Management Authority

TDA Hydraulic Performance and Geomembrane Damage Potential

Final Report

October 2019



15th October 2019

Brad Schultz
Operations Manager, Alberta Recycling Management Authority
1800 Scotia 1 Tower, 10060 Jasper Avenue
Edmonton Alberta
T5J 3R8

Dear Brad:

Re: Final Report
TDA Hydraulic Performance and Geomembrane Damage Potential

Please find attached our final report describing the work performed by Adelantar Consulting in connection with the study of the landfill leachate collection characteristics of Tire Derived Aggregate ('TDA'). The report is the culmination of several years of work and provides important insights into the hydraulic performance of TDA in a landfill leachate collection system and the potential for TDA to damage geomembrane landfill liners. We trust this work will meet your needs at this time, and wish to thank Alberta Recycling Management Authority for allowing us to execute this project on your behalf.

Yours truly
Adelantar Consulting



Pete Marshall
Principal

Adelantar Consulting
Suite 502
10339 – 124th Street
Edmonton, Alberta
T5N 3W1

A division of 1219146
Alberta Ltd
t: +1.780.932.3434



Table of Contents

1.0	INTRODUCTION	1
2.0	BACKGROUND.....	1
2.1	General	1
2.2	Principles of Landfill Leachate Collection	2
2.3	Alberta Regulatory Setting - Leachate	3
3.0	PARTICLE SIZE CHARACTERIZATION.....	4
3.1	TDA	4
3.2	Gravel	5
4.0	TASK 1 – HYDRAULIC PERFORMANCE TESTING	5
4.1	Objectives	6
4.2	Design, Construction and Commissioning of Test Equipment	7
4.3	Testing Equipment and Procedures	8
4.3.1	One dimensional consolidometer.....	8
4.3.2	Two-dimensional permeameter	9
4.4	Results and Interpretation.....	10
4.5	Task 1 Summary and Recommendations	11
5.0	TASK 2 – POTENTIAL FOR DAMAGE TO GEOMEMBRANES FROM LEACHATE DRAINAGE MATERIALS.....	11
5.1	General	11
5.2	Objectives	12
5.3	Testing Equipment	12
5.4	Role of Compacted Clayey Subgrade.....	14
5.5	Materials Tested	15
5.5.1	Geomembrane	15
5.5.2	Protective geosynthetics	15
5.5.3	TDA.....	15
5.5.4	Gravel	16
5.6	Puncture Testing Methods and Results	16
5.6.1	Laboratory testing	16
5.6.2	Implications for field scale performance.....	22
5.7	Geomembrane Strain Testing and Results	24
5.8	Task 2 Summary and Recommendations	26

List of Figures

	Page
Figure 1 Relative shape and size of multi-, double- and single-pass TDA	5
Figure 2 1-D vertical consolidometer and 2-D permeameter	7
Figure 3 Permeameter configured to measure temperature effects on compression	8
Figure 4 Schematic representation of puncture testing compression chamber	13
Figure 5 TDA/geomembrane testing apparatus	13
Figure 6 Prepared clay subgrade in testing equipment	14
Figure 7 Geomembrane punctures induced by protruding TDA wire	17
Figure 8 TDA puncture risk examples	18
Figure 9 Loading and flipping of frozen box sample	20
Figure 10 Strain area distribution curves for TDA and gravel	25

List of Tables

	Page
Table 1 Predicted frequency of geomembrane punctured by TDA	21

List of Appendices

Appendix 1	Physical properties of TDA affecting performance in leachate collection systems
Appendix 2	Damage to geomembrane by coarse uniform TDA or gravel drainage aggregate



1.0 INTRODUCTION

Adelantar Consulting ('Adelantar') was retained by Alberta Recycling Management Authority ('Alberta Recycling') to undertake a testing program which would provide new information regarding the performance of Tire Derived Aggregate ('TDA') when used as a drainage material in landfill leachate collection systems. Adelantar was responsible to deliver the program, and retained the University of Saskatchewan ('the University') to construct new testing equipment, modify existing testing equipment and execute the testing work, and work collaboratively with Adelantar to interpret the test results in the context of Alberta landfill applications. The University team was led by Professor Ian Fleming, who has an impressive track record of directly related work over the past two decades.

The current document presents the results of the work in the following format:

- **Task 1 – Hydraulic performance.** This task addresses the drainage behaviour of TDA in landfill leachate collection systems typical of Alberta landfills, with a focus on permeability and compressibility.
- **Task 2 – Geomembrane puncture potential.** This task addresses the extent to which TDA can be expected to puncture geomembrane landfill liners.

Both tasks assess the relevant characteristics of TDA relative to mineral aggregates (i.e. gravel). Detailed reports prepared by the University are presented as appendices to the current document.

2.0 BACKGROUND

2.1 General

TDA has been used as an alternative to mineral leachate drainage media (i.e. sand or gravel) in Alberta landfill leachate collection systems for almost 20 years. While operational experience with these TDA-based systems has been good and there have been no reports of unacceptable performance, technical questions have emerged from industry and academia regarding the hydraulic performance of the material (i.e. can TDA adequately convey landfill leachate such that regulatory leachate control limits can be met). In addition, the increasing use of plastic liners ('geomembranes') in landfills has raised questions regarding the extent to which exposed wires in TDA might have the potential to puncture these liners. The testing program described in the current document was designed to respond to these questions.

The technical literature makes it clear that conventional soil testing equipment is poorly suited to the testing of TDA due to the large size of TDA particles compared to typical soils. The Department of Civil, Geological and Environmental Engineering at the University was recognized for their strong track record in TDA research supported by the design and construction of dedicated testing equipment. Adelantar therefore retained the University to undertake the testing work including the design and construction of new testing equipment and the modification of equipment previously developed by the University for other TDA testing work. The testing program was conducted from mid 2016 to early 2019 and formed the basis for the current report.

2.2 Principles of Landfill Leachate Collection

A landfill leachate collection system is a drainage system which is used to remove liquids from the base of a landfill. This system usually comprises a permeable layer (usually including pipes), which directs leachate towards one or more extraction points from where it can be removed by pumping or gravity flow. The efficiency of the leachate drainage system is controlled by the following principal factors:

- **the slope on which the drainage system is constructed** (given that steeper slopes lead to a higher rate of liquid flow than shallower slopes);
- **the length of drainage pathways** within the drainage layer (given that a short path to a pipe or an extraction point will allow faster rates of extraction than a longer path); and
- **the permeability of the drainage material** (given that more permeable materials allow a higher rate of liquid flow than less permeable materials).

The permeability of the drainage material is the focus of Task 1 of the current study.

Leachate drainage layers comprise solid particles separated by spaces (or 'voids'). These voids (including the small connections between larger voids) control the rate at which leachate can flow under a given set of conditions. Biological, chemical and physical processes in a landfill lead to these voids becoming progressively clogged over time, and as such the nature of the voids both at the time of initial placement of waste and later in the life of the landfill is key to the performance of the leachate collection system.



Leachate drainage layers composed of gravel have the following general characteristics:

- they are incompressible; and
- they are composed of particles that are approximately the same size in every direction.

These characteristics are important for the following reasons:

- because gravel drainage layers are incompressible, the void structure in these layers does not change significantly in response to pressure from overlying waste in a landfill. While the material that forms the TDA particles does not compress significantly, TDA particles and layers constructed of these particles definitely do compress under load and this means that the voids are smaller after the layer is compressed. Smaller voids result in reduced rates of leachate flow, so this aspect of TDA must be understood to allow TDA-based leachate collection systems to be properly designed. In addition, clogging occurs in these voids so the nature of the void structure in both gravel and TDA layers is of real importance; and
- each particle within a gravel drainage layer can reasonably be characterized by a single size measurement, and bulk aggregate can be characterized as the combination of these individual particle sizes. TDA particles generally have very different sizes in their length, width and thickness, and this configuration makes them difficult to characterize. Given that the size of the particles was expected to be a factor in the size and configuration of voids, this property of TDA was identified as being relevant to hydraulic performance.

Each of these characteristics was investigated in the study and is described in the current document.

2.3 Alberta Regulatory Setting - Leachate

Regulatory expectations for the routine design and operation of landfills in Alberta are presented in the *Standards for Landfills in Alberta* (the 'Standards for Landfills', Alberta Environment, February 2010). Sections 4.10(b), (d) and (e) of the Standards for Landfills identify applicable leachate head management requirements as follows:

- (b) During active landfill life, final landfill closure and post-closure the maximum acceptable leachate head in landfill cells constructed after July 1, 2009 shall not exceed 300 mm.

- (d) *The person responsible for a landfill shall remove leachate from the cell at a frequency that maintains the level of leachate at or below the maximum acceptable leachate head.*
- (e) *Notwithstanding the requirements in 4.10(b),[4.10(c)] and 4.10(d), upon detection of any exceedances of the maximum acceptable leachate head, the person responsible shall reduce the leachate head level to below the maximum acceptable leachate head level within a maximum of 14 calendar days subsequent to the detection.*

The leachate collection system comprises a drainage system at the base of a landfill which must be capable of meeting these maximum leachate head requirements assuming leachate is removed from the drainage layers at an adequate rate. The hydraulic performance of the leachate collection material is one of a number of key factors in the functioning of the leachate collection system in this regard. Task 1 of the current assignment is intended to provide new information regarding the expected performance of TDA relative to these requirements.

3.0 PARTICLE SIZE CHARACTERIZATION

The importance of particle size to the hydraulic performance of drainage materials is described in Section 2 of the current document. Because of this, the study included a detailed assessment of TDA particle size. The results of the assessment are presented relative to typical leachate collection gravel in the following subsections of the current document.

3.1 TDA

The size and shape of TDA particles varies based on the type and extent of tire processing undertaken. Three different types of TDA material, varied by the level of processing as either multi pass, double pass or single pass, were supplied by Alberta Recycling and characterized to evaluate the particle size distribution and other properties of the sample. Figure 1 illustrates the size and shape of typical particles of each of these types of TDA.





Figure 1: Relative shape and size of multi-, double- and single-pass TDA

In order to adequately describe the size of TDA particles, a measure termed 'equivalent dimension' was developed which was considered to be able to describe a range of particle sizes from those with a tabular form (i.e. length less than approximately twice the width) to those with an elongate form (i.e. where the length was many times more than the width). It was notable that multi-pass material contained almost 10% (by mass) with an equivalent dimension less than 50 mm, while the single- and double-pass material contained almost no particles with an equivalent dimension less than 100 mm.

3.2 Gravel

It is clear from the technical literature that an 'ideal' gravel for use as a leachate collection material would have a particle size in the order of 50 mm, and would be essentially single-sized (i.e. poorly graded). This type of gravel has a high voids content (see Section 2 of the current document for discussion of the relevance of voids) and therefore provides both significant permeability and significant space for the storage of the clog material that results from biological, chemical and physical process in the landfill. It is recognized however that this type of material, while theoretically ideal, may not be available at reasonable cost on most landfill projects and cannot therefore be reasonably used as the only basis of comparison for TDA. On that basis, a more typical drainage gravel which included a greater range of fine and coarse particles (i.e. better graded) was included in the study.

4.0 TASK 1 – HYDRAULIC PERFORMANCE TESTING

Loss of hydraulic performance of landfill leachate collection media due to the accumulation of clog material in voids is well documented in normal landfill service conditions, and is common to all such

media (rather than being restricted to TDA). Concern has been raised regarding the possibility of relatively high rates of loss of hydraulic performance in TDA-based as opposed to gravel-based landfill leachate collection systems. This concern was expressed in a notable technical paper published in 2005 by Kerry Rowe and his co-authors at Queens University in Ontario. Subsequent authors (especially Richard Beaven and his colleagues at the University of Southampton, UK) have suggested that additional factors not fully considered in Rowe's paper may have led to the over-estimating of clogging rates in TDA.

The hydraulic performance testing component of the current assignment was developed to respond to the uncertainties described above, and to provide a better understanding of the extent to which TDA produced in accordance with Alberta Recycling specifications could be expected to meet the leachate management requirements of the Standards for Landfills. The testing work was intended to complement previous work conducted by Daryl McCartney for Alberta Recycling on behalf of the University of Alberta / Edmonton Waste Management Centre of Excellence (whose earlier report provided new information regarding some aspects of TDA behaviour, but was not conclusive in several key areas of interest). Details of the hydraulic performance task are presented in the following sub-sections of the current document.

4.1 Objectives

The objective of Task 1 was to investigate the hydraulic behaviour of TDA in a laboratory setting intended to simulate typical Alberta landfill service conditions, so as to provide confidence to key stakeholders including design engineers, landfill owners and regulators of the extent to which Alberta TDA can meet reasonable performance expectations in Alberta landfill leachate collection applications.

The testing program was designed to evaluate the combined effects of sustained load, temperature and particle size/shape for various TDA materials in order to determine the change in void characteristics and permeability in both vertical and horizontal directions. The testing program was designed to improve the fundamental understanding of the material behaviour and correlate fundamental performance-related parameters.

4.2 Design, Construction and Commissioning of Test Equipment

Task 1 of the testing program included the modification and use of the following equipment:

- **a large-diameter one dimensional vertical consolidometer** – this equipment was developed to investigate immediate compression and creep compression (and associated void characteristics); and
- **a two-dimensional permeameter** – this equipment was developed primarily to investigate horizontal and vertical permeability, and was also used to investigate the effects of elevated temperature on TDA compression.

This equipment had initially been developed to test the behaviour of TDA produced in Saskatchewan, and while it had operated satisfactorily during this work a number of issues had been identified that warranted significant overhauls to make it suitable for the current project. The equipment was modified such that it could reliably impose vertical stresses that simulated waste pile thicknesses typical of Alberta landfills. In order to improve the performance of the testing equipment for the current testing program, modifications were made to the equipment. Both pieces of equipment were designed and constructed to handle large strains while maintaining a constant vertical load.

The equipment is shown in Figures 2 and 3.

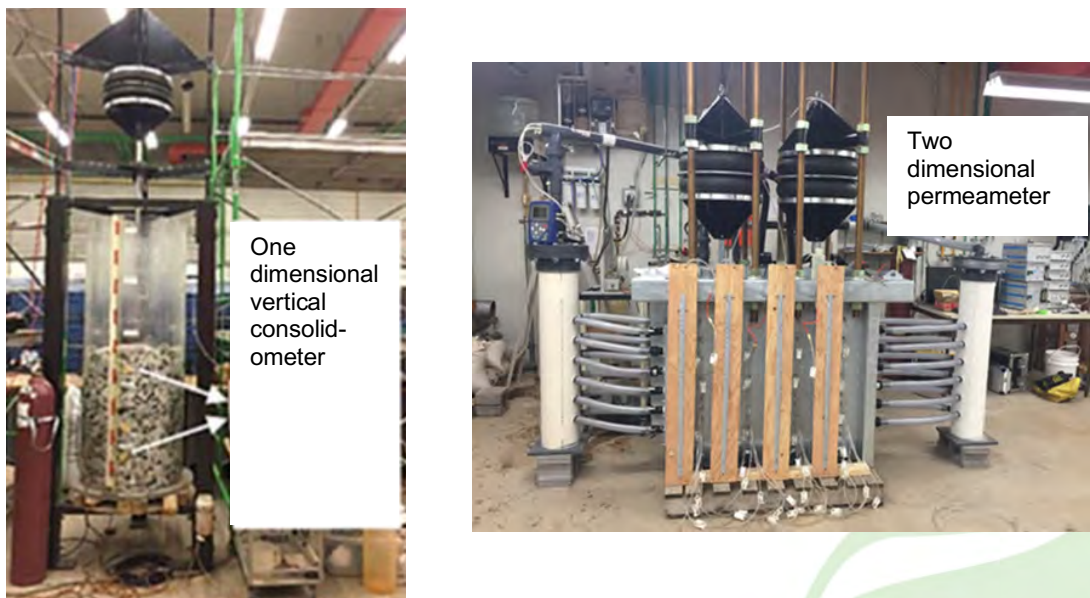


Figure 2: 1-D vertical consolidometer and 2-D permeameter

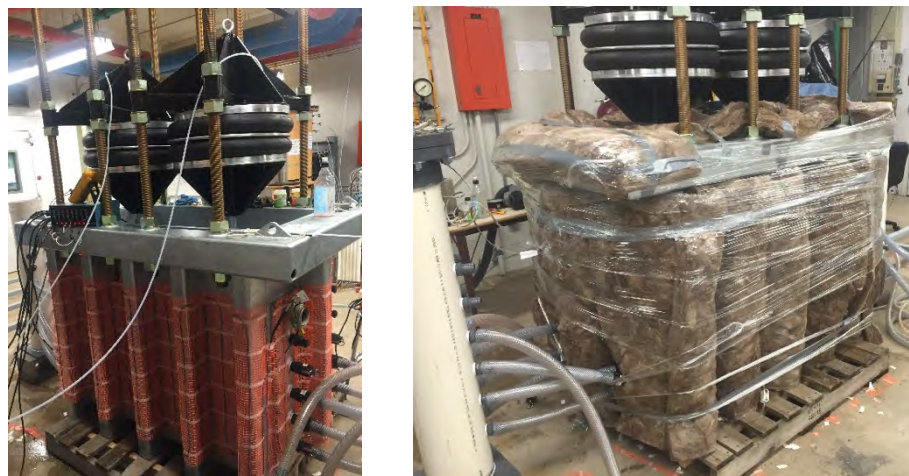


Figure 3: Permeameter configured to measure temperature effects on compression

4.3 Testing Equipment and Procedures

4.3.1 One dimensional consolidometer

The one-dimensional consolidometer was used to investigate void volume changes occurring in TDA as a result of vertical load. The testing methods may be summarized as follows:

- the consolidometer (which is transparent) was loaded with multi-pass TDA, and visual markers were inserted within the TDA to allow monitoring of the compression response to vertical load at known vertical intervals;
- TDA was subjected to progressively larger vertical loads which were applied and held for at least 20 days each;
- three separate tests were conducted in load stages of 100, 200 and 300 kPa (equivalent to approximately 10, 20 and 30 m of landfill waste thickness respectively);
- one test was conducted at 220 kPa, with the load being applied quickly; and
- one test was conducted at 220 kPa with the load being applied over a total duration of 126 days.

Void reduction and compressibility of the TDA were monitored over time for each of the tests. Initial void characteristics were varied to investigate whether the starting degree of compaction affected the compression response. The change in void volume indicated by monitoring of the visual markers was verified by directly filling and draining the consolidometer (with water).

4.3.2 Two-dimensional permeameter

The two-dimensional permeameter was used primarily to investigate the permeability of the TDA under a variety of compression conditions. The testing method may be summarized as follows:

- the permeameter was loaded with TDA and the target vertical stress applied for each particular test. Most tests were conducted on multi-pass TDA, with a smaller number of tests being conducted on single-pass TDA;
- permeant fluid was introduced at the target flow rate, either at one side of the permeameter (to allow the calculation of horizontal permeability) or from the base (to allow the calculation of vertical permeability);
- most tests were conducted using air as the permeant fluid due to the inherent difficulties of sustaining flows sufficient to generate adequate liquid head losses in such a high permeability material. A limited number of tests were conducted with water to validate the air flow test results;
- pressures were measured at multiple ports along the flow paths, and the pressure results were used to calculate the intrinsic permeability of the TDA; and
- intrinsic permeability results were then used to calculate hydraulic conductivity.

It should be noted that friction between the inside wall of the permeameter and the TDA was recognized as introducing a stress response characteristic that was an attribute of the testing but would not occur in a landfill setting. Measures were taken to correct mathematically for this characteristic, and ‘corrected’ void characteristics were used in the analysis of the data.

In addition to permeability testing, the permeameter was used to investigate the following effects of elevated temperature on the response of TDA to compression:

- the effect of elevated temperature applied after the TDA was subjected to vertical load; and
- the effect of elevated temperature applied prior to vertical loading.

The high temperature testing method may be summarized as follows:

- following permeability testing at an applied load of 315 kPa, heating mats were applied to the permeameter and the testing equipment was insulated to protect against heat loss;

- a temperature of 58°C was maintained for 90 days, and the effects recorded by temperature probes within the TDA mass and in the headspace in the test cell.

4.4 Results and Interpretation

The hydraulic performance testing provided the following principal results:

- **initial compression versus creep** - TDA exhibited compression behaviour that was slightly different to conventional soils, but in general demonstrated that initial compression was significantly greater than longer term creep;
- **effect of elevated temperature** - the compression response of TDA was not significantly changed by elevated temperature;
- **void characteristics** - TDA exhibited less void volume than gravel under typical Alberta landfill conditions on a volumetric basis (i.e. one cubic metre of compressed TDA would have less void volume than one cubic metre of gravel). ‘Ideal’ leachate collection gravel with a nominal particle size of 50 mm was reported to have a void ratio of approximately 0.65, while more typical graded drainage gravel was reported to have a void ratio of approximately 0.5. Void ratios for TDA were reported to range from 0.2 to 0.38 at under a vertical load of 300 kPa (equivalent to a landfill height of 30 to 40 m). This result indicates that a larger total volume of TDA would be required to provide the same volume of storage for clog material compared to a mineral aggregate. This could be achieved by installing a thicker TDA layer than would be required for mineral aggregate. It should be noted that this result addresses only the volume available for storage of clog material, and is independent of leachate flow characteristics (which are addressed below). A possible weak correlation was identified between void characteristics at the start and end of testing, which suggested that loosely-placed TDA material may retain higher void volumes than more compacted equivalent materials, even after compression and creep;
- **permeability characteristics** – TDA was demonstrated to exhibit horizontal hydraulic conductivities well above 10^{-2} cm/s under a vertical load of 375 kPa (equivalent to a waste column height of approximately 30 to 40 m). Vertical hydraulic conductivities were confirmed to be only slightly lower than horizontal hydraulic conductivities, and still greater than 10^{-2} cm/s. Continued testing indicated that permeability results after approximately 8 months of creep were not statistically different than the preliminary results. The technical literature indicates that a leachate collection system with this characteristic should perform well, even if clogging reduces the hydraulic conductivity by two orders of magnitude. It

should be noted that single-pass TDA exhibited slightly higher hydraulic conductivity results than multi-pass TDA.

4.5 Task 1 Summary and Recommendations

The results of the hydraulic performance testing indicate that TDA can be expected to convey leachate to an extraction point in accordance with the leachate head control requirements of the Standards for Landfills in Alberta provided care is taken in design. This conclusion was reached on consideration of test results regarding void characteristics under compression (including the effects of elevated temperature), and permeability. While it was confirmed that TDA does not provide as much void volume as some mineral aggregates under reasonable landfill loading conditions, this characteristic is to be considered relative to the need for storage of clog materials. ‘Ideal’ mineral aggregates with a nominal particle size of approximately 50 mm are often not available at reasonable cost on Alberta landfill projects, and more typical (and affordable) aggregates would have significantly less void volume than the ‘ideal’ mineral materials. It is concluded that on the basis of hydraulic performance, TDA is worthy of consideration as a leachate collection material for Alberta landfills provided care is taken to assess the implications of all applicable design factors.

5.0 TASK 2 – POTENTIAL FOR DAMAGE TO GEOMEMBRANES FROM LEACHATE DRAINAGE MATERIALS

5.1 General

Geomembranes (i.e. plastic liners) are increasingly being used as a component of lining systems in modern landfills. Geomembranes can offer excellent containment performance provided they remain intact, however given that they are typically between 1.5 mm and 2 mm thick, the risk of them being damaged (and their containment performance therefore being compromised) is higher than for more traditional clay liners which are typically 0.6 m to 1 m thick. Geomembrane damage can take the form either of punctures caused directly by sharp objects, or by excessive localized tensile strains which can lead to longer term stress cracking.

Leachate drainage materials typically lie directly above or in immediate proximity to geomembranes in landfill lining systems, and consequently represent a potential source of damage to these geomembranes. It was expected that TDA and gravel drainage materials might represent different damage risks to geomembranes, with the exposed wires in otherwise generally malleable TDA

particles being in contrast to more rigid and potentially sharper-edged gravel particles. The extent to which the TDA mechanisms of geomembrane puncture might compare with the behaviour of gravel to compromise the integrity of geomembranes was not well documented in the technical literature, and closing this gap in understanding was the focus of the geomembrane damage task within the current assignment.

5.2 Objectives

The objective of the testing was to determine the extent to which TDA and gravel drainage materials can be expected to cause damage to a geomembrane under varying conditions. It was recognized that landfill designs sometimes provide protection from these damage mechanisms by the inclusion of a geotextile (i.e. protective fabric) or other geosynthetic materials between the lower surface of the drainage layer and the upper surface of the geomembrane. A testing protocol was therefore developed as part of the current assignment to investigate the ability of different protective materials to protect against geomembrane damage, using similar techniques for damage assessment.

5.3 Testing Equipment

The testing program included the development of a large diameter compression chamber designed to simulate vertical stresses equivalent to waste pile thicknesses typical of Alberta landfills. The maximum force capable of being applied in this equipment was 352 kN at 1,724 kPa, which results in an applied sample pressure of 550 kPa (representative of a municipal waste pile approximately 45 m high, depending on the type of waste involved and other landfill conditions). The testing equipment was designed and constructed by the University of Saskatchewan for the current project.

The TDA testing apparatus was large by soil laboratory standards (0.9 m diameter), and comprised a steel frame within which a layer of clay could be compacted (to represent a clay liner), and over which a geomembrane and a drainage layer could be placed prior to a vertical load being applied. This configuration of key components is illustrated schematically in Figure 4.

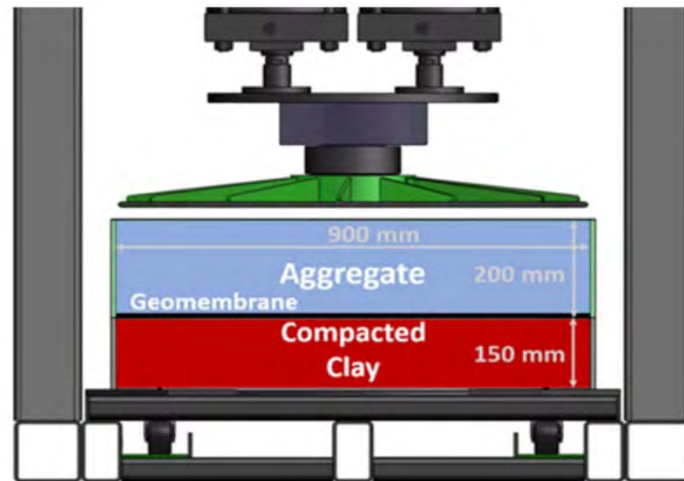


Figure 4: Schematic representation of puncture testing compression chamber

The equipment was designed during Summer 2016, and fabrication of the components commenced at the University machine shops in September 2016. Testing began following installation, calibration and the establishment of the data acquisition system. Figure 5 illustrates the completed/installed purpose-built compression chamber that was used in testing the geomembrane puncture behaviour of TDA.



Figure 5: TDA/geomembrane testing apparatus

For comparison testing of gravel drainage materials, smaller but otherwise similar test cells (400 mm diameter) were fabricated and placed in load frames. These smaller diameter cells could be used for this purpose due to the smaller size of mineral aggregate particles compared to Alberta TDA.

5.4 Role of Compacted Clayey Subgrade

The condition of the clayey subgrade was identified as a factor that could affect the puncture response of the overlying geomembrane under load. Multiple clayey materials typical of those used to construct landfill clay liners were sourced from Alberta, Saskatchewan, and Ontario, and were subjected to routine geotechnical testing to characterize key material properties. These materials were then prepared and installed in the testing equipment to conditions representative of a typical landfill as illustrated in Figure 6.



Figure 6: Prepared clay subgrade in testing equipment

5.5 Materials Tested

5.5.1 Geomembrane

Geomembrane used in the testing was supplied by Solmax from the plant in Varrennes, Quebec. Materials were tested in nominal 1.5 mm thick and 2 mm thick configurations, without textured surfaces.

5.5.2 Protective geosynthetics

Protective geosynthetics were supplied by the following manufacturers:

- AGRU provided two grades of non-woven needle-punched geotextiles;
- Tencate provided a woven geotextile; and
- Skaps provided a drainage geocomposite.

The protection available from heavy geotextiles was simulated using multiple layers of lighter geotextiles.

5.5.3 TDA

The following grades of TDA were provided by Alberta Recycling:

- **multi-pass** material – this is representative of the grade of TDA routinely produced in accordance with the Alberta Recycling specification, and having a nominal particle size of 150 mm
- **double pass** material – this is material which resulted from two passes through the TDA production equipment, and while generally characterized by particles larger than the multi-pass material, is not produced to meet a target particle size; and
- **single pass** material – this is the material which resulted from a single pass through the TDA production equipment and is generally characterized by large particles.

Each of these materials was carefully characterized in terms of particle size as described in Section 3 of the current document. Additional information regarding characterization in terms of protruding wires is presented in Section 5.6.1 of the current document.

5.5.4 Gravel

As described in Section 3 of the current document, ‘ideal’ drainage gravel comprises uniform material with a grain size of the order of 50 mm. Material of this general type was sourced in Saskatoon and tested for the current assignment. Materials of this ideal nature are often not available at reasonable cost for landfill construction projects, consequently a more typical landfill drainage gravel was sourced from Alberta and tested to provide comparison. The Alberta material was less uniform, having a wider distribution of fine and coarse material.

5.6 Puncture Testing Methods and Results

5.6.1 Laboratory testing

It was recognized during the design of the testing program that only a relatively small proportion of TDA particles exhibited wire protrusions that were considered likely to cause geomembrane puncture. While the testing equipment was large on a laboratory scale, it was evident that an impossibly large number of tests would be required to produce punctures that could be readily studied and be representative of conditions at a landfill scale. Placing TDA randomly over the geomembrane in the test chamber was therefore not a viable testing strategy, and the following approach was therefore developed to allow immediate puncture to be estimated on a field scale:

- **Step 1** – estimate the proportion of ‘high risk particles¹ in a given quantity of TDA.
- **Step 2** – assess the likelihood of high risk TDA particles landing such that the wires would impinge directly on the geomembrane / geosynthetic protection (i.e. being unfavourably oriented).
- **Step 3** – assess the likelihood of high risk TDA particles puncturing the geomembrane/geosynthetic protection by landing unfavourably.

Similar testing was undertaken using gravel to allow the potential for geomembrane puncture by both TDA and gravel on a field scale to be estimated. Summaries of these activities are provided below.

¹ Where ‘high risk’ particles are those that contain protruding wires that are expected to puncture a geomembrane if they impinge directly on it

Step 1 – Estimate the proportion of ‘high risk’ TDA particles

The nature of wires protruding from an individual particle of TDA depends on a number of TDA manufacturing factors, including the sharpness of the knives and the orientation of a used tire or tire fragment into the knives. It was recognized that some wires are not rigid enough to puncture a geomembrane, and of those wires that are rigid enough the nature of the wire configuration (and corresponding potential to puncture a geomembrane) can vary from particle to particle. TDA particles representing various levels of puncture risk were identified and subjected to puncture testing using geomembranes with light geotextile protection.

Twelve initial tests were completed with moderate geotextile protection about a 1.5 mm thick High Density Polyethylene ('HDPE) geomembrane. Immediate puncture holes ranging from 1 mm in diameter (caused by individual wires) to 5 mm in diameter (for groups of wires) were recorded. Large groups of wires were found to behave in a manner similar to gravel, i.e. that they caused indentations but not immediate punctures. Examples of punctures observed are shown in Figure 7.



Figure 7: Geomembrane punctures induced by protruding TDA wire

Somewhat unexpectedly, the occurrence of immediate punctures was not observed to increase with higher normal loads.

The puncture results allowed TDA particles to be broadly classified as follows:

- **high puncture risk** – contains at least one rigid bead wire (1 to 2 mm in diameter), and/or a group of wires with at least one wire protruding beyond the others in the group;
- **medium puncture risk** – contains groups of bead wires that are approximately 2 mm in length;
- **low puncture risk** – contains groups of bead wires with no wires protruding beyond the others in the group; and
- **no significant puncture risk** – contains no significant protruding bead wires.

Examples of particles in the high, medium and low risk categories are shown in Figure 8.

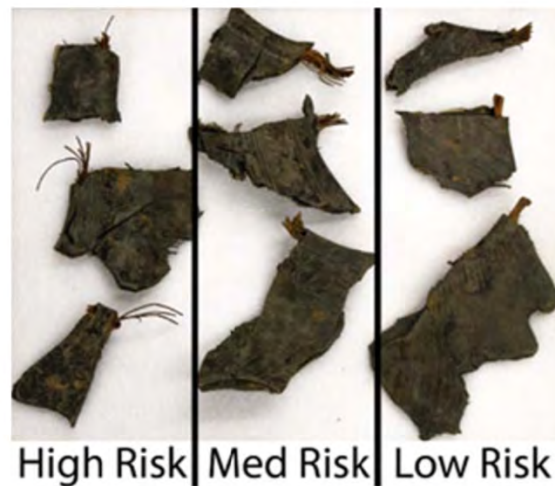


Figure 8: TDA puncture risk examples

Samples of TDA resulting for different degrees of processing (single pass, double pass and multi pass) were assessed to identify any effects on the proportion of high risk TDA particles. It was found that each type of processing resulted in approximately 2 to 3% of particles representing a high puncture risk. Additional discussion of the implications to field puncture performance is presented in Section 5.6.2 of the current document.

The visual assessment process used to classify the puncture risk of TDA particles was acknowledged to be subjective, however some validation of the process was undertaken by having different people classify 100 particles and comparing the results. While some variance was observed, the classification techniques were confirmed to provide an acceptable level of consistency for the purpose.

Step 2 – Assess probability of high risk particles being unfavourably oriented

Step 1 of the puncture testing process confirmed the proportion of high risk TDA particles which can be expected for a given quantity of TDA. Step 2 of the testing was designed to investigate the extent to which high risk TDA particles could be expected to be oriented unfavourably towards the geomembrane such that they could potentially cause puncture to the underlying geomembrane / protective geosynthetics.

To investigate the orientation of TDA particles, a 6 m² open-topped wooden box was constructed, and filled with TDA from a loader bucket (to simulate field placement conditions). The following procedure was then undertaken:

- the box was placed in the laboratory and the TDA was flooded carefully with water;
- the box was then relocated using a loader to an external location during the Saskatoon Winter. This resulted in the water freezing, and the TDA particles becoming locked in position;
- the box was then returned to the laboratory, where it was turned upside down to expose the base of the TDA/ice mass; and
- warm water was used to progressively thaw the ice and reveal the orientation and condition of the TDA particles (which were then classified, measured and photographed).

Photographs depicting the loading and flipping of the frozen box are presented in Figure 9.





Figure 9: Loading and flipping of frozen box sample

Four tests were undertaken using the procedure described above, and using bulk TDA samples as received from the TDA producer. A smaller (2.4 m^2) box was also constructed to investigate the orientation of high risk TDA particles intentionally placed close to the base of the TDA layer (to increase the understanding of the orientation of high risk TDA particles at the base of the TDA layer).

The results of this testing may be summarized as follows:

- in the small box test using controlled multi pass TDA (i.e. a sample with a high proportion of high risk TDA particles), the box contained 1,250 particles;
- 150 particles were recorded at the base, of which approximately 7% were recorded to be oriented towards the base (i.e. unfavourably);
- in the large box testing using as-received multi pass TDA, the box contained 3,600 particles of which 485 particles were at the base;
- in the large box testing using double pass TDA, the box contained 1,390 particles of which 244 particles were at the base;
- in both the multi pass and double pass large box tests, only one particle was recorded to be oriented unfavourably towards the base.

The results of the random sample large box testing and the controlled sample small box testing are consistent, and suggest that approximately 7% of the high risk pieces would be expected to be oriented unfavourably towards the geomembrane.

It should be noted with regard to the expected number of punctures from high risk TDA particles that while the extent of processing (i.e. single pass, double pass, multi pass) does not appear to affect the proportion of high risk TDA particles, there are fewer large particles in a given quantity of TDA (and consequently fewer high risk particles in that same quantity) than would occur with smaller particles. This finding suggests that reduced levels of TDA processing and the resulting smaller number of high risk TDA particles impinging on geomembrane liners should result in reduced geomembrane puncture.

Step 3 – assess probability of puncture from unfavourably oriented high risk TDA particles

Initial testing confirmed that geomembranes with moderate geotextile protection can be punctured by high risk TDA particles intentionally oriented with the wires facing the geomembrane/geotextile protection. Step 3 of the testing was designed to investigate the extent to which different geosynthetics would protect against geomembrane puncture under these conditions. The following protective geosynthetics were tested:

- 544 and 814 g/m² non-woven needle punched geotextiles;
- a planar drainage geocomposite (i.e. a geonet core enveloped top and bottom with geotextiles); and
- a 26.3 kN/m (CD) woven geotextile.

Various combinations of these materials were tested (e.g. the two non-woven needle-punched geotextiles were used in combination, representing a 1,358 g/m² geotextile). Five tests were conducted using combinations of non-woven needle-punched geotextiles above a 1.5 mm thick geomembrane, four tests were conducted using combinations of non-woven needle-punched geotextiles above a 2 mm thick geomembrane and three tests were run using combinations of non-woven geotextiles, woven geotextiles and planar drainage geocomposite above a 2 mm thick geomembrane. The results of this testing may be summarized as follows:

- greater thicknesses of geotextile protection were confirmed to provide higher levels of protection against geomembrane puncture. For example, the protection efficiency of a

- 1.5 mm thick geomembrane ranged from 86.7% to 96.4% for geotextiles with mass per unit area of 1,088 and 1,628 g/m² respectively;
- greater geomembrane thickness was confirmed to provide a higher level of protection against geomembrane puncture. For example, the protection efficiency offered by a 1,088 g/m² geotextile ranged from 86.7% to 98.3% for geomembranes of 1.5 and 2 mm thick respectively; and
 - combinations of non-woven geotextiles, woven geotextiles and a planar drainage geocomposite were found to provide a protection efficiency equivalent to a heavy (1,628 g/m²) non-woven needle-punched geotextile.

The test results confirmed that protruding wires from TDA can be expected to puncture geomembranes, to an extent determined by the thickness of the geomembrane and the level of overlying geotextile protection. Additional discussion of the implications to field puncture performance is presented in Section 5.6.2 of the current document.

With regard to the testing approach described above, it should be noted that the intentional placing of high risk TDA particles above the protective geotextile/geomembrane in the test chamber, and the intentional orienting of these particles towards the protective geotextile/geomembrane so that they would tend to impinge on the geomembrane is conservative, i.e. the approach would overestimate the frequency of any punctures while realistically representing the mechanics of geomembrane puncture itself under reasonable worst case conditions.

5.6.2 Implications for field scale performance

The laboratory scale testing described above identified the following characteristics of TDA with regard to puncture of geomembranes:

- the proportion of high risk TDA particles;
- the frequency with which these particles are expected to be oriented unfavourably towards underlying geomembranes / protective geosynthetics; and
- the extent to which these particles could puncture different geomembranes protected with different types of geosynthetics if the particles were oriented unfavourably towards the geomembrane.

A simple equation was derived to express how these factors could be used to predict the number of geomembrane punctures due to TDA in a field setting. These results are summarized in Table 1.

Table 1: Predicted frequency of geomembrane puncture by TDA

	Single pass	Double pass	Multi pass
TDA particles on base (#/m ²)	25	41	72
TDA particles on base (#/ha)	250,000	410,000	720,000
Proportion of high risk TDA particles	3.1%	1.9%	1.8%
High risk TDA particles on base (#/ha)	7,750	7,790	12,960
High risk TDA particles oriented unfavourably	7%	7%	7%
High risk TDA particles oriented unfavourably (#/ha)	523	525	874
Protection efficiency ^{*1}	97.5%	97.5%	97.5%
Punctures (#/ha)	13	13	22

^{*1} Assuming 2 mm thick geomembrane with 1,088 g/m² geotextile protection

The following conclusions were drawn from the results:

- less TDA processing results in larger TDA particle size and fewer TDA particles for a given quantity of TDA. Given that the proportion of high risk particles was similar for all grades of TDA at around 2 to 3%, larger TDA particle size would result in fewer high risk TDA particles being available at the base of a TDA layer to cause puncturing of underlying geosynthetics. Review of TDA specifications regarding particle size may be warranted;
- a 2 to 3% proportion of high risk TDA particles appears to be achievable using conventional TDA processing equipment and good processing techniques. Incorporation of this factor into production QA/QC requirements may be warranted;
- geomembrane protection efficiency should be considered by landfill design engineers during the preparation of specifications for TDA-related projects, giving due consideration to clay subgrade conditions, geomembrane type, drainage material and thickness of waste pile.

5.7 Geomembrane Strain Testing and Results

In addition to the risk of immediate puncture of geomembranes by high risk TDA particles in the leachate collection system, it was evident from the technical literature that leachate drainage media can produce indentations in the geomembranes which represent local stretching (or 'strain') in the material. The literature suggests that strain should be kept below 3% to avoid compromising the integrity of the geomembrane in the long term. The testing program therefore included measures to investigate the extent to which TDA and typical leachate drainage gravel materials would induce strains above 3% given the conditions of the geomembrane puncture testing described in Section 5.3 of the current document.

The puncture testing method presented in Section 5.6 of the current report involved multiple compression tests of different configurations of geomembrane, geosynthetic protection, drainage material and load. Following each loading event, the drainage materials, protective geotextile and geomembrane were removed to expose the clay subgrade and allow the indentations imparted by the drainage materials to be observed and recorded photographically, and any penetrative punctures to be identified. A photogrammetric method was developed at the University to compare and evaluate the strains induced by the TDA and gravel materials in the geomembrane and captured in the clay. Images were correlated using a point cloud, which allowed the comparison and evaluation of the strains caused by TDA and mineral aggregate. An approximate mathematical method developed by Tognon et al. (2000) was initially used to calculate the distribution of localized high strains.

The data captured by these techniques allowed strain area distribution curves to be developed, which showed the proportion of the affected surface that had suffered greater than the target 3% strain. Strain area distribution curves for TDA and gravel for 1.5 mm and 2 mm thick geomembranes are presented as Figure 10.



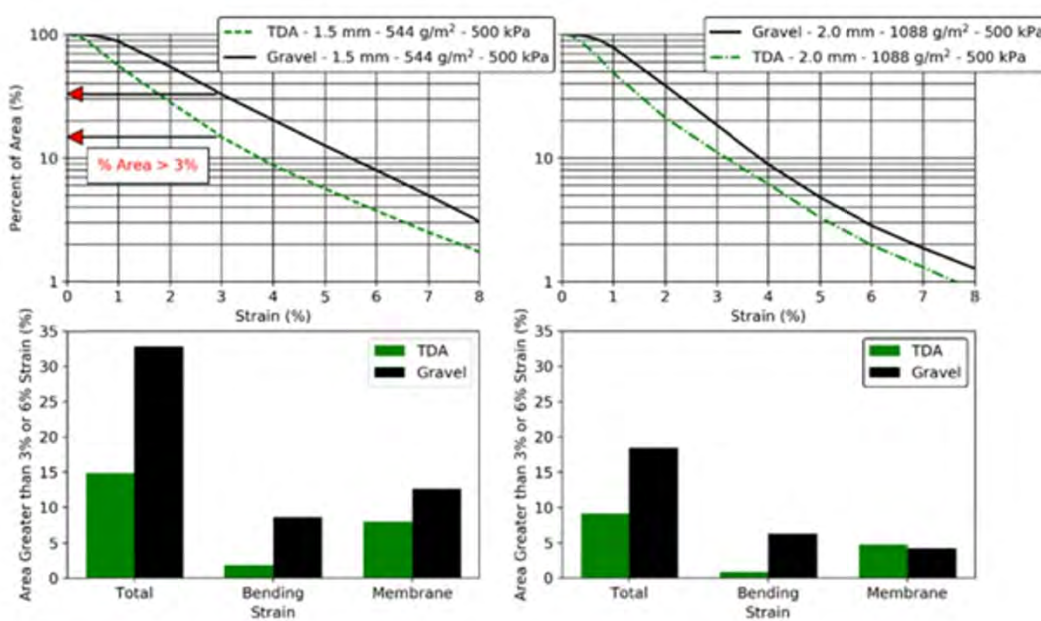


Figure 10: Strain area distribution curves for TDA and gravel

These curves clearly show that TDA results in a smaller proportion of the geomembrane suffering strains greater than 3% than gravel (using equivalent subgrade, geosynthetic protection and load conditions).

Information became available during the testing program indicating that Tognon's data analysis method would underestimate strain for small, deep indentations (such as those caused by gravel) and overestimates strain for large, shallow indentations (such as those caused by TDA). This data analysis anomaly would suggest unreasonably poor strain performance for TDA as the 'rebounding' behaviour of the geomembrane for large, shallow indentations would affect the results. A revised test method was developed as part of the testing program to address this issue.

The revised data analysis method considered radial or lateral displacements to reduce the effects of the simplifying assumptions inherent in Tognon's method. Testing was re-run for TDA and gravel using the following method to prevent the geomembrane from rebounding:

- a pattern was painted onto the geomembrane prior to testing;
- epoxy was pumped in to the system to "lock" the geomembrane in place while normal loads were still in place; and

- the pattern before and after geomembrane deformation was compared to more accurately measure the strain induced, using optical techniques.

The testing procedure was used for both TDA and gravel in order to compare the relative performance of each drainage material. The revised analysis suggested that the difference in strain performance between TDA and gravel may be even more pronounced than indicated on Figure 10.

5.8 Task 2 Summary and Recommendations

The testing confirmed the potential for both TDA and gravel to cause damage to geomembrane liners, even with heavy geosynthetic protection. The mechanisms by which this damage is caused differed between TDA and gravel as follows:

- protruding wires in TDA were confirmed to be a higher risk for immediate puncture than typical leachate drainage gravel; and
- TDA was confirmed to be a lower risk for excessive local strain associated with long term geomembrane stress cracking than typical leachate drainage gravel.

These risks could not be reduced to zero by the inclusion of protective geosynthetics between the base of the TDA/gravel layer and the top of the geomembrane liner.

Initial indications are that lower levels of TDA processing resulting in larger TDA particle size may reduce the risk of geomembrane puncture from TDA. Detailed investigation of this factor was not an objective of the current study, and the finding should be considered preliminary. Further study is warranted to identify the ideal TDA particle size that would optimize hydraulic performance and geomembrane puncture behaviour.

Appendix 1

Physical properties of TDA affecting performance in leachate collection system

University of Saskatchewan, October 2019





Tire derived aggregate as a drainage medium for landfill leachate collection

I.R. Fleming, Ph.D., P.Eng.

A.R. Hammerlindl, M.Eng., P.Eng.

B.A. Marcotte, B.Sc.

D. Adesokan, M.Sc.

October, 2019

Geotechnical Engineering Laboratories

Department of Civil, Geological & Environmental Engineering

57 Campus Drive, Saskatoon S7N 5A9 Canada

Tire derived aggregate as a drainage medium for landfill leachate collection

Structure and format of reporting

This two volume report documents work carried out at the University of Saskatchewan Geotechnical Labs since 2016 to evaluate tire derived aggregate (TDA) for use as a drainage medium in landfill leachate collection systems (LCS). These reports have been prepared for Adelantar Consulting on behalf of Alberta Recycling (AR). Accordingly, each of the two volumes covers separate (but related) workplans as follows:

Volume 1 Physical properties of TDA affecting performance in LCS

This report covers the testing of large samples to evaluate the compression of TDA under load and the resulting decrease in void ratio (or porosity) as well as the resulting change in both vertical and horizontal permeability.

Testing was carried out using two different systems: i) a large 1-dimensional cylindrical consolidometer designed to handle large strains while maintaining constant vertical load under compression and subsequent creep; and ii) a large rectangular 2D permeameter that allowed for measurement of horizontal and vertical hydraulic conductivity of a large specimen under load.

The effects of immediate compression by application of vertical stress were evaluated, along with the effect of creep over time at constant load. The inherent nature of TDA required innovative design of the laboratory testing equipment (and iterative re-design and upgrading of the system and its components). A total of 5 compression/creep tests were carried out over a combined 315 days with individual tests ranging in duration from 24 to 126 days.

Hydraulic conductivity was evaluated by dozens of tests at different flow rates and pressures. Interpreting the resulting data to yield hydraulic conductivity values required some complex analyses to account for high velocities, inertial effects and the inevitable artifacts of even the largest scale laboratory testing. These complex analyses are included as an appendix.

Volume 2 Damage to geomembranes by coarse uniform TDA or gravel drainage aggregate

This report evaluates the potential for damage to a geomembrane from an overlying coarse drainage aggregate. The testing program was designed to evaluate the relative risks associated with tire derived aggregate (TDA) and gravel when used in conjunction with a geomembrane in a base barrier for a landfill. The testing equipment consists of a large compression device capable of applying over 700 kPa to a 0.9 m diameter sample of TDA over geomembrane (GM) over clay.

The work addressed two separate types of damage to a geomembrane: short term puncture from point loading of the coarse drainage aggregate (Objective 1); and the development of high localised tensile strains which are detrimental to geomembrane integrity on a longer timeline (Objective 2) when such localised strain exceeds a threshold above which stress cracking becomes likely.

Multiple trials were carried out to evaluate various protective layers that may be placed between the GM and the drainage medium. In addition, work was carried out to highlight the significant role of the compacted clay sub-liner material in controlling the strains in an overlying geomembrane.

Tire derived aggregate as a drainage medium for landfill leachate collection

Volume 1, Physical properties of TDA affecting performance in LCS

Table of Contents

1.	Background – performance of leachate collection systems	1
2.	Scope of work and objectives	3
3.	Characterization of TDA materials	4
4.	Hydraulic conductivity	7
5.	Void volume	10
6.	Discussion of results	16
7.	Key findings	19
	References	20
	Appendices	
	Attachment	

List of Tables

Table 1:	Average corrected values for horizontal and vertical hydraulic conductivity and corresponding anisotropy	9
Table 2:	Compression tests	10
Table 3:	Required thickness of TDA at time of placement	17

List of Figures

Figure 1:	Variation of maximum head on liner with hydraulic conductivity of drainage media	2
Figure 2:	TDA samples	4
Figure 3:	Size distribution of single and multi-pass TDA samples compared with gravel	5
Figure 4:	Triaxial cell set up for assessing isotropic solid volume compression in individual TDA particles	6
Figure 5:	The 2D permeameter	7
Figure 6:	2D permeameter – two typical trials - vertical test data	8
Figure 7:	2D permeameter – two typical trials - horizontal test data	9
Figure 8:	Large 1-D compression test cell	10
Figure 9:	Progression of creep test showing positions of visual markers during the tests	11
Figure 10:	Porosity inferred from vertical compression compared with direct measurements	11
Figure 11:	Raw data from compression / creep test	12
Figure 12:	Results of compression / creep test expressed as void ratio over time	12
Figure 13:	Results of compression / creep test expressed as void ratio vs stress	13
Figure 14:	Results of compression / creep test #1	13
Figure 15:	Results of compression / creep test #2	14
Figure 16:	Comparison of fast and slow loading on compression of TDA	14
Figure 17:	Heating pads affixed to 2D permeameter-consolidometer	15
Figure 18:	Comparison of volumetric strain induced by immediate and creep compression	16
Figure 19:	Compressed TDA impregnated with dyed epoxy and sliced to image void space	17
Figure 20:	Sample mapping of void geometry	18

Final Report – Physical properties of TDA affecting performance in LCS

1. Background – performance of leachate collection systems

The performance of a drainage layer used in a landfill leachate collection system (LCS) depends upon two key considerations:

- i. high hydraulic conductivity (or permeability) of the material so as to minimise mounding of leachate head on the base barrier; and
- ii. resilience to clogging, which is strongly related to the total volume of large voids (typically expressed as porosity or void ratio).

These two parameters are not independent of each other and each will change over time as a result of accumulation of mineral deposits within the pores. Testing for clogging potential was outside the scope of work, however based on a thorough understanding of the mechanisms; it is possible to draw conclusions regarding the likely effect of clogging on materials with varying void ratio and void size.

The purpose of the work described in this report is to evaluate the TDA material received from Alberta Recycling (AR) relative to the properties as described above that are required for satisfactory performance in LCS.

1.1. Control of leachate head

A material with a high permeability allows for leachate to flow easily under gravity without “mounding” or ponding up on the base barrier. Such mounding increases the fluid pressure of the leachate on the base barrier thus forcing more leachate to leak through any defects in a geomembrane or in the case of compacted clay or geosynthetic clay liner (GCL) resulting in greater flow through the pores of the clay. For this reason, several jurisdictions have regulated the maximum hydraulic head (height of the “mound”) over a base barrier system in a landfill. For example, the Province of Alberta requires no more than 0.3 m of leachate head over a landfill base barrier under the *Standards for Landfills in Alberta* (2010).

There are various relationships that may be used to estimate the hydraulic head in a granular drainage blanket. Assuming that drainage pipes function as intended to remove leachate with little additional head loss (not always true, see Fleming et al, 1999), the maximum head (h_{MAX}) can be expressed as a function of the following:

- the hydraulic conductivity of the drainage media (k);
- the length of the drainage path, i.e. half the distance between drainage pipes (L);
- the slope toward the drainage pipe (s or $\tan\beta$);
- the average infiltration into the drainage system from the overlying waste (q_0).

One useful such relationship was published by Giroud & Houlihan (1995). This equation provides inaccurate results, however, when the saturated zone extends above the top of a finite thickness of drainage layer. Accordingly, where the calculated value of h_{MAX} was greater than 0.5 m, a steady state finite element solution was used to estimate the value of h_{MAX} numerically. The FE simulations incorporated reasonable values for the hydraulic conductivity of waste at the bottom of a landfill (Fleming, 2011, Beaven et al, 2008). The resulting relationship between h_{MAX} and k is presented in Figure 1 for reasonable values of L and $\tan\beta$ and for reasonable upper and lower bound values of q_0 applicable to Alberta.

It is evident from Figure 1 that for hydraulic conductivity greater than about 3×10^{-5} m/s, hydraulic head is easily maintained less than 0.3m. If k decreases to lower values somewhat less than 10^{-5} m/s, hydraulic performance of a drainage blanket will depend on limiting the length of the drainage path or increasing the slope. If k is less than about 5×10^{-6} m/s the drain will simply not function as such for a reasonable slope or length of drainage path, given values of q_0 representative of Alberta.

It is equally evident that for (long term) k greater than or only slightly less than 10^{-4} m/s, the drainage blanket may be expected to function well under the conditions and range of variables described above.

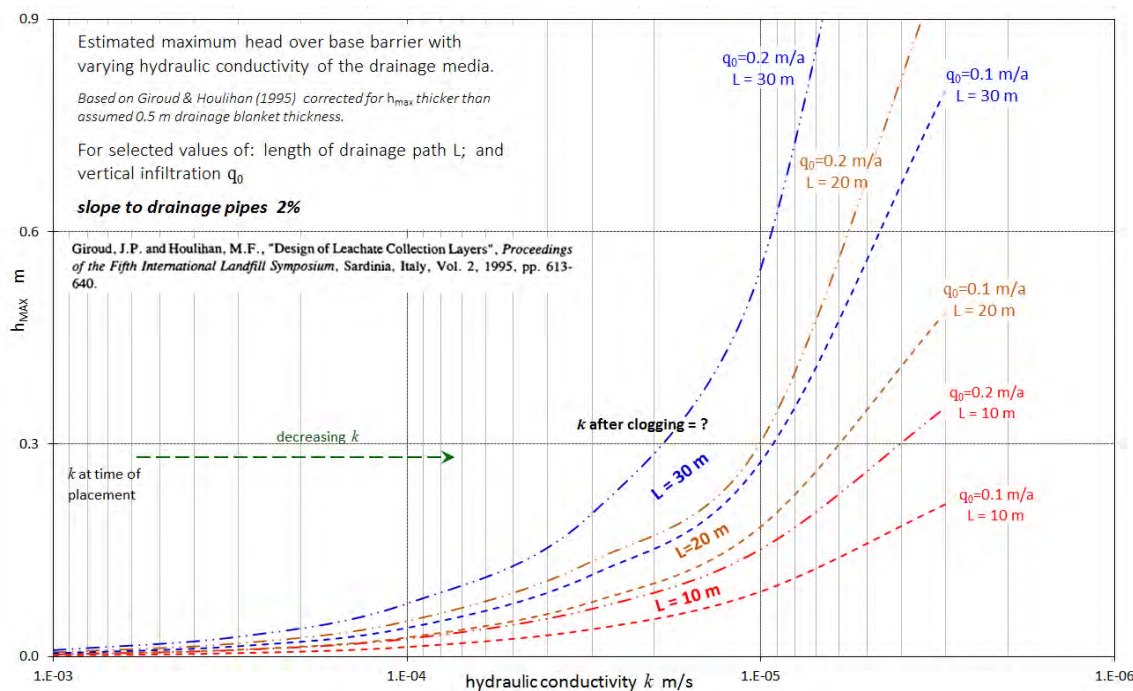


Figure 1: Variation of maximum head on liner with hydraulic conductivity of drainage media

1.2. Void volume

The permeability of the drainage media at the time of placement, while important, is not in fact the key consideration. As a result of biogeochemical clogging processes, a mineral deposit is likely to precipitate and accumulate in the voids of the drainage media (Fleming et al, 1999, Fleming & Rowe, 2004) thus decreasing k over time (which may only be a few years). A key function of a drainage layer is thus to have a sufficient pore volume to store this inevitable mineral clog without the clog deposit inhibiting the interconnectedness of the pore network and significantly reducing k .

A simple approach to estimate the required minimum pore volume for resilience against clogging was proposed by Rowe & Fleming (1998) based on the mass (and therefore volume) of clog deposit and a spatial distribution of the mineral clog deposit within the drainage blanket based on field observations (Fleming et al, 1999). Essentially, for the same functioning service life against clogging, if the void ratio of TDA is lower than that of an available gravel, then the thickness of the TDA layer must be increased, the spacing between drainage pipes decreased, or both.

It is not enough that there be a large volume of pores, the pores must also be large in size. For example, consider a uniform (approx. 50 mm diameter) coarse gravel aggregate ($k \approx 10^{-1}$ m/s) with a large volume of pores (void ratio $e \approx 0.7$) that are themselves individually large (average pore dimension ≈ 15 mm). For such a material, the decrease in k due to clogging may be about 2 orders of magnitude (Rowe & Fleming, 1998, Fleming et al, 1999) and leachate heads should not build up to problematic levels. For a uniform-sized fine "pea" gravel (about 8 mm diameter and void dimension ≈ 3 mm), while the clean unclogged k may be sufficiently high at $\le 10^{-2}$ m/s and the initial void ratio may also be about 0.7, the individual pores are smaller and the effect on k of the accumulation of mineral clog deposit will be much more pronounced - k may decrease by over 3 orders of magnitude with potential consequences in terms of significant head on the base barrier, saturation of wastes etc.

2. Scope of work and objectives

In the context of the issues discussed in Section 1 above, the scope of this work was established. Fundamentally, the objective was to determine the physical properties of TDA that will affect its performance as drainage media in LCS.

Specific aspects of the workplan included the following:

- *Evaluate and characterise the TDA in terms of particle size and exposed wires. This is reported primarily in Volume II.*
- *Design and construct large laboratory test cells (or otherwise modify existing equipment) to enable constant load to be applied during compression to >50% vertical strain. For practical considerations, it was determined that separate test cells would be used to evaluate both vertical and horizontal hydraulic conductivity on the one hand, with one-dimensional vertical compression and creep being tested separately in a different testing system.*
- *Apply constant vertical loads representative of a medium to large landfill in Alberta (15 to >40 m total thickness of waste).*
- *Measure the immediate and time-delayed creep compression under load and determine the effect of compression from sustained loading on void ratio.*
- *Measure the vertical and hydraulic conductivity of the material under applied vertical stress up to 500 kPa.*
- *Evaluate whether elevated temperature (up to about 60°C) affects the compression or creep behaviour of TDA.*
- *Prepare a report synthesising the results and conclusions.*

3. Characterization of TDA materials

3.1. Particle size distribution

Several large samples of TDA material were received from Alberta Recycling (AR) in autumn, 2016. This material had been processed with multiple passes through the shredder and screens to yield a nominal 150 mm particle size. This material, for the purpose of this report is termed multi-pass TDA. All of the compression testing was carried out using multi-pass TDA, as was most of the hydraulic conductivity testing. AR supplied in late 2017 additional materials which had been subject to less processing and consequently exhibited a larger particle size relative to the multi-pass TDA material. This larger particle-size material was intended principally for the testing of damage to geomembranes (Volume 2) but hydraulic conductivity tests were conducted for the single-pass material. Figure 2 shows the three TDA materials.

Because of the irregular particle shape of TDA, particle size cannot practically be determined using conventional sieve analysis as is done for mineral aggregates or granular soils. Large bulk samples of TDA, representing well over 100 kg were instead sorted by hand and the length, width and mass of each individual particle was measured, and any exposed wire was characterised. This procedure is described in detail in Volume 2. In order to best characterise the size of particles that range from tabular (with length less than about 2X width) to elongated ($L>>W$), an equivalent dimension was defined as:

$$D_{EQ} = \sqrt{LW} \quad \text{Eq. 1}$$

The multi-pass TDA material contained almost 10% by mass of particles with $D_{EQ}<50$ mm. In contrast, particles with D_{EQ} less than 100 mm were essentially absent from the single or double-pass material. Figure 3 shows particle size distribution of the 3 TDA materials. For context, typical particle size distributions are also presented for some natural gravels. The “ideal” drainage media for LCS would almost always be uniform 50 mm gravel with $C_u=d_{60}/d_{10}<1.5$, although such material is not always readily available and where it is available, the cost may be high. Accordingly, Figure 3 also presents an “acceptable” less uniform gravel (with C_u of 1.5 to 3) as actually used at a large landfill in Alberta.

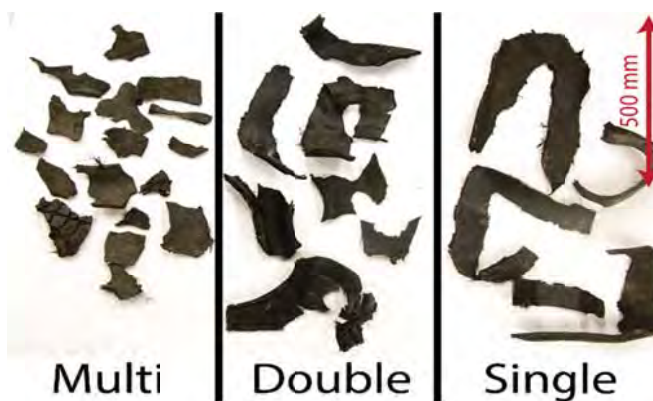


Figure 2: TDA samples: left – multi-pass, middle – double-pass, right – single-pass

It must be emphasized that the particle sizes for TDA and gravel cannot really be compared. For natural soils, or any material that is roughly equidimensional, the pore size can generally be related to the size of the particles. For elongated TDA, the pore shape is substantially different and the pore sizes are decreased with load as discussed further later in this report. Accordingly, the particle sizes of unloaded TDA do not relate to the pore size of loaded TDA in the same way as do the particle size and pore size distributions in gravel, and the different materials cannot be directly compared.

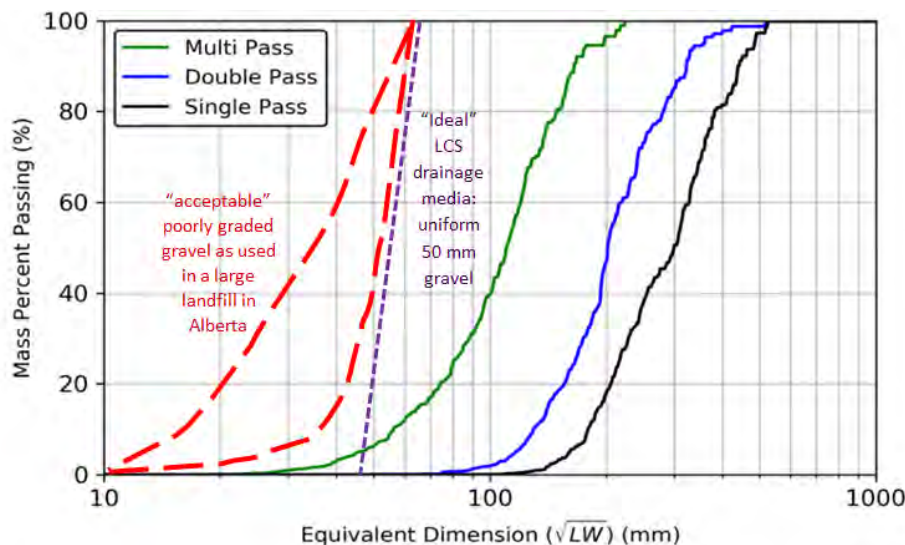


Figure 3: Size distribution of single and multi-pass TDA samples compared with gravel by conventional sieve analysis

3.2. Contribution of solid volume compression in individual TDA particles to void volume reduction in the TDA mass

Since the physical properties of TDA have not been systematically evaluated, there are fundamental questions regarding the nature of tire fragments as part of a porous material. One important such question is whether there is any change in the total volume of an individual tire fragment when subjected to sustained loading. In soil mechanics, the volume of each individual mineral particle may reasonably be taken to be sufficiently close to zero so as to not affect the property of the bulk porous media which consists of many such particles and the associated pores (and pore fluid). As a result, when a soil is subjected to loading, the volumetric strain can be expressed as follows:

$$\Delta V = \Delta V_V \text{ and } \Delta V_S = 0 \text{ so: } \varepsilon_V = \frac{\Delta V}{V_0} = \frac{\Delta e}{1+e_0} \quad \text{Eq. 2}$$

Where V is total volume, V_V is void volume, V_S is solid=phase volume, ε_V is volumetric strain and e is void ratio. For TDA, a reasonable question is therefore whether sustained loading causes volume change in an individual particle or whether the response is purely a change in particle shape with no change in volume.

To evaluate solid volume compression in individual TDA particles, testing was completed in a large triaxial cell (0.6 m high, 0.3 m diameter) (Figure 4). A known volume of water was added to a known volume of TDA mass in the triaxial cell; vacuum pressure was applied to the top of the cell to de-air the TDA sample to enhance saturation, after which isotropic stresses were applied using a pressure - volume (PV) controller. Isotropic stresses of 50 and 100 kPa were applied and each left for a total of 30 days, followed by a stress of 200 kPa which was maintained for an additional 60 days.

An increase in water demand in the test cell from the PV controller was taken as an indication of solid volume compression of the individual TDA particles. Portions of the test results that may have been indicative of the compression of air within the TDA mass were eliminated from the final dataset for assessing the solid phase compression of the individual TDA particles.

The resulting data suggest that the volume compression of the TDA was negligible and could not be differentiated from the response of the test cell itself.



Figure 4: Triaxial cell set up for assessing isotropic solid volume compression in individual TDA particles

4. Hydraulic conductivity

A specialised testing device (Figure 5) was designed and fabricated at the U of S for the purpose of measuring the hydraulic conductivity of TDA. The device allows for a large sample to be compressed under load and air or water introduced on one side and removed on the other (as shown) or vertically from bottom to top. The resulting variation in fluid pressure reflects the resistance to flow and is used to calculate the hydraulic conductivity in either the horizontal or vertical direction.



Figure 5: The 2D permeameter

Measuring hydraulic conductivity of low or moderate-permeability materials is usually quite straightforward, however there are significant challenges for materials with $k >$ about 10^{-2} m/s. In order to generate a loss of head or pressure that is sufficiently large so as to be measured reliably, a large fluid flow, or a very long sample are required, or both. Analysis of test results may also be somewhat more complicated; for example, large flow velocities introduce inertia into the flow system, whereas Darcy flow is assumed to be at sufficiently low velocity that the inertia term is negligible. The data collected during a test of high k material carried out with very high flow must often be analysed using corrections for inertia.

Most of the testing was carried out using air as the fluid rather than water. The resulting values of intrinsic permeability were then used to calculate hydraulic conductivity based on the relative values of density and viscosity of air and water. It should be emphasized that several tests were carried out with water as the permeating fluid, and results were in good agreement, although the tests carried out this way were far more difficult and time consuming, given the extremely large flow of water required to generate a measurable head loss in the system. Since the actual physical testing represented by far the more significant challenge, most of the measurements were made with air as the test results so obtained were found to be more consistent and repeatable.

In the case of TDA, there are other factors that also contribute to the complexity of testing hydraulic conductivity. While it is relatively simple to compress TDA in a cylinder and induce flow vertically through the cylinder (e.g. Rowe & McIsaac, 2005) such a test would inherently measure only the vertical hydraulic conductivity k_z . Given that TDA consists of flat or tabular shaped particles in which the shortest dimension (thickness) is substantially lower than the others (Figure 2) it is entirely plausible to consider that the material may exhibit anisotropy in hydraulic conductivity, especially when loaded vertically as is the case in practice. Such anisotropy as a result of the physical properties of the material may be termed *fabric anisotropy*.

Given that it is necessary to load the sample in order to measure a meaningful result, the loading conditions did introduce complexity – not only to the test apparatus but also to the analysis of results. Up to 270 kN of

vertical load (28 tonnes) was applied to the sample. While every effort was made to reduce sidewall friction, it cannot be eliminated entirely (see Adesokan et al, 2018). The result is that the vertical stress is not homogeneous through the sample and in fact is greatest at the top and lowest at the bottom. The result is that the material properties, while reasonably consistent in the horizontal plane, vary from top to bottom. Given the relation between vertical stress and void ratio (as discussed in the following section 5), permeability may be expected to decrease upward, which is exactly what occurred as indicated by Figure 6. This variation of k in the vertical direction has a greater effect on k_z than k_x and introduces a “compression anisotropy” to the test that is entirely different than the real fabric anisotropy which reflects the material properties. During data analysis, this effect must be removed in order to yield consistent and correct interpretations of hydraulic conductivity. Adesokan & Fleming (2019) discuss this and other challenges in detail.

A series of hydraulic conductivity tests were carried out to measure both k_x and k_z under varying vertical stress and at various flow rates. In the permeameter, most of the tests were carried out using the multi-pass TDA. A series of tests was also carried out using single-pass TDA. Tests were carried out primarily using air flow, although a limited number of tests for multi-pass TDA were carried out using water. A total of 40 measurement ports for air pressure or hydraulic head are located on each side of the permeameter, in four vertical lines, separated horizontally by 290 mm. Each vertical line consists of 10 ports on each side, separated vertically by 63mm. As the TDA material compresses under load, the top of the TDA moves below the uppermost ports which sequentially are shut in the for remainder of the test.

During the testing presented in Figures 6 & 7, the TDA had compressed to approximately half the initial height and only the lowermost 40 ports were still available. Each data point presented in Figure 6 thus represents the average of the readings from the 8 ports at the same elevation. Similarly, each point in Figure 7 represents an average of the 10 lowermost ports along each vertical line. Where air was used as the perment fluid, the distribution of pressure was measured and the intrinsic permeability (k_i) of the material was determined using:

$$k_i = \frac{Q_A}{A} \mu_A \left(\frac{\Delta P}{\Delta \ell} \right)^{-1} \quad \text{Eq. 3}$$

where Q_A/A is the air flow per unit cross-section area, μ_A is the viscosity of air and $\Delta P/\Delta \ell$ is the pressure gradient in the direction of flow. Intrinsic permeability (k_i) is then converted to hydraulic conductivity (k) using:

$$k = k_i \frac{\rho_w g}{\mu_w} \quad \text{Eq. 4}$$

where ρ_w is the density of water, μ_w is the viscosity of water and g is gravity.

Typical results (single-pass TDA) are presented in Figures 6& 7, in each case showing the results of two trials carried out at different flow rates of air. In most tests, results were consistent, although there was noise associated with individual manometer ports being blocked off by TDA particles.

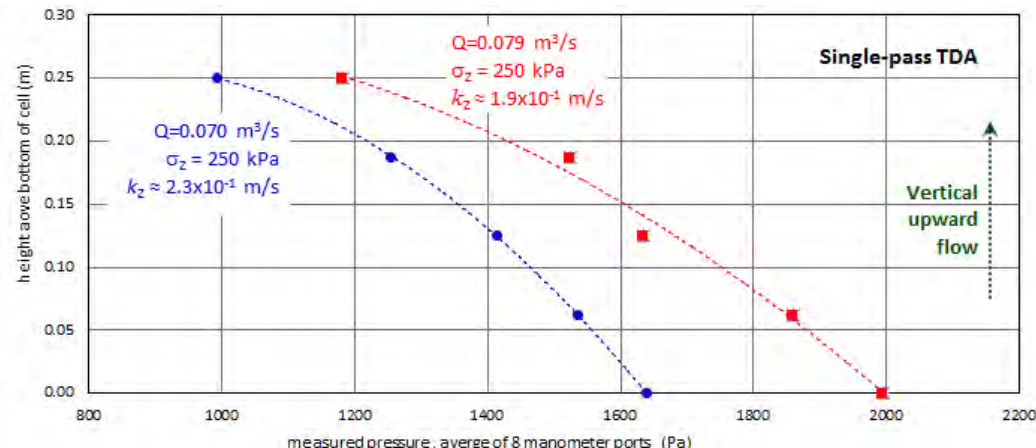


Figure 6: 2D permeameter – two typical trials - vertical test data

The pressure drop with vertical flow distance (Figure 6) shows that the pressure gradient increased upward, suggesting that the permeability of the material decreased closer to the load plate. This compression anisotropy is purely an artifact of the test conditions and its effect must be removed from the data in the determination of vertical and horizontal hydraulic conductivity and the true (fabric) anisotropy under field conditions where there is no sidewall friction to decrease vertical stress across the thickness of the TDA layer.

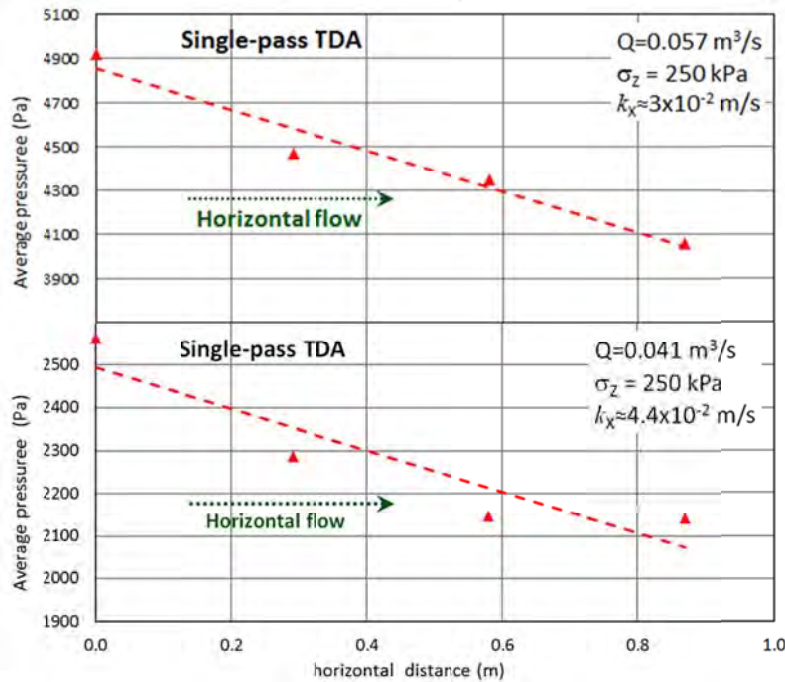


Figure 7: 2D permeameter – two typical trials - horizontal test data

Table 1 provides a summary of the permeability testing results for single-pass and multi-pass TDA. Under vertical loads up to 375 kPa (30-40 m height of municipal waste) the hydraulic conductivity of the TDA was determined to be greater than 10^{-2} m/s. This value is sufficiently high for use as LCS drainage media. It must be emphasized that this value reflects the fresh “clean” material (either gravel or TDA) before it has been subject to the inevitable clogging processes that may be expected to quite quickly decrease k by about 2 to 3 orders of magnitude (within a few years, Fleming et al, 1999). In the longer term, the effect of clogging on the hydraulic performance of TDA and gravel cannot be compared based on existing knowledge.

The hydraulic conductivity of the single-pass TDA is slightly higher than that of the multi-pass TDA material.

Table 1: Average corrected values for horizontal and vertical hydraulic conductivity and corresponding anisotropy

TDA material	Applied surface load, kPa	Corrected estimated mean vertical hydraulic conductivity, k_x m/s	Corrected estimated mean horizontal hydraulic conductivity, k_z m/s	Anisotropy in hydraulic conductivity k_x / k_z
multi-pass	112	3.3×10^{-1}	5.2×10^{-1}	2
	224	1.1×10^{-1}	3.0×10^{-1}	3
	375	2.4×10^{-2}	5.1×10^{-2}	2
single-pass	250	2×10^{-1}	3.6×10^{-2}	<1

5. Void volume

For gravel drainage aggregate, the void ratio of the material will not change upon the application of vertical stress. The volume of voids (per unit area of drain) is important because that volume must be sufficient to "store" the accumulated mineral clogging deposits while maintaining sufficient interconnection of large voids as to ensure that permeability remains sufficiently high to avoid large buildup of hydraulic head in the system.

5.1. Testing strategy

In the case of TDA, compression of the layer results in a decrease of the void ratio even before clogging material can accumulate. During sustained loading, some additional creep compression also occurs. A large compression chamber was designed and built to test immediate and creep compression behaviour (Figure 8).

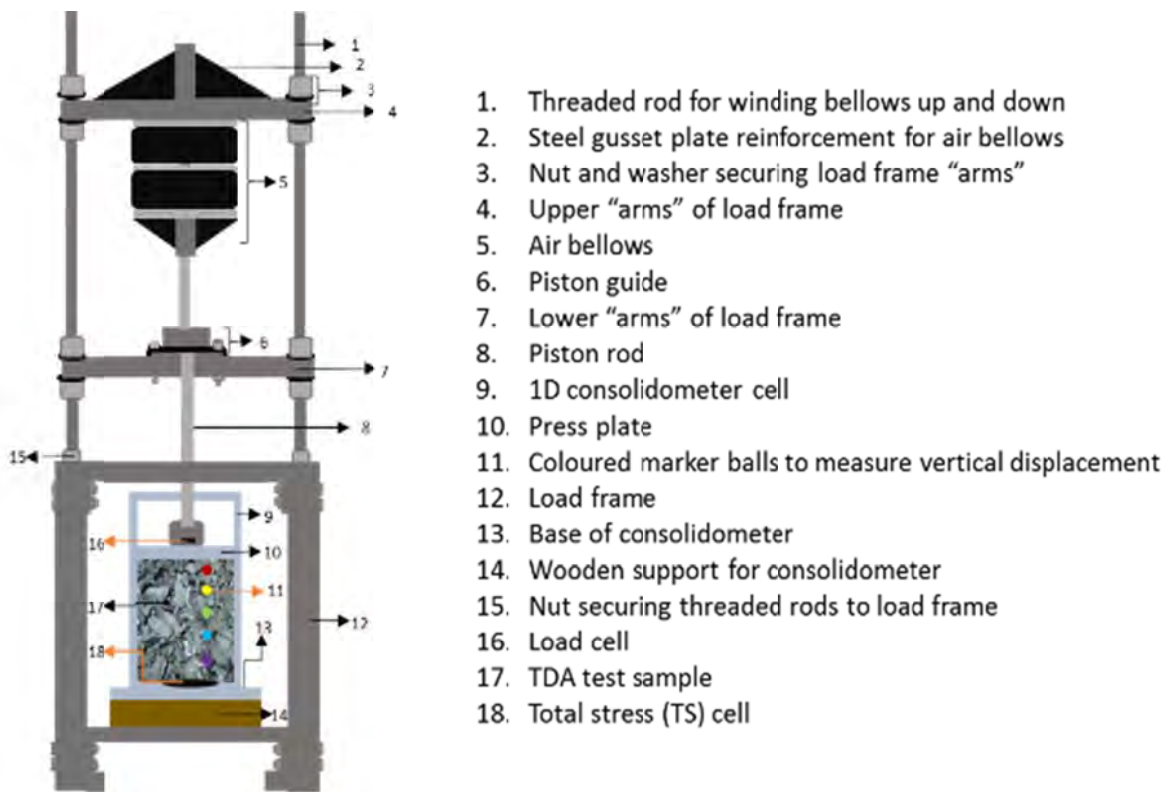


Figure 8: Large 1-D compression test cell

A total of 5 different compression tests were conducted on TDA material received from AR.

Table 2 Compression tests

Test #	Material	Load steps (kPa)	Total duration (d)
1	multi-pass	100, 200, 300	54
2	multi-pass	100, 200, 300	36
3	multi-pass	100, 200, 300	75
4	multi-pass	220 (applied quickly)	24
5	multi-pass	220 (applied slowly over ≈50 d)	126

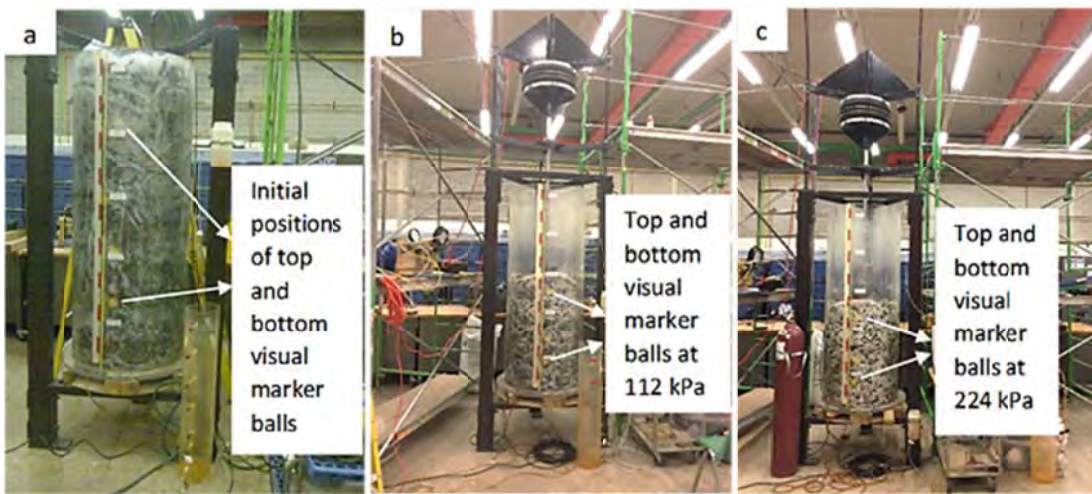


Figure 9: Progression of creep test: (a) unloaded (b) 112 kPa (c) 224 kPa. Sample positions of visual markers during the tests are indicated (using the topmost and bottom

During the compression tests, void ratio (or porosity) was calculated from the reduction in total volume, assuming that the overall volume reduction is attributable only to a reduction in void volume (Section 3.2 above). As a check, porosity was directly measured by filling and draining the 1D compression cell. Figure 10 clearly shows the good agreement between the two, with the direct measurement tending to slightly underestimate porosity relative to the calculated values, as should be expected from retained water or entrapped air.

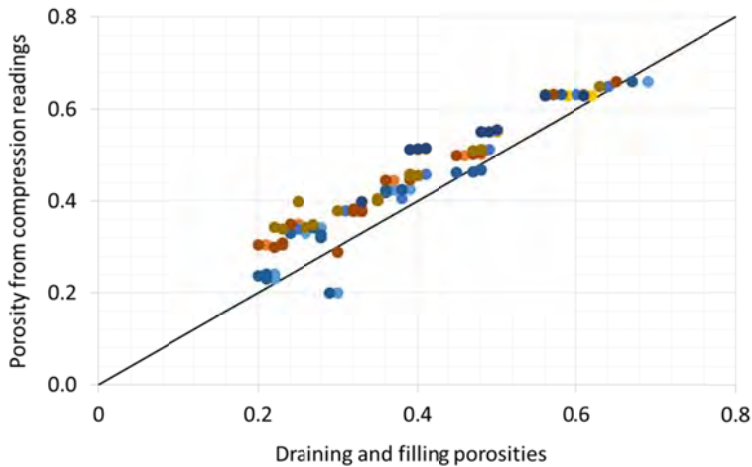


Figure 10: Porosity inferred from vertical compression compared with direct measurements

5.2. Compression and creep testing results

The following figures present the results of a series of compression tests carried out over a two year period. The mass of TDA in the tall 1-dimensional compression cell can be considered to be a series of thinner “slices”. Due to sidewall friction, the average vertical stress is not the same in each slice.

For each test, the raw data for the elevation of the top of each sublayer may be presented as shown in Figure 11 for Test 3. Since the vertical movement of two sets of intermediate reference points were tracked over time, this test effectively represents 3 compression tests of sublayers subject to slightly different vertical stress (Adesokan et al, 2018). It is evident that the markers for the top of the layer

moved downward by the greatest amount since these were affected by the compression of all three sublayers while the markers representing the top of the lowest sublayer moved the least, reflecting only compression of that bottom layer. It is also evident that most of the compression happened very quickly and that the subsequent creep represented much less displacement than the immediate compression.

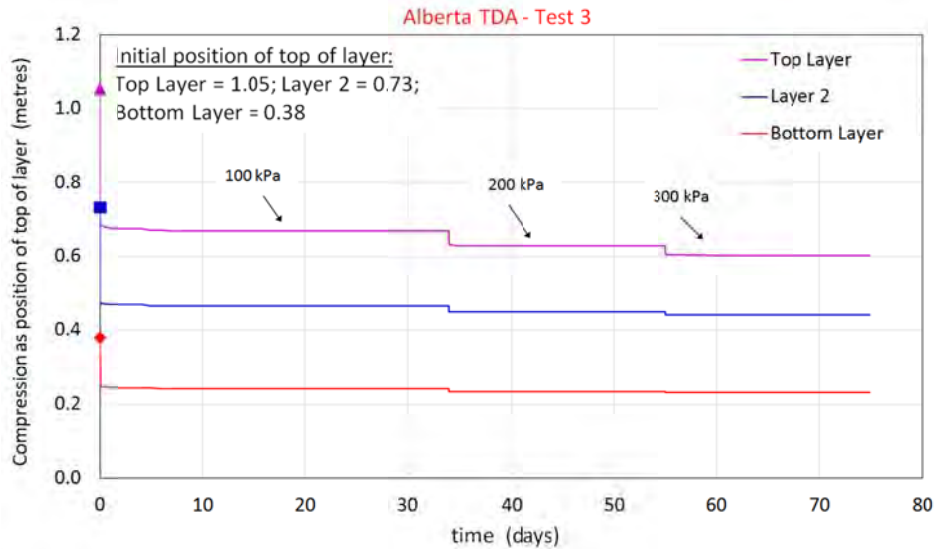


Figure 11: Raw data from compression / creep test

The changing heights of the top of each sublayer in Figure 11 reflect compression of the various layers and can be expressed as a change in void ratio over time (Figure 12).

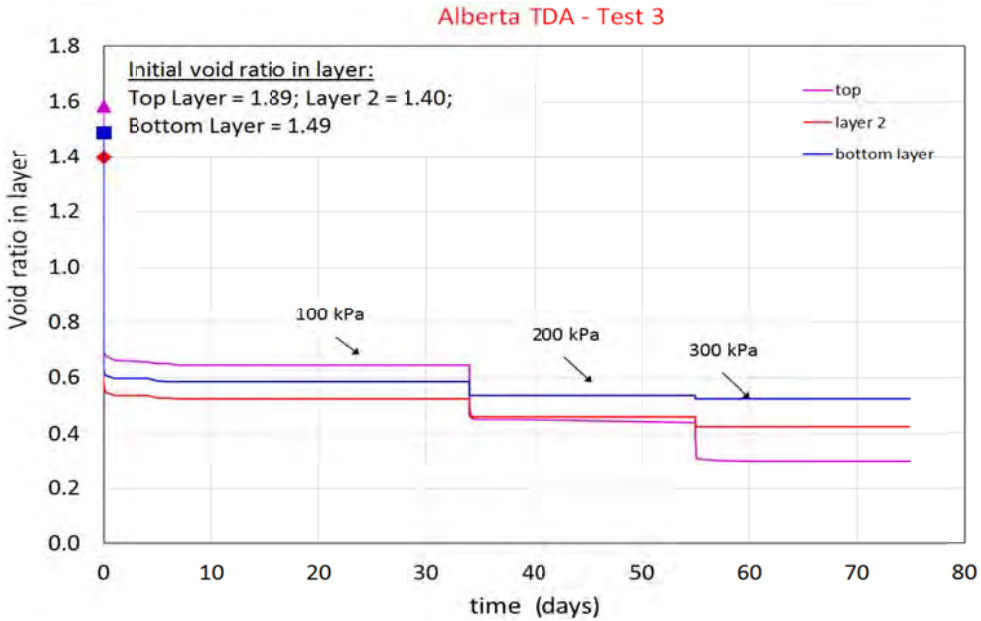


Figure 12: Results of compression / creep test expressed as void ratio over time

Consolidation tests in geotechnics are typically presented at semi-log scale as void ratio vs log vertical stress (Figure 13 for test 3). A consistent value of the compression index (c_c , the slope at semi-log scale) is expected for most soils however for TDA, there was not found to be a consistent representative value for the compression index. In fact, in many cases it appears that the slope flattened (i.e. decreasing c_c) at the largest increments of stress.

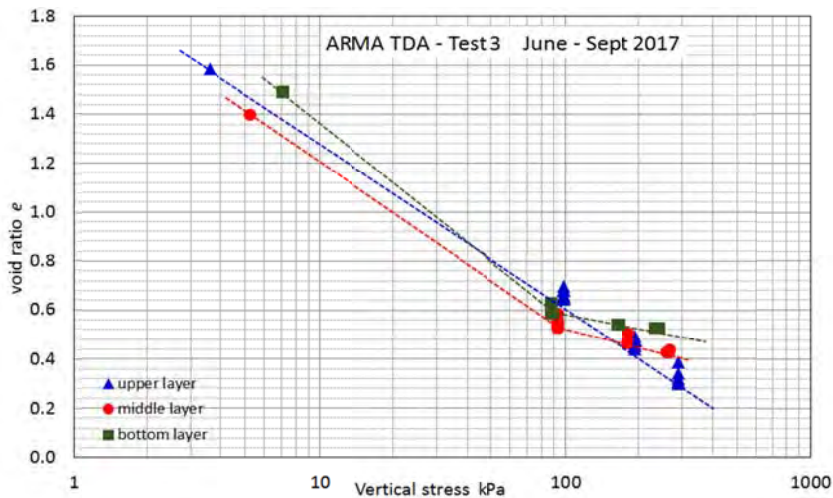


Figure 13: Results of compression / creep test expressed as void ratio vs stress

The plots of void ratio vs time and void ratio vs vertical stress are presented below for tests 1 & 2. In test #1 the initial void ratio of the three layers was generally lower and in test #2, the TDA was intentionally placed with as high an initial void ratio as possible – it can be seen from the initial values that it is very difficult to achieve highly consistent results between the various sublayers.

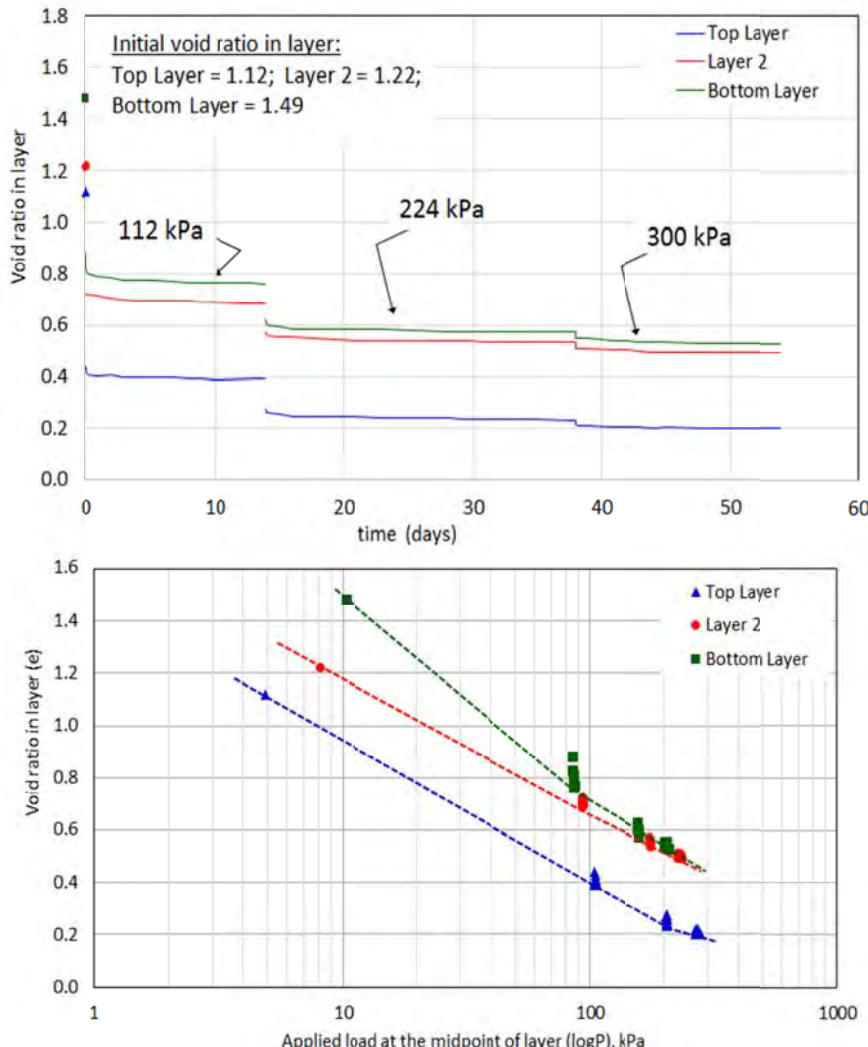


Figure 14: Results of compression / creep test #1

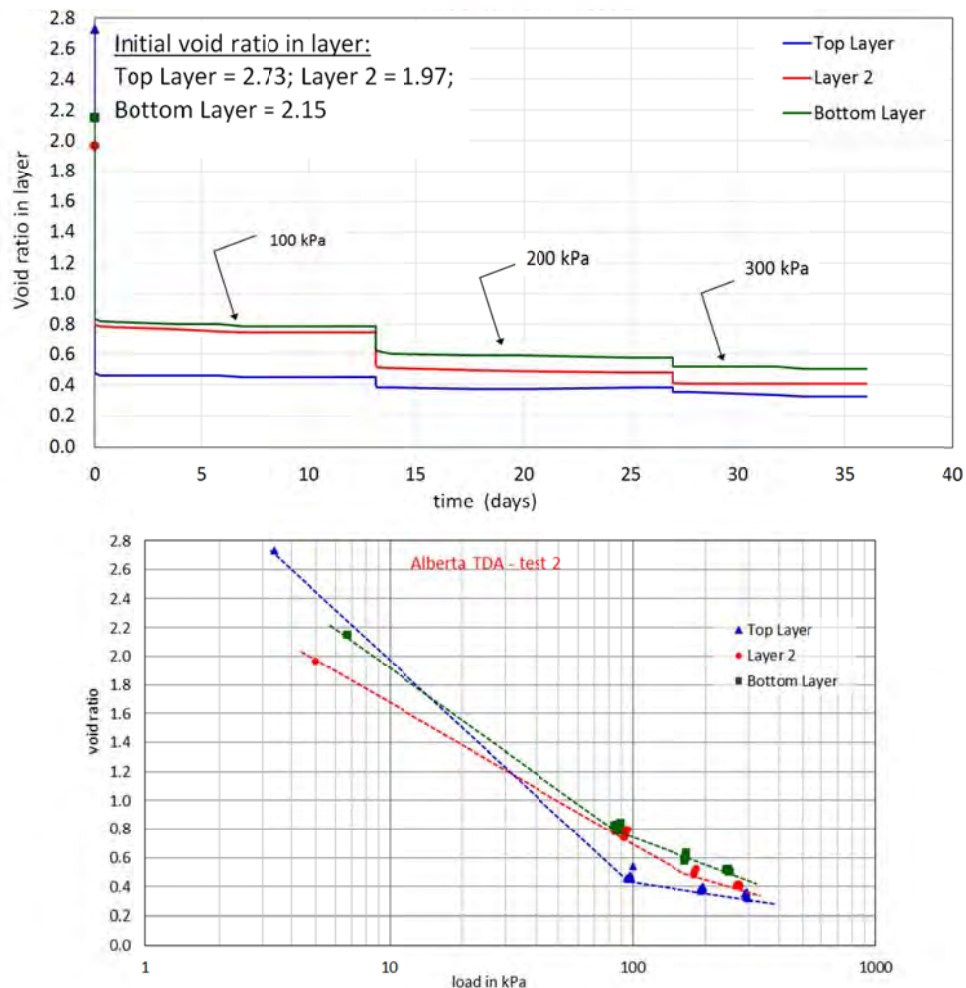


Figure 15: Results of compression / creep test #2

From these results, it is evident that the compression behaviour of TDA is complicated and may depend on many factors including initial void ratio. In order to evaluate the effect of loading rate, tests 4 and 5 were carried out with fast and slow loading respectively. The initial void ratio was almost exactly the same (≈ 1.8) and the final void ratios were close, with perhaps slightly less compression under slow loading.

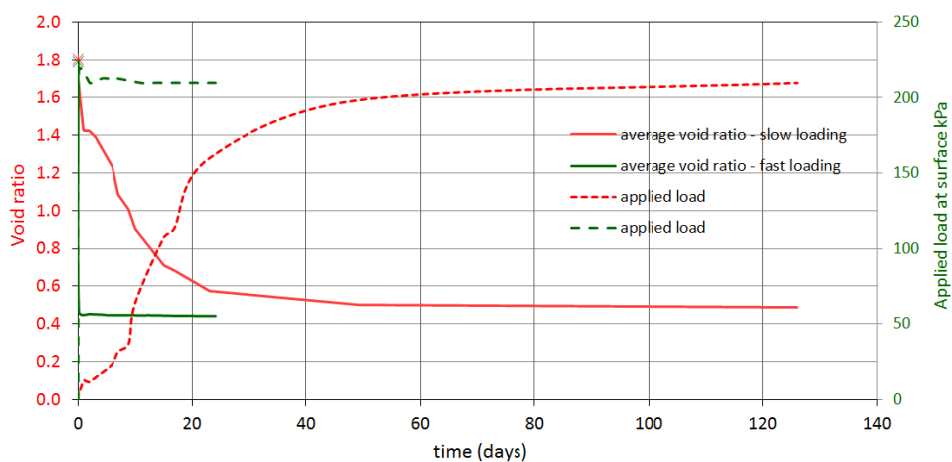


Figure 16: Results of compression / creep test #4 & #5. These tests were carried out differently than tests 1-3. For test #4, 210 kPa was applied as quickly as possible. For test #5, the same load was applied very gradually over a period of weeks.

5.3. Effect of temperature

The contribution of elevated temperatures to void volume reduction in a TDA mass following compression and creep was evaluated in the 2D consolidometer-permeameter following the horizontal and vertical hydraulic conductivity testing. After the hydraulic conductivity tests at an applied load of 315 kPa, heating mats were wrapped around the test cell (Figure 17) and covered with insulation. The heating mats were set at a temperature of 58°C for 90 days and temperature readings were taken from probes that were inserted into the TDA mass and the headspace of the 2D cell.

Two aspects of the effects of temperature on a TDA mass were investigated: (1) how much further void volume reduction would occur if there was surface load on the TDA mass before increasing the temperature, and (2) how much compression would occur if the temperature of the TDA mass was increased before increasing the applied surface load?

No further compression was observed in the TDA mass after heating it up for 90 days. Similarly, after unloading to 224 kPa, and reloading to 375 kPa to evaluate any softening in the TDA particles that may induce further compression and creep, no additional strain was observed. No plastic strain was observed as the TDA mass returned to its original position at the 375 kPa load step. .

There was no observed increment of further creep as a result of elevating the temperature of the TDA – the material did not display any increase in compressibility or accelerated rate of strain at a temperature of 58°C.



Figure 17: Heating pads affixed to 2D permeameter-consolidometer – these were covered with insulation and the temperature raised to 54°C

6. Discussion of results

6.1. Hydraulic conductivity

Based on the results described in this report, the horizontal hydraulic conductivity of the AR multi-pass TDA remains well above 10^{-2} m/s when compressed under a vertical stress of 375 kPa. The comparable vertical hydraulic conductivity is only slightly lower, with the anisotropy k_x/k_z being only about 2. Using reasonable and typical parameters for Alberta, a series of calculations based on Giroud & Houlihan (1995) can be made (Figure 1) suggesting that a drainage blanket with $k > 10^{-2}$ m/s should perform well, and should continue to do so even if clogging reduces hydraulic conductivity by 2 orders of magnitude.

On a site specific basis, designers should consider whether this value is sufficiently high for the specific requirements of a particular site.

6.2. Compression and void ratio

For load applied quickly, there is some indication (tests #4 & 5) that faster loading may cause slightly greater compression (and thus decrease in void ratio) than if the load is applied slowly. The lower values of $e \approx 0.2$ to 0.25 may thus be somewhat lower than might be expected with slower loading, but until further testing confirms this, these lower values should be considered by designers of facilities incorporating TDA in a LCS.

Creep compression, while certainly observed, was much less significant than immediate compression. The vertical scales in Figure 18a & 18b show that clearly. While less important than immediate compression, it would not be prudent to ignore the reduction in void ratio associated with creep.

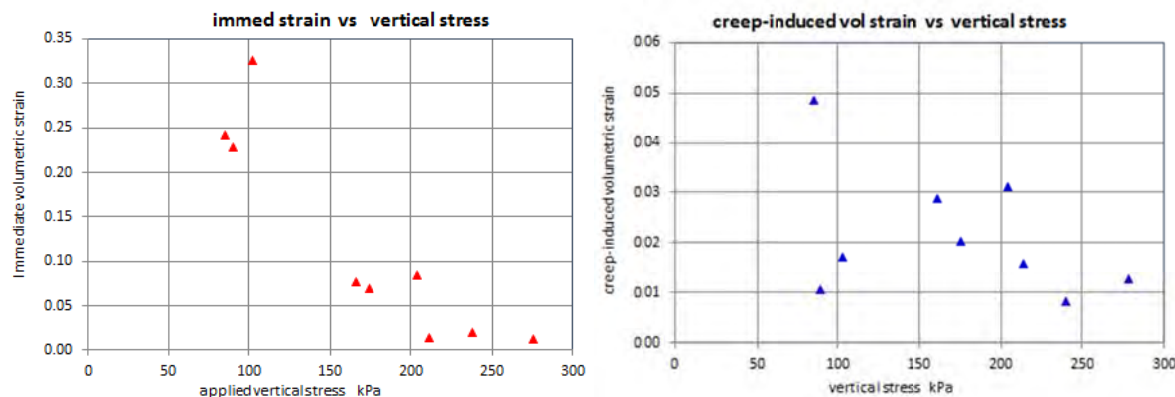


Figure 18: Comparison of volumetric strain induced by immediate compression with that caused by creep compression (AR test #1 shown)

The effect of a lower value of void ratio is that a greater thickness of material must be placed in order to ensure an equivalent void volume at some point in the future when the material has compressed and creeped to its final lower void ratio.

In order to compare TDA with gravel, an evaluation of void volume may be made and compared with that of reasonable gravel aggregate. The thickness of the gravel layer was selected based on considerations in Rowe & Fleming (1998). For a range of assumed values of post-compression & creep TDA void ratio based on this testing, the thickness of TDA may be calculated at the time of placement and after compression in order to provide a particular volume of voids per unit area. Table 3 presents typical calculated values of thickness to provide the same (unclogged) pore volume as a drainage blanket 0.3 m thick composed of the typical poorly graded pit run gravel (as per Figure 3) used at a large landfill in Alberta. For comparison, an "ideal" uniform-sized coarse gravel may be seen to provide a greater void volume.

Given the uncertainties involved, designers using any natural or TDA material other than the “ideal” uniform 50 mm gravel should consider the thickness of drainage blanket as well as potentially decreasing the drainage pipe spacing and/or steepening the slope to the drainage pipes.

Table 3 Required thickness of TDA at time of placement

	void ratio under load	loaded thickness (m)	void volume (m ³ / m ²)	void ratio when placed	thickness req'd when placed (m)
coarse uniform gravel	0.65	0.30	0.12	0.65	0.3
graded pit run gravel	0.50	0.30	0.10	0.50	0.30
TDA low final e	0.20	0.60	0.10	1.5	1.25
TDA moderate final e	0.25	0.50	0.10	1.5	1.00
TDA higher final e	0.38	0.38	0.10	1.5	0.69

6.3. Resilience to clogging

Testing for clogging potential was outside the scope of work, however based on a thorough understanding of the mechanisms, it is possible to draw tentative conclusions regarding the likely effect of clogging on materials with varying void ratio and void size. Assuming that the total void volume is sufficient to store the accumulated volume of mineral clog material over the design service life (Rowe & Fleming, 1998), the resilience to clogging may be considered to improve significantly with larger size pores as explained in detail in a number of papers, for example Rowe & Yu (2013). Essentially, large interconnected pores clog less easily and less severely.

While outside the scope of work, it was considered important to understand the size and shape of the pores of compressed TDA under load. A sample of TDA was loaded to 225 kPa and left for several weeks until creep was (mostly) complete. A two-part low-viscosity epoxy was dyed with a fluorescent dye and pumped into the test cell which was left under load while the epoxy cured. Subsequently, the large mass of epoxy-impregnated TDA (Figure 19c) was sliced into 25 mm sections at a waterjet cutting facility. Figure 20 shows a digital photograph of a typical section after being loaded into image analysis software.

Figures 19 and 20 clearly show the size and shape of the voids (fluorescent green) and the TDA particles (black). It is evident that the pores tend to be elongated, with the smaller dimension at least 10's of mm, which is generally similar in size to that of coarse uniform 40-60 mm gravel.



Figure 19: (a) Compressed TDA being impregnated with dyed epoxy; (b) left to set under sustained loading; (c) slice of epoxied TDA showing void space (0.58 m diameter)

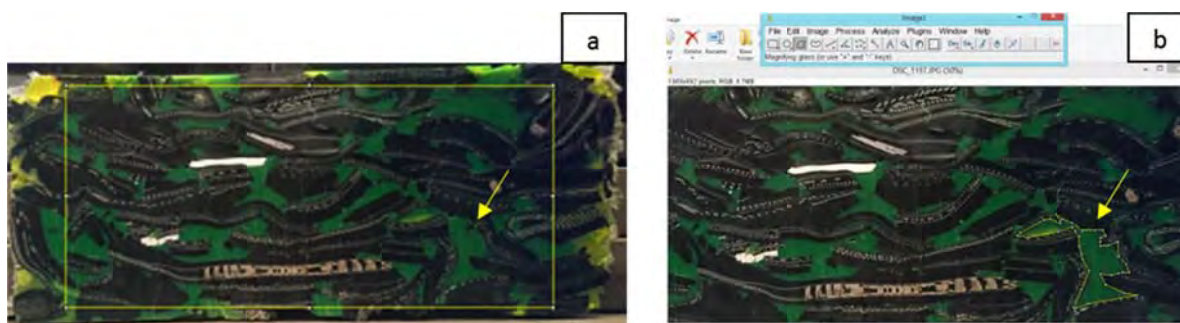


Figure 20: (a) Light coloured box used to isolate edge effects and highlight region to map on slice. Void to be mapped is indicated by light coloured arrow; (b) sample mapping of individual void geometry for analysis

Considering Figures 19 and 20 in the context of Table 3, it may be concluded that the pores generally appear to be sufficiently large so as to be generally comparable in size with those of the ideal uniform gravel, however not as uniform in size and shape. The continuity of the pores must be considered, however and there may potentially be large pores that dead-end and do not thus not contribute to permeability. In general, however, Figure 19 and 20 tend to support the other results presented in this report that suggest that the pore volume and pore size of TDA compressed under load are sufficient for use in a LCS drainage blanket provided other considerations are met (e.g. protection of underlying geomembrane, provision of adequate filter/sePARATOR over drainage blanket).

7. Key findings

The various challenges associated with testing this rather difficult material have resulted in test results that inevitably incorporate some artifacts of the testing methods or test conditions. Nonetheless, for the TDA tested, the following key conclusions may be made.

- *Under vertical load up to about 300 kPa, the void ratio of TDA decreases to as low as 0.2, (although more often about 0.3).*
- *There is a strong relationship between vertical stress and the final void ratio.*
- *Immediate compression dominates over creep, although creep should not be neglected. The effect of creep may be covered if reasonably conservative values are selected for the degree of compression and the compressed void ratio.*
- *Depending on the load, a significant uncompressed thickness of TDA should be used which should be at least 0.7 m and perhaps greater than 1.2 m.*
- *There appears to be a weak correlation between void ratio at the time of placement and final void ratio (for a particular load). There are almost certainly some artifacts of the test conditions that have led to differing responses, and this conclusion should be considered somewhat tentative. There remains, however a reasonably strong indication that a higher void ratio at the time of placement may be beneficial.*
- *In the range of temperatures expected within a landfill (20-60°C), there appears to be no effect of temperature on the compression or creep of TDA.*
- *At up to 375 kPa applied stress, the hydraulic conductivity of the material remained higher than 10² m/s. Single-pass TDA exhibits somewhat higher hydraulic conductivity compared with multi-pass TDA.*
- *Little anisotropy was found in the hydraulic conductivity of TDA in the horizontal and vertical directions.*
- *Given all of the above, TDA can be considered suitable for use in LCS provided care is taken. TDA cannot be considered to be "as good as" coarse uniform 50 mm gravel in terms of its performance in LCS. The material tested does have properties that are sufficient for the required functions, provided care is taken.*
- *In addition to the properties of the material used for drainage media (permeability, void ratio, pore size) long term LCS performance depends upon the interaction of a number of other considerations and design variables including:*
 - ✓ *the height of the landfill and expected rate of infiltration into the waste fill;*
 - ✓ *thickness of the drainage blanket;*
 - ✓ *slope to collection pipes;*
 - ✓ *length of drainage path (pipe spacing);*
 - ✓ *the presence of a high quality filter/sePARATOR over the drainage blanket (and underneath where compacted clay is used).*

Where a designer chooses to use any drainage media other than "ideal" uniform 50mm gravel (e.g. graded natural gravel, TDA, geosynthetic drainage products, recycled concrete aggregate) it would be prudent to consider adjustments to these other design variables to ensure long term performance.

References

- Adesokan, D., Fleming, I.R., Hammerlindl, A., McDougall, J.R., 2019 Strategies for testing large particle sized tire-derived aggregate (TDA) under applied load. *ASTM Geotechnical Testing Journal* Vol 42 Issue 5, Sept 2019. Available online: Oct 26, 2018. DOI: 10.1520/GTJ20170091
- Adesokan, D. & Fleming, I.R., 2019 Hydraulic properties of tyre derived aggregate (TDA) under sustained loading. *Environmental Geotechnics* (under review)
- Beaven, R.P., Powrie, W., Zardava, K., 2008. Hydraulic properties of MSW. In: Geotechnical Characterization, Field Measurement and Laboratory Testing of Municipal Solid Waste. *Proceedings of the 2008 International Symposium on Waste Mechanics. ASCE Geotechnical Special Publication No. 209*, pp. 1–43.
- Fleming, I.R. (2011) Indirect measurements of field-scale hydraulic conductivity of waste from two landfill sites. *Waste Management*, **31**(12), pp2455–2463.
- Fleming, I.R. and R.K. Rowe (2004) Laboratory studies of clogging of landfill drainage systems. *Canadian Geotechnical Journal* **41**(1), pp134–153.
- Fleming, I.R., Rowe, R.K. & Cullimore, D.R. (1999) Field observations of clogging in a landfill leachate collection system. *Canadian Geotechnical Journal*, **36**(4), pp685-707.
- Giroud, J.P. and Houlihan,.F. (1995) Design of leachate collection layers. *Proceedings of 5th International Landfill Symposium*, Cagliari, Sardinia, Italy, Vol 2, pp.613-640.
- Rowe, R.K. and Fleming, I.R. (1998). Estimating the time for clogging of leachate collection systems. *3rd International Congress on Environmental Geotechnics*, Lisbon, Sept, pp 23-38.
- Rowe, R.K. and McIsaac, R. 2005 Clogging of tire shreds and gravel permeated with landfill leachate. *ASCE Journal of Geotechnical & Geoenvironmental Engineering*, **131** (6) pp 682-693.
- Rowe, R.K and Yu, Y. (2013) A practical technique for estimating service life of MSW leachate collection systems. *Canadian Geotechnical Journal*, **50** (2): pp165-178.

Appendix A: Detailed methodology for determination of hydraulic conductivity from air permeability tests

Hydraulic properties of tyre derived aggregate (TDA) under sustained loading

Doyin Adesokan, Adam Hammerlindl, Ian Fleming

Department of Civil, Geological & Environmental Engineering, Saskatoon, Canada

This paper presents the systematic approach to analyse anisotropy in the hydraulic conductivity of TDA by formulating pressure distribution and hydraulic conductivity forms that were used to determine the vertical distribution of both vertical and horizontal hydraulic conductivity at any point across the thickness of the TDA. The analytical forms described were used to strip the laboratory data of all sidewall friction induced anisotropy and then systematically introduce anisotropy to determine the “true” anisotropy values of TDA that may be used for design.

Materials

TDA was sourced from tyre recycling facilities in Saskatchewan (Sask TDA) and Alberta (Alberta TDA) for the study. The particle sizes of the TDA ranged from 50 to over 305 mm. The description of the TDA tested, including the particle size distribution and specific gravity, in addition to the compression and creep results, the 1D compression testing equipment, testing challenges and strategies implemented to overcome the testing challenges are presented in Adesokan et al. (2019).

Equipment

A large sized 2D consolidometer and permeameter (2D cell) was custom-built to complete both horizontal and vertical air and water flow testing of the large particle sized TDA under sustained loading. The 2D cell (Figure 1) is 1 m high, 0.6 m wide, 1.2 m long and weighs approximately 8 kN. The loading plate of the cell weighs approximately 1 kN and contains housings for two load cells to be placed under the applied load sources - air bellows, for surface load measurements. The loading plate has forty eight 12.7 mm diameter holes for outflow of fluids during testing.



Figure 1: The 2D consolidometer and permeameter – in use for horizontal airflow testing

On the front panel of the cell, there are four columns of piezometer ports, with each column containing ten piezometer ports for measuring gauge pressure during airflow testing and hydraulic head during water flow testing (Figure 1). On each end of the cell, there are twenty 50 mm diameter openings (Figure 2) for

horizontal fluid flow measurements. At the bottom flange on the front panel of the cell, there are four similar sized openings for vertical flow through the system.

Plastic cookies were used to cover the holes at the ends of the cell before loading with TDA to provide a smooth flush along the inner wall of the cell during loading (Figure 2). The plastic cookies were removed for the horizontal flow tests to allow for introduction and flow of fluids through the TDA. They were replaced for the vertical flow tests.

Steel plate facings were bolted into place to cover the openings at the ends (Figure 2). Gasket fittings were placed around the openings before bolting the steel plate facings on. The steel plate facing has six openings with connectors to attach hoses for horizontal flow testing.



Figure 2: Side openings and fittings on the 2D cell for horizontal flow measurements

Methods

Air permeability and hydraulic conductivity measurements

Before loading up the 2D cell with TDA, two pancake type VW total stress cells manufactured by Durham GeoSlope indicator (DGSI) were placed at the bottom of the cell to measure applied loads reaching the bottom of the TDA in order to account for sidewall friction loss. Sidewall friction treatment consisting of two layers of high temperature grease and two layers of 2 mm plastic was applied prior to loading up the cell with TDA (Adesokan et al., 2009), and the openings on the ends of the cell were plugged with the plastic cookies.

Applied loads from of 56, 112, 224 and 375 kPa were applied to the TDA. The 56 kPa applied load was only applied to Sask TDA. Compression of the TDA was measured using a meter long ruler placed at locations that were pre-marked on the top of the loading plate.

Both air and water flow testing were performed in the 2D cell. Horizontal and vertical water flow testing was performed at the end of the final applied load of 375 kPa to determine corresponding hydraulic conductivity with the air permeability measurements at that load. The TDA was maintained dry for the airflow measurements and water was introduced at the final load step for direct hydraulic conductivity measurements.

An advantage of performing airflow testing is that the time required establishing pressure and flow equilibrium is less than with hydraulic conductivity testing (Long, 1988; Wells et al., 2007; Huang et al., 2015; Huang et al., 2016). Another advantage of airflow testing is that access to interstitial voids within the test particles is more rapid than with hydraulic conductivity testing because air is less viscous (Wells et al., 2006; Wells et al., 2007; Huang et al., 2015).

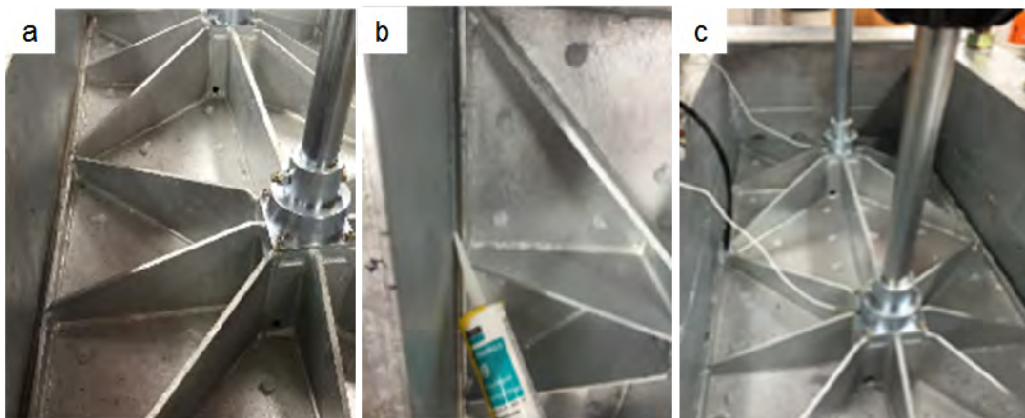
Airflow into the cell was supplied by three industrial ShopVacs (blowers) that could deliver a combined flow rate of up to 170 m³/s. Inflow and outflow was measured using calibrated pitot tube assemblies and differential and static pressure were measured using a high-resolution digital manometer. Flow was left to stabilize before taking readings, typically after approximately 5 to 10 minutes.

Three airflow rates for high, medium and low flows, corresponding to the number of blowers used, were completed per testing cycle for each applied surface load. Flow rates for horizontal airflows ranged from 152 SCFM with three blowers to 34 SCFM with one blower. Those for vertical airflows ranged from 179 SCFM with three blowers to 34 SCFM with one blower.

Gauge pressure within the TDA during airflow testing was measured using large sized custom-made water manometers that were connected to the piezometer ports on the front panel of the tank (Figure 1). Before taking readings, the ports were pierced through with a long 1/8 inch diameter steel needle to break through the layers of plastic treatment that had been applied for minimizing sidewall friction along the sidewalls of the cell. The arrangement of the piezometer ports across the front of the 2D test cell made it possible to collect data that were essential for evaluating both vertical and horizontal air permeability and subsequently the hydraulic conductivity of the TDA.

To perform vertical airflow testing, inflow was introduced at the bottom of the cell and outflow was at the top of the cell through the openings in the loading plate and the clearance between the loading late and the walls of the cell. To perform horizontal airflow testing, the steel cover plates on the ends of the tank were removed to take out the cookie plugs from the flow openings, then the fittings for the steel facing, and the hoses and tubing for the flows were all connected. One end of the hoses were attached to the connectors on the steel plate and the other ends connected to cylindrical pipes to which well heads were attached (Figure 1).

To leak proof the cell for horizontal airflow testing, the clearance between the loading plate and the walls of the cell were stuffed with flexible tubing (Figure 3a), then silicon was applied (Figure 3b) and smoothed into place over and around the tubing to ensure good sealing (Figure 3c). The silicon was allowed a minimum of 12 hours to set before commencing the testing.



Figures 3 a to c: Top openings through and around the loading plate for vertical flow measurements being sealed for horizontal flow measurements.

For vertical and horizontal hydraulic conductivity measurements, water was introduced into the TDA at the final loading step (375 kPa) to measure flow rates and hydraulic gradients. A minimum of five flow rates were measured for each of the vertical and horizontal hydraulic conductivity measurements.

The flow rates for vertical and horizontal flows ranged from 55 L/min to 8 L/min. The flow rate of water during the testing was determined both manually and electronically. The manual approach involved collecting the effluent from the cell into a large graduated clear cylinder and using a stopwatch to estimate the flow time.

A Rosemount 8732 integral mount magnetic flow reader was used for some of the flow readings to check the accuracy of the manually obtained flow measurements. Readings obtained with the flow reader were found to be consistent with readings from the manual measurements within a 5% error margin.

The measurement of hydraulic conductivity was to compare the intrinsic permeability of the TDA for measurements with both air and water. Theoretically, it is expected that the intrinsic permeability of a porous media should be the same for measurements with air and with water (Long et al., 1988; Huang et al., 2015; Huang et al., 2016), but this may not always be the case (Huang et al., 2015; Huang et al., 2016). A comparison of the air and water hydraulic conductivity results for both TDA tested is presented at the end of this report.

Determination of specific surface

In a complementary porosimetry evaluation, TDA – Sask TDA, was compressed and impregnated with a mixture of epoxy resin, hardener and fluorescent yellow dye to make the voids more identifiable for mapping, while under sustained loading. The porosimetry evaluation was done to look within the fabrics of TDA to assess particle orientation and void geometry under sustained high loading.

From the evaluation, the specific surface of TDA was determined and used in the analysis to determine the vertical distribution of both horizontal and vertical hydraulic conductivity to evaluate anisotropy in the hydraulic conductivity of TDA. A 60 kN hydraulic unit was used to apply approximately 224 kPa of surface load to the TDA. The epoxy mixture was pumped into the TDA and the epoxied TDA was left to set under applied load (Figures 4 a, b).

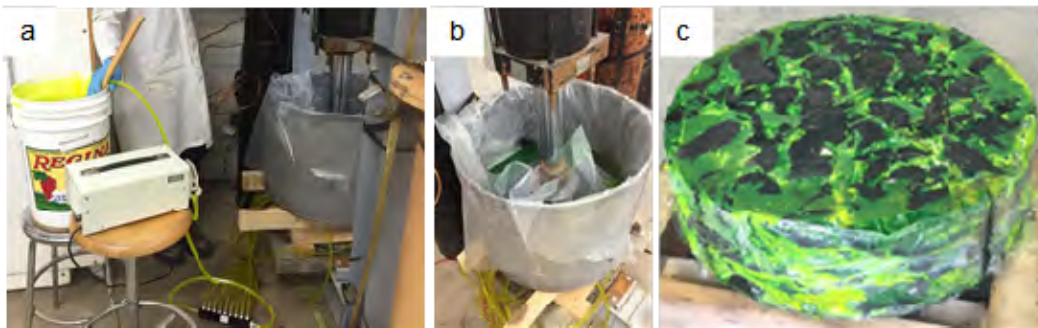


Figure 4: (a) Compressed TDA being pumped full with Epoxy resin, hardener and fluorescent yellow dye, (b) impregnated TDA left to set under sustained loading, (c) Epoxied TDA extruded

The solidified epoxied TDA (Figure 4c) was thin sectioned into 0.025 m thick slices using a water jet cutter with Garnet 80 mesh spec sand. ImageJ – an image processing program written in Java, for analyzing multidimensional images was used to map and analyze void and particle volume geometry across the sections (Figure 5). Individual surface area, total surface area, perimeter and volume of the voids and particles across the thin sections were estimated to determine the specific surface area and void ratio for each slice.



Figure 5: (a) Light coloured box used to isolate edge effects and highlight region to map on slice. Void to be mapped is indicated by light coloured arrow; (b) sample mapping of individual void geometry for analysis

Analysis

Assessing the applicability of Darcy's law

Darcy's law is generally accepted to be valid for laminar flows, that is Reynold's number (Re) ranges from 1 to 10. A transitional flow range (nonlinear laminar or unsteady laminar flow) is accepted to exist for $10 < Re < 1000$ and turbulent flows for $Re \geq 1000$.



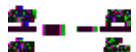
(1)

In equation 1, ρ is the density of the fluid (kg/m^3); v is the specific discharge (m/s); a is the characteristic pore dimension – in this case, diameter of 30% smaller than the longest dimensions for each TDA type; μ is the viscosity of the fluid (kg/ms).

The Re for all the air and water flow tests fell within the transitional nonlinear laminar flow range. As a result, there was a need to add correctional parameters to the basic Darcy's equation of flow to account for the non-linearity and unsteadiness in the flows.

Forchheimer suggested a second order term for nonlinear effects relating to inertia $\frac{\rho}{K_a} - \beta$ is Forchheimer's constant, Q is the flow rate through the porous medium and ρ is the density of the fluid.

Incorporating Forchheimer's inertia term into Darcy's flow equation gives a modified Darcy's equation (equations 2, 3).



(2)

Then,

$$\frac{Q}{A} = -\frac{K_a}{L} \Delta P - \beta Q^2 \quad (3)$$

(3)

In equations 2 and 3, K_a is the intrinsic permeability determined from the airflow measurements.

Effects of nonlinear laminar flows

Equation 3 was linearized to determine the K_a (m^2) and the β terms to evaluate the effects of the Forchheimer inertia term on the flows. The values of K_a (m^2) with inertia were then used to estimate corresponding k (m/s) with inertia using equation 4:

$$k (\text{m/s}) = (K_a \rho g) / \mu \quad (4)$$

In equation 4, K_a is the hydraulic conductivity of the TDA, ρ is the density of water (kg/m^3), g is acceleration due to gravity (m/s^2), μ is the dynamic viscosity of water (kg/ms).

Since the TDA was dry during the airflow testing, it was possible to estimate equivalent hydraulic conductivity (m/s) values directly from the measured airflow values using equation 4. The mean hydraulic conductivity values with the inertia term were up to 5 times greater than those values without the inertia term (Figures 6a and 6b).

The mean hydraulic conductivity values in Figures 6 a and b had been determined from measurements at discrete points taken from the manometer port readings. An issue with the discrete values is that TDA partially or completely blocked some of the measurement ports; hence, readings were low or nonexistent at some locations. It was necessary to determine the hydraulic conductivity at all the ports and at any given point across the thickness of the TDA for both the vertical and horizontal flows, in order to complete a detailed evaluation of the hydraulic conductivity, and anisotropy in the hydraulic conductivity of the TDA.

To determine the continuous vertical distribution of both the vertical and horizontal hydraulic conductivity, a functional hydraulic conductivity form was derived and used to analyze the laboratory data. In the data analysis, the correction factors for inertia determined here were applied to the mean hydraulic conductivity values that were determined using the functional hydraulic conductivity form.

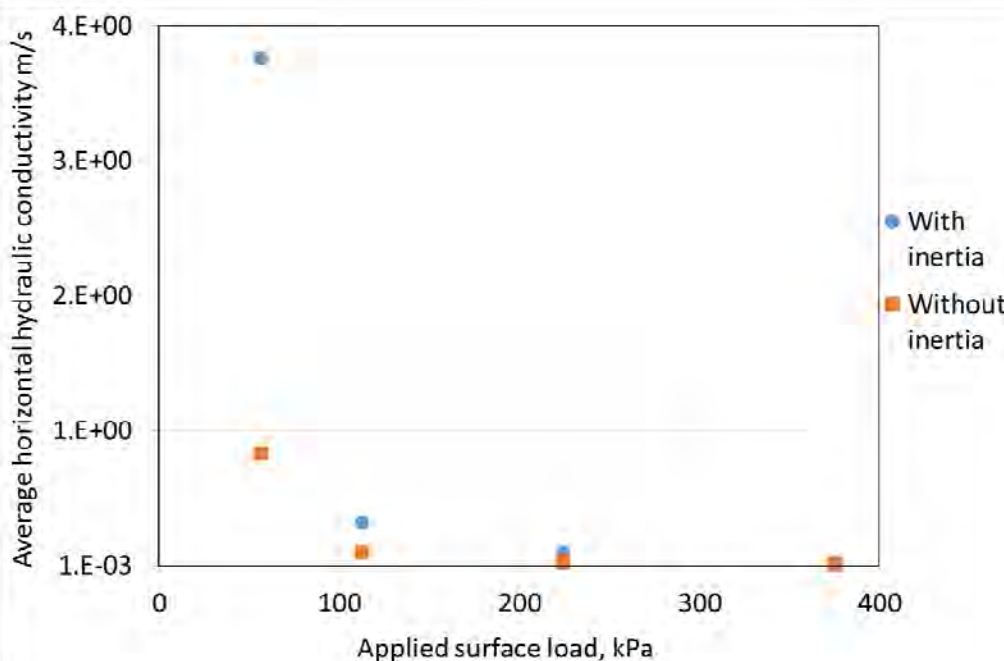


Figure 6a: horizontal hydraulic conductivity with and without the inertia considerations – Sask TDA shown.

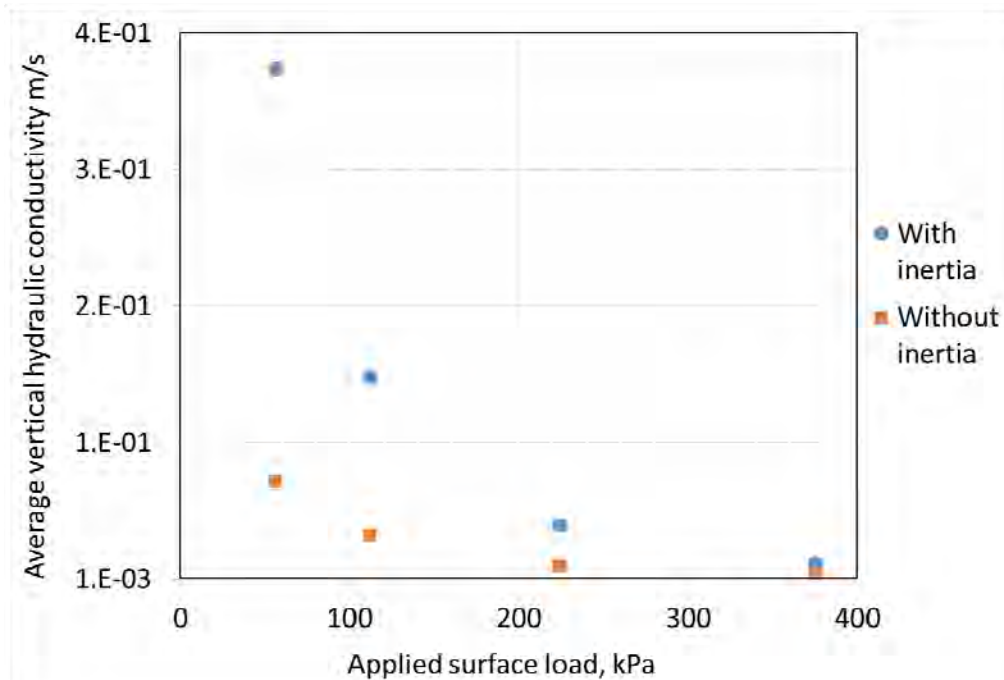


Figure 6b: vertical hydraulic conductivity with and without the inertia considerations – Sask TDA shown.

From Figures 6a and b, inertia increased the hydraulic conductivity by up to 5 times at the 56 kPa applied load, indicating that hydraulic conductivity may be grossly underestimated if inertia is not considered at certain applied loads. The inertia effects however appeared to decrease with applied loads after the 112

kPa applied load. Possibly because the void volume reduction from compression at higher applied loads results in a reduction in flows through the TDA, in turn causing a reduction in inertia effects.

Anisotropy in the hydraulic conductivity of TDA

Two forms of anisotropy exist in the laboratory data of TDA: (1) the “true” anisotropy and (2) the sidewall friction induced anisotropy. The “true” anisotropy is created by the orientation and alignment of the TDA particles. This is essentially the fabric anisotropy in the TDA.

Sidewall friction induced anisotropy is created by the apparent layering caused by sidewall friction between the TDA particles and the sidewall of testing units when surface load is applied to the TDA. Sidewall friction causes the top layers of TDA closer to the applied surface loads to compress more than the bottom layers farther away from the load.

This creates a layering that causes the vertical and horizontal hydraulic conductivity values to increase across the thickness of the TDA, such that the bottom layer of the TDA will have the highest hydraulic conductivity and the topmost layer will have the lowest. Then, for the horizontal hydraulic conductivity, the highest hydraulic conductivity value (at the bottom) will govern the total flow, and for the vertical hydraulic conductivity, the lowest hydraulic conductivity value (at the top) will govern the flow.

The mean horizontal hydraulic conductivity for such a layered system will therefore be higher than the mean vertical hydraulic conductivity, creating a form of anisotropy. This anisotropy may not necessarily represent the fabric anisotropy of the TDA, and it has to be separated from the laboratory data to accurately evaluate the hydraulic properties of the TDA for field conditions where sidewall friction will not be encountered.

To evaluate fabric anisotropy, the continuous distribution of both the vertical and horizontal hydraulic conductivity across the thickness of the TDA had to be known. For these, functional forms of pressure distribution and vertical hydraulic conductivity with position – $P(z)$ and $k_z(z)$ were derived and applied to the laboratory data. With the functions forms, data was estimated for those locations with nonexistent or inconsistently low data because of TDA partially or completely blocking measurement ports.

The functional forms of $P(z)$ and $k_z(z)$ were formulated in terms of the same known inputs and unknown parameters. Knowing $P(z)$ at any vertical position across the TDA, it was possible to determine the unknown parameters in the $k_z(z)$ function and estimate $k_z(z)$. The unknown parameters were determined using high efficiency data solvers in combination with error minimizing statistical analytical methods – root mean square error (RMSE) and normalized error methods to match the estimated $P(z)$ and $k_z(z)$ values from the functional forms to the laboratory data. The estimated distribution of $k_z(z)$ was used to determine relative $k_x(z)$ at any vertical position.

Functional forms of $P(z)$ and $k_z(z)$

The functional form of $\sigma_z(z)$ was first determined and then inserted into the $P(z)$ form. The $P(z)$ form is presented here afterwards. The functional form of $\sigma_z(z)$ was derived by incorporating a series of relations that had been determined from previous and complementary laboratory testing and analysis completed in this study into the Kozeny Carman relation for hydraulic conductivity.

The relations used in the derivation of $k_z(z)$ are as follows: (i) applied stress as a function of position ($\sigma_z = f(z)$); (2) void ratio as a function of applied stress ($e = f(\sigma_z)$); (3) void ratio as a function of position ($e = f(z)$); (4) vertical hydraulic conductivity as a function of void ratio (e) and specific surface ($S_s = f(e, S_s)$), and (5) specific surface (S_s) as a function of void ratio (e) ($S_s = f(e)$).

Applied stress as a function of position ($\sigma_z = f(z)$)

This relation was determined for testing in a cylindrical 1D consolidometer (Adesokan et al. 2019) as:

$$\sigma_z = \sigma_a + \frac{K_o}{D} z \tan(\delta) \quad (5)$$

Where:

σ_a = applied surface stress, kPa

K_o = is the lateral earth pressure coefficient,

δ = sidewall friction angle

D = diameter of the 1D consolidometer, m

z = depth, m

For the 2D test cell, a geometric relation was applied to account for the difference in the shape of the 2D cell relative the 1D consolidometer. The corresponding relation for the 2D cell is given as:

$$\sigma_{z_2} = \sigma_a + \frac{K_o}{D} z \tan(\delta) \quad (6)$$

Void ratio as a function of applied stress($e = f(\sigma_z)$), and void ratio as a function of position ($e = f(z)$)

It had been established from the 1D compression tests (Adesokan et al. 2019) that the relationship between e and σ_z in TDA can be described using the consolidation equation for soils as follows:

$$e_s = e_a - C_c \log \left(\frac{\sigma_z}{\sigma_{z_0}} \right) \quad (7)$$

Where,

e_s = void ratio

e_a = initial void ratio

C_c = slope of the curve

σ_z = applied vertical stress, kPa

σ_{z_0} = initial applied vertical stress, kPa

Representing equation 6 in terms of its constants and variables gives:

$$\sigma_{z_2} = A z^2 + B \quad (8)$$

Where:

$A = \sigma_a$

$$B = \frac{\sigma_{z_0} + K_o D \tan(\delta)}{D}$$

Substituting equation 8 into 7 gives:

$$e_s = e_a - C_c \log \left(\frac{\sigma_{z_2}}{\sigma_{z_0}} \right) \quad (9)$$

Let:

$$e_a = C \text{ and } C_c = D$$

Equation 9 then becomes:

$$e_s = C - D \log \left(\frac{A z^2 + B}{\sigma_{z_0}} \right)$$

Then,

$$e_s = C - D \log \left(\frac{A z^2 + B}{\sigma_{z_0}} \right) \quad (10)$$

Using the following relation:

$$\log(e(z)) = -\log(-z) = z$$

Equation 10 becomes:

$$e_z = C - (C \times z)$$

Then,

$$e_z = C + (Cz) \quad (11)$$

Vertical hydraulic conductivity as a function of void ratio and specific surface ($k_z(z) = f(e, S_s)$)

The Kozeny-Carman equation was represented for this as follows:

$$k_{z,0} = \left(\frac{C}{4} \right) \left(\frac{1}{e_z} \right) \left(\frac{g}{\mu} \right) \left(\frac{S_s}{1} + e_z \right) \quad (12)$$

Where:

$k_{z,0}$ = hydraulic conductivity

y = unit weight of permanent

μ = viscosity of permanent

C_{K-C} = Kozeny-Carman empirical constant

S_s = specific surface/susceptibility

e_z = void ratio

Let

$$\left(\frac{C}{4} \right) \left(\frac{1}{e_z} \right) = a$$

Then,

$$k_{z,0} = \frac{ay^2}{\mu^2} \quad (13)$$

Specific surface as a function of void ratio ($S_s = f(e)$)

Having measured the specific surface as earlier described, a correction factor was applied to the measured values to account for variations in the image dimensions. Plot of specific surface and void ratio for all the epoxied slices was generated and a best-fit relation was applied as a power function:

$$S_s = 466.68 e_z^{0.7} \quad (14)$$

Represented as:

$$S_s = 466.68 e_z^{-1}$$

Then,

$$S_s = Fe_z, \text{ where } F = 466.68$$

Thus,

$$S_s^2 = (Fe_z)^2 \quad (15)$$

Substituting equation 15 into 13 gives k_z in terms of e_z

$$k_{z,0} = \frac{ay^2}{(Fe_z)^2 \mu^2} \quad (16)$$

Then,

$$k_z(z) = \frac{m_{z,z}}{P(z)} \quad (17)$$

Substituting equation 11 into 17 gives a portmanteau vertical hydraulic conductivity form:

$$k_z(z) = \frac{\alpha P(z)}{P(z) + \alpha z} \quad (18)$$

With equation 18, a portmanteau functional hydraulic conductivity form, it was possible to determine $k_z(z)$ at any point across the thickness of the TDA (Figure 7), not just at the points where readings had been taken from the measurement ports. This was essential for determining corresponding $k_z(z)$ values to evaluate anisotropy. The terms D, F, and the Ck-c term embedded in the α term were determined by using root mean square error and normalized error methods in combination with data solvers to match the estimated mean values of $k_z(z)$ determined using equation 18 to the mean values determined from the laboratory data.

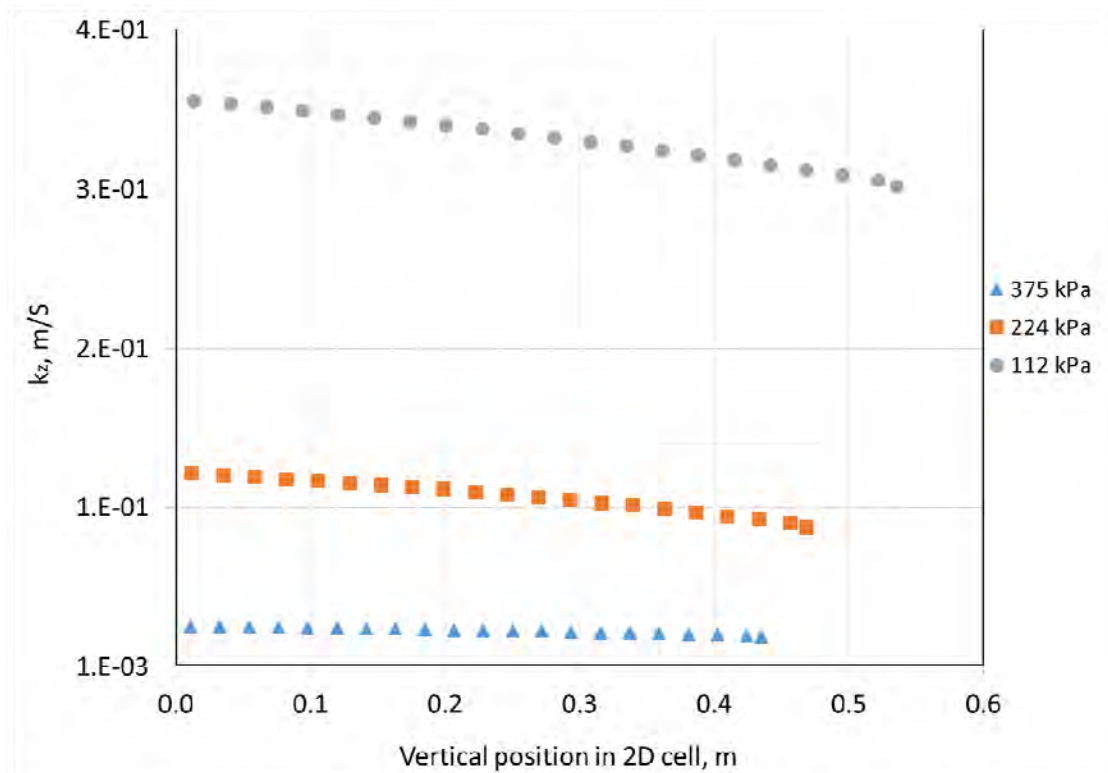


Figure 7: Vertical distribution of k_z i.e. $k_z(z)$ across the TDA thickness – Alberta TDA shown

Functional form of $P(z)$

Using the flow equation for air permeability:

$$\frac{dP}{dz} = -\left(\frac{A}{\mu_a} \frac{dy}{dz}\right) \quad (19)$$

Where,

dP = differential pressure

$$A = \left(\frac{\rho_w g}{\mu_a}\right)$$

μ_a = dynamic viscosity of air (kg/ms)

ρ_w = density of water (kg/m³)

g = acceleration due to gravity (m/s²)

μ_w = dynamic viscosity of water (kg/ms)

dz = change in length in flow direction (m)

Then, substituting for $\frac{dP}{dz}$ in Equation 19 gives:

$$dz = -\frac{\mu_w}{\rho g} \left(\frac{1}{C} + 1 \right) dz \quad (20)$$

Integrating dP gives:

$$P_{out} = -\frac{\mu_w}{\rho g} \left[\frac{1}{C} \ln(C + Dz) + z \right] + \text{constant} \quad (21)$$

When $Dz = 0$

$$\text{constant} = \frac{\mu_w}{\rho g} \left[\frac{1}{C} \ln(C) \right] \quad (22)$$

Hence,

$$P_{out} = -\frac{\mu_w}{\rho g} \left[\frac{1}{C} \ln(C + Dz) + z \right] + \frac{\mu_w}{\rho g} \left[\frac{1}{C} \ln(C) \right] \quad (23)$$

Then,

$$P_{out} = \frac{\mu_w}{\rho g} \left[\frac{1}{C} \right] - \frac{\mu_w}{\rho g} \left[\frac{1}{C} \ln(C + Dz) + z \right] \quad (24)$$

The $P(z)$ function (equation 24) was fit to the laboratory $P(z)$ data (Figure 8), using RMSE to minimize errors and data solvers to vary and determine the unknown parameters in the equation. The parameters were determined simultaneously for the $P(z)$ form since the unknown parameters are the same.

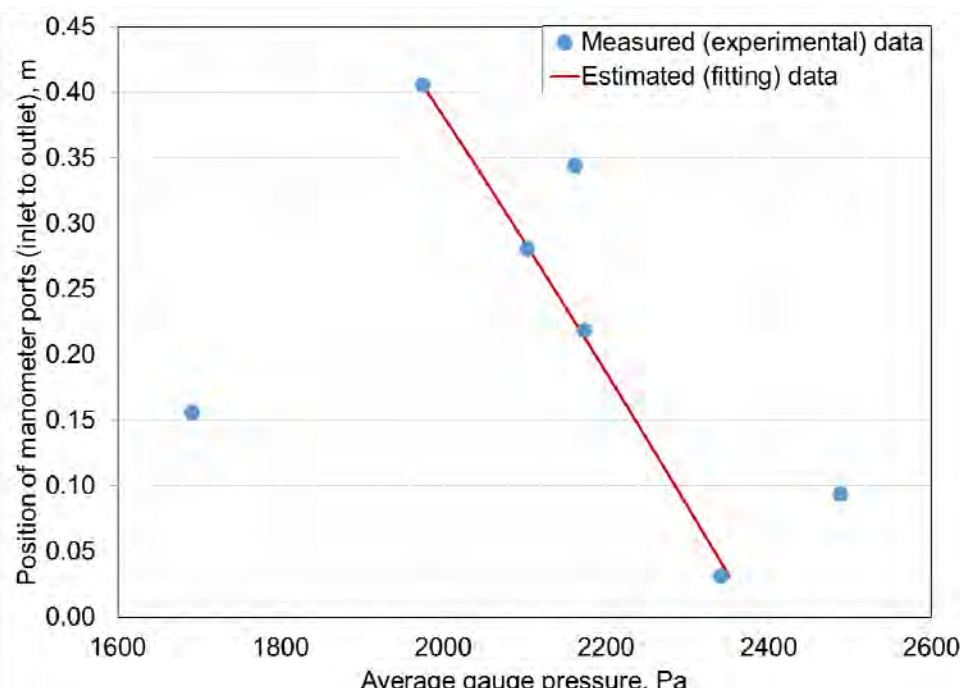


Figure 8: Sample measured and estimated $P(z)$ data – high flow 375 kPa Alberta TDA presented

Determining the distribution of $\frac{Dz}{C}$

The distribution of $\frac{Dz}{C}$ (Figure 9) was determined by initially assuming an isotropic condition where the λ_{xx} and λ_{yy} values were the same and then introducing anisotropy by varying the λ_{yy} values until the

mean of the estimated values matched the measured discharge velocity q (m/s) and the mean k_x from the laboratory measurements.

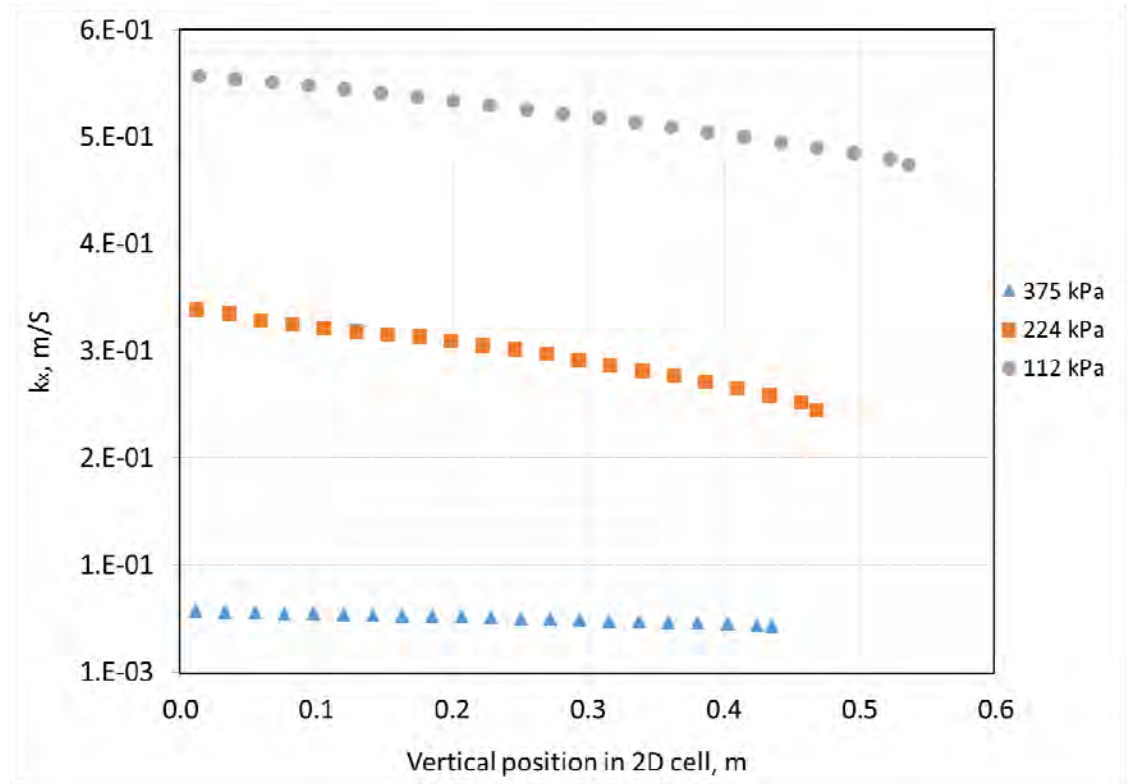


Figure 9: Vertical distribution of k_x i.e. k_x across the TDA thickness – Alberta TDA shown

Once the mean values of the estimated and measured k_x values were matched, implying that any existing fabric anisotropy had been systematically uncovered, the estimated k_x and k_z values were corrected for inertia effects and used to assess fabric anisotropy (Table 1).

Table 1: Hydraulic conductivity values estimated using the $k_z(z)$ function and corrected for inertia; and corresponding anisotropy in the hydraulic conductivity values

Applied surface load, kPa	Sask TDA			Alberta TDA		
	Corrected estimated mean vertical hydraulic conductivity, m/s	Corrected estimated mean horizontal hydraulic conductivity, m/s	Anisotropy in the hydraulic conductivity	Corrected estimated mean vertical hydraulic conductivity, m/s	Corrected estimated mean horizontal hydraulic conductivity, m/s	Anisotropy in the hydraulic conductivity
56	3.61E-01	4.16E+00	12		Not completed	
112	3.03E-01	3.24E-01	1	3.32E-01	5.21E-01	2
224	7.70E-02	9.96E-02	1	1.08E-01	2.98E-01	3
375	3.35E-02	2.48E-02	1	2.35E-02	5.09E-02	2

From Table 1, anisotropy in hydraulic conductivity appeared to be constant after a certain applied load. For the Sask TDA, there seemed to be no anisotropy after the 56 kPa; and for the Alberta TDA, the 56 kPa applied load was not applied, but the anisotropy was largely 2 for the same applied loads as the Sask TDA. Fabric anisotropy under applied loads thus seems to be material dependent as it was higher for the

Alberta TDA than the Sask TDA at similar applied loads. For both TDA, the mean vertical and horizontal values presented in Table 4 exceeded the commonly prescribed hydraulic conductivity value for landfill drainage – 10^{-4} m/s by more than one order of magnitude.

For a comparison of the hydraulic conductivity obtained from airflow measurements and that from water flow measurements at 375 kPa – the mean hydraulic conductivity from the water flow measurements for both TDA were 2 to 3 times higher than the average airflow values. This disparity is however within reason, given the large sized voids within the TDA and the large flows through.

REFERENCES

- Adesokan, D., Fleming, I., Hammerlindl, A., and McDougall, J. (2019). Strategies for One Dimensional (1D) Compression Testing of Large-Particle-Sized Tire Derived Aggregate. *Geotechnical Testing Journal*, Advance online publication. Retrieved from <https://doi.org/10.1520/GTJ20170091>
- Ahmed, I., and Lovell, C. W. 1993. Tire chips as permeable aggregate in landfills. Proceedings of the 1st Annual Great Lakes Geotechnical/Geoenvironmental Conference, Toledo, Toledo Section of the American Society of Civil Engineers: 83-90.
- Beaven, R. P. (1994). The technical aspects of controlled waste management: Assessment of the physical and hydraulic properties of tyres for leachate collection and drainage systems in landfills. London: Wastes Technical Division, Department of the Environment.
- Beaven, R. P., Hudson, A. P., Knox, K., Powrie, W., and Robinson, J. P., "Clogging of landfill tyre and aggregate drainage layers by methanogenic leachate and implications for practice," *Waste Management*, Vol. 33, 2013, pp. 431- 444
- Beaven, R. P., Powrie, A. P., Hudson, A. P., and Parkes, D. J., "Compressibility of tyres for use in landfill drainage systems," *Waste and Resource Management*, Vol. 159, No. WR4, 2007, pp. 173-180
- Cooke, A. J., and Rowe, R. K. (2008a). 2D modelling of clogging in landfill leachate collection systems. *Canadian Geotechnical Journal*, 45(10), 1393-1409.
- Cooke, A. J., and Rowe, R. K. (2008b). Modelling landfill leachate-induced clogging of field-scale test cells (mesocosms). *Canadian Geotechnical Journal*, 45(11), 1497-1513.
- Cooke, A. J., Rowe, R. K., Rittman, B. E., VanGulck, J., and Millward, S. (2001). Biofilm Growth and Mineral Precipitation in Synthetic Leachate Columns. *Journal of Geotechnical and Geoenvironmental Engineering*, 127, 849-856.
- Cooke, A. J., Rowe, R. K., Rittmann, B. E., and Fleming, I. R. (1999). Modelling biochemically driven mineral precipitation in anaerobic biofilms. *Wat. Sci. Tech.*, 39(7), 57-64.
- Cooke, A. J., Rowe, R. K., VanGulck, J., and Rittman, B. E. (2005). Application of the BioClog model for landfill leachate clogging of gravel-packed columns. *Canadian Geotechnical Journal*, 42(6), 1600-1614.
- Donovan, R., Dempsey, J., and Owen, S., "Scrap tire utilization in landfill applications, "presented at the 17th Biennial Waste Processing Conference, 1996, pp. 353-383
- Duffy, D. P., "Using tire chips as leachate drainage layer," *Waste Age*, Vol. 26, No. 9, 1995, pp. 113-122
- Evans, P., "Use of tire shred in landfill construction," presented at the Geotechnical Society of Edmonton Third Annual Symposium Environmentally Friendly Technologies in Geotechnical Engineering, Edmonton, Alberta, 1997, pp. 1-8
- Fleming, I. R., and Rowe, R. K., "Laboratory studies of clogging of landfill leachate collection and drainage systems," *Canadian Geotechnical Journal*, Vol. 41, 2004, pp. 134-158

- Fleming, I. R., Rowe, R. K., and Cullimore, D. R., "Field observations of clogging in landfill leachate collection systems," Canadian Geotechnical Journal, Vol. 36, 1999, pp. 605- 787
- Hall, T. J., "Reuse of shredded tire material for leachate collection systems," presented at the 14th Annual Madison Waste Conference, University of Madison, Wisconsin, 1991, pp. 367-376
- Huang, M., Rodger, H., and Barbour, L. 2015. An evaluation of air permeability measurements to characterize the saturated hydraulic conductivity of soil reclamation covers. Canadian Journal of Soil Science, 95: 15-26.
- Huang, M., Zettl, J. D., Barbour, L. S., and Pratt, D. 2016. Characterizing the spatial variability of the hydraulic conductivity of reclamation soils using air permeability. *Geoderma*, 262: 285-293.
- Hudson, A. P., Beaven, R. P., Powrie, W., and Parkes, D., "Hydraulic conductivity of tyres in landfill drainage systems," Waste and Resource Management, Vol. 160, No. WR2, 2007, pp. 63-70
- Long, R. P., Demars, K. R., Mankbadi, R. R., and Covo, A. 1988. Final Report: The Relationship Between Permeability Coefficients for Soil Obtained Using Liquid and Gas. University of Connecticut, Department of Civil Engineering.
- McIsaac, R., and Rowe, K., "Change in leachate chemistry and porosity as leachate permeates through tire shreds and gravel," Canadian Geotechnical Journal, Vol. 42, 2005, pp. 1173-1188
- McIsaac, R. S., Rowe, R. K., Fleming, I. R., & Armstrong, M. D. (2000). Leachate collection system design and clog development. 6th Environmental Engineering Specialty Conference of the CSCE & 2nd Spring Conference of the Geoenvironmental Division of the Canadian Geotechnical Society, (pp. 66-73). London, Ontario. Retrieved December 6, 2013, from http://www.civil.queensu.ca/Research/Environmental/R-Kerry-Rowe/publications/documents/ConfLondon83_90%20Leachate%20Collection.p
- Mwai, M., Wichuk, K., and McCartney, D., "Implications of using Tire-derived Aggregate for landfill leachate collection and drainage systems". In the Proceedings of the Solid Waste Association of North America, 5th Canadian Symposium . Banff, Alberta, 2010, pp. 18- 21
- Narejo, D. B., and Shettima, M. (1995). Use of recycled automobile tires to design landfill components. *Geosynthetics International*, 2(3), pp. 619-624.
- Qian, X., Koerner, R. M., and Gray, D. H. (2002). *Geotechnical Aspects of Landfill Design and Construction*. Upper Saddle River, New Jersey: Prentice-Hall, Inc.
- Reddy, K. R., and Marella, A., "Properties of different size scrap tire shreds: Implications on using as drainage material in landfill cover systems, "presented at the Seventeenth International Conference on Solid Waste Technology and Management, Philadelphia, USA, 2001, pp.1-16
- Reddy, K. R., and Saichek, R. E., "Characterization and performance assessment of shredded scrap tires as leachate drainage material in landfills," presented at the Fourteenth International Conference on Solid Waste Technology and Management, Philadelphia, USA, 1998
- Rowe, K. R., and Yu, Y. (2013). A Practical technique for estimating service life of MSW leachate collection systems. Canadian Geotechnical Journal, 50, 165-178. doi:dx.doi.org/10.1139/cgj-2012-0257
- Rowe, R. K., Armstrong, M. D., and Cullimore, D. R. (2000a). Mass Loading and the Rate of Clogging due to Municipal Solid Waste Leachate. Canadian Geotechnical Journal,, 37(2), 355-370.
- Rowe, R. K., Armstrong, M. D., and Cullimore, D. R. (2000b). Particle Size and Clogging of Granular Media Permeated with Leachate. ASCE Journal of Geotechnical and Geoenvironmental Engineering, 126(9), 775-786.
- Rowe, K. R., and Babcock, D., "Modelling the clogging of coarse gravel and tire shreds in column tests," Canadian Geotechnical Journal, Vol. 44, 2007, pp. 1273-1285

- Rowe, K. R., and McIsaac, R., "Clogging of tire shreds and gravel permeated with landfill leachate," *Journal of Geotechnical and Geoenvironmental Engineering*, Vol. 131, 2005, pp.682-693
- Rowe, R. K., "Long-term performance of contaminant barrier systems," *Geotechnique*, Vol. 55, No. 9, 2005, pp. 631-678
- Rowe, R. K., and Fleming, I. R., "Estimating the time for clogging of leachate collection systems," presented at the 3rd International Congress: Environmental Geotechniques, Lisbon, Vol. 1, 1998, pp. 23-28.
- Rowe, R. K., Quigley, R. M., Brachman, R. W., and Booker, J. R., 2004, *Barrier Systems for Waste Disposal Facilities*, Taylor and Francis Books Ltd (E and FN Spon), London, pp. 587
- Warith, M. A., Evgin, E., and Benson, P., "Suitability of shredded tires for use in landfill leachate collection systems," *Waste Management*, Vol. 24, 2004, pp. 967-979
- Wells, T., Fityus, S., and Smith, D. W. 2007. Use of In Situ Air Flow Measurements to Study Permeability in Cracked Clay Soils. *Journal of Geotechnical and Geoenvironmental Engineering*, 133(12): 1577-1586.
- Wells, T., Fityus, S., Smith, D. W., and Moe, H. 2006. The indirect estimation of saturated hydraulic conductivity of soils, using measurements of gas permeability. *Australian Journal of Soil Research*, 44: 719-725.
- Yu, Y., and Rowe, K. R., "Modelling leachate-induced clogging of porous media," *Canadian Geotechnical Journal*, Vol. 49, 2012, pp. 877-890
- Zekkos, D., Bray, J. D., Kavazanjian, E. J., Matasovic, N., Rathje, E. M., Reimer, M. F., and Stokoe II, K. H., "Unit Weight of Municipal Solid Waste," *Journal of Geotechnical and Geoenvironmental Engineering*, Vol. 132, 2006, pp. 1250-1261
- Zimmerman, P. S., 1997, "Compressibility, Hydraulic Conductivity and Soil Infiltration of Tire Shreds and Field Testing of a Shredded Tire Horizontal Drain," MS Thesis, Iowa State University, Ames, Iowa

Attachments: Volume 1



Geotechnical Testing Journal

Doyin Adesokan,¹ Ian Fleming,² Adam Hammerlindl,² and
John McDougall³

DOI: 10.1520/GTJ20170091

Strategies for One Dimensional
(1D) Compression Testing of
Large-Particle-Sized Tire Derived
Aggregate

Doyin Adesokan,¹ Ian Fleming,² Adam Hammerlindl,² and John McDougall³

Strategies for One Dimensional (1D) Compression Testing of Large-Particle-Sized Tire Derived Aggregate

Reference

Adesokan, D., Fleming, I., Hammerlindl, A., and McDougall, J., "Strategies for One Dimensional (1D) Compression Testing of Large-Particle-Sized Tire Derived Aggregate," *Geotechnical Testing Journal* <https://doi.org/10.1520/GTJ20170091>. ISSN 0149-6115

ABSTRACT

Laboratory testing of a mass of large-particle-sized tire derived aggregate (TDA) to assess performance-related properties such as void ratio, compressive creep, and hydraulic conductivity under large loads poses a number of experimental challenges. Large-particle-sized TDA is shredded scrap tires with particle sizes from 50 mm to over 305 mm. The large particle size of the TDA mass results in experimental challenges, such as the need for a large test chamber and the need for a load application system with a capacity to apply and sustain large loads, while accommodating large vertical displacements from the compression of the TDA mass. As an example, to put these requirements into perspective, a mass of TDA with a nominal particle size of 150 mm requires a test cell diameter of at least 600 mm and preferably a diameter of 700 mm. If a load of 400 kPa were to be applied onto the TDA mass to simulate approximately 35 m to 40 m of overlying material (waste and routinely applied cover materials) in an application such as a landfill, the test apparatus must be capable of delivering over 150 kN of applied load. Furthermore, for a reasonable initial mass of TDA that is 1.2 m thick, the test cell will have to be designed to maintain that load over 0.6 m of vertical displacement because of the compression of the TDA mass. This article presents a number of practical strategies that were implemented to overcome the experimental challenges with testing large particle size, highly compressible TDA mass to establish the performance related properties for use in service. In some instances, components of the test equipment had to be re-engineered to accommodate

Manuscript received March 21, 2017; accepted for publication June 28, 2018; published online October 26, 2018.

¹ Department of Civil, Geological, and Environmental Engineering, University of Saskatchewan, 57 Campus Dr., Saskatoon, Saskatchewan S7N 5A2, Canada (Corresponding author), e-mail: ada477@mail.usask.ca, <https://orcid.org/0000-0002-2166-5111>

² Department of Civil, Geological, and Environmental Engineering, University of Saskatchewan, 57 Campus Dr., Saskatoon, Saskatchewan S7N 5A2, Canada

³ School of Engineering and the Built Environment, Edinburgh Napier University, 10 Colinton Rd., Edinburgh EH10 5DT, United Kingdom

exigencies that had not been anticipated, such as differential compression of the TDA mass. The focus of this article is on equipment design and experimental methodologies. A few sample results from the study are presented to illustrate the successful implementation of the design methodologies. Although TDA has been studied in this work, the strategies described herein can be applied to a wide range of highly compressible materials under large loads.

Keywords

scrap tire, tire derived aggregate, tire shreds, landfill, consolidometer, creep, drainage blanket, large strains, solid waste, and highly compressible materials

Introduction

Over the past two decades, in large part for economic considerations and as a means for reusing the large stream of scrap tires generated at the end of the useful life of automobile tires, TDA derived from scrap tires shredding into sizes from 25 mm to over 305 mm has been suggested (Hall 1991; Duffy 1995; Reddy and Saichek 1998; Warith, Evgin, and Benson 2004), researched (McIsaac and Rowe 2005; Rowe and McIsaac 2005; Hudson et al. 2007; Beaven et al. 2006; Beaven et al. 2013), and used (Donovan, Dempsey, and Owen 1996; Evans 1997; Zimmerman 1997; Reddy and Saichek 1998; Warith, Evgin, and Benson 2004) as a substitute for gravel in the blanket drainage layers of leachate collection and disposal systems. In the western Canadian provinces of Saskatchewan and Alberta, TDA is used in over thirty landfills that receive between a quarter and a third of the combined municipal solid waste stream of the two provinces.

TDA is a polymeric composite, as such a mass of TDA subjected to vertical loading is expected to exhibit viscoelastic behavior (Reddy and Marella 2001; Warith, Evgin, and Benson 2004) typically consisting of an immediate elastic spring-like response followed by a time-dependent viscous dashpot-like response (creep). It is important to understand both responses and their individual and combined effects on long-term performance and service life when designing load-bearing applications such as drainage layers in waste disposal sites with TDA. The performance and service life of any drainage layer is expected to exceed the contaminating lifespan of the waste disposal facility, which has been estimated to be several centuries (Rowe and Fleming 1998; Fleming, Rowe, and Cullimore 1999; Fleming and Rowe 2004; Rowe 2005; Yu and Rowe 2012). This expected service life and performance depends on a number of factors including: (1) the ability of the drainage layer to maintain a sufficient vertical and more importantly horizontal permeability to rapidly transmit infiltrating leachate from the overlying waste into collection pipes and sumps to minimize excessive head on basal barrier materials (Fleming, Rowe, and Cullimore 1999; Qian, Koerner, and Gray 2001; Rowe et al. 2004; Yu and Rowe 2012); (2) the ability of the drainage layer to retain a sufficient pore volume following physical and inevitable biogeochemical clogging to ensure continuous transmission of leachate into collection and removal units (Fleming, Rowe, and Cullimore 1999; Qian, Koerner, and Gray 2001; Rowe and McIsaac 2005; Rowe and Babcock 2007; Beaven et al. 2013); (3) the ability of the drainage layer to transfer vertical load to underlying basal barrier materials without inducing or making worse localized strains and other forms of physical damage (Dickinson and Brachman 2008).

Various studies such as Hall (1991), Reddy and Saichek (1998), Warith, Evgin, and Benson (2004), Rowe and McIsaac (2005), and McIsaac and Rowe (2005) have shown that different TDA (differing in terms of shape, particle size, mode of shredding, exposed and loose wire content) perform differently in compression under similar applied loads and loading conditions. Strenk et al. (2007) highlighted the variability and scale dependence of TDA particle size and performance-related properties. Similarly, studies by Beaven et al. (2006), Mwai, Wichuk, and McCartney (2010), and Beaven et al. (2013) showed that particle size matters in the behavior of a TDA mass under applied loads.

The one dimensional (1D) compression results presented in the Beaven and Mwai studies showed that TDA masses with large-sized particles (particles greater than 200 mm) compressed more than those with smaller-sized particles (200 mm and less) under similar applied loads. A higher compression implies a higher void volume reduction, and void volume reduction is a key parameter for assessing the performance of TDA in service, especially for drainage applications under service loads. For these reasons, testing smaller particle-sized TDA in smaller test equipment to eliminate the need for large-sized testing equipment may result in errors in estimating the performance and service life of large-particle-sized TDA.

In assessing the service life of a TDA mass for drainage applications in waste disposal sites under high compressive loads imposed by overlying materials, it is imperative to perform the required tests on a TDA mass with particle sizes and attributes that are suitable for such applications—ideally, large-particle-sized TDA with the longest particle dimension from 50 mm to over 305 mm. Testing such large-sized particles will require large test cells and large systems for applying and sustaining high compressive loads on the test cells.

Laboratory testing of a mass of TDA with large-sized particles requires the use of largescale testing equipment and this may present a number of challenges. Zimmerman (1997) appeared to have alluded to this in the study in which 200-mm to 400-mm particle-sized TDA mass was tested. The author stated that it was “impractical” to have a test chamber several times larger than the largest particle size. “Practicality,” as stated by Zimmerman, could have been related to potential challenges associated with having a large-sized test chamber, and in the study, a smaller test chamber equal in width to the longest TDA particle dimension was used.

Testing a mass of TDA in a chamber with the same dimensions as the longest particle size may increase sidewall friction along the walls of the test chamber. Sidewall friction is an artefact of 1D constrained loading tests (Olson 1986; Sarby and Vickers 1986) and, given the flexibility of TDA particles, there is an increased tendency for the particles to stick to the walls of test cells, potentially increasing sidewall friction. Sidewall friction reduces the amount of applied load reaching the bottom of a test specimen, causing larger strains in materials at the top of the test cell than at the bottom (Sarsby and Vickers 1986).

Sidewall friction has been noted to increase as the ratio of chamber size to longest TDA particle dimension decreases (ASTM D6270-08, *Standard Practice for Use of Scrap Tires in Civil Engineering Applications*). The effects of sidewall friction could result in the erroneous estimation of the properties of the TDA mass, potentially causing an underestimation of compression and an overestimation of porosity in the TDA mass if unaccounted for in the analyses of the laboratory test results.

It was deemed important from the outset to be able to measure and account for sidewall friction. Because sidewall friction was anticipated to be significant, the stress state could be expected to vary across the thickness of the TDA mass in the consolidometer. Accordingly, it was deemed necessary to measure the total vertical stress reaching the base of the TDA mass and to estimate compressive response at intermediate positions within the test specimen.

Because the test cell was fabricated from transparent acrylic, colored lacrosse balls were placed as visual markers at intermediate levels to enable the TDA mass to be treated as if it were a stack of thinner slices, each subjected to differing vertical and horizontal stress conditions. In later tests, the colored balls were replaced by fluorescent paint spots applied to individual particles of TDA placed near the cylinder sidewall. In order to determine the actual vertical stress reaching the base of the TDA mass, a total stress (TS) cell was placed on the acrylic base of the apparatus prior to filling with TDA.

Each slice created by a top and bottom visual marker thus may be considered to represent a compression test at an applied load. The progression of compression in each slice was measured from the displacement of the visual markers, and each slice was analyzed as an individual compression test at the applied load reaching the slice. The vertical stress reaching each slice was estimated from considerations of sidewall friction along with the observed variation in vertical strain and the measured TS at the base of the TDA mass.

Evaluating the performance determining properties of large-particle-sized TDA under large applied and sustained vertical loads is the basis of a series of completed and ongoing studies at the University of Saskatchewan (U of S), Canada. Two pieces of custom, largescale laboratory testing equipment—a 1D consolidometer and a two-dimensional (2D) consolidometer/permeameter unit—were designed and fabricated at the U of S as part of these studies.

The equipment and procedures for the 1D consolidometer for evaluating compression, creep and ensuing void ratio reduction in the TDA mass are described in this article. The 2D consolidometer/permeameter unit was used to evaluate the effects of void volume reduction on horizontal and vertical permeability under increasing applied vertical load; this equipment and the experimental methodologies employed will be discussed in a complementary article.

The equipment design and experimental methodologies for the 1D consolidometer are presented in this article as a series of technical challenges that were overcome in order to successfully operate largescale geotechnical laboratory equipment to evaluate the field performance of a mass of TDA under large sustained loads.

The challenges described include the following:

- the geometry of the test chamber and the associated structural considerations, given the large particle size of the TDA mass;
- a system for applying and sustaining high loads on the TDA mass under large compressive strains;
- managing differential compression in the heterogeneous TDA mass;
- measuring and reducing sidewall friction; and
- measuring phase (solid and void) volume change under increasing applied loads.

In view of the previously mentioned challenges, the three fold objectives of this article are to (1) describe the design aspects of the 1D consolidometer and the experimental challenges that were encountered, (2) describe the strategies that were developed and implemented to overcome these challenges, and (3) present some test results from the implementation of the experimental designs and test equipment.

Material

The TDA used in this study ([Fig. 1](#)) was supplied by Shercom industries, Saskatoon, Saskatchewan. Shercom produces TDA from scrap passenger and light truck tires.

FIG. 1

TDA used in the study.



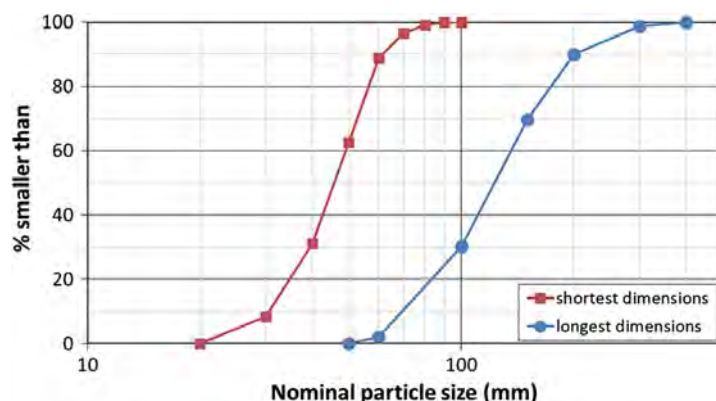
Quantitative analyses were performed to determine the particle size distribution (PSD) and specific gravity of the TDA mass. For the PSD, approximately 20 kg of TDA was selected randomly and the length, width, thickness, and mass of individual shreds (particles) were measured. Plots of PSD using the cumulative percentage smaller than the longest dimension of each TDA particle and the cumulative percentage smaller than the smallest dimension of each particle are presented in **Fig. 2a** and **b**. The specific gravity of the TDA mass was measured according to ASTM C127-12, *Standard Test Method for Density, Relative Density (Specific Gravity), and Absorption of Coarse Aggregate*, to be 1.27.

CHALLENGE 1: A SUITABLE TEST CHAMBER

Given the large dimensions of the TDA particles, a large test chamber several times larger in diameter than the longest dimension of the TDA particles was required to minimize sidewall friction as recommended in ASTM D6270-08. In addition, the height of the test chamber had to be sufficient to accommodate an initially greater thickness of a mass of TDA that would undergo large compressive strains as loading progressed.

FIG. 2

Particle size distribution plots for the TDA mass using both longest and shortest dimensions of individual particles.



A 1.8-m-high 1D consolidometer with a diameter of 0.7 m was fabricated from a cylinder of transparent acrylic material with a wall thickness of 0.1 m, an ultimate tensile strength of approximately 50 MPa, and an elastic modulus of 3.2 GPa ([Fig. 3a](#)). In the load frame, the consolidometer was placed on a wooden base plate of the same diameter as the outer diameter of the consolidometer; the base plate had sufficient clearance underneath for a forklift to move the consolidometer in and out of the load frame. A schematic of the 1D consolidometer setup with details of the load application system is presented in [Fig. 3b](#).

It was important to be able to move the consolidometer in and out of the loading frame with minimal obstructions and to have a load frame that was sufficiently sturdy with adequate capacity to withstand applied loads. It was also important to have a system for loading and unloading the consolidometer. A triangular design was implemented for the load frame to facilitate easy movement of the consolidometer in and out of the load frame ([Fig. 3a](#)), and a gantry system allowing for various degrees of inclination of the consolidometer was fabricated for loading and unloading the consolidometer ([Fig. 4](#))

CHALLENGE 2: THE LOADING SYSTEM

The large-sized consolidometer meant a large loaded area, the application of large vertical loads of over 150 kN, and a loading system capable of applying and maintaining the large vertical loads constantly at high strains greater than 50 %. A loading system such as this

FIG. 3 (a) The 1D consolidometer placed in the triangular-shaped load frame showing a compression test in progress; (b) schematic of the 1D consolidometer and its components. 1. Threaded rod for winding bellows up and down; 2. Steel gusset plate reinforcement for air bellows; 3. Nut and washer securing load frame “arms”; 4. Upper “arms” of load frame; 5. Air bellows; 6. Piston guide; 7. Lower “arms” of load frame; 8. Piston rod; 9. 1D consolidometer cell; 10. Press plate; 11. Colored marker balls to measure vertical displacement; 12. Load frame; 13. Base of consolidometer; 14. Wooden support for consolidometer; 15. Nut securing threaded rods to load frame; 16. Load cell; 17. TDA test sample; 18. Total stress (TS) cell.

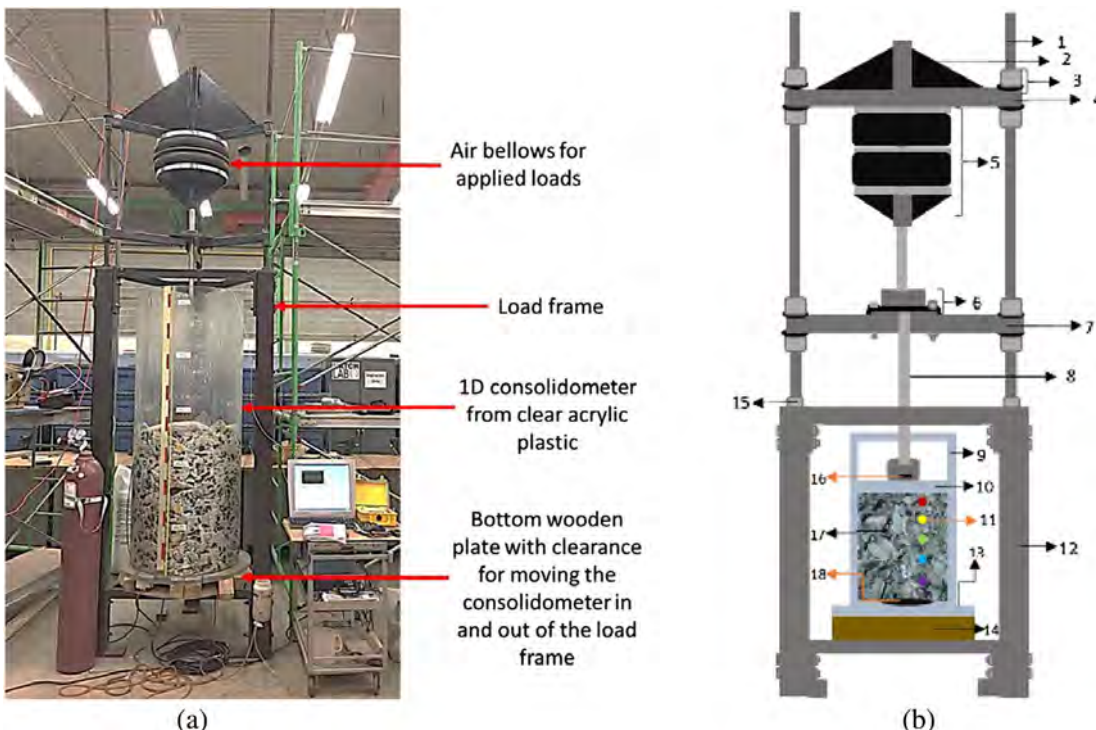


FIG. 4 Gantry system for unloading and loading the consolidometer outside the load frame.

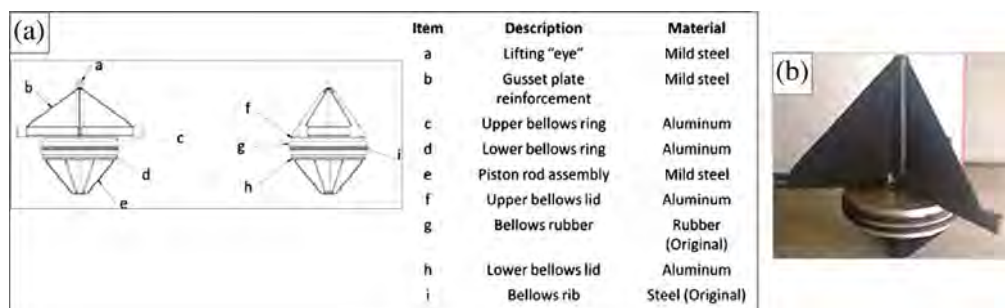
would require a long extension stroke with means for lowering and raising the system while maintaining constant load on the TDA mass.

In addition, components that would facilitate the transfer and distribution of the applied vertical load uniformly across the surface of the TDA mass in the consolidometer were required. To apply the large constant loads, 21 ½-inch-diameter stock units of double convolution air bellows (model 9109150) were sourced from Parker Hannifin, Cleveland, OH. The air bellows were subsequently modified by removing the factory-fitted upper and lower plates—items “f” and “h” in **Fig. 5a**—and replacing them with steel plates and gusset reinforcement (**Fig. 5b**) to enhance the load bearing capacity of the air bellows and prevent excessive bending of the inset ring plates during loading.

The re-engineered air bellows (**Fig. 5b**) weigh 123 kg and have the capacity to generate over 150 kN, which could be used to apply vertical stresses of up to 600 kPa. The maximum applied vertical stress in the testing described in this article was 224 kPa to simulate 20 m to 25 m of overlying waste (Zekkos et al. 2006) above a mass of TDA in a landfill drainage application.

A 0.04-m by 1.64-m piston rod fabricated out of steel was used to transfer the load from the air bellows to the loading plate on the test sample. The loading plate was fabricated from the same acrylic material as the consolidometer, is 20 mm thick, and is 5 mm smaller in diameter than the inner diameter of the consolidometer, providing sufficient clearance along the walls of the consolidometer during loading.

A piston guide was incorporated into the loading system to provide alignment for the piston rod during loading. Both the piston guide and air bellows were connected to the load frame by upper and lower “arms” that were attached to threaded rods bolted onto the top of the load frame (see **Fig. 3b**). The length of threaded rods was designed to allow for

FIG. 5 (a) Components of re-engineered air bellows; (b) re-engineered air bellows with gusset reinforcement.

sustained loading on the TDA mass over a total displacement associated with vertical strains exceeding 50 %.

The “arms” were manually wound down while maintaining constant pressure in the air bellows by means of pressure relief valves. This ensured that a constant load was supplied to the TDA mass as the applied vertical stress increased and compressive strains became larger.

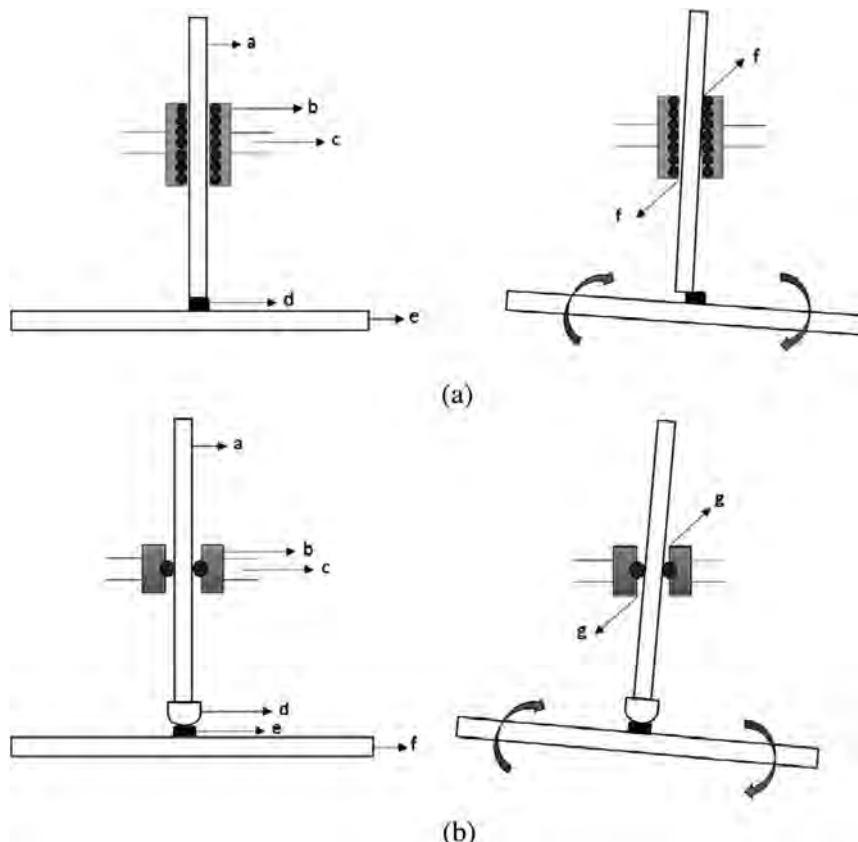
A button-type load cell with a capacity of over 150 kN, sourced from Futek Inc., Irvine, CA, USA (model LLB500), was positioned between the lower end of the piston rod and the press plate to determine the actual load supplied by the air bellows to the consolidometer. The load cell was placed in a housing and this was bolted to the top of the press plate to ensure that the load cell was held in place during the tests. The load cell was connected to a PC-controlled readout unit, and the vertical load supplied to the TDA mass was displayed in real time.

A pancake-type vibrating wire (VW) TS cell (P/N 52608220, S/N 11-1282) with a capacity of over 300 kPa manufactured by Durham Geo-Enterprises, Inc., (Durham Geo Slope Indicator (DGSI), Richmond, BC, Canada) was used to measure the load reaching the bottom of the consolidometer. The TS cell readings were useful for estimating the effectiveness of the sidewall treatments that were applied to the walls of the 1D consolidometer for reducing sidewall friction. They were also useful for developing a theoretical approach for estimating the loss of applied surface load across the thickness of the TDA mass resulting from sidewall friction.

FIG. 6

(a) Representation of the initial piston guide design and deflection of the load application system; a. Piston rod; b. Linear bearing cartridge piston guide; c. Lower “arms” of the load frame; d. Load cell; e. Press plate; f. Binding and loss of applied vertical load to the piston guide.

(b) Representation of the redesigned piston guide and deflection of the load application system; a. Piston rod; b. Annular single row piston guide; c. Lower “arms” of the load frame; d. Conical tip fitting for piston rod; e. Load cell; f. Press plate; g. No binding – sufficient clearance between piston guide and piston rod.



The TS cell was placed in the 1D consolidometer prior to filling with TDA, resting flat on the rigid base of the consolidometer to avoid poor conformance and stiffness–compatibility related errors in the TS measurement that may occur with placing the TS cell within the TDA mass. Descriptions of poor conformance and stiffness compatibility errors in TS measurements are provided in Dunilcliff (1988).

A 25-mm-thick plywood disc that was the same diameter as the TS cell was placed on top of the TS cell before loading the consolidometer with TDA to ensure an even distribution of applied stresses on the TS cell. The TS cell was connected to a VW data recorder (P/N 52613500, S/N 42182) by DGSI to obtain readings.

CHALLENGE 3: DIFFERENTIAL COMPRESSION

Because of the variations in shapes and sizes of the particles in the TDA mass and an initially large void volume from the large sizes of the TDA particles, differential compression and misalignment of the load application system occurred at the early stages of the testing. Following an increase of load from 112 kPa to 224 kPa, uneven settlement of the TDA mass occurred, and this caused the press plate to tilt and the piston rod misaligned such that only a small portion of the lower end of the piston rod was left in contact with the load cell.

A diagnostic evaluation of the occurrence showed that the clearance between the piston rod and the annulus of the piston guide was insufficient, and this had caused the piston rod to bind at the ends of the piston guide during the misalignment (**Fig. 6a**). This binding resulted in significant fluctuations in the load reaching the surface of the TDA mass.

The piston guide that was originally used had been a linear bearing cartridge placed inside a cylindrical canister base. Embedded inside the cartridge were rings of small-sized ball bearings to provide alignment of the piston rod. The linear bearing design provided motion and full contact in the direction of the cartridge but did not allow for misalignment of the piston rod. The piston guide had to be redesigned and refabricated to accommodate deflections and misalignments in subsequent tests.

The redesigned piston guide has an annular single row consisting of 5/8-sized ball bearings to provide a single point of contact around any given point of the piston rod. The ball bearings in the piston guide are capped in two halves that are bolted together to form a canister base. The redesigned piston guide provides better alignment and freer movement of the piston rod and is able to accommodate misalignments up to 15°, creating a diametric clearance of almost 3 mm within the annulus of the piston guide.

In addition to redesigning the piston guide, the lower end of the piston rod was fitted with a cylindrical hollow base having a conical tip to create a wider contact area between the lower end of the piston rod and the surface of the load cell during misalignment. With the conical tip attachment, the piston rod is able to revolve or rotate on the load cell during differential settlements and misalignments without slipping off completely (**Fig. 6b**).

With the re-engineered piston assembly, during subsequent testing, the piston rod was able to move freely within the annulus of the piston guide and was able to misalign slightly without binding at the edges of the piston guide while maintaining maximum contact with the load cell. The re-engineered piston assembly reduced the fluctuations in applied load reaching the TDA mass during subsequent tests considerably.

CHALLENGE 4: MEASURING COMPRESSIVE STRAINS AND VOID VOLUME REDUCTION

There are currently no standard test methods for evaluating compression and void volume reduction in a mass of TDA under applied loads. The following standard methods for

evaluating creep in polymers were adapted as required: ASTM D2990–09, *Standard Test Methods for Tensile, Compressive, and Flexural Creep and Creep-Rupture of Plastics*, and ASTM D7406–07, *Standard Test Method for Time-Dependent (Creep) Deformation Under Constant Pressure for Geosynthetic Drainage Products*.

Evaluating Solid Volume Compression in TDA Particles

Before setting out to measure the compression and void volume reduction in the TDA mass, it was deemed essential to identify the contribution of solid volume compression in individual TDA particles to the overall void volume reduction so that appropriate means for evaluating the resulting void volume reduction may be established. A complementary study was completed as part of this research work to evaluate the contribution of solid volume compression of individual TDA particles to overall compression and creep.

In that study, isotropic stresses from 50 kPa to 200 kPa were applied incrementally to a mass of TDA in a 0.6-m by 0.3-m triaxial cell for over 90 days. Upon application of load, there appeared to be some elastic compression, but subsequently, there was little or no further compression over the test period to the end of the final isotropic stress of 200 kPa.

Given the minimal solid volume compression observed in that study, it was determined that void volume reduction may be the principal mechanism for compressive strains in a mass of TDA under applied loads and compressive solid volume change in the individual TDA particles may be ignored. Hence, any change in void volume in a mass of TDA under applied loads may be represented by the change in the height of the TDA mass using Eq 1.

$$\frac{\Delta H}{H} = \frac{\Delta e}{1 + e_0} \text{ and } \Delta V_s = 0 \quad (1)$$

where:

H = height;

e = void ratio; and

V_s = volume of solids.

Measuring 1D Compression and Change in Void Volume in the TDA Mass—Primary Strategy

Having fabricated the consolidometer cell from transparent plastic, it was possible to place visual markers at various depths within the TDA mass and the vertical displacement of the markers could be tracked periodically to measure intermediate strains. Three colored four-inch diameter balls with a comparable elastic modulus to the modulus of individual TDA particles were placed at predetermined heights as visual markers against the inside walls of the consolidometer adjacent to three 1.8-m-long measuring tapes that had been glued to the outside wall of the cell 120 degrees apart.

The positions of the visual markers were read across the measuring tapes as loading progressed. Adjacent visual markers separated the TDA mass into slices. The slices were analyzed to represent a series of tests running simultaneously in the test cell. The mass of TDA placed in each slice separated by the visual markers was determined during loading, and because the specific gravity of the TDA had been previously measured, the dry unit weight of each mass of TDA slice was estimated. Knowing these, it was possible to estimate the initial void volume in the slices and the change in void volume with the progression of the test using Eq 2.

$$e = \left(\frac{G_s \gamma_w}{\gamma_{dry}} \right) - 1 \quad (2)$$

where:

G_s = specific gravity;

γ_w = the unit weight of water, kN/m³; and

γ_{dry} = the unit weight of dry TDA mass in the slices, kN/m³.

Measuring 1D Compression and Change in Void Volume in the TDA Mass—Auxiliary Strategy

Drainable porosity was measured periodically as an auxiliary method for estimating compression and change in the void ratio within the TDA mass. Drainable porosity measurements for void ratio evaluation in a mass of TDA have been done by previous researchers, e.g., McIsaac and Rowe (2005), Rowe and McIsaac (2005), and Hudson et al. (2007).

The fabrication of the consolidometer included threaded ports at the base for introducing fluids into the TDA mass. The threaded ports made it easy to remove the fittings when they were not in use to recover a smooth flush base for transporting the cell around on a forklift. The ports were barb fitted to allow for connection of flexible tubing for fluid flow. The barb fitting design was to ensure a smooth flush on the inside of the consolidometer at the base and to prevent intrusion of fittings into the consolidometer or standing water at the base during drainable porosity tests.

Both filling and draining porosities were evaluated in the drainable porosity tests. For the filling porosity, a graduated cylinder was placed on a scaffold and a flexible tubing was connected to the bottom of the graduated cylinder and to the ports at the bottom of the 1D consolidometer. The tubing connection allowed water to drain by gravity from the graduated cylinder into the 1D consolidometer for filling porosity measurements. Water from the graduated cylinder flowed under gravity to fill up the consolidometer to the elevation of the visual markers, and the transparent cell made it easy to see the water level rise to the required elevation.

The consolidometer was filled from bottom to top to ensure saturation of the TDA mass for the measurements. Each TDA mass slice was filled within 24 hours—this period may not have been sufficient to ensure complete saturation of the voids in the TDA mass. Because of this, the void ratio measurements from drainable porosity presented in this article may have underestimated the values slightly. A comparison of the void ratio values from drainable porosity and those from measuring the displacement of the visual markers is presented later on.

For the draining porosity, the consolidometer cell was drained by gravity into the graduated cylinder, and it was observed that draining the cell too quickly resulted in delayed drainage. Delayed drainage is a situation whereby water from preceding layers, if not allowed enough time to drain completely, seeps into lower layers while draining those layers.

Delayed drainage ultimately results in erroneous readings of draining porosity because lower layers would drain a larger volume of water, while upper layers would drain less water and the void volume in the various layers would be misrepresented. To manage delayed drainage during the draining porosity tests, a constant head container was attached to the load frame and a flexible tubing was connected to the top of the constant head container and the ports at the bottom of the 1D consolidometer (**Fig. 7**).

The constant head container was lowered to predetermined heights—usually the height of the visual markers—and water from the 1D consolidometer drained by gravity into the constant head container through the flexible tubing. Overflow from the constant head container was collected into the graduated cylinder, and when the head of water in the 1D

FIG. 7

Draining porosity test in progress showing the constant head addition (container) for collecting delayed drainage during draining porosity.



consolidometer was equal to that of the water inside the constant head container, the setup was left undisturbed for a few hours to collect any delayed drainage from the upper layers.

Following the drainable porosity tests, filling and draining porosity values of the TDA mass slices were determined using Eq 3. Corresponding void ratio values were estimated from the porosity values.

$$n = \frac{V_{water}}{V_{TDA}} \quad (3)$$

where:

n = porosity;

V_{water} = volume of water; and

V_{TDA} = volume of the TDA mass slice filled or drained.

CHALLENGE 5: MANAGING SIDEWALL FRICTION

Sidewall Friction Reduction

In the conventional 1D oedometer standard testing procedure ASTM D2435/D2435M-11, *Standard Test Methods for One-Dimensional Consolidation Properties of Soils Using Incremental Loading*, a test cell is used to minimize sidewall friction, height-to-specimen diameter ratios of 1:2.5 are recommended, and height-to-diameter ratios greater than 1:4 are preferred. The height to diameter ratio of the 1D consolidometer used in this study was 2.5:1. Significant sidewall friction was anticipated because of this, and methods for reducing and accounting for sidewall friction were required.

Two treatment methods for reducing sidewall friction were evaluated. Treatment 1 involved applying a layer of high-temperature grease to the inside walls of the consolidometer and placing a layer of 0.15-mm polyethylene plastic on top of the greased wall. Treatment 2 involved applying two layers of the same plastic and two layers of the high-temperature grease to the inside walls of the consolidometer. The grease was applied directly to the wall of the consolidometer and in between the two layers of plastic.

TABLE 1

Effects of sidewall friction treatments at 112 kPa.

Operation	% Load Reaching the Bottom at 112 kPa
No sidewall treatment	46 %
Treatment 1	50 %
Treatment 2	54 %

Both treatments resulted in a reduction of over 50 % in sidewall friction as shown in the sample results for an applied load of 112 kPa (**Table 1**) for readings from the TS cell placed beneath the TDA mass in the consolidometer. Treatment 2 achieved a slightly higher reduction and was applied in subsequent tests.

Sidewall Friction Evaluation

Despite applying sidewall treatments, it may not be possible to eliminate sidewall friction in 1D constrained testing of a TDA mass. With this in mind, an approach that may be used to evaluate sidewall friction loss to enable a detailed evaluation of the compression behavior of the TDA mass for design was developed and is presented here. The evaluation approach presented in this study is similar to a theoretical approach that was previously developed by Beaven (2000) from the testing of municipal solid waste.

The Beaven approach related the vertical effective stress (σ'_v) at a depth, z , in the cell to the internal angle of friction (ϕ') of the waste and to the interface shear friction angle (δ) between the waste and the wall of the test cell. The Beaven approach assumed that ϕ' , δ and the unit weight (γ) of the waste were constant with applied load and depth, and the resulting equation was given as

$$\sigma'_v = \frac{\gamma}{B} (1 - e^{-Bz}) + P \cdot e^{-Bz} \quad (4)$$

where: $B = \left[\frac{4(1-\sin\phi') \cdot \tan\delta}{d} \right]$; and

P = the applied surface load.

Although the theoretical approach by Beaven and the approach presented in this article share some similarities, the techniques that were applied to develop the resulting equations are different. In the Beaven approach, there was a reliance on the internal angle of friction of the waste mass, additionally, the actual stress reaching the bottom of the test cell and intermediate strains within slices of the waste mass were not measured.

In addition, in the Beaven approach, the unit weight of the TDA mass was assumed to be constant. This assumption of a constant unit weight may result in errors in estimating the void ratio with applied loads and with depth. This is because the unit weight of a mass of TDA will depend on the applied loads and the resulting compression from the applied loads.

Additionally, because the applied loads in a constrained loading test of a TDA mass will vary across the thickness of the specimen as a result of sidewall friction, unit weight will not be constant throughout the specimen. As such, assuming a constant unit weight with applied load and thickness for the TDA mass may result in errors in estimating the effects of sidewall friction and may additionally cause a misrepresentation of the void volume reduction in the TDA mass with applied stress.

The sidewall friction equation presented in this article considers intermediate slices of the TDA mass and evaluates the compression and void volume change in each slice. As

such, the equation accounts for the changes in unit weight with depth across the thickness of the TDA mass and presents a range of sidewall friction angle (δ) values for various applied loads that were obtained from the test results. The sidewall evaluation equation and approach in this study are described in the following sections.

The parameters governing sidewall friction were determined using the load cell readings at the top, the intermediate strains measured from the displacement of the visual markers, and the TS cell readings beneath the TDA mass. Using these readings, it was possible to integrate applied load with depth and to evaluate strains at any point within the TDA mass to account for sidewall friction loss.

In the evaluation procedure, sidewall friction was assumed to be analogous to the Mohr-Coulomb model, which may be used to evaluate interface shear resistance given in Eq 5.

$$\tau = K_o \sigma'_z \tan \delta + c_a \quad (5)$$

where:

τ = shear stress;

K_o = lateral “earth” pressure coefficient;

σ'_z = applied vertical stress;

$\tan \delta$ = angle of interface shearing resistance; and

c_a = adhesion.

It was assumed that K_{oTDA} and $\tan \delta$ were constant with depth, giving a first-order decay of vertical stress with depth as follows:

$$\sigma' z_{(z)} = \sigma z_o e^{(-4K_{oTDA} \tan \delta Z/D)} \quad (6)$$

where:

$\sigma' z_{(z)}$ = vertical load at a particular depth;

σz_o = the applied vertical load at the top;

K_{oTDA} = lateral pressure coefficient for a TDA mass;

δ = the interface shearing angle between the TDA mass and the walls of the test cell;

Z = the depth from the applied stress; and

D = the diameter of the test cell.

Because the applied load at the top (σz_o) and the stress reaching the bottom of the TDA mass were known, the term $K_{oTDA} \tan \delta$ that is analogous to the parameter β for skin friction of piles was estimated from a simple root mean square error (RMSE) analysis. The parameters K_{oTDA} and $\tan \delta$ were subsequently separated and determined independently from specific individual measurements. These measurements are described in the following sections.

The RMSE analysis of the top and bottom stresses in the TDA mass yielded a $K_{oTDA} \tan \delta$ value of 0.75 for no sidewall friction treatment and 0.12 for sidewall friction Treatment 2. To estimate the value of K_{oTDA} , the hoop strain was measured in the thick-walled acrylic test cylinder, and this value was used with a three-dimensional (3D) finite element (FE) model of the acrylic test cell as described in the following paragraphs. The focus of the FE modeling and the completed independent direct shear tests was to determine the approximate values of K_{oTDA} and $\tan \delta$ that may tease out the lumped β parameter and not to conduct a detailed analysis of the TDA mass.

Estimation of K_{oTDA}

Three high precision strain gauges were glued to the outer wall of the consolidometer 120° apart at a height corresponding to the region of estimated maximum hoop strain upon increasing applied load. The strain gauges were connected to a readout unit, and the resultant hoop strains were recorded as vertical stresses increased.

A 3D FE model was developed for the consolidometer apparatus using the software package Abaqus (Dassault Systèmes, Vélizy-Villacoublay, France). The mechanical response of the acrylic cylinder was simulated using a linear elastic model for small strains in acrylic in order to estimate the value of K_{oTDA} by adjusting the horizontal earth pressure of the TDA to match the hoop strain values measured by the strain gauges on the sidewalls of the apparatus. The TDA itself was not explicitly part of the FE model except in that the outward horizontal stress applied by the vertically loaded mass of TDA was applied as a load boundary condition to the surface of the acrylic cylinder. This outward horizontal stress decreased with height along this boundary in accordance with the vertical stress distribution $\sigma'_z(z)$ throughout the TDA mass and the shear stress distribution $\tau_z(z)$ along the walls of the consolidometer (**Fig. 8**).

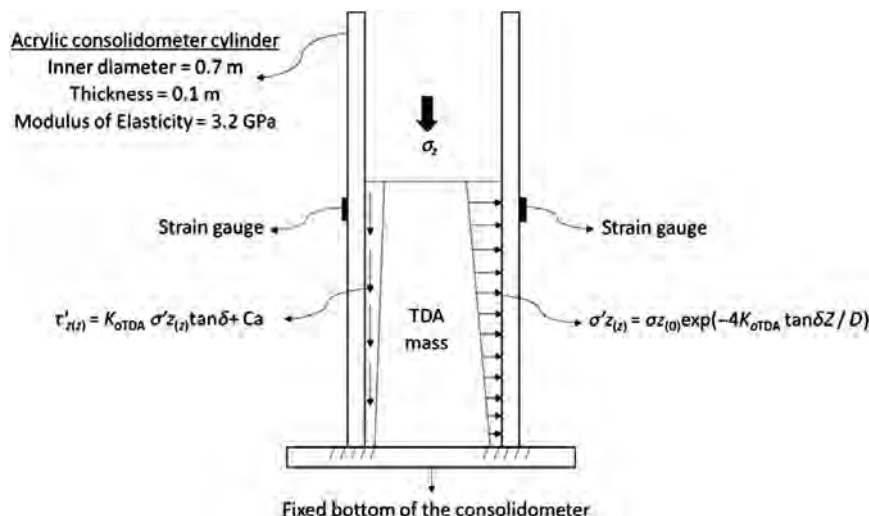
The FE model was run multiple times using Eqs 5 and 6 and the thickness of the TDA mass. The value of K_{oTDA} was varied until the hoop strain predicted by the FE model matched the observed values. The resulting best-fit value of K_{oTDA} obtained using the FE model was 0.7. It should be noted that a mass of TDA is not a perfectly homogeneous isotropic linearly elastic material and representing the lateral and shear stress from the TDA mass as a boundary condition for the FE model of the acrylic cylinder is necessarily a simplification. The FE modeling did yield a reasonable value of K_{oTDA} for the analyses. Furthermore, the value was useful for estimating the maximum load that may be safely applied to a TDA mass in the test apparatus without the risk of damaging the acrylic cylinder.

Estimation of $\tan \delta$

Using $K_{oTDA} = 0.7$, an RMSE analysis was applied to vary the value of $\tan \delta$ in Eq 6 until the calculated measurements at the bottom of the cell matched the readings from the TS

FIG. 8

A schematic representation of the consolidometer cell as it was used in the 3D FE model to determine the value of K_{oTDA} for the TDA mass.



cell at the bottom of the TDA mass. The estimated value of δ from this approach was between 10° to 12° for the applied loads.

For an independent evaluation of $\tan \delta$, testing was conducted in a 300-mm by 450-mm direct shear box to determine an approximate value for the interface friction angle δ between the TDA mass and the walls of the acrylic test cell with sidewall Treatment 2 applied. The applied normal stresses and sidewall conditions in the 1D consolidometer were simulated as closely as possible. It should be noted that the dimensions of the TDA particles (ranging from 50 mm to 305 mm) being close to the direct shear box dimensions could have resulted in edge effects between the TDA particles and the walls of the direct shear box. This may have contributed to the interface shear friction values recorded for the TDA mass and acrylic interface.

Another aspect of the direct shear test to point out is that the plastic layers were replaced and the grease layers were reapplied for each test in the direct shear box. These were not done in the compression tests in the 1D consolidometer; the initial grease layers and plastic applied in the 1D consolidometer were used from start to finish in the compression tests. As such, the δ values that were determined independently in the direct shear box may have underestimated the friction values. The results from the direct shear interface friction tests are presented in **Table 2**.

The results from the evaluation approaches for δ as described in the preceding sections suggest that $\tan \delta$ may not depend on the applied stress significantly. This may substantiate the premise that δ may be assumed to be constant with depth in the formulation of the sidewall evaluation strategy for evaluating stress distribution within the TDA mass presented in Eq 6. The values of δ estimated from measurements in the 1D consolidometer were higher than the values from the individual direct shear tests in **Table 2**.

The higher δ values may be related to the ripping of the plastic sidewall liners with increased loading, causing direct contact (sticking) of some TDA particles to the wall of the consolidometer. This may have caused nonuniform displacements along the TDA mass and wall interface, potentially increasing the sidewall friction compared with the direct shear tests in which the plastic layers were replaced for each test run and had fewer rips.

Notwithstanding, because the vertical stress applied to each slice was known and the compressive response of the TDA had been determined across a range of loads, it was important to have a good estimate of the degree to which sidewall friction changed the vertical stress from the top to the bottom of the TDA mass. However, had the sidewall friction effect been more or less pronounced, the results in the 1D consolidometer would have still been usable as long as a good estimate of the distribution of vertical stress could be made.

TABLE 2

Results from the measurement of δ° with sidewall Treatment 2.

Applied Stress, $\sigma(z)$, kPa	Shear Stress τ , kPa	$\tan \delta$	δ°
39.4	3.8	0.01	0.7
65.3	5.9	0.04	2.3
195.0	9.4	0.03	1.8
255.0	10.9	0.03	1.7
304.4	12.1	0.03	1.7

Discussion

IMMEDIATE COMPRESSION AND CREEP

The progression of compression at the applied surface loads of 112 kPa and 224 kPa, simulating approximately 10 m to 25 m of waste above the drainage layer, respectively, is presented in [Fig. 9](#). Compression in the TDA mass as measured periodically from the vertical displacement of the colored visual markers is presented in [Fig. 10](#), where H1 to H5 are the labels for the visual markers from the topmost marker H1 to the bottom marker H5.

The initial positions of the visual markers (H1 to H5) before applying the 112 kPa surface load were H1 = 1.78 m, H2 = 1.42 m, H3 = 1.06 m, H4 = 0.72 m, and H5 = 0.32 m. At both load steps of 112 kPa and 224 kPa, there was a large immediate compression followed by some creep ([Table 3](#)).

FIG. 9

Progression of the 1D compression test: (a) no applied surface load; (b) after applying 112 kPa surface load; (c) after applying 224 kPa surface load.

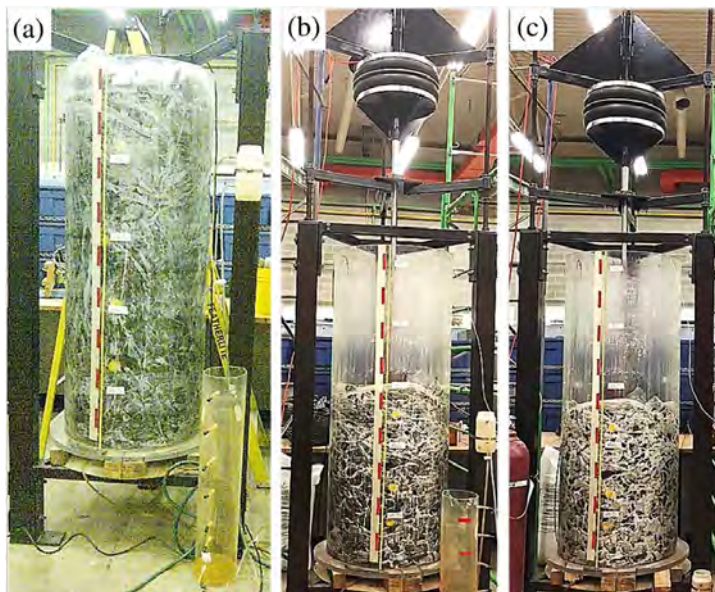


FIG. 10

Elevation of the visual markers at the applied surface loads of 112 kPa and 224 kPa. H1 to H5 are the labels for the visual markers from the topmost marker H1 to the bottom marker H5. The initial positions of the visual markers (H1 to H5) before applying the 112 kPa surface load are as follows: H1 = 1.78 m, H2 = 1.42 m, H3 = 1.06 m, H4 = 0.72 m, H5 = 0.32 m.

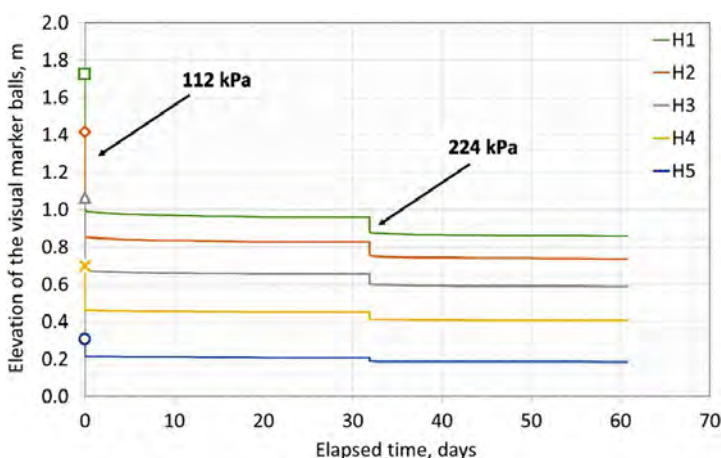


TABLE 3

Immediate and time-dependent compression of the TDA mass.

Applied Top Stress, kPa	Overall Compression, %	Immediate Compression, %	Time-Dependent Compression, %
112	44	41.5	2.5
224	Additional 10.5	7.8	2.7

The total compression at the end of the final load step of 224 kPa was approximately 55 %, and the contribution of creep to this was approximately 5 %. Immediate compression upon application of the loads was larger at 112 kPa and reduced significantly at the 224 kPa load step. This is indicative of strain stiffening in the TDA mass with increased applied vertical stress. Strain stiffening in a TDA mass has been presented in studies by other researchers. For instance, the compression results presented by Beaven et al. (2006) and Mwai, Wichuk, and McCartney (2010) for different sizes and types of TDA showed reduced compression–strain stiffening at stresses from 200 kPa and greater.

VOID RATIO EVALUATION

Before and after creep plots of void ratio with applied stress (e -log p plots) for the slices in the TDA mass are presented collectively as series of tests running concurrently and are shown in Fig. 11a. The onset of creep (in this study) is 24 hours after the application of the surface vertical load. Because of sidewall friction, the applied load at the top of the TDA mass was reduced throughout the specimen thickness; this resulted in a higher compression and void volume reduction in slices closer to the applied load than in slices farther away from it.

In addition to the Fig. 11a plots, e -log p plots for the end of creep for individual slices of the TDA mass, taking each slice as a separately run test and tracking the void ratio change in the individual slices in relation to the applied surface loads, are presented in Fig. 11b. The void ratio e was estimated using Eq 1, and the applied stress reaching the slice from the surface load (p) was determined using Eq 6.

The void ratio in the top TDA slice (H1 to H2) decreased by approximately 57 % upon application of the initial load of 112 kPa and further decreased by approximately 19 % when the applied load was increased from 112 kPa (end of creep) to 224 kPa. The void ratio reduction induced by creep was approximately 10 % at 112 kPa and 8 % at 224 kPa. These were smaller than the void ratio reduction induced by immediate compression before the onset of creep.

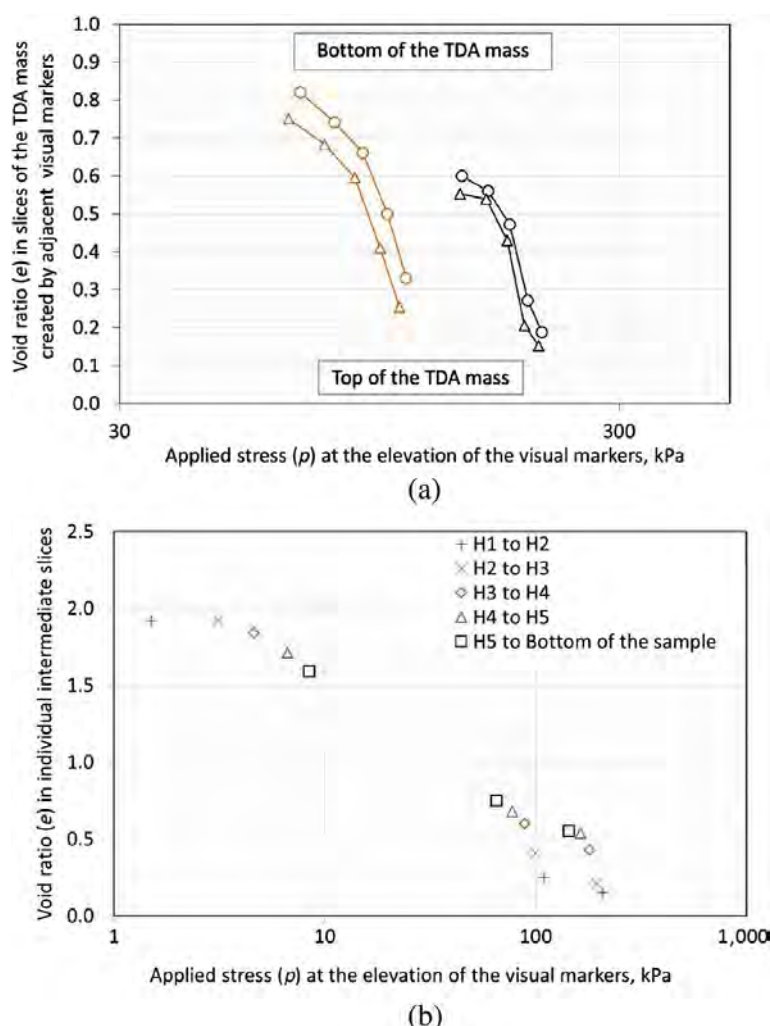
The shapes of the e -log p curves in Fig. 11a and b suggest that there may not be a unique relationship between void ratio and applied loads for a mass of TDA as measured from constrained loading. The void ratio of a TDA mass at a particular load appears to depend on the loading stress path taken to get to that void ratio, thus indicating that the compressive behavior of a mass of TDA under controlled conditions may be complicated and that there is need for field measurements to calibrate laboratory test results.

DRAINABLE POROSITY

A representation of average drainable porosity and porosity estimated from the displacement of the visual markers is presented in Fig. 12. The plot indicates some

FIG. 11

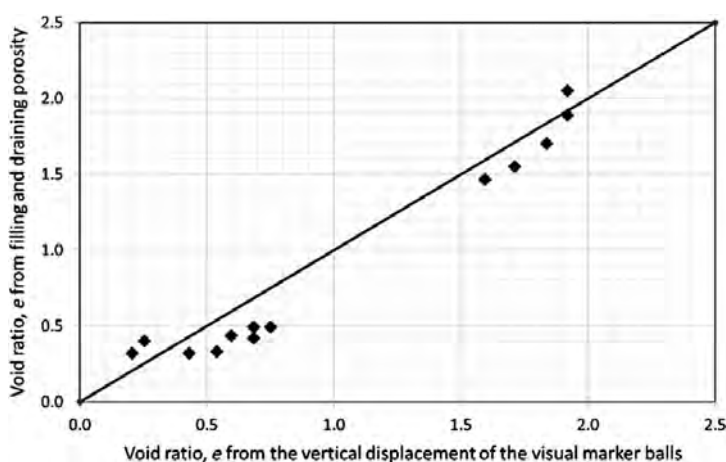
(a) e - $\log p$ curves for the entire thickness of the TDA mass, treating the slices collectively as a series of tests running concurrently. Adjacent visual markers in the test cell formed individual slices—for instance, visual markers H1 to H2 formed the topmost slice and visual marker H5 to the bottom of the cell formed the bottom slice. The applied loads in the slices were estimated using Eq 6. The trend lines connecting circular markers on the plots represent the before creep values and those connecting triangular markers represent after creep values. The onset of creep in this study was taken as 24 h after the applied load. The initial e values in the slices before the 112 kPa surface load were H1 to H2 = 1.92, H2 to H3 = 1.92, H3 to H4 = 1.84, H4 to H5 = 1.71, and H5 to the bottom of the cell = 1.51. (b) e - $\log p$ curves for individual slices of the TDA mass at the end of creep, treating each slice as a separately run test and tracking the void ratio change in the individual slices for the applied loads. For each slice, there are three marker points indicated on the plot: the first series of marker points indicate the initial void ratio values for each slice (under no external applied loads, just the weight of overlying TDA mass); the second and third points indicate the void ratio values at the end of 122 kPa and 224 kPa, respectively.



consistency between the void ratio values estimated from drainable porosity and those estimated from the displacement of the visual markers. However, the void ratio values that were estimated from drainable porosity measurements appear to be generally lower than those estimated from the displacement of the visual markers. This may be indicative of incomplete saturation of the TDA mass during the filling process for drainable porosity.

FIG. 12

Void ratio estimated from drainable porosity versus void ratio from tracking the vertical displacement (elevation) of the visual markers.



The void ratio results in Fig. 12 further highlight the benefits of the primary approach, involving the use of a transparent test cell and visual markers that were employed for measuring 1D compression and void ratio in the TDA mass. Nonetheless, in the absence of a clear test cell, drainable porosity values may still be used with a good degree of reliability to estimate void ratio change in a TDA mass in compression tests. Filling of the TDA mass should be completed over a longer period to potentially increase saturation and improve the accuracy of the measured values.

IMPLICATIONS OF CURRENT FINDINGS FOR PRACTICE AND FURTHER COMPLETED AND ONGOING RESEARCH WORK ON TDA

As stated previously in this article, the performance of a mass of TDA as the drainage layer in waste disposal facilities depends on the porosity, permeability, and pore volume of the TDA mass following (1) compressive strains from overlying waste and cover materials and (2) biogeochemical clogging from leachate flowing through the drainage layer. The porosity of the TDA mass under simulated overlying waste was evaluated in this study; this was found to reduce by over 50 % from an unloaded state to about 0.26 at the maximum applied load of 224 kPa.

Although the porosity of 0.26 at an applied load of 224 kPa—equivalent to between 20 m and 25 m of waste (Zekkos et al. 2006)—may seem low, the coefficient of vertical and horizontal permeability values of the TDA mass at a comparable porosity and applied stress have been evaluated and the results show high permeability values for the TDA mass. The measured coefficients of the vertical and horizontal permeability of the TDA mass at an applied vertical stress of 219 kPa were 7.9E-03 m/s and 1.9E-02 m/s, respectively. These values are higher than the regulatory requirement of 1E-04 m/s in the Western Canada jurisdiction for a landfill drainage layer.

The details of the 2D permeability testing, including the equipment design and experimental strategies employed, will be presented in a companion article. In addition, a porosimeter is being used with image analysis to analyze the pore geometry of a mass of TDA under applied vertical loading to obtain parameters, such as specific surface, pore volume, and pore size distribution, that may be used to evaluate the performance of a TDA mass against biogeochemical clogging under various mass loading and flow scenarios. The findings from this study will be presented in an upcoming article.

Conclusions and Summary

The challenges with testing large-particle-size TDA for use under large stresses imposed by overlying material have been discussed and some strategies for overcoming the challenges have been presented. The highlights of this article include the following:

- (1) Laboratory testing of large-particle-sized TDA is challenging, and it unavoidably requires the use of large-sized test equipment with the capacity to apply large vertical loads and accommodate large vertical strains.
- (2) The use of air bellows that can be wound down manually made it possible to apply and sustain large loads onto the test specimen while experiencing high vertical strains greater than 0.5 m.
- (3) A mass of TDA with large-sized particles has an initially large void volume that reduces considerably upon loading because of a large immediate compression and some creep.
- (4) Compression in a mass of TDA has been determined to be from void volume reduction, and the compression of individual solid particles may be ignored.
- (5) The use of a clear, “see-through” consolidometer provided the opportunity to measure intermediate strains and void ratio in slices within the test specimen. A single test can therefore yield information regarding a range of stresses concurrently if intermediate strains in slices are measured.
- (6) There is a need for unconstrained field testing of TDA to eliminate the effects of sidewall friction and to calibrate laboratory test data obtained from constrained 1D compression testing.
- (7) It is essential to account for sidewall friction in the laboratory testing of TDA to avoid overestimating the applied stresses and void ratio throughout the test specimen. For instance, if methods for measuring and estimating sidewall friction, such as using a clear test cell, placing visual markers at intermediate levels to separate the test specimen into slices, placing a TS cell at the bottom of the specimen to account for sidewall friction loss, and using a theoretical model to estimate applied stresses in intermediate slices, were not employed, the actual applied stresses within the specimen thickness, the resulting strains, and void volume reduction may have been overestimated. Dividing the test specimen into slices and determining the applied stress and void ratio in each slice made it possible to determine the actual void ratio at an applied stress following the effects of sidewall friction.
- (8) The sidewall friction evaluation approach that was presented in this article can be used to estimate stresses and strains at any point within the consolidometer, potentially eliminating the need for TS cells beneath the test specimen.
- (9) Void volume reduction in a TDA mass was found to reduce significantly as applied vertical stresses increased. This confirms the strain stiffening behavior of a mass of TDA under applied loads, substantiating similar findings from previous researchers (e.g., Beaven et al. 2006; Mwai, Wichuk, and McCartney 2010).
- (10) Nonlinearities in the e -log p consolidation curves indicate that the 1D constrained creep compression of a mass of TDA might be complicated.
- (11) Although TDA has been tested in this study, the strategies that were implemented in this study may be applicable to a wide range of highly compressible materials with initially large void volumes that would reduce significantly following compressive displacements under vertical loading.

ACKNOWLEDGMENTS

The equipment described in this article was fabricated and subsequently modified by the University of Saskatchewan Engineering Machine Shops. The assistance and financial support of SNC-Lavalin and Shercom Industries is acknowledged.

References

- ASTM C127-12, 2012, *Standard Test Method for Relative Density (Specific Gravity), and Absorption of Coarse Aggregate* (Superseded), ASTM International, West Conshohocken, PA, www.astm.org
- ASTM D2435/D2435M-11, 2011, *Standard Test Methods for One-Dimensional Consolidation Properties of Soils Using Incremental Loading*, ASTM International, West Conshohocken, PA, www.astm.org
- ASTM D2990-09, 2009, *Standard Test Methods for Tensile, Compressive, and Flexural Creep and Creep-Rupture of Plastics* (Superseded), ASTM International, West Conshohocken, PA, www.astm.org
- ASTM D6270-08, 2008, *Standard Practice for Use of Scrap Tires in Civil Engineering Applications* (Superseded), ASTM International, West Conshohocken, PA, www.astm.org
- ASTM D7406-07, 2007, *Standard Test Method for Time-Dependent (Creep) Deformation under Constant Pressure for Geosynthetic Drainage Products*, ASTM International, West Conshohocken, PA, www.astm.org
- Beaven, R. P., 2000, “The Hydrogeological and Geotechnical Properties of Household Waste in Relation to Sustainable Landfilling,” Ph.D. dissertation, University of London, London, United Kingdom.
- Beaven, R. P., Hudson, A. P., Knox, K., Powrie, W., and Robinson, J. P., 2013, “Clogging of Land Fill Tyre and Aggregate Drainage Layers by Methanogenic Leachate and Implications for Practice,” *Waste Manage.*, Vol. 33, No. 2, pp. 431–444, <https://doi.org/10.1016/j.wasman.2012.10.021>
- Beaven, R. P., Powrie, W., Hudson, A. P., and Parkes, D. J., 2006, “Compressibility of Tyres for Use in Landfill Drainage Systems,” *Proc. Inst. Civ. Eng. Waste Resour. Manage.*, Vol. 159, No. 4, pp. 173–180.
- Dickinson, S. and Brachman, R. W. I., 2008, “Assessment of Alternative Protection Layers for a Geomembrane-Geosynthetic Clay Liner (GM-GCL) Composite Liner,” *Can. Geotech. J.*, Vol. 45, No. 11, pp. 1594–1610, <https://doi.org/10.1139/T08-081>
- Donovan, R., Dempsey, J., and Owen, S., 1996, “Scrap Tire Utilization in Landfill Applications,” presented at the *17th Biennial Waste Processing Conference*, Atlantic City, NJ, American Society of Civil Engineers, Reston, VA, pp. 353–383.
- Duffy, D. P., 1995, “Using Tire Chips as Leachate Drainage Layer,” *Waste Age*, Vol. 26, No. 9, pp. 113–122.
- Dunicliff, J., 1988, *Geotechnical Instrumentation for Monitoring Field Performance*, John Wiley and Sons, New York, NY, pp. 165–177.
- Evans, P., 1997, “Use of Tire Shred in Landfill Construction,” presented at the *Third Annual Symposium Environmentally Friendly Technologies in Geotechnical Engineering*, Edmonton, Canada, Geotechnical Society of Edmonton, Edmonton, Canada, pp. 1–8.
- Fleming, I. R. and Rowe, R. K., 2004, “Laboratory Studies of Clogging of Landfill Leachate Collection and Drainage Systems,” *Can. Geotech. J.*, Vol. 41, No. 1, pp. 134–153, <https://doi.org/10.1139/t03-070>
- Fleming, I. R., Rowe, R. K., and Cullimore, D. R., 1999, “Field Observations of Clogging in Landfill Leachate Collection Systems,” *Can. Geotech. J.*, Vol. 36, No. 4, pp. 685–707, <https://doi.org/10.1139/t99-036>
- Hall, T. J., 1991, “Reuse of Shredded Tire Material for Leachate Collection Systems,” presented at the *14th Annual Madison Waste Conference*, Madison, WI, University of Wisconsin, Madison, WI, pp. 367–376.

- Hudson, A. P., Beaven, R. P., Powrie, W., and Parkes, D., 2007, "Hydraulic Conductivity of Tyres in Landfill Drainage Systems," *Proc. Inst. Civ. Eng. Waste Resour. Manage.*, Vol. 160, No. 2, pp. 63–70.
- McIsaac, R. and Rowe, R. K., 2005, "Change in Leachate Chemistry and Porosity as Leachate Permeates through Tire Shreds and Gravel," *Can. Geotech. J.*, Vol. 42, No. 4, pp. 1173–1188, <https://doi.org/10.1139/t05-050>
- Mwai, M., Wichuk, K., and McCartney, D., 2010, "Implications of Using Tire-Derived Aggregate for Landfill Leachate Collection and Drainage Systems," presented at the *Solid Waste Association of North America, Fifth Canadian Symposium*, Banff, Canada.
- Olson, R. E., 1986, "State of the Art: Consolidation Testing," *Consolidation of Soils: Testing and Evaluation, ASTM STP892*, Yong, R. N. and Townsend, F. C., Eds., ASTM International, West Conshohocken, PA, pp. 7–70, <https://doi.org/10.1520/STP34606S>
- Qian, X., Koerner, R. M., and Gray, D. H., 2001, *Geotechnical Aspects of Landfill Design and Construction*, Pearson Education, Upper Saddle River, NJ, pp. 294–330.
- Reddy, K. R. and Marella, A., 2001, "Properties of Different Size Scrap Tire Shreds: Implications on Using as Drainage Material in Landfill Cover Systems," presented at the *17th International Conference on Solid Waste Technology and Management*, Philadelphia, PA, 19p.
- Reddy, K. R. and Saichek, R. E., 1998, "Characterization and Performance Assessment of Shredded Scrap Tires as Leachate Drainage Material in Landfills," presented at the *14th International Conference on Solid Waste Technology and Management*, Philadelphia, PA.
- Rowe, R. K., 2005, "Long-Term Performance of Contaminant Barrier Systems," *Géotechnique*, Vol. 55, No. 9, pp. 631–678, <https://doi.org/10.1680/geot.2005.55.9.631>
- Rowe, R. K. and Babcock, D., 2007, "Modelling the Clogging of Coarse Gravel and Tire Shreds in Column Tests," *Can. Geotech. J.*, Vol. 44, No. 11, pp. 1273–1285, <https://doi.org/10.1139/T07-057>
- Rowe, R. K. and Fleming, I. R., 1998, "Estimating the Time for Clogging of Leachate Collection Systems," presented at the *Third International Congress on Environmental Geotechniques*, Lisbon, Portugal, A. A. Balkema, Rotterdam, the Netherlands, pp. 23–28.
- Rowe, R. K. and McIsaac, R., 2005, "Clogging of Tire Shreds and Gravel Permeated with Landfill Leachate," *J. Geotech. Geoenviron. Eng.*, Vol. 131, No. 6, pp. 682–693, [https://doi.org/10.1061/\(ASCE\)1090-0241\(2005\)131:6\(682\)](https://doi.org/10.1061/(ASCE)1090-0241(2005)131:6(682))
- Rowe, R. K., Quigley, R. M., Brachman, R. W. I., and Booker, J. R., 2004, *Barrier Systems for Waste Disposal Facilities*, Taylor and Francis Group, London, United Kingdom, 587p.
- Sarsby, R. W. and Vickers, B., 1986, "Side Friction in Consolidation Tests on Fibrous Peat," *Consolidation of Soils: Testing and Evaluation, ASTM STP892*, Yong R. N. and Townsend F. C., Eds., ASTM International, West Conshohocken, PA, pp. 485–489, <https://doi.org/10.1520/STP34629S>
- Strenk, P. M., Wartman, J., Grubb, D. G., Humprey, D. N., and Natale, M. F., 2007, "Variability and Scale-Dependency of Tire-Derived Aggregate," *J. Mater. Civ. Eng.*, Vol. 19, No. 3, pp. 233–241, [https://doi.org/10.1061/\(ASCE\)0899-1561\(2007\)19:3\(233\)](https://doi.org/10.1061/(ASCE)0899-1561(2007)19:3(233))
- Warith, M. A., Evgin, E., and Benson, P. A., 2004, "Suitability of Shredded Tires for Use in Landfill Leachate Collection Systems," *Waste Manage.*, Vol. 24, No. 10, pp. 967–979, <https://doi.org/10.1016/j.wasman.2004.08.004>
- Yu, Y. and Rowe, K. R., 2012, "Modelling Leachate-Induced Clogging of Porous Media," *Can. Geotech. J.*, Vol. 49, No. 8, pp. 877–890, <https://doi.org/10.1139/t2012-052>
- Zekkos, D., Bray, J. D., Kavazanjian, E., Jr., Matasovic, N., Rathje, E. M., Reimer, M. F., and Stokoe, K. H., II, 2006, "Unit Weight of Municipal Solid Waste," *J. Geotech. Geoenviron. Eng.*, Vol. 132, No. 10, pp. 1250–1261, [https://doi.org/10.1061/\(ASCE\)1090-0241\(2006\)132:10\(1250\)](https://doi.org/10.1061/(ASCE)1090-0241(2006)132:10(1250))
- Zimmerman, P. S., 1997, "Compressibility, Hydraulic Conductivity, and Soil Infiltration Testing of Tire Shreds and Field Testing of a Shredded Tire Horizontal Drain," M.S. thesis, Iowa State University, Ames, IA.

Appendix 2

*Damage to geomembrane by coarse uniform TDA or gravel drainage
aggregate*

University of Saskatchewan, October 2019





Tire derived aggregate as a drainage medium for landfill leachate collection

I.R. Fleming, Ph.D., P.Eng.

A.R. Hammerlindl, M.Eng., P.Eng.

B.A. Marcotte, B.Sc.

D. Adesokan, M.Sc.

October, 2019

Geotechnical Engineering Laboratories

Department of Civil, Geological & Environmental Engineering

57 Campus Drive, Saskatoon S7N 5A9 Canada

Tire derived aggregate as a drainage medium for landfill leachate collection

Structure and format of reporting

This two volume report documents work carried out at the University of Saskatchewan Geotechnical Labs since 2016 to evaluate tire derived aggregate (TDA) for use as a drainage medium in landfill leachate collection systems (LCS). These reports have been prepared for Adelantar Consulting on behalf of Alberta Recycling (AR). Accordingly, each of the two volumes covers separate (but related) workplans as follows:

Volume 1 Physical properties of TDA affecting performance in LCS

This report covers the testing of large samples to evaluate the compression of TDA under load and the resulting decrease in void ratio (or porosity) as well as the resulting change in both vertical and horizontal permeability.

Testing was carried out using two different systems: i) a large 1-dimensional cylindrical consolidometer designed to handle large strains while maintaining constant vertical load under compression and subsequent creep; and ii) a large rectangular 2D permeameter that allowed for measurement of horizontal and vertical hydraulic conductivity of a large specimen under load.

The effects of immediate compression by application of vertical stress were evaluated, along with the effect of creep over time at constant load. The inherent nature of TDA required innovative design of the laboratory testing equipment (and iterative re-design and upgrading of the system and its components). A total of 5 compression/creep tests were carried out over a combined 315 days with individual tests ranging in duration from 24 to 126 days.

Hydraulic conductivity was evaluated by dozens of tests at different flow rates and pressures. Interpreting the resulting data to yield hydraulic conductivity values required some complex analyses to account for high velocities, inertial effects and the inevitable artifacts of even the largest scale laboratory testing. These complex analyses are included as an appendix.

Volume 2 Damage to geomembranes by coarse uniform TDA or gravel drainage aggregate

This report evaluates the potential for damage to a geomembrane from an overlying coarse drainage aggregate. The testing program was designed to evaluate the relative risks associated with tire derived aggregate (TDA) and gravel when used in conjunction with a geomembrane in a base barrier for a landfill. The testing equipment consists of a large compression device capable of applying over 700 kPa to a 0.9 m diameter sample of TDA over geomembrane (GM) over clay.

The work addressed two separate types of damage to a geomembrane: short term puncture from point loading of the coarse drainage aggregate (Objective 1); and the development of high localised tensile strains which are detrimental to geomembrane integrity on a longer timeline (Objective 2) when such localised strain exceeds a threshold above which stress cracking becomes likely.

Multiple trials were carried out to evaluate various protective layers that may be placed between the GM and the drainage medium. In addition, work was carried out to highlight the significant role of the compacted clay sub-liner material in controlling the strains in an overlying geomembrane.

Tire derived aggregate as drainage media for landfill leachate collection

Volume 2, TDA damage to geomembranes

Table of Contents

1.0 Summary	1
2.0 Materials & Testing Equipment	4
3.0 Details of Puncture Testing Results	11
4.0 Details of Strain Testing and Results	21
5.0 Conclusions	31
6.0 Implications of findings and areas requiring further study	31
References	32
Appendices	34
Attaachments	

List of Tables

Table 1: Index properties of soil subgrades used in testing	6
Table 2: Index properties of geomembranes	8
Table 3: Index properties of geotextiles	9
Table 4: Summary of preliminary test results to determine hazardous wire types	13
Table 5: Proportion of high risk wires in single, double, and multi pass TDA	14
Table 6: Variability when sorting TDA	14
Table 7: Data from frozen ice block testing	17
Table 8: Summary of puncture protection efficiency results	18
Table 9: Probability of puncture based on test results	20

List of Figures

Figure 1: Schematic of test device	4
Figure 2: Large 0.9m diameter test device used for puncture testing using TDA and smaller 0.4 m diameter test cylinders used for testing gravel	5
Figure 3: Proctor curves of clay soils tested	6
Figure 4: Storage of 500 kg of clay in coolers; compaction of clay in cylinder and compaction hammer	7
Figure 5: Smoothed clay surface for testing	7
Figure 6: Geomembrane strain and compacted water content	8
Figure 7: Tire derived aggregate samples	9
Figure 8: Size distribution of single, double and multi-pass TDA samples	10
Figure 9: Size comparison of gravel to multi-pass TDA	10
Figure 10: Punctures of the geomembrane by different types of wires	12
Figure 11: Geomembrane puncture and pressure	12
Figure 12: High, medium, and low risk TDA pieces for puncture of geomembranes	13
Figure 13: Simulated field placement of TDA into constructed wooden box and flipping of ice block	15
Figure 14: Frozen double pass TDA sample representing the orientation of TDA in contract with geomembrane	16
Figure 15: Frozen small ice block testing with labeled high risk pink pieces	16
Figure 16: High risk multi pass TDA oriented unfavourably in small box test	17
Figure 17: Intentionally placed TDA pieces on geotextile protection layer above geomembrane to test protection efficiency	18
Figure 18: Punctures of geomembrane	19
Figure 19: Photogrammetry and mesh creation	23
Figure 20: Deformed surface and interpreted strain map for 1.5 mm geomembrane loaded by gravel and TDA at 500 kPa with a 544g/m ² protection layer	24
Figure 21: Deformed surface and interpreted strain map for 2.0 mm geomembrane loaded by gravel and TDA at 500 kPa with a 1088g/m ² protection layer	24
Figure 22: Strain area distributions for TDA and gravel under similar conditions	25
Figure 23: Pattern on geomembrane before and after strain	26
Figure 24: Epoxy and gravel in test cylinder to determine geomembrane strains	26
Figure 25: Strain map of epoxy gravel test based on new method	27
Figure 26: Strain map of gravel epoxy test using the method developed by Tognon	27
Figure 27: Strain area distribution comparing methods of calculating strain for gravel	28
Figure 28: Strain map of epoxy TDA test by new method	28
Figure 29: Strain map of epoxy TDA test using the method developed by Tognon	29
Figure 30: Strain area distribution comparing methods of calculating strain for TDA	29

Final Report – TDA damage to Geomembranes

1.0 Summary

The object of this testing program was to compare and evaluate the relative risks associated with tire derived aggregate (TDA) and gravel when used in conjunction with a geomembrane in a base landfill liner scenario. The study focused on two issues: short term geomembrane puncture (Objective 1); and induced high localised tensile strain, which is detrimental to geomembrane integrity on a longer timeline (Objective 2).

The **1st objective** of this testing program was to answer the question “how significant is the potential for puncture of a geomembrane by TDA and what can be done to mitigate it?” The first part of this aimed to estimate how many punctures of a geomembrane might be caused by placing TDA as a LCS blanket drain over a geomembrane/compacted clay composite barrier system and ten subjecting it to vertical loading. The second aspect of this objective aimed to establish whether a geotextile protection layer could be used to prevent or limit puncture of the geomembrane from tire derived aggregate (TDA) under the vertical load expected under a landfill. Prior to this study, no conclusions have been made with regards to geomembrane punctures from TDA, although the only previous study (Reddy and Saichek, 1998) had supported the idea of a protection layer to prevent puncture.

The **2nd objective** aimed to answer the different but related question “if we don’t expect puncture of a geomembrane from gravel used as LCS drainage media, how can we compare TDA and gravel in terms of damage to the geomembrane?” As explained in detail in subsequent sections, the localised areas of high strain induced in the geomembrane from TDA drainage aggregate were accordingly identified, characterized and compared to those caused by coarse uniform gravel drainage aggregate. Although gravel may not result in short term punctures, gravel has the disadvantage of leaving prominent “dimples” in the geomembrane. If localised strain within or adjacent to a dimple exceeds a threshold strain (approximately 3-5% according to Rowe and Yu, 2019) stress cracking is likely to occur (over time) at this location. The onset of stress cracking is accelerated by the adverse conditions and elevated temperatures at the bottom of a landfill, and dimples from gravel could result in thousands of holes per hectare (Abdelaal et al. 2014). Given the different shape of TDA compared to gravel, a different dimple shape would be expected and may result in less strain.

An “apples to apples” comparison between TDA and gravel cannot really be made based on either Objective 1 or Objective 2 independently and separate from the other. The results of this study, as well as others previously (Brachman and Gudina 2008; Tognon et al. 2000) have indicated that a thick, nonwoven protection layer would be required if localised strains from coarse uniform gravel are to be kept to a minimum threshold. On the other hand, TDA will require a thick, nonwoven protection layer to reduce short term punctures from the high-risk wires, but may in fact perform better from a standpoint of long-term strains.

The objectives of this work were narrowed down as follows:

- A. *For the TDA material supplied by AR, what is the required thickness of geomembrane and nonwoven geotextile protection layer combination to reduce the number of holes per hectare to a reasonable number?*

B. Given adequate puncture prevention as determined in A) above, how does the localised distribution of strain (in dimples) vary between TDA and readily-available natural gravel?

The following conclusions can be made regarding Objective A:

- Based on the puncture testing program, it was found that geosynthetic protection layers of a reasonable thickness were unable to eliminate 100% of puncture through the geomembrane from TDA.
- Gravel under simulated loads with typical protection layers did not result in short term punctures, consistent with the findings of others (Brachman and Gudina 2008; Rowe et al. 2013).
- All geomembranes can be expected to be installed with some number of holes varying from 5-25 per hectare based on installation damage (Giroud 2016). Therefore, if less than 20 holes are expected for TDA, it falls within the range of holes that one might expect in design due to installation damage (given good geomembrane installation).

The following key recommendations are suggested to reduce expected punctures to less than 20 per hectare:

- a. Increase the size of TDA particles by reducing processing (ie. double pass instead of multi-pass)
- b. Limit the proportion of high-risk wires (see report for description) within the sample to under 2% and monitor to ensure processing is consistent
- c. Use a thicker geomembrane, e.g. 2 mm rather than 1.5 mm
- d. Use at minimum a 1088 g/m² protection layer or alternatively a soil protection layer (depending on local regulations, availability and constructability)

Since TDA is expected to puncture the geomembrane to some extent, it is important that this be accounted for in design and steps are taken to ensure leakage is kept to a minimum using a risk-based approach (Marcotte and Fleming 2019).

The following conclusions can be made regarding Objective B:

Results have demonstrated that TDA outperforms gravel with regards to undesirable tensile strains within the geomembrane.

For gravel, a very heavy (likely in excess of 2000 g/m²) would be required to severely limit or eliminate indentations where local strain exceeds 3%.

TDA, on the other hand induces less strain in the geomembrane. This finding actually understates the difference between gravel and TDA, given the known inaccuracies in the existing method used to date. A new method was developed and confirmed that Tognon's method inaccurately estimates strain. Specifically it was found to underestimate the strain for gravel and overestimate strains for TDA.

In summary, a thick non-woven protection layer is required for both TDA and gravel but for different failure mechanisms. However, when comparing the cost of TDA and gravel, the same thickness of geotextile protection layer (greater than 1088 g/m²) should be assumed.

The following report will presents the testing program and results. Further detailed test results are found in Appendices A-D.

The conclusions outlined in this report are limited to the scope of analysis and testing that was commissioned by AR:

- All testing was carried out using non-textured HDPE geomembranes of various thickness manufactured by Solmax International Inc. in Varennes, QC. Different polymers, or even HDPE geomembranes manufactured in different plants or by different manufacturers may yield different results;
- The effect of textured HDPE geomembranes was not considered;
- The vertical loads associated with landfills of small size (<15 m in height) or very large size (>50 m in height) were not considered;
- Loading was relatively rapid and represents undrained loading conditions. In order to evaluate the effects of slower drained loading a different experimental strategy would be required.
- The effects of varying levels of processing (i.e. single-pass, double-pass and multi-pass TDA) have not been characterized in a comprehensive, exhaustive manner, and the tentative conclusion stated in this report that there may be a benefit to reduced degree of processing must be read in that light.

2.0 Materials and Testing Equipment

2.1 Equipment

A large cylinder pressure device was used to evaluate puncture of the geomembrane under high loads that represent the large pressure of overlying waste. Many other researchers and industry professionals have developed devices to evaluate puncture and strains in geomembrane liners (Laine et al. 1988; Brummerman et al. 1994; Tognon 1999; Rowe et al. 2013). However, many of these devices utilize an air bladder to apply load. The drawback to an air bladder is the inability to undergo large vertical strain.

Pneumatic cylinders were selected to apply a constant load to the sample and to accommodate the large vertical strain expected to occur. Each pneumatic cylinder had a diameter of 254 mm (10 inches) and a stroke of 150 mm (6 inches). The air cylinders acted in tandem by attaching each of the rods to a 19.05 mm steel plate as shown in Figure 1. The maximum force that can be applied is 352 kN (88 kN per cylinder) at 1724 kPa (250 PSI) air pressure, which results in an applied sample pressure of 550 kPa. If the unit weight of municipal solid waste (MSW) is taken between 10-14 kN/m², this would represent a MSW landfill approximately 45 metres high.

To accommodate the large size of TDA, a cylindrical test apparatus with a sufficient diameter was required. The size was dictated by maximizing the diameter to particle size ratio, while also achieving a sufficiently high applied total pressure on the sample. The average diagonal TDA (multi-pass) particle length used in the testing was 96 mm. Therefore, a 901.7 mm inner diameter steel pipe (36 inch outer diameter) was selected due to its availability and ease of fabrication. This resulted in a test area of 0.639m².

A 445 kN load cell was mounted to the base of the plate as shown in Figure 1. A swivel button joint was machined to ensure the cylinders moved in tandem regardless of any differential vertical strain within the layer of TDA. The button ensured that minimal eccentric forces were transmitted to the load cell. The load button was machined to have a convex surface that would fit inside a concave surface on the load plate.

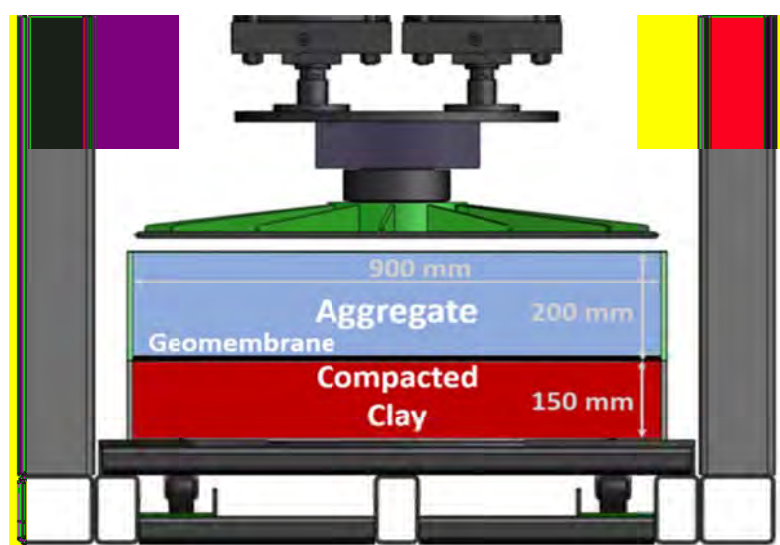


Figure 1: Schematic of test device

The device was designed in-house and fabricated at the U of S Engineering Machine Shops with laser-cutting of sheet metal at a local shop in Saskatoon. The test cylinder was designed to be two rings as shown in Figure 2. The upper (green) ring is removable which allows for surface preparation of the subgrade which is compacted in the lower (black) ring. The lower ring is 150 mm in height and the upper ring is 200 mm in height.



Figure 2: Large 0.9m diameter test device used for puncture testing using TDA (L) Smaller 0.4 m diameter test cylinders used for testing gravel (R)

The mass of the base assembly is approximately 400 kg when full of compacted clay. To facilitate ease of operation and testing, retractable wheels are used to move the cylinders and base in and out of the loading area and preparation area. By retracting or extending the wheels, the assembly can be slid in and out. The entire assemble weighs approximately 1600 kg. For comparison testing of gravel, smaller test cells of diameter 400 mm were fabricated and were placed in load frames as shown in Figure 2.

2.2 Materials Used

2.2.1 Clay materials

The importance of the clay subgrade or foundation layer has been well established for composite barriers subject to point loading (Rowe et al, 2013a). Multiple clay liner materials were sourced from Alberta, Saskatchewan, and Ontario. Standard index tests and proctor curves were completed for each as shown in Figure 3 and Table 1.

The TDA testing was primarily completed above the pottery clay, Battleford Till, and Floral Till. The other soils were used to evaluate the influence of subgrade on geomembrane strains, as the subgrade plays a key role in strains that develop. The clay is mixed in 40 kg batches using a paddle mixer. It is then stored in coolers, as shown in Figure 4, and placed in a moisture controlled room for at least 48 hours.

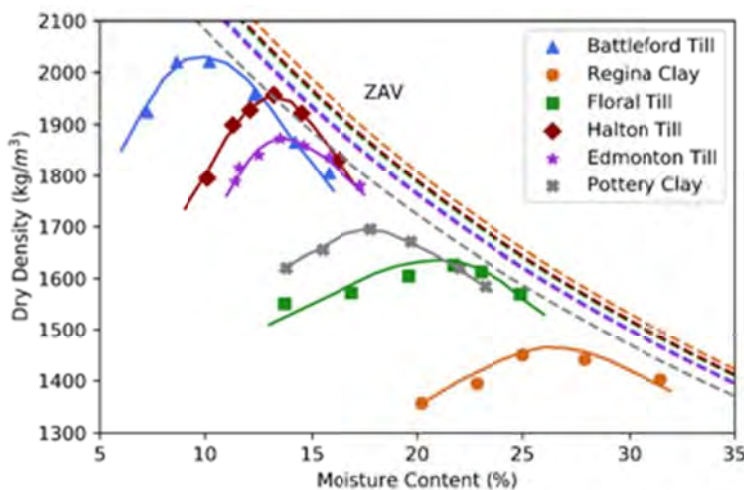


Figure 3: Proctor curves of clay soils tested

Table 1: Index properties of soil subgrades used in testing

Soil	USCS	G_s	LL (%)	PI (%)	Activity	w_{opt} (%)	ρ_{Dmax} (kg/m^3)	Sand & Gravel (%)	Silt (%)	Clay (%)
Regina Clay (southern Sask.)	CH	2.83	74.7	47.7	0.8	26.0	1460	21.0	21.0	58.0
Battleford Till (central Sask.)	CL	2.73	23.3	9.7	0.65	10.0	2030	49.5	35.6	14.9
Floral Till (central Sask.)	CL	2.78	42.9	20.9	0.54	21.0	1620	9.2	51.7	39.0
Halton Till (southern Ont.)	CL	2.79	31.5	13.5	0.75	13.0	1960	33.8	48.3	17.9
Edmonton Till (Alberta)	CL	2.72	32.8	17.8	0.87	13.5	1875	36.7	43.0	20.4
Pottery Clay	CL	2.63	46.0	27.2	0.64	18.0	1680	5.5	52.3	42.2

LL -liquid limit; PI – plasticity index; w_{opt} – optimum moisture content using standard compaction; ρ_{Dmax} – maximum dry density using standard compaction; G_s – Specific Gravity

The clay is then compacted in the test device to a specified density using a 22.7 kg large steel compacted hammer. It is important to ensure that the moisture and density of the clay are pre-determined and consistent as they can alter the magnitude of any measured deformations or strains (Marcotte & Fleming, 2019). Upon completion of a lift, multiple moisture samples and torvane measurements were taken to ensure variability and confirm soil conditions. The upper lift (50 mm) of soil is removed and replaced after each test. The entire clay is removed and replaced after approximately 5-6 tests. The final clay surface is smoothed with a large rolling pin, as shown in Figure 5, similar to a smooth drum roller used during placement in the field.

Compacted clayey soils used for liners are always compacted wet of the line of optimums to ensure adequately low hydraulic conductivity (Benson & Daniel 1990; Benson et al. 1999). Typically, shear strength of the soil is a secondary consideration. The upper water content limit has historically been based on the trafficability limit

(other geotechnical considerations aside); that is, the limit where excessive rutting does not occur (Leroueil et al. 1992). However, the wetter the soil, the higher the resulting geomembrane strains, as shown in Figure 6.



Figure 4: Left - 500 kg of clay in coolers for storage; Right - compaction of clay in cylinder and compaction hammer



Figure 5: Smoothed clay surface for testing

Therefore, from the perspective of localised areas of high strain in the geomembrane, it would be preferred to compact at lower water content (within the specifications) near the geomembrane, as long as sufficiently low hydraulic conductivity could be maintained. The type of clayey soil also affects the geomembrane strain differently, as seen by the Floral Till points falling above the best fit line and the Regina Clay points below the best fit line in Figure 6. This is further discussed in Section 4 and additional information about the role of the clayey soil in controlling geomembrane strains can be found in Marcotte and Fleming, 2019 (Attachment A).

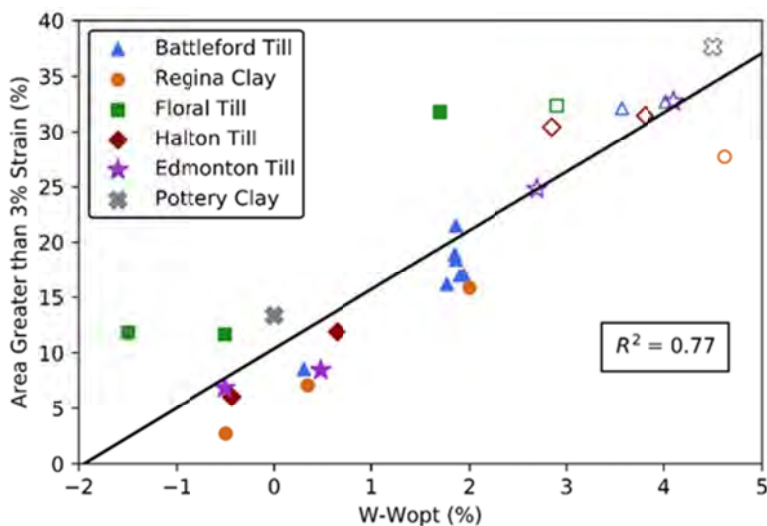


Figure 6: Geomembrane strain and compacted water content

2.2.2 Geomembranes

Geomembranes were received from Solmax in Varrennes, QC. Index properties as provided by the manufacturer are given in Table 2.

Table 2: Index properties of geomembranes

Geomembrane (mm)			1.5	2
Thickness (min)	ASTM D1599	mm	1.35	1.8
Density	ASTM D792	g/cm ³	>0.94	>0.94
Strength at Yield	ASTM 6693	kN/m	23	31
Elongation at Yield	ASTM 6693	%	13	13
Strength at Break	ASTM 6693	kN/m	43	57
Elongation at Break	ASTM 6693	%	700	700
Tear Resistance	ASTM D1004	N	187	250
Puncture Resistance	ASTM D4833	N	534	695

Testing with geomembranes manufactured at different plants or from other manufacturers may result in some variations with the results reported herein.

2.2.3 Geosynthetic protection layers

Various protection geotextiles were acquired from multiple manufacturers. Agru provided the nonwoven needle punched (NWNP) geotextiles. Skaps provided the planar drainage geocomposite (PDG). Tencate provided the woven geotextile (W). Heavier geotextiles were achieved by placing multiple layers of geotextiles above each other (Tognon et al. 2000). Therefore, a 1358 g/m² geotextile is actually a 544 g/m² placed above a 814 g/m² textile. As provided index properties are given in Table 3.

2.2.4 TDA and Gravel

Three different bulk samples of TDA were provided by AR as shown in Figure 7. The TDA varied based on the level of processing. A particle size distribution was completed manually, by individually measuring the mass, length and width (and documenting all exposed wire) for each of hundreds of TDA particles. Results

are presented below in Figure 8 as the equivalent dimension (square root of length X width). Less processing results in a large size, although the shape of the distribution remains relatively constant.

Table 3: Index properties of geotextiles

Thickness	Test Method	Units	NWNP	NWNP	PDG	W
		mm	-	-	6*	
Mass per Unit Area	ASTM D-5261	g/m ²	544	814	272**	
Grab Tensile	ASTM D-4632	N	1736	2002	1000**	
Elongations	ASTM D-4632	%	50	50	50**	
CBR Puncture	ASTM D-6241	kN	5	5.8	2.9**	
Trapezoidal Tear	ASTM D-4533	N	668	900	400**	
Apparent Opening Size	ASTM D-4751	mm	0.15	0.15	0.177**	
Tensile Strength @ 2% strain (MD)	ASTM D4595	kN/m				7
Tensile Strength @ 2% strain (CD)	ASTM D4595	kN/m				26.3
Apparent Opening Size		mm				0.425

Individual TDA particles may exhibit protruding wires and these may puncture a geomembrane. Not all wires cause puncture, however, so a key aspect of the material characterisation is to determine the proportion of high risk particles in a batch of TDA. Because the determination of what constitutes a high-risk TDA particle required puncture testing, this aspect of the work is reported separately in Section 3.2.

Sub-angular crushed gravel was sourced locally in Saskatoon. This material was between 50.8 mm and 31.5 mm with 65% passing the 37.5 mm screen. The gravel was routinely screened to ensure large particles were used. For comparison, rounded less-uniform drainage stone was collected during construction of a landfill cell in north-central Alberta. Both materials are shown along with multi-pass TDA in Figure 9.



Figure 7: Tire derived aggregate samples: left - multi pass, middle – double pass, right – single pass

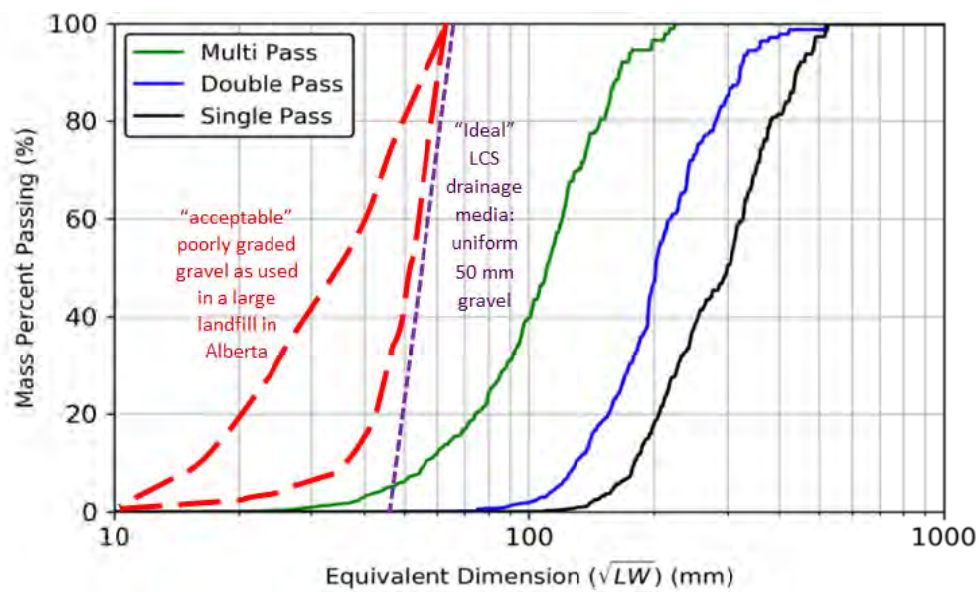


Figure 8: Size distribution of single, double and multi-pass TDA samples by hand sorting and gravel by conventional sieve analysis

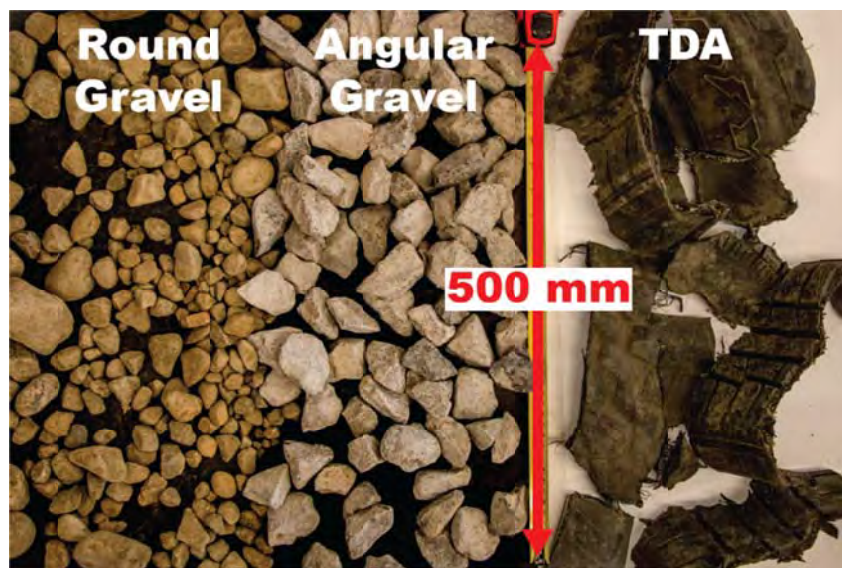


Figure 9: Size comparison of gravel to multi-pass TDA

3.0 Details of Puncture Testing Results

3.1 Overall Strategy for Puncture Testing

A custom testing apparatus was constructed to carry out puncture testing (see Figures 1,2). While large (900 mm diameter), the geomembrane sample represents only 0.6 m² and a single puncture would represent thousands of punctures per hectare at field scale. It is obviously not practical to carry out thousands of replicate tests for each test configuration (protective layer thickness). Accordingly, placing TDA randomly over the geomembrane was not a viable testing strategy. To quantify the rate of puncture on a larger area, the puncture testing was therefore carried out by evaluating three controlling factors:

1. Proportion of high-risk wires within a sample of TDA;
2. Probability of landing with the wires facing the geomembrane (“unfavourably”);
3. Probability of puncturing the geomembrane/geotextile protection layer given that they land unfavourably (in other words the protection layer efficiency).

By evaluating the three factors, the probability of a TDA piece containing a wire, landing unfavourably, and subsequently puncturing the liner and protection layer could be estimated for a larger area. Each factor will now be described in detail.

3.2 Proportion of High-risk Wires (Factor 1)

3.2.1 Evaluation of Wire Types

A majority of the TDA particles contain some sort of protruding wire, however, most are not rigid enough to cause puncture and buckle under any load. Of the wires that are rigid enough, the arrangement, length, and orientation of the wires differs from piece to piece. Before a proportion of high-risk wires could be determined, the wires that are most ‘high risk’ for geomembrane puncture had to be determined.

To evaluate the different wire types, TDA pieces were selected to be representative of the different wires shapes and sizes in a given sample. Some of the pieces contained individual wires, whereas others contained short bundles of wires.

A number of preliminary puncture tests were completed to evaluate what types of wires have the potential to puncture the geomembrane. Each piece was placed intentionally in an unfavourable orientation (in terms of the geomembrane) to try to induce puncture. Images of punctures are shown in Figure 10. A total of twelve initial tests were completed with relatively light protection layers. A summary is given in Table 4.

The holes ranged from 1mm in diameter when caused by individual wires, to 5 mm in diameter when caused by groupings of wires. When heavier protection layers were used, large groups of wires did not puncture the geomembrane, but rather resulted in indentations similar to gravel. In the range 200-460 kPa, no significant trend was found to occur with pressure, as shown in Figure 11. It is expected that the force required to puncture would decrease with reduced pressure (Koerner et al. 2012). However, to eliminate another variable, all further testing was completed at 500 kPa to remain conservative.



Figure 10: Punctures of the geomembrane by different types of wires

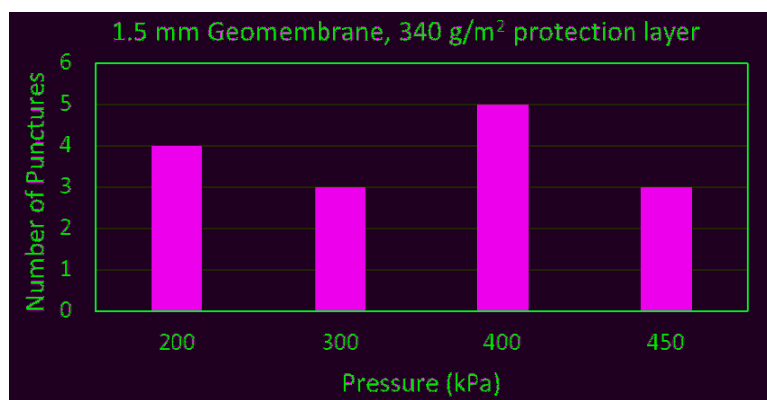


Figure 11: Geomembrane puncture and pressure

Table 4: Summary of preliminary test results to determine high-risk wire types

Test ID	Geomembrane Thickness (mm)	Protection Layer MUA (g/m ²)	Pressure Applied (kPa)	HR	MR	LR
GS10	1.5	None	200	3	1	1
GS11	1.5	340	300	2	1	
GS12	1.5	340	400	5		
GS13	1.5	340	200	3	1	
GS14	1.5	340	450	2	1	
GS15	1.5	542	550	1		
GS16	1.5	PGD	550	4		
GS17	2	None	350	3	2	
GS18	2	PDG	350	1		
GS19	2	680	550	5		
GS20	2	340	350			
GS21	2	400	500	3		
GS22	3	None	350			

HR – High risk; MR – Medium risk; LR – low risk

3.2.2 Classification of Pieces

Based on the results in of the preliminary testing, the TDA particles were classified as either high, medium, or low risk as shown in Figure 12. Additional images of example high, medium, and low risk pieces are given in Appendix A: Classification of High-risk Pieces. Medium and low risk pieces pose little to no risk when used in conjunction with a 2.0 mm geomembrane and a sufficient protection layer (at least 1088 g/m²).

The TDA particles were classified based on the following characteristics, as shown in Figure 12.

- High (Category A): contains at least 1 rigid individual wire (1-2 mm in diameter). May also be a group of wires, where one wire protrudes out longer than the others surrounding it.
- Medium (Category B): contains groups of wires that are the same length (+-2 mm in length) and are grouped together
- Low risk (Category C): contains group of rigid wires, with no wires protruding further than the other

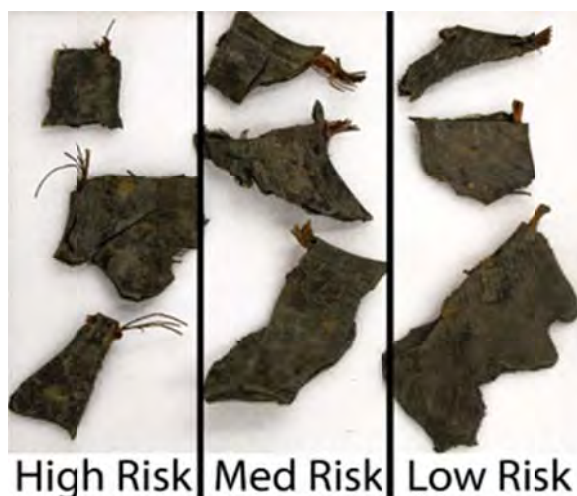


Figure 12: From left to right: high (A), medium (B), and low (C) risk TDA for puncture of geomembranes

3.2.3 Proportions of High-risk Wires

To evaluate the proportion of pieces with high-risk wires, large random bulk samples of as supplied TDA were sorted into bins of high, medium, low and no risk and the results are given in Table 5.

Table 5: Proportion of high risk wires in single, double, and multi pass TDA

Risk	Single Pass		Double Pass		Multi-Pass	
	#	%	#	%	#	%
High (A)	10	3.1	28	1.9	25	1.8
None	300	92.9	1390	94.3	1323	95.5
Sample Mass (kg)	88.8		430		134	

The results suggest that the proportion of high-risk wires is independent of the number of passes. However, the proportion of high-risk wires should be kept to a minimum (no higher than 3%) and processing methods should be evaluated accordingly. Conversations with the processor have indicated that the sharpness and age of the shears effect the quality, and periodic checks should be made to confirm the proportion of high-risk wires.

To estimate variability between different people estimating the high-risk wire proportions, 100 pieces including high, medium, and low risk was given to two individuals with no prior experience with TDA. Based on the description and picture above, the sample was sorted into its categories, with results given in Table 6.

Table 6: Variability when sorting TDA

Risk	Author	Person 2	Person 3
High (A)	26	23	27
Med (B)	20	17	23
Low (C)	17	22	15
None	37	38	35
Total	100	100	100

As can be seen in Table 6, there is relatively low variability between people when sorting TDA if given the above description. While a subjective process, it seems sufficiently consistent from person to person. This is promising in terms of QA/QC for geomembranes with high-risk wires.

3.3 Probability of TDA Landing in an Unfavourable Manner (Factor 2)

If a TDA piece contains a high-risk wire, it is only at risk of puncturing a liner if the piece lands such that the wire is oriented towards the geomembrane. A large box was constructed, filled with TDA, frozen and flipped to evaluate the probability of TDA landing “unfavourably” (wires facing towards geomembrane). The box was filled with TDA by dumping from a loader bucket to simulate field operations as shown in Figure 13.

Hot water was used to slowly reveal the lowest (upper) layer of the frozen ice block while visually inspecting the surface for wires. A sample of double pass TDA is shown in Figure 14. Images from the tests with multi-pass TDA can be found in Appendix B.

Four frozen TDA ice box flip tests were completed. A smaller box was constructed to evaluate the probability of TDA pieces falling unfavourably when a larger proportion of high risk pieces are intentionally placed in the

sample so that they would fall near the bottom. 145 high-risk TDA pieces were selected and the corner of the piece with the wire was spray painted bright pink. A large plastic tote was filled and dumped into the box with regular and painted high risk TDA to increase the probability of the high risk landing on the bottom of the box. An image of the resulting ice blocks are given in Figure 15 for two duplicate tests.



Figure 13: Simulated field placement of TDA into constructed wooden box and flipping of ice block

The surface was carefully examined to check if pieces had landed unfavourably, as shown in example photos in Figure 16. Every piece near the bottom was counted, and those pieces landing with unfavourable orientation were identified and counted.

From the small ice box testing, the probability of a high-risk TDA piece landing with unfavourable orientation (with the wires facing the geomembrane) was estimated to be approximately 7%. The results of the ice block testing are summarised in Table 7. The results of the controlled small box confirm the results of the random large box test. In the large box multi pass test, approximately 485 pieces landed near the bottom. Assuming 2% of pieces are high risk, this equates to about 10 high risk pieces at the bottom. If only 7% of those pieces land with unfavourable orientation, one would expect at most only 1 high risk piece to orient unfavourably during the test – which is what occurred from a completely random sample of multi-pass TDA. The small block testing may really be considered a “reality check” for the large box results.

It should be emphasized that whether or not a TDA piece lands unfavourably is not really binary (0 or 1), however for simplicity and practical application of these results it may be considered to be so. During examination, this was interpreted conservatively (I.e. a very liberal definition of “unfavourable orientation”).

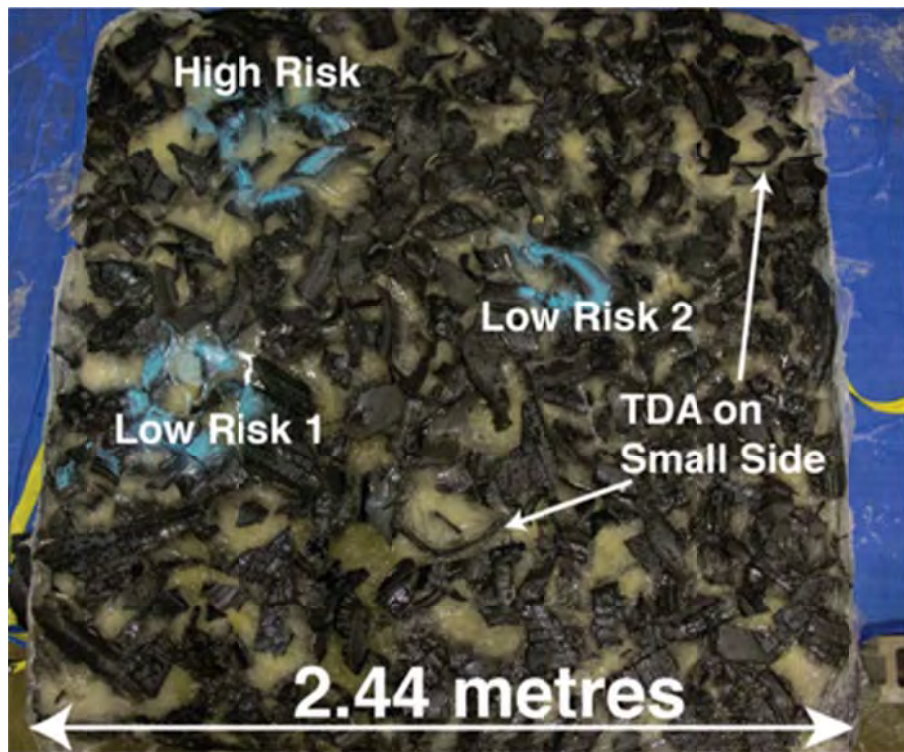


Figure 14: Frozen double pass TDA sample representing the orientation of the TDA that would be in contact with a geomembrane

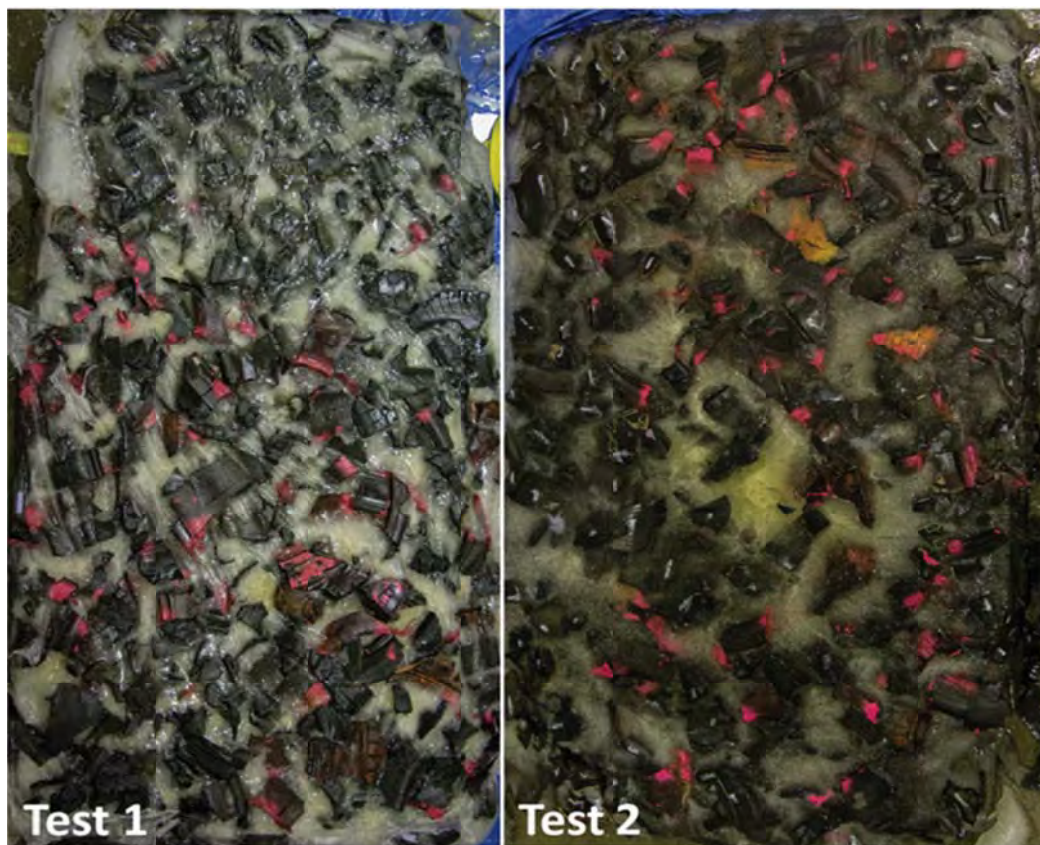


Figure 15: Frozen small ice block testing with labeled high risk pink pieces



Figure 16: High risk multi pass TDA oriented unfavourably in small box test

Table 7: Data from frozen ice block testing

	Total Pieces	Pieces on Bottom	Area of Test	TDA/m ²	High Risk on Bottom	HR Landed Unfavourably	Probability of Landing Unfavourably
Small Box							
MP 1	1250	150	2.4	63	65	5	7.7%
MP 2	1250	150	2.4	63	69	4	5.8%
Average		150	2.4	62.5	67	4.5	7%
Large Box							
Multi Pass	3600	485	6	81		1	
Double Pass	1390	244	6	41		1	

A second important piece of information from the frozen block testing is the number of pieces on the bottom. Larger particle size results in a reduction of pieces near the bottom (larger pieces results in fewer pieces over the same area). This is beneficial since fewer pieces near the bottom (while the proportion of high-risk pieces is relatively constant, see Table 5) would directly result in less high-risk pieces near the bottom. For this reason, it is recommended that reduced processing and larger particle sizes may reduce punctures.

3.4 Protection Layer Efficiency (Factor 3)

If a TDA piece has a protruding high-risk wire and lands in such a way that the wire is facing the geomembrane (unfavourably), there is also a chance that the protection layer prevents a puncture. The protection efficiency of the geomembrane represents the ability of the geomembrane/protection layer system to prevent puncture. For each case, a higher proportion of high risk pieces were intentionally placed on the geomembrane to try to induce puncture, as shown in Figure 17, thus testing the efficiency of the protection layer/geomembrane given that multiple pieces had “landed” with unfavourable orientation.



Figure 17: Intentionally placed TDA pieces on geotextile protection layer above geomembrane to test protection efficiency

A number of geomembranes and geotextile protection materials were evaluated, as described above in Section 2.2.3. A summary of results is given in Table 8. Results of all 22 individual tests are given in Appendix C.

In general, better performance could be expected with a 2.0 mm geomembrane as opposed to a 1.5 mm geomembrane. It is therefore recommended that at least 2.0 mm geomembranes be used in conjunction with TDA, with improved performance expected for thicker geomembranes as well (2.5 mm or 3.0 mm). At least a 1088 g/m² geotextile cushion should be used to ensure a protection layer efficiency of at least 97%. Alternative protection layers such as woven geotextiles or planar drainage geocomposites were found to perform no better than a thick nonwoven geotextile. If permitted, a sand or soil protection layer should eliminate all punctures, given it can be placed without construction damage to the geomembrane. A few example images of puncture can be seen in Figure 18.

Table 8: Summary of puncture protection efficiency results

GM	Protection Layer	MUA	# Tests	# High Risk	# Punctures	Probability Puncture	Protection Efficiency
1.5	NWNP	544	1	15	5	33.3%	66.7%
		814	1	15	3	20.0%	80.0%
		1088	1	15	2	13.3%	86.7%
		1358	2	55	4	7.3%	92.7%
		1628	2	55	2	3.6%	96.4%
2	NWNP	1088	3	120	2	1.7%	98.3%
		1358	3	120	4	3.3%	96.7%
		1628	3	120	3	2.5%	97.5%
		2442	1	40	0	0% (1 test only)	100%
2	NWNP+W	814	1	40	1	2.5%	97.5%
	NWNP+W	1358	1	40	1	2.5%	97.5%
	PDG+NWNP	814	1	40	1	2.5%	97.5%

GM – geomembrane thickness (mm); NWNP – nonwoven needlepunched; PDG – planar drainage geocomposite; W – woven geotextile; MUA – mass per unit area (g/m²)

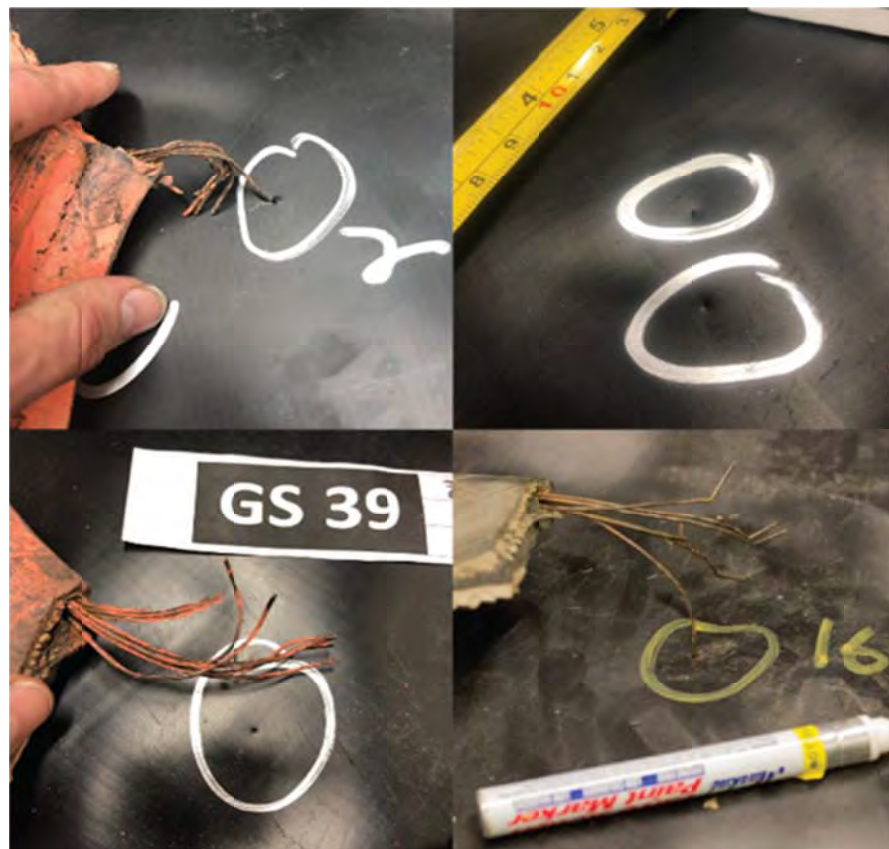


Figure 18: Punctures of geomembrane

3.5 Estimating number of punctures at field scale

Given the results of each factor as described previously, the anticipated number of holes per hectare may be estimated using Equation 1 with: the number of pieces near the bottom; the proportion of high risk pieces; the probability of landing unfavourably; and the puncture protection efficiency.

$$H = (0.07)(T_{bot})(P_{hr})(1 - E_p)(A) \quad \text{Eq. 1}$$

Where H is number of holes, T_{bot} is the number of pieces on the bottom layer (pieces/m^2), P_{hr} is the proportion of high risk pieces (fraction) and E_p is the efficiency of the protection layer (fraction), and A is the area (m^2). The 0.07 represents the probability of a TDA piece landing unfavourably. Table 9 presents the values and the anticipated number of punctures per hectare assuming the protection layer is a nonwoven geotextile with mass per unit area 1088 g/m^2 with a protection efficiency of about 97.5%.

The following conclusions can be drawn from the results:

- Less processing results in a larger particle size, and therefore fewer pieces at the bottom. This in turn reduces the expected number of holes per hectare.
- If the proportion of high-risk wires is increased, there will be an increase in the number of expected holes. At the current time, limiting the proportion of high-risk wires to less than 2.5-3% appears to be a reasonable and achievable objective for manufacturers and QA/QC protocols should reflect this.

- A protection layer efficiency of at least 97% is recommended. Based on the materials used in this study, this represents at minimum a 2.0 mm geomembrane with a 1088 g/m² nonwoven needle punched geotextile protection layer.

Table 9: Probability of puncture based on test results

	Single Pass	Double Pass	Multi Pass
Bottom pieces per m ²	25	41	72
Bottom pieces per Ha (10 ⁵)	2.5	4.1	7.2
High risk proportion	3.1%	1.9%	1.8%
Bottom high risk per Ha	7,750	7,790	12,960
Probability landing unfavourably	7%	7%	7%
High risk unfavourably per hectare	523	525	874
Protection efficiency*	97.5%	97.5%	97.5%
Punctures per hectare	13	13	22

* Protection efficiency is for a 2.0 mm geomembrane with a 1088 g/m² nonwoven protection layer

For example, if a 1088 g/m² non-woven geotextile is placed above a 2.0 mm geomembrane and double pass TDA is used (high risk proportion = 1.9%), approximately 13 holes per hectare (diameter of 1 mm) could be anticipated to occur and be accounted for during design.

4.0 Details of Strain Testing and Results

4.1 Strain in Geomembranes

If short term punctures do not occur, another concern with large angular aggregate such as TDA and gravel is stress induced cracking from indentations in the geomembrane. The weight of the overlying waste and non-uniform loading of the geomembrane results in indentations. Strains (localized stretching of the geomembrane) from these indentations must be kept to a minimum to ensure the longest service life possible. A typical target strain threshold is 3% (Rowe and Yu 2019). Protection layers, such as geotextiles or layers of sand are often placed over the geomembrane to limit strains to this target threshold. Several researchers have suggested that very heavy nonwoven protection layers exceeding 2000 g/m^2 may be required to control geomembrane strains (Tognon et al. 2000; Brachman et al. 2018). Abdelaal et al. (2014) warn that using less an insufficient protection layer could result in potentially thousands of holes per hectare considering the number of localized strain concentrations susceptible to stress cracking that result from point loading by gravel particles. Furthermore, the subgrade should be compacted as stiff as possible (high shear strength and density) as the clay plays a major role in the development of geomembrane strains (Marcotte and Fleming 2019).

4.2 Estimating the Strain Distribution from Point loading

The complex pattern of strain induced in a geomembrane by point loading from gravel has been evaluated through scanning the surface of a lead sheet placed between the geomembrane and the underlying clay to acquire a surrogate profile of the geomembrane (i.e. Brachman and Gudina 2008; Brachman and Sabir 2013; Hornsey and Wishaw 2012; Tognon et al. 2000).

To actually estimate the amount of strain in and around these localised dimples, the method that is most widely used was developed by Tognon et al. (2000). Using kinematic deformations to estimate strain at a given location, this method considers the membrane and bending components of strain through numerical approximations. The estimate of membrane strain is based, in part on an assumption of zero shear strain and that every point is displaced solely in the vertical direction, which is a significant simplification that leads to inaccuracies in the estimated strain.

Despite its known limitations, Tognon's method is in practical terms best practice for estimating localised strain from irregular point loading (Rowe and Yu 2019). Recent research however, has demonstrated that it inaccurately estimates strain (Eldesouky and Brachman 2018). The current research suggests that Tognon's method underestimates strain for small and deep dimples, such as those caused by gravel. The study also indicates that Tognon's method may overestimates strain in large dimples, such as those caused by TDA (Eldesouky and Brachman 2018). Tognon's method can still be used to evaluate TDA and gravel strain, but may well be overestimating strains from TDA and underestimating strains from gravel.

In Section 4.5, the effect of Tognon's simplifying assumption is evaluated, through application of a novel (and very time consuming) method that attempts to measure lateral and radial displacements of thousands of points on the surface of a geomembrane.

Using Tognon's simplified approximation, and a grid of points with uniform horizontal spacing (Δx), using the measured vertical positions (z), the membrane strain can be approximated by:

$$\varepsilon_M = \sqrt{\left[1 + \left(\frac{1}{2\Delta x} [z_{i+\Delta x} - z_{i-\Delta x}]\right)\right]} - 1 \quad \text{Eq. 2}$$

Where $z_{i+\Delta x}$ and $z_{i-\Delta x}$ are the vertical displacements at point $i+\Delta x$ and $i-\Delta x$, and Δx is the horizontal spacing. The bending strain considers differences in strain through the thickness of the geomembrane (Brachman & Eastman, 2013). The bending strain will be the greatest at the geomembrane surface and zero at the middle. It is considered by a second-order finite difference approximation:

$$\varepsilon_B = \frac{m}{(\Delta x)^2} [z_{i+\Delta x} - 2z_i + z_{i-\Delta x}] \quad \text{Eq. 3}$$

Where m is the distance from the centre of the geomembrane. The resulting strain is the sum of the membrane and bending strain:

$$\varepsilon_T = \varepsilon_M + \varepsilon_B \quad \text{Eq. 4}$$

In the current testing program, the areal distribution of strain was calculated using Tognon's combined bending and membrane strain (Tognon et al. 2000) with the grid scanning method developed by Hornsey and Wishaw (2012) as described in the introduction. A uniform 1.5 mm by 1.5 mm grid was developed and elevation values from the digital elevation model were interpolated onto each grid "cell". For each cell, the membrane strain for the geomembrane was computed using Eq. 1 for the eight surrounding neighbor cells – two orthogonal and two diagonal calculations.

Similarly, bending strain was calculated using Eq. 2 for the surrounding orthogonal and diagonal cells. The bending strain was calculated for both the bottom and top of the geomembrane. The total maximum calculated strain was then the sum of the maximum bending and maximum membrane strain for each grid point. The total maximum strain was then assigned to the strain array. The procedure continued iterating until all strains were calculated across the grid.

4.3 Photogrammetry Procedure

Laser scanners (LIDAR) have been used to develop profiles of deformed lead sheets for evaluating geomembrane strains. However, high resolution laser scanners are often expensive. A new method was developed to create a mesh of the deformed surface using photogrammetry. It requires a digital camera and a computer sufficiently powerful enough to perform the calculations. Photogrammetry involves the triangulation of common points between overlapping images. Once common points from multiple images are obtained, relative distances and camera orientations can be calculated. To relate the relative distances to real-world distances, a scale bar must be placed within the scene as shown in Figure 19. To facilitate the matching of points, the clay surface was spray painted with multiple colours in a random speckle pattern.

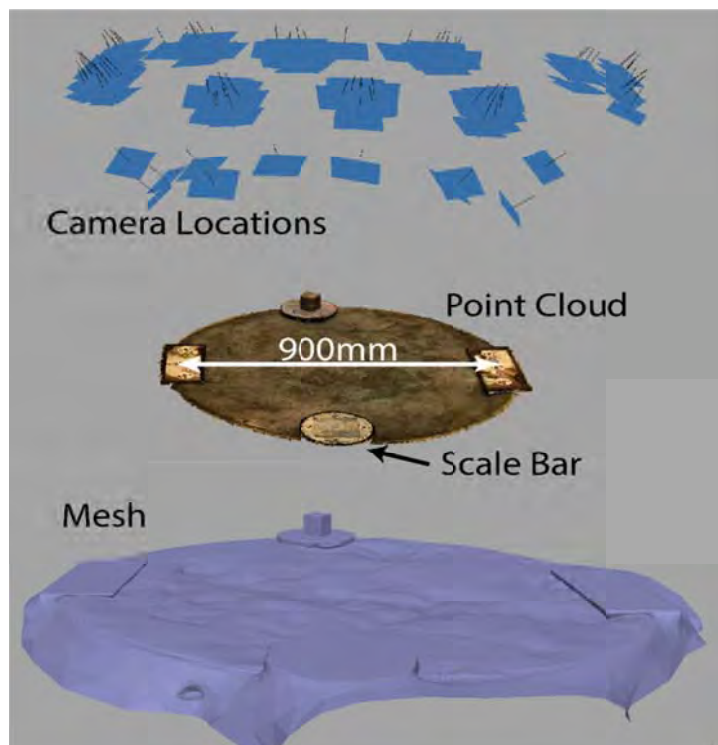


Figure 19: Photogrammetry and mesh creation

The mesh was interpreted onto a uniform grid. Strain was calculated for each point using the equations developed by Tognon et al. (2000) and the mesh calculation method developed by Hornsey and Wishaw (2012).

4.4 Strain Results using Tognon's Method

Although incorrect, the method developed by Tognon is simple, quick, and can be used to evaluate different test configurations. Multiple tests were completed to evaluate and compare the relative performance of TDA and gravel under identical conditions. Additional strain maps can be found in Appendix D.

Although likely insufficient, a 544 g/m² geotextile is a commonly used protection layer for gravel in practice. Duplicate tests were completed for gravel and TDA as shown in Figure 20. Both tests were completed above a Battleford Till compacted clayey soil liner compacted at approximately 2% wet of standard Proctor Optimum and at 100% relative Proctor compaction.

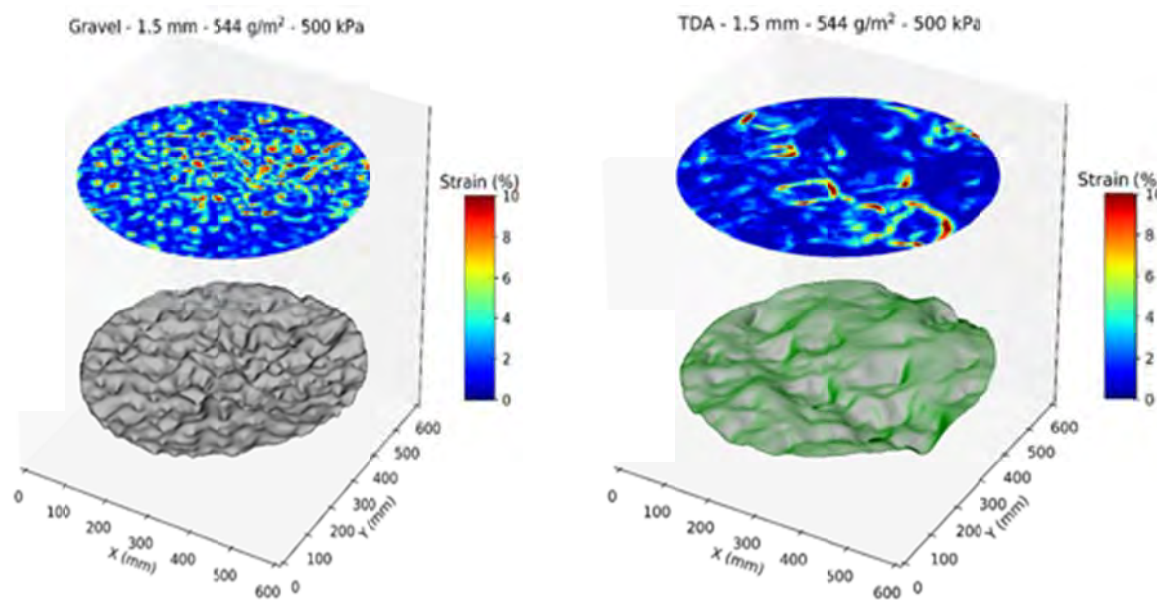


Figure 20: Deformed surface (vertically exaggerated) and resulting interpreted strain map for 1.5 mm geomembrane loaded by gravel and TDA at 500 kPa with a 544g/m² protection layer

The large TDA particles result in fewer areas of high localised strain when compared to gravel. Based on the recommendations of the puncture testing as described previously, a minimum of 2.0 mm thick geomembrane with a 1088 g/m² geotextile was used to ensure performance with TDA. The test configuration was done for both TDA and gravel and is shown in Figure 21.

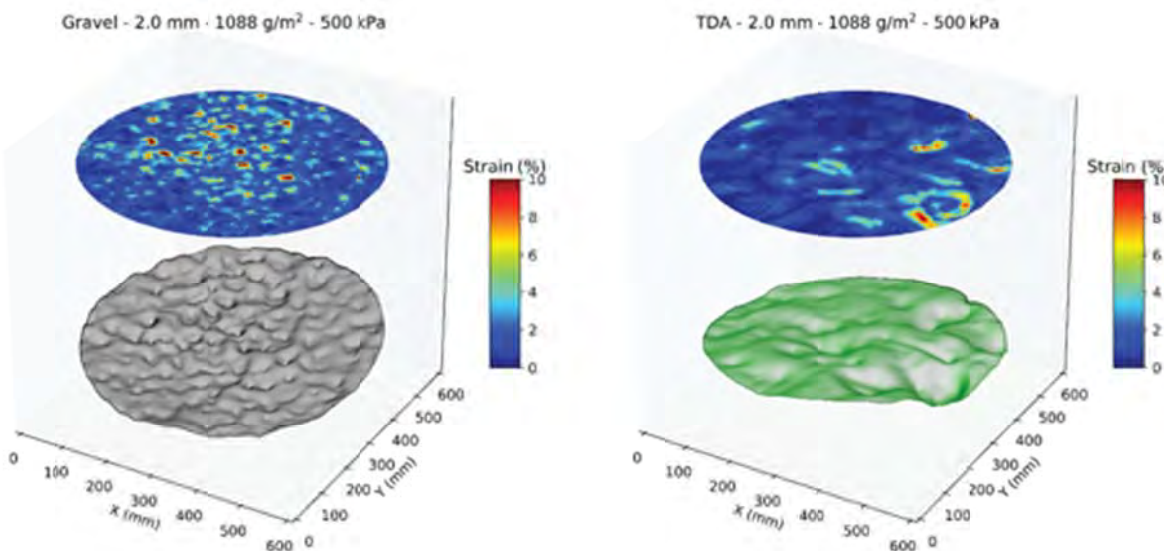


Figure 21: Deformed surface (vertically exaggerated) and resulting interpreted strain map for 2.0 mm geomembrane loaded by gravel and TDA at 500 kPa with a 1088g/m² protection layer

The cumulative percent of the area exceeding the threshold can be used to best compare the relative performance between the two aggregates as shown in Figure 22. Often, 3% strain is a common target “threshold” strain when calculated using Tognon’s method (Rowe and Yu 2019).

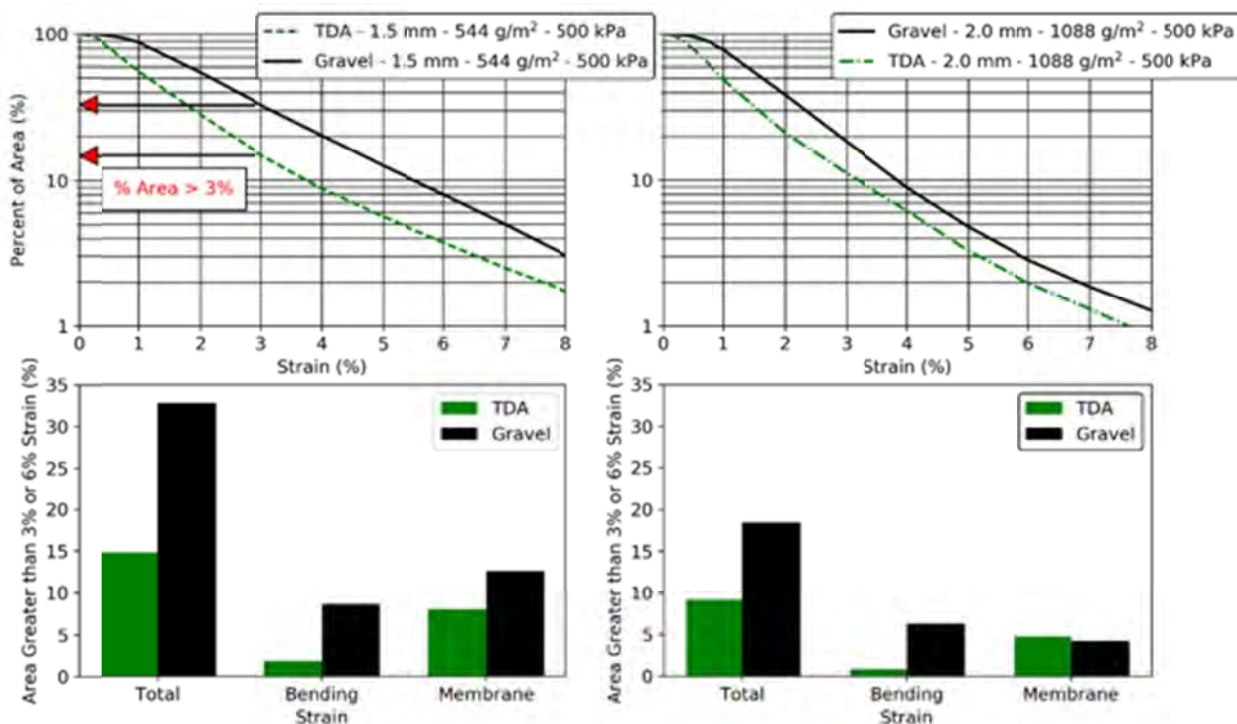


Figure 22: Strain area distributions for TDA and gravel under similar conditions

A common protection layer in Western Canada is often a 544 g/m² geotextile above a 1.5 mm geomembrane for gravel. However, this protection layer is likely insufficient, and could potentially result in many thousands of holes per hectare if subject to adverse conditions (Abdelaal et al. 2014). When compared to TDA, from a strain standpoint (under the same conditions), the TDA performs significantly better (the gravel had double the area of TDA exceeding the threshold strain in both cases).

However, as demonstrated in the previous section, a 544g/m² geotextile and a 1.5 mm geomembrane would be insufficient in limiting short term punctures from TDA wires. As previously stated, it is recommended that a 2.0 mm geomembrane and a 1088 g/m² protection layer is used for TDA to prevent wire puncture. Under these conditions, gravel and TDA still result in a proportion of the area exceeding the 3% threshold, but again TDA outperformed gravel in terms of strains. Heavier protection layers further decrease strains in TDA and protection layers in excess of 2000 g/m² are expected to keep strains greater than 3% to a minimum.

4.5 Strain Estimations using New Method

To evaluate the strains in the geomembrane without the simplifying assumptions used by Tognon, a new test method was developed. The new method considers radial or lateral displacements, thus reducing the known inaccuracy associated with the simplifying assumptions inherent in Tognon's method. A challenge with measuring strain in the geomembrane is that the geomembrane rebounds elastically and viscoelastically.

To overcome the challenge of rebound, the geomembrane was secured in place using epoxy. A precise 4mm grid was produced on the surface of a white geomembrane using a laser cut stencil as shown in Figure 23.

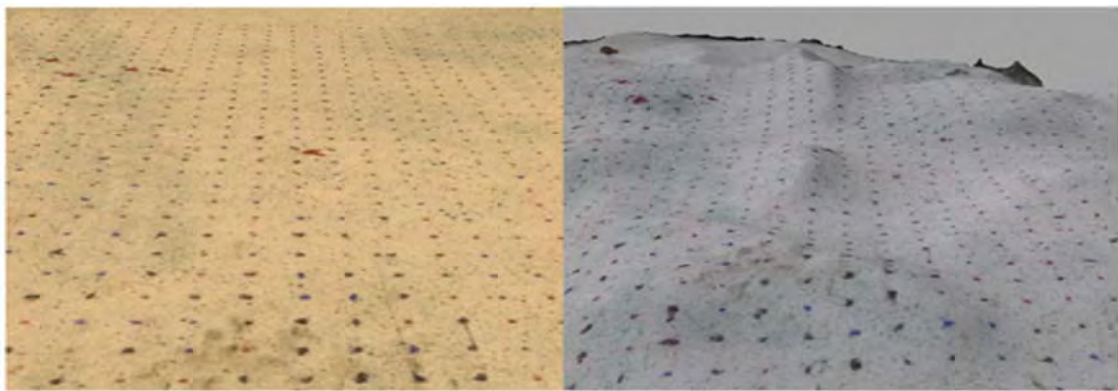


Figure 23: Pattern on geomembrane: Left - before strain; Right - after strain

The geomembrane was placed with the grid pattern down on the compacted clay. Very slow cure epoxy was added into above the geomembrane prior to the placement of gravel as shown in Figure 24. Once gravel was added, load was applied to deform the geomembrane while also locking the strains in place.

Once the epoxy had cured, the geomembrane was removed and the photogrammetry procedure was performed to create a three dimensional mesh. The deformed coordinates for each marked point were found based on the reference scale bar. The strain calculation method used by Vogel and Lee (1989) was performed for all 3,600 points in the grid to determine the engineering strain and a strain map is shown in Figure 25. To compare, Tognon's method was calculated over the same area using the same 4 mm regular grid spacing. A strain map using Tognon's method is given in Figure 26.



Figure 24: Epoxy and gravel in test cylinder to determine geomembrane strains

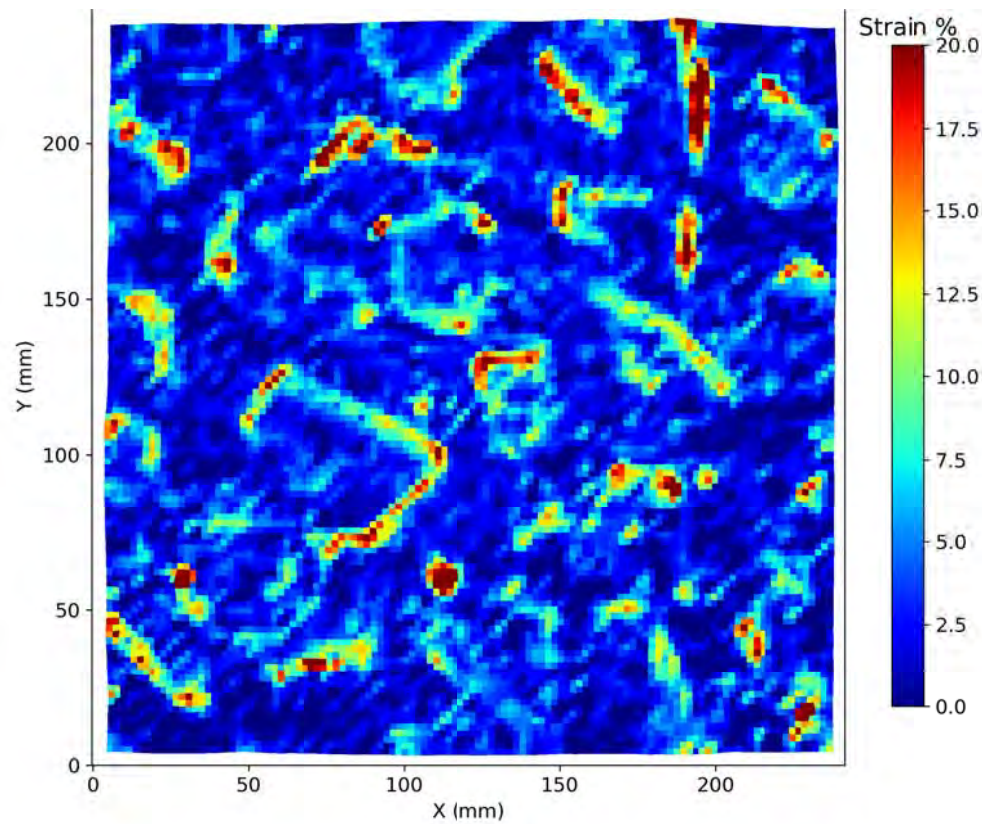


Figure 25: Strain map of epoxy gravel test based on new method

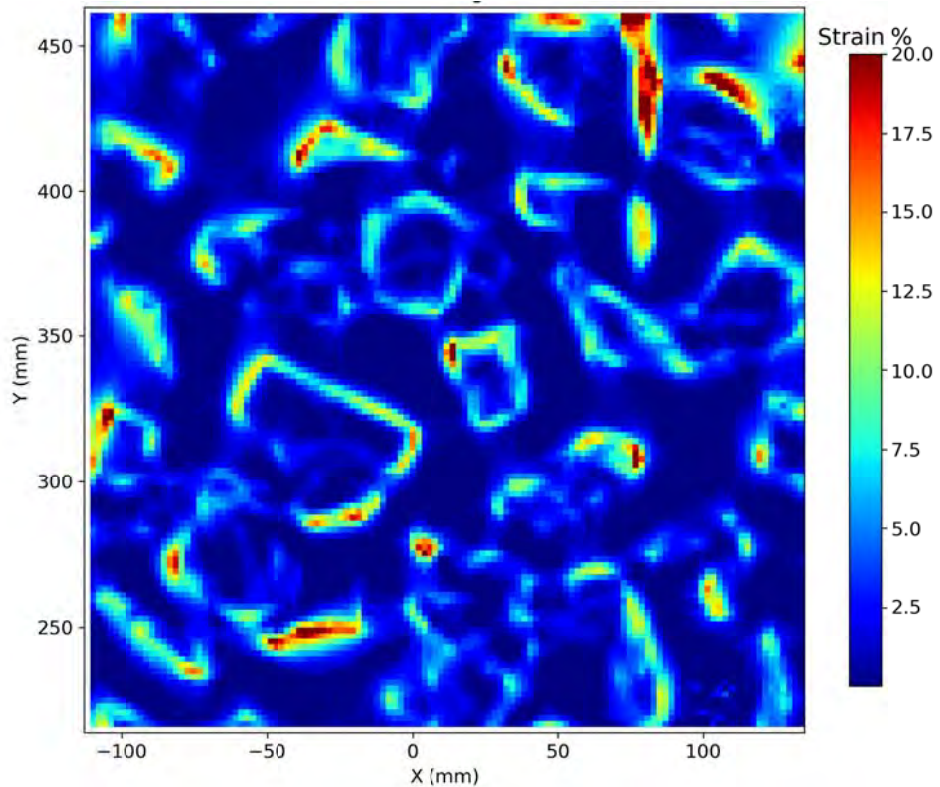


Figure 26: Strain map of gravel epoxy test using the method developed by Tognon

The similarity of the two strain maps demonstrate that both methods predict the areas of high strain. However, the magnitude of the strain when calculated using the epoxy method is larger, shown clearly by comparing the strain area distribution in Figure 27. Strain area distribution (SAD) curves give the percentage of the total area that exceeds a threshold strain. As expected, based on the work by Eldousouky and Brachman (2018), the Tognon method underestimates the strain for dimples that are deep and narrow such as those caused by gravel.

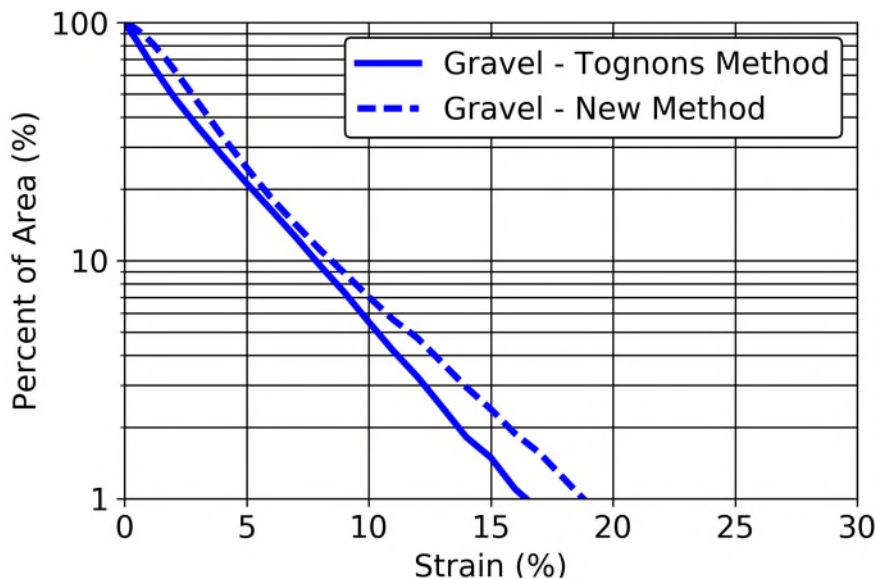


Figure 27: Strain area distribution comparing methods of calculating strain for gravel

The procedure was repeated using TDA (no protection layer) with a grid of 11,236 pre-marked points. The resulting strain maps using the new method and Tognon's method are shown in Figure 28 and Figure 29 respectively.

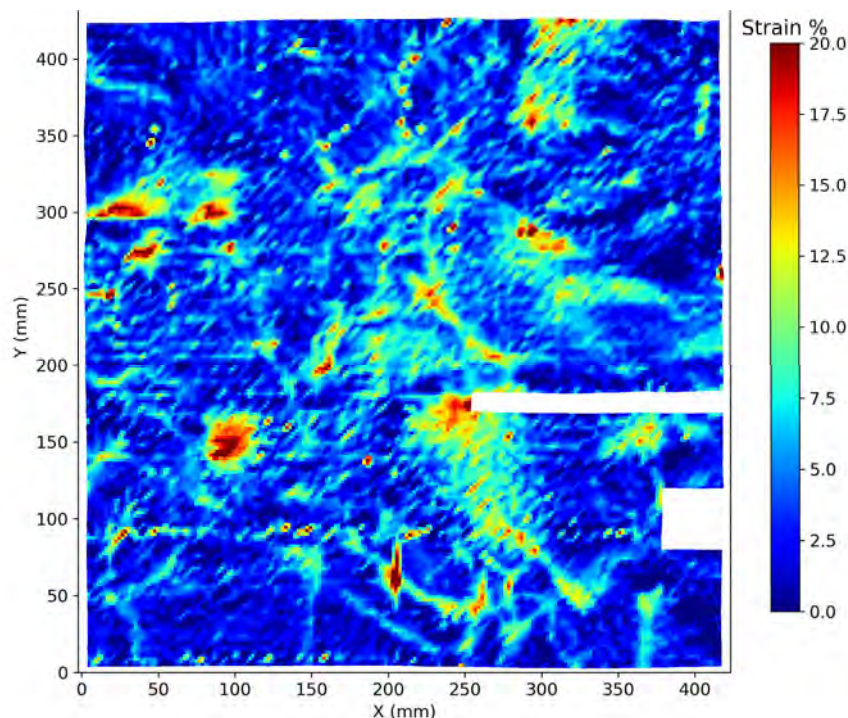


Figure 28: Strain map of epoxy TDA test by new method (white areas are where epoxy stuck to the geomembrane obscured the grid)

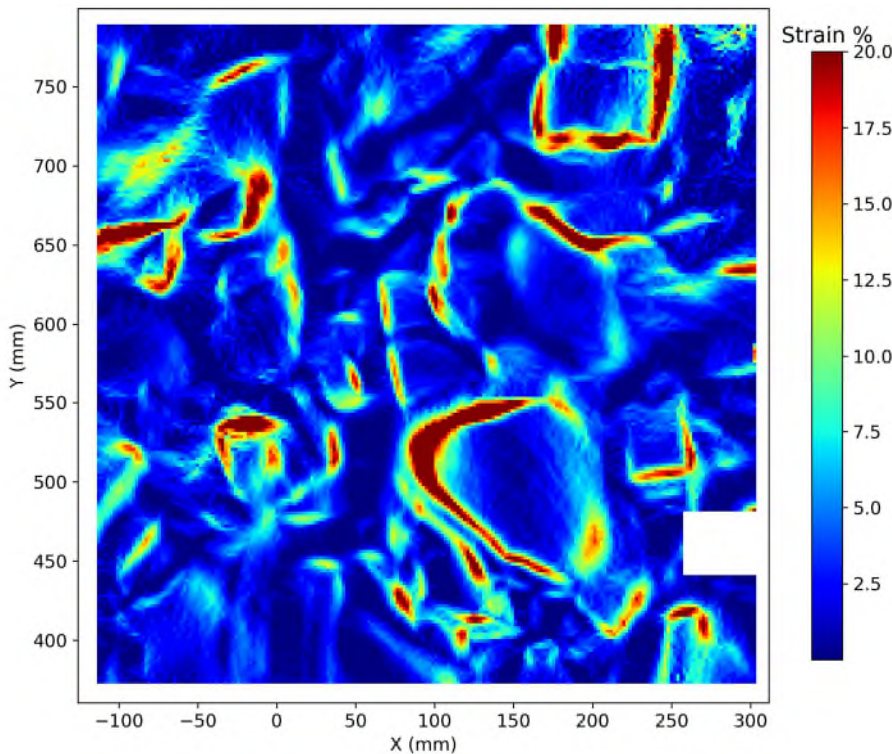


Figure 29: Strain map of epoxy TDA test using the method developed by Tognon

A comparison of the SAD distribution calculated using the two methods for TDA is shown below in Figure 30.

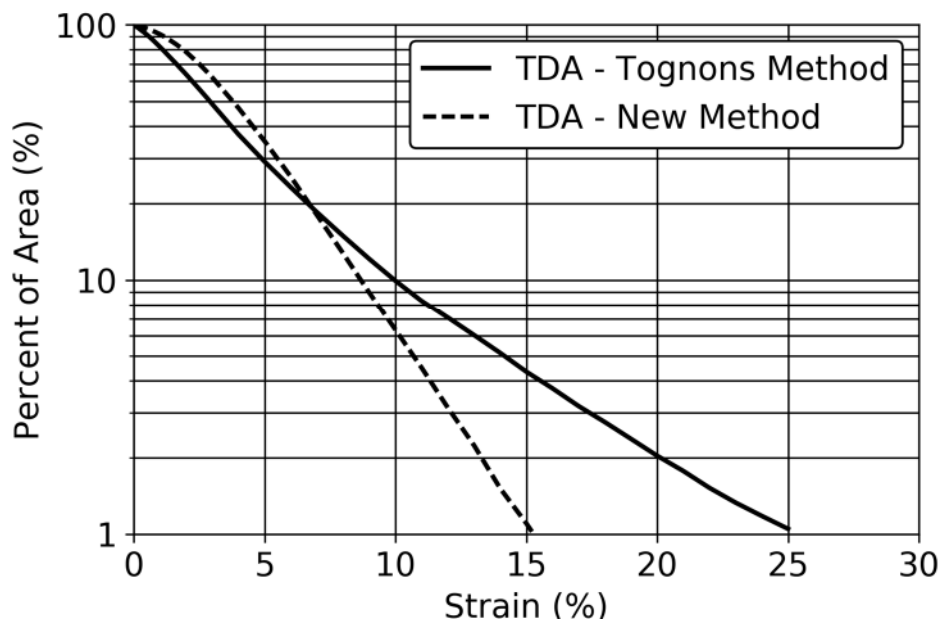


Figure 30: Strain area distribution comparing methods of calculating strain for TDA

For strains greater than 6%, Tognon's method appears to overestimate the strain in the geomembrane for larger flatter dimples induced by TDA confirming that Tognon's method may overestimate strain associated with large shallow indentations.

These “epoxy tests” were carried out with no protection layers and resulted in large areas of high strains for both aggregates. With heavy protection layers, these high strain areas could have been limited as shown in Figure 22. and the numerous other tests shown in Appendix D. The actual amount of strain, however, was not the point of these tests. These tests were carried out to evaluate the relative error introduced by the known limitations of the Tognon method on strain patterns induced by TDA and gravel respectively. The results do strongly suggest that Tognon’s method will over or under-estimate strain differently for different aggregates based on the shape of the indentations.

In general, it may thus be concluded that other considerations being equal, the difference in localised strain induced by TDA and gravel is likely to be even more significant than suggested by Figure 22.

5.0 Conclusions:

Based on the current state of knowledge, the following conclusions can be made with regards to the use of TDA and gravel as drainage aggregate in landfill applications:

- Gravel and TDA both require heavy protection layers (nonwoven geotextiles in excess of at minimum 1088 g/m²) or soil protection layers if they can be placed within regulatory requirements and without damage to the geomembrane
- Gravel requires heavy protection layers primarily to prevent the development of long term tensile strains (likely heavier than 1088 g/m²). Ideally testing should be done with site-specific clay, geomembrane and gravel to develop a series of SAD curves for various weights of protection layer;
- TDA requires heavy protection layers primarily to prevent the short-term puncture from protruding wires
- The following guidelines are recommended for TDA:
 - At least a 2 mm geomembrane;
 - At minimum a 1088 g/m² nonwoven needle punched geotextile or soil protection layer;
 - Ensuring the percentage of high-risk wires in the TDA does not exceed 3%;
 - Using larger TDA (double pass recommended);
 - Compacting the subgrade to ensure sufficient strength and stiffness while maintaining hydraulic conductivity requirements.

6.0 Implications of findings and areas requiring further study:

Based on the findings described in this report, it may be concluded that the use of TDA as drainage media for landfills may be associated with a greater degree of risk of short term puncture as compared to a conventional gravel drainage medium used for LCS, all other considerations being equal;

On the other hand, all else being equal, a LCS drainage blanket composed of TDA may be associated with a decreased risk of longer term stress-cracking defects associated with localised areas of high strain caused by the point loading.

Loading was relatively rapid and represents undrained loading conditions. In order to evaluate the effects of slower drained loading a different experimental strategy is required.

The effects of varying levels of processing (i.e. single-pass, double-pass and multi-pass TDA) have not been characterized in an exhaustive manner, and the conclusion reached in this report regarding the potential benefit of larger-sized TDA must be read in that light. Additional work in this regard would be appropriate:

Existing specifications for TDA in terms of grain size and amount of exposed wire are not appropriate for the LCS function of large particle-sized TDA. A specification should be developed for this specific purpose.

References:

- Abdelaal, F. B., Rowe, R. K., & Brachman, R. W. I. (2014). Brittle rupture of an aged HDPE geomembrane at local gravel indentations under simulated field conditions. *Geosynthetics International*, **21**(1), 1–23.
- Agisoft, L. L. C. (2016). Agisoft PhotoScan User Manual: Professional Edition, Version 1.2. Retrieved from http://www.agisoft.com/pdf/photoscan-pro_1_2_en.pdf
- Brachman, R. W. I., & Eastman, M. K. (2013). Calculating local geomembrane indentation strains from measured radial and vertical displacements. *Geotextiles and Geomembranes*, **40**, 58–68.
- Brachman, R. W. I., Eastman, M. K., & Eldesouky, H. M. G. (2018). Screening Tests to Limit Geomembrane Strain from Gravel Indentations. *Journal of Geotechnical and Geoenvironmental Engineering*, **144**(6), 04018031.
- Brachman, R. W. I., & Gudina, S. (2008). Gravel contacts and geomembrane strains for a GM/CCL composite liner. *Geotextiles and Geomembranes*, **26**(6), 448–459.
- Brachman, R. W. I., Rowe, R. K., & Irfan, H. (2014). Short-Term Local Tensile Strains in HDPE Heap Leach Geomembranes from Coarse Overliner Materials. *Journal of Geotechnical and Geoenvironmental Engineering*, **140**(5), 1–7.
- Brachman, R. W. I., & Sabir, A. (2010). Geomembrane puncture and strains from stones in an underlying clay layer. *Geotextiles and Geomembranes*, **28**(4), 335–343.
- Brummermann, K., Blumerl, W., & Stoewahse, C. (1994). Protection layers for geomembranes: Effectiveness and testing procedures. *Proc., 5th International Conference on Geosynthetics*, 1003–1006.
- Eldesouky, H. M. G., & Brachman, R. W. I. (2018). Calculating local geomembrane strains from a single gravel particle with thin plate theory. *Geotextiles and Geomembranes*, **46**(1), 101–110.
- Giroud, J.P. (2016). Leakage control using geomembrane liners. *Soils and Rocks, São Paulo*, **39**(3), 213–235.
- Hornsey, W. P., & Wishaw, D. M. (2012). Development of a methodology for the evaluation of geomembrane strain and relative performance of cushion geotextiles. *Geotextiles and Geomembranes*, **35**, 87–99.
- Koerner, R. M., Wong, W. C., & Koerner, G. R. (2012). Index puncture resistance of geomembranes using various protection geosynthetics. *Geotechnical Testing Journal*, **35**(5), 762–770.

Laine, D.L., Miklas, M.P., Parr, C.H. (1989). Loading point puncturability analysis of geosynthetic liner materials. *Proceedings geosynthetics 89'*, San Diego, IFAI Publishers

Marcotte, B. A., & Fleming, I. R. (2019). The role of undrained clay soil subgrade properties in controlling deformations in geomembranes. *Geotextiles and Geomembranes*, **47** pp327-335. Available online 22 February, 2019. DOI: 10.1016/j.geotexmem.2019.02.001

Reddy, K. R., & Saichek, R. E. (1998). Assessment of damage to geomembrane liners by shredded scrap tires. *Geotechnical Testing Journal*, **21**(4), 307-316.

Rowe, R. K. (2005). Long-term performance of contaminant barrier systems. *Géotechnique*, **55**(9), 631–678.

Rowe, R. K., Brachman, R. W. I., Irfan, H., Smith, M. E., & Thiel, R. (2013a). Effect of underliner on geomembrane strains in heap leach applications. *Geotextiles and Geomembranes*, **40**, 37–47.

Rowe, R. K., Abdelaal, F.B., Brachman, R. W. I. (2013b). Antioxidant depletion of HDPE geomembrane with sand protection layer. *Geosynthetics International*, **20**(2), 73-89

Rowe, R. K., & Yu, Y. (2019). Magnitude and significance of tensile strains in geomembrane landfill liners. *Geotextiles and Geomembranes*. In Press

Rowe, R. K. (2012). Short-and long-term leakage through composite liners. The 7th Arthur Casagrande Lecture. *Canadian Geotechnical Journal*, **49**(2), 141-169.

Seeger, S., & Muller, W. (2003). Theoretical approach to designing protection: selecting a geomembrane strain criterion. In: Dixon, N., Smith, D.M., Greenwood, J.H., Jones, D.R.V. (Eds.), *Geosynthetics: Protecting the Environment*. London: Thomas Telford.

Tognon, A. R., Kerry Rowe, R., & Moore, I. D. (2000). Geomembrane Strain Observed in Large-Scale Testing of Protection Layers. *Journal of Geotechnical and Geoenvironmental Engineering*, **126**(12), 1194–1208.

Vogel, J. H., & Lee, D. (1988). An automated two-view method for determining strain distributions on deformed surfaces. *Journal of Materials Shaping Technology*, **6**(4), 205-216.

Zanzinger, H. (1999). Efficiency of Geosynthetic Protection Layers for Geomembrane Liners: Performance in a Large-Scale Model Test. *Geosynthetics International*, **6**(4), 303–317.

Appendix A: Classification of High-risk Pieces



Figure A1: Examples of High Risk Wires



Figure A2: Examples of High Risk Wires 2



Figure A3: Examples of High Risk Wires 3



Figure A4: Examples of High Risk Wires 4



Figure A5: Examples of Low Risk Wires



Figure A6: Examples of Low Risk Wires 2



Figure A7: Examples of Low Risk Wires 3



Figure A8: Examples of Low Risk Wires 4

Appendix B: Additional Images from Ice Block Testing

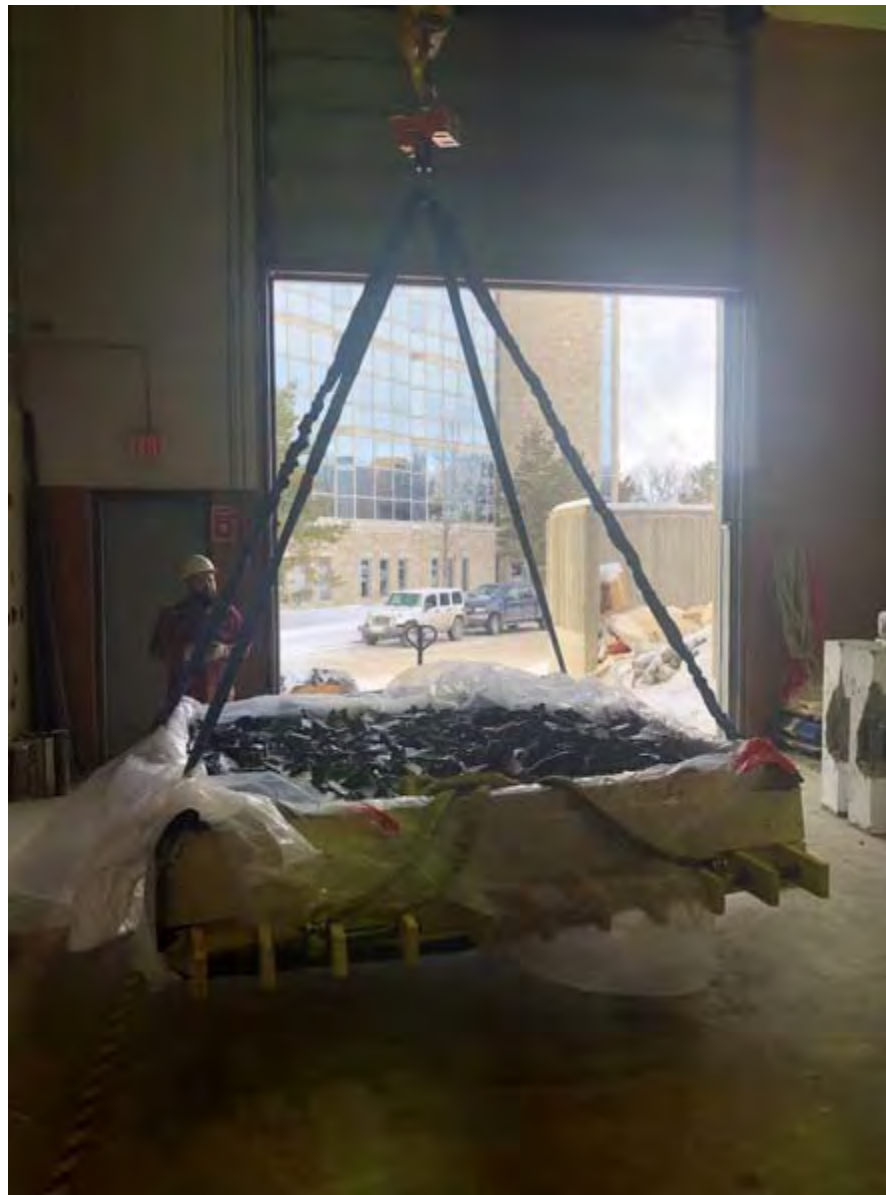


Figure A9: Moving frozen TDA block back inside after freezing



Figure A10: Frozen TDA ice blocks upon flipping

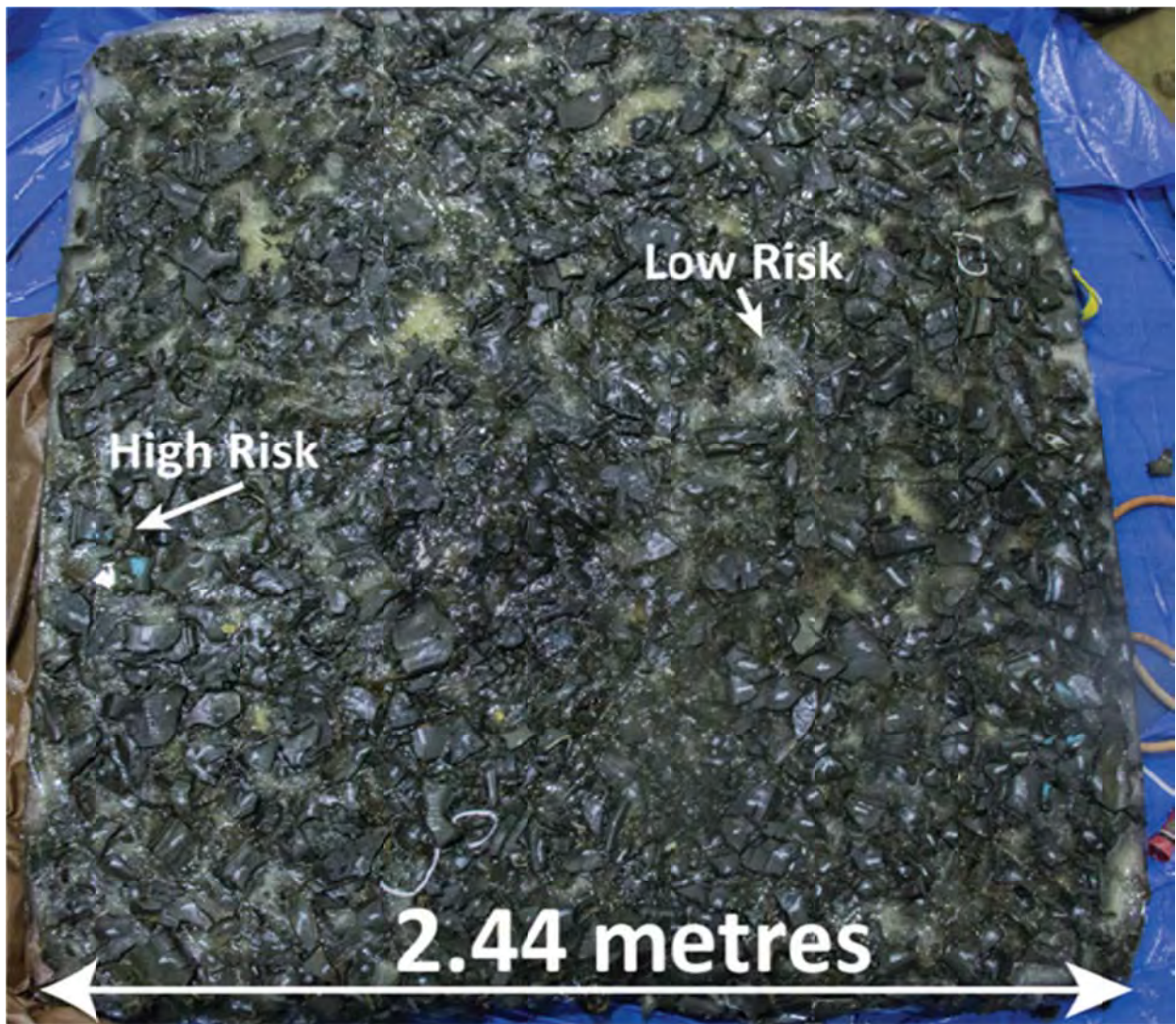


Figure A11: Single pass TDA ice block



Figure A12: Examples of TDA pieces oriented in unfavourably upon melting of top surface of ice



Figure A: Examples of TDA pieces oriented in unfavourably upon melting of top surface of ice

Appendix C: Results of Puncture Tests

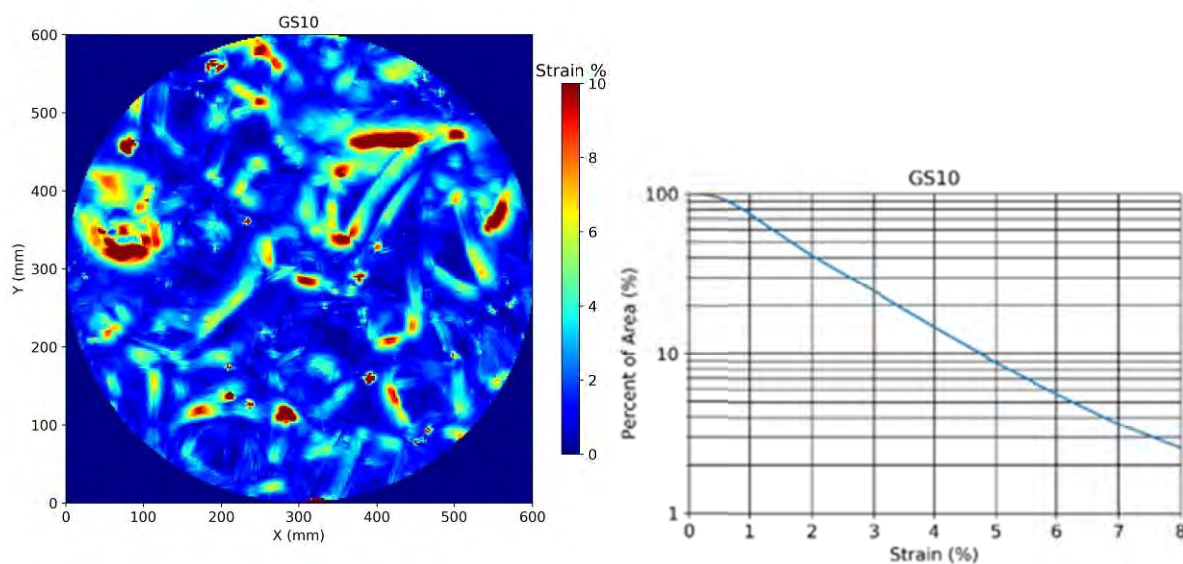
Table A1: Results of all GS protection efficiency testing

Name of Test	Geomembrane (mm)	Protection Layer Type	Protection Layer MUA (g/m ²)	Total Load (kPa)	Pre Test Moisture	Post Test Moisture	% Wet OMC	Relative Density	S _u (kPa)	# Selected Puncture Pieces	Number of Punctures
GS27	1.5	NW	544	500	12.7%	12.8%	2.2%	100%	93	15	5
GS28	1.5	NW	814	500	12.2%	12.7%	1.7%	100%	109	15	3
GS31	1.5	NW	1080	500	11.6%	11.5%	1.1%	100%	115	15	2
GS29	1.5	NW	1360	500	12.2%	12.8%	1.7%	100%	113	15	0
GS30	1.5	NW	1628	500	11.8%	12.1%	1.3%	100%	110	15	0
GS32	2	NW	1080	500	11.2%	11.1%	0.7%	100%	132	40	0
GS33	2	NW	1080	500	11.6%	11.9%	1.1%	100%	127	40	0
GS34	2	NW	1080	500	11.4%	11.4%	0.9%	100%	129	40	2
GS35	2	NW	1360	500	11.7%	11.5%	1.2%	100%	125	40	4
GS36	2	NW	1624	500	11.7%	11.6%	1.2%	100%	126	40	1
GS37	2	NW	2448	500	11.7%	10.7%	1.2%	100%	120	40	0
GS39	2	NW	1624	500	11.6%	11.5%	1.1%	100%	135	40	1
GS40	2	NW	1360	500	11.4%	11.7%	0.9%	100%	133	40	2
GS41	2	NW	1624	500	11.7%	11.8%	1.2%	100%	129	40	1
GS42	2	NW	1360	500	11.4%	11.3%	0.9%	100%	132	40	0
GS43	1.5	NW	1624	500	11.3%	-	0.8%	100%	130	40	2
GS44	1.5	NW	1360	500	11.7%	11.7%	1.2%	100%	130	40	4
GS45	2	NW and W	812 + Woven	500	12.0%	11.9%	1.5%	100%	127	40	2
GS46	2	NW and W	1360 + woven	500	11.7%	12.0%	1.2%	100%	126	40	2
GS47	2	NW and PDG	PDG + 814 W	500	12.3%	11.6%	1.8%	100%	128	40	1
GS48	2	NW	1080		12.2%	11.2%	1.7%	100%	127	Gravel	
GS49	1.5	NW	544		12.1%	10.2%	1.6%	100%	124	Gravel	

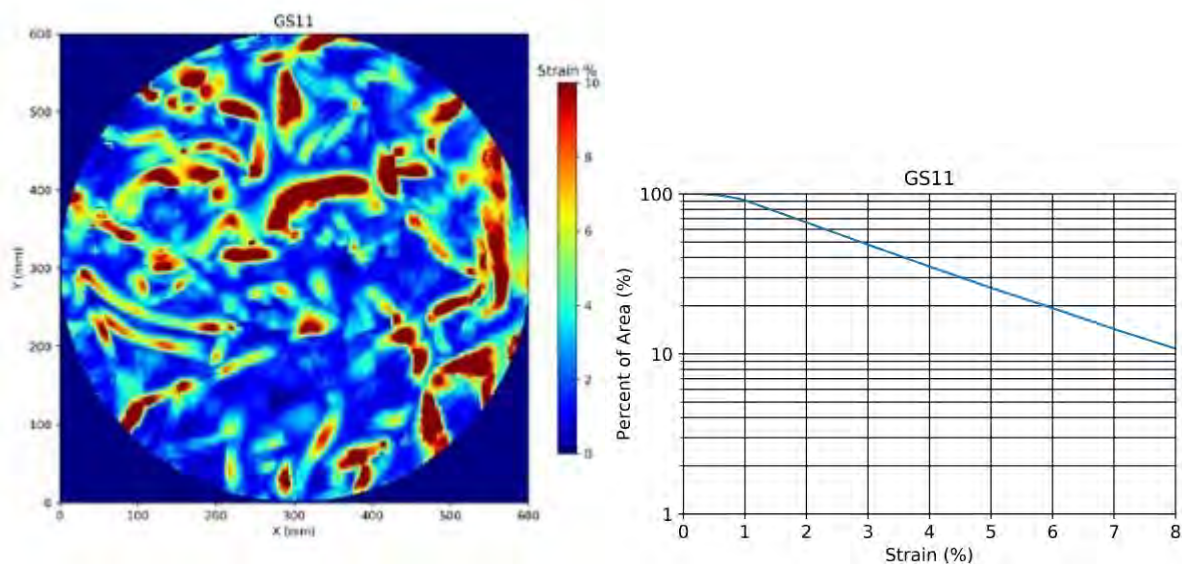
Appendix D: Strain maps and SAD curves

note: strain estimated using Tognon's method

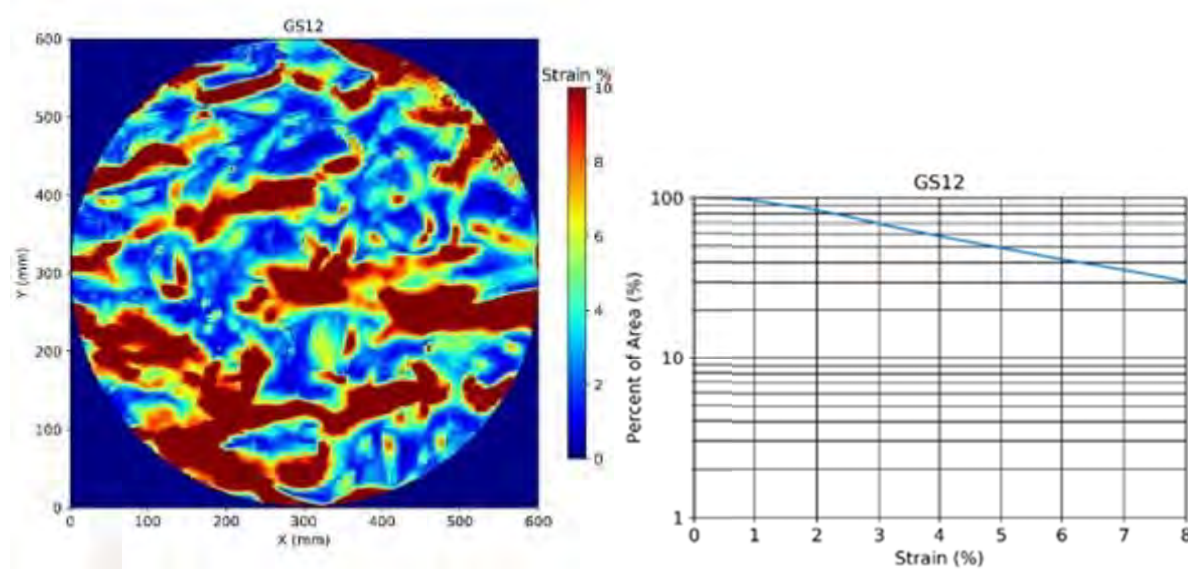
Test ID	GS10
Aggregate Above Geomembrane	TDA
Aggregate Description	ARMA
Soil Name	Floral Till
Water Content	28%
Percent wet of Proctor optimum	6.0%
Undrained Shear Strength (kPa)	47
% Standard Proctor Optimum	94%
Loading Rate	100 kPa every 10 min
Time Held at Load (hours)	24
Pressure (kPa)	200
Geomembrane Manufacturer	Solmax
Geomembrane Thickness (mm)	1.5
Geomembrane Type	HDPE
Protection Layer	None
Protection Layer MUA (g/m ²)	



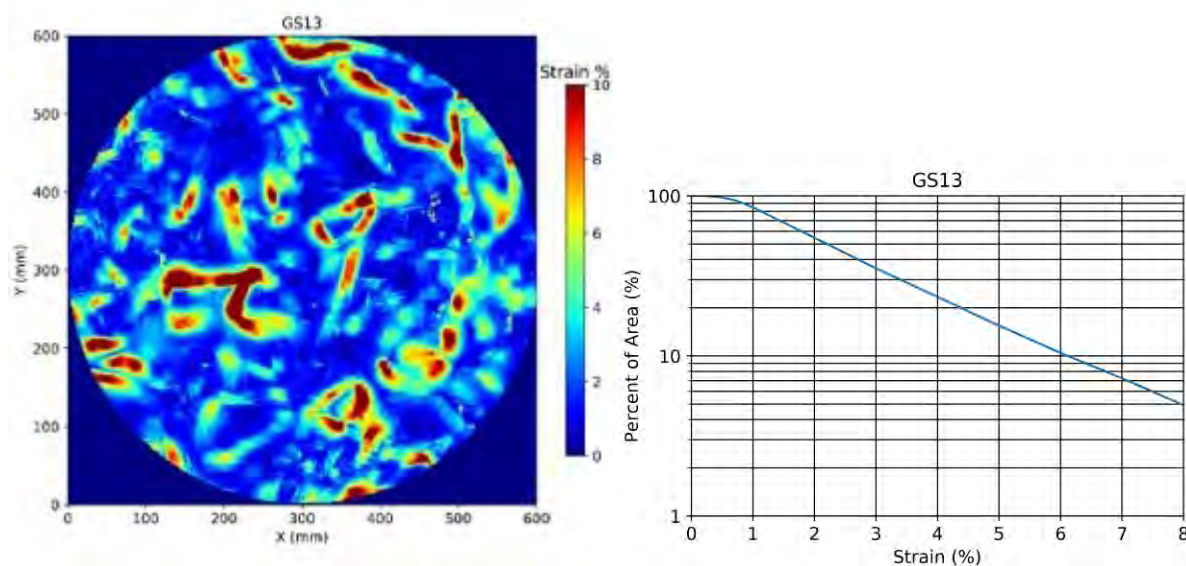
Test ID	GS11
Aggregate Above Geomembrane	TDA
Aggregate Description	ARMA
Soil Name	Floral Till
Water Content	28%
Percent wet of Proctor optimum	6.3%
Undrained Shear Strength (kPa)	48
% Standard Proctor Optimum	94%
Loading Rate	100 kPa every 10 min
Time Held at Load (hours)	24
Pressure (kPa)	300
Geomembrane Manufacturer	Solmax
Geomembrane Thickness (mm)	1.5
Geomembrane Type	HDPE
Protection Layer	Non-Woven
Protection Layer MUA (g/m ²)	340



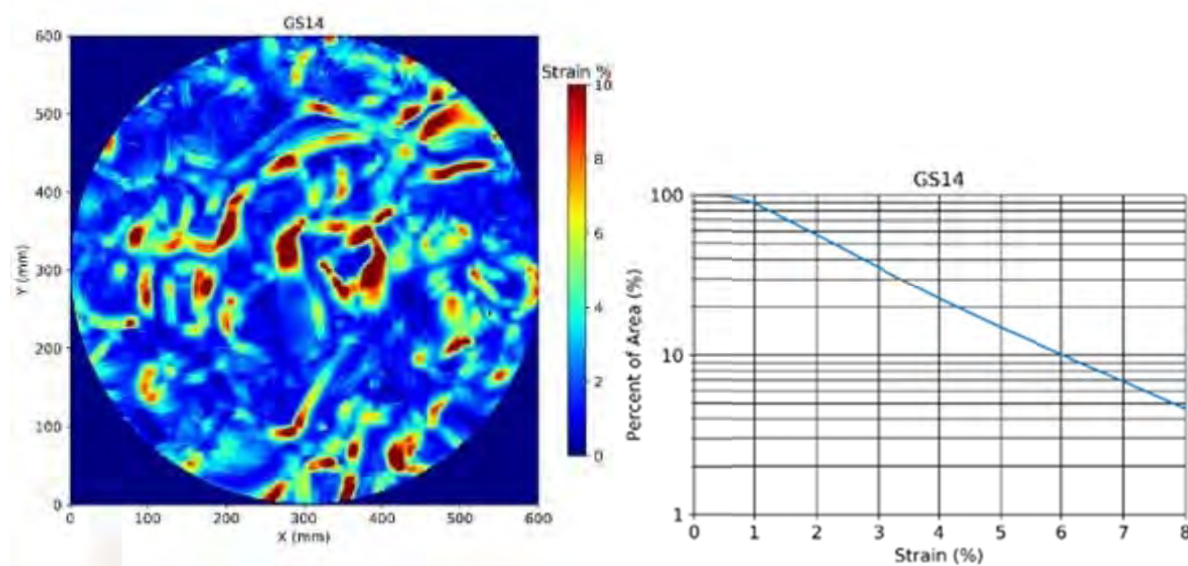
Test ID	GS12
Aggregate Above Geomembrane	TDA
Aggregate Description	ARMA
Soil Name	Floral Till
Water Content	28%
Percent wet of Proctor optimum	6.2%
Undrained Shear Strength (kPa)	53
% Standard Proctor Optimum	94%
Loading Rate	100 kPa every 10 min
Time Held at Load (hours)	24
Pressure (kPa)	400
Geomembrane Manufacturer	Solmax
Geomembrane Thickness (mm)	1.5
Geomembrane Type	HDPE
Protection Layer	Non-Woven
Protection Layer MUA (g/m ²)	340



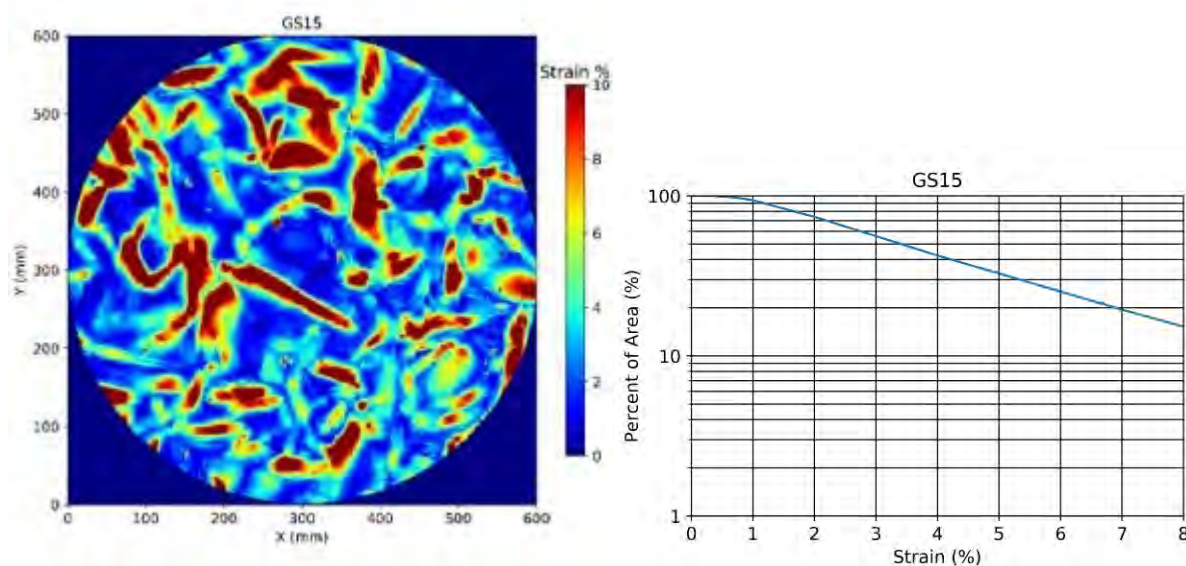
Test ID	GS13
Aggregate Above Geomembrane	TDA
Aggregate Description	ARMA
Soil Name	Floral Till
Water Content	27%
Percent wet of Proctor optimum	5.5%
Undrained Shear Strength (kPa)	53
% Standard Proctor Optimum	94%
Loading Rate	100 kPa every 10 min
Time Held at Load (hours)	24
Pressure (kPa)	200
Geomembrane Manufacturer	Solmax
Geomembrane Thickness (mm)	1.5
Geomembrane Type	HDPE
Protection Layer	Non-Woven
Protection Layer MUA (g/m ²)	340



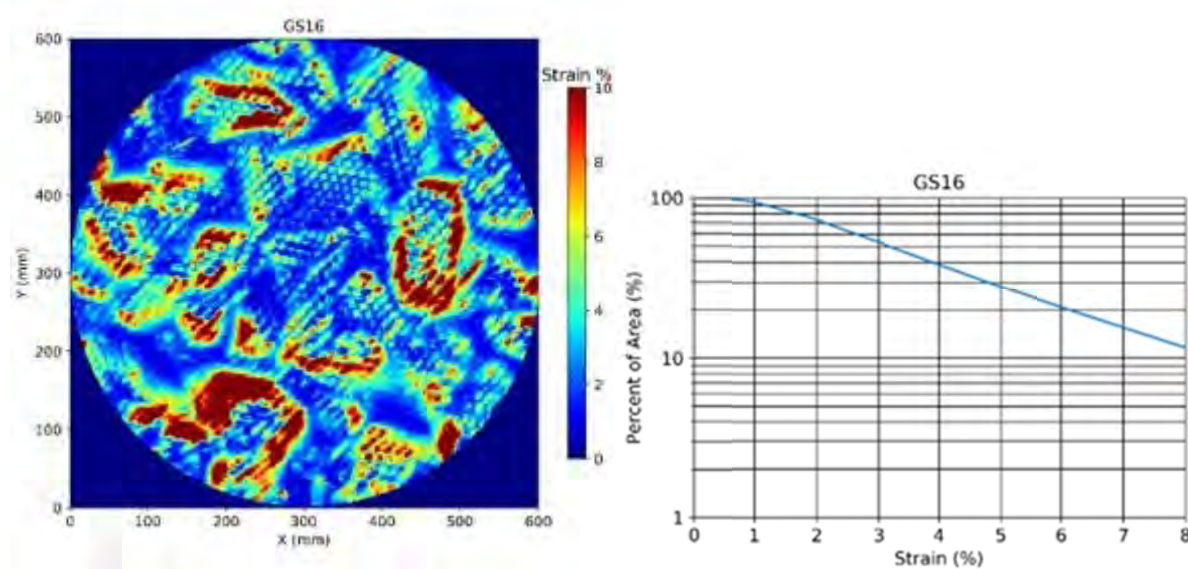
Test ID	GS14
Aggregate Above Geomembrane	TDA
Aggregate Description	ARMA
Soil Name	Floral Till
Water Content	27%
Percent wet of Proctor optimum	5.2%
Undrained Shear Strength (kPa)	53
% Standard Proctor Optimum	94%
Loading Rate	100 kPa every 10 min
Time Held at Load (hours)	24
Pressure (kPa)	450
Geomembrane Manufacturer	Solmax
Geomembrane Thickness (mm)	1.5
Geomembrane Type	HDPE
Protection Layer	Non-Woven
Protection Layer MUA (g/m ²)	340



Test ID	GS15
Aggregate Above Geomembrane	TDA
Aggregate Description	ARMA
Soil Name	Floral Till
Water Content	27%
Percent wet of Proctor optimum	4.6%
Undrained Shear Strength (kPa)	53
% Standard Proctor Optimum	94%
Loading Rate	100 kPa every 10 min
Time Held at Load (hours)	24
Pressure (kPa)	550
Geomembrane Manufacturer	Solmax
Geomembrane Thickness (mm)	1.5
Geomembrane Type	HDPE
Protection Layer	Non-Woven
Protection Layer MUA (g/m ²)	540

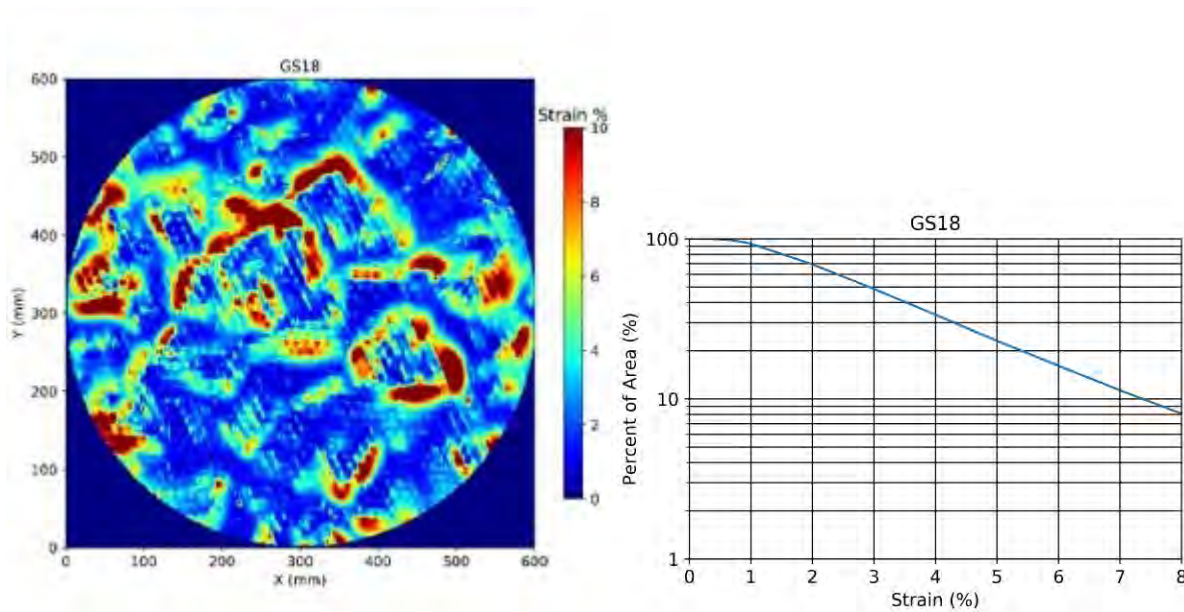


Test ID	GS16
Aggregate Above Geomembrane	TDA
Aggregate Description	ARMA
Soil Name	Floral Till
Water Content	26%
Percent wet of Proctor optimum	3.8%
Undrained Shear Strength (kPa)	59
% Standard Proctor Optimum	94%
Loading Rate	100 kPa every 10 min
Time Held at Load (hours)	24
Pressure (kPa)	550
Geomembrane Manufacturer	Solmax
Geomembrane Thickness (mm)	1.5
Geomembrane Type	HDPE
Protection Layer	PDG
Protection Layer MUA (g/m ²)	

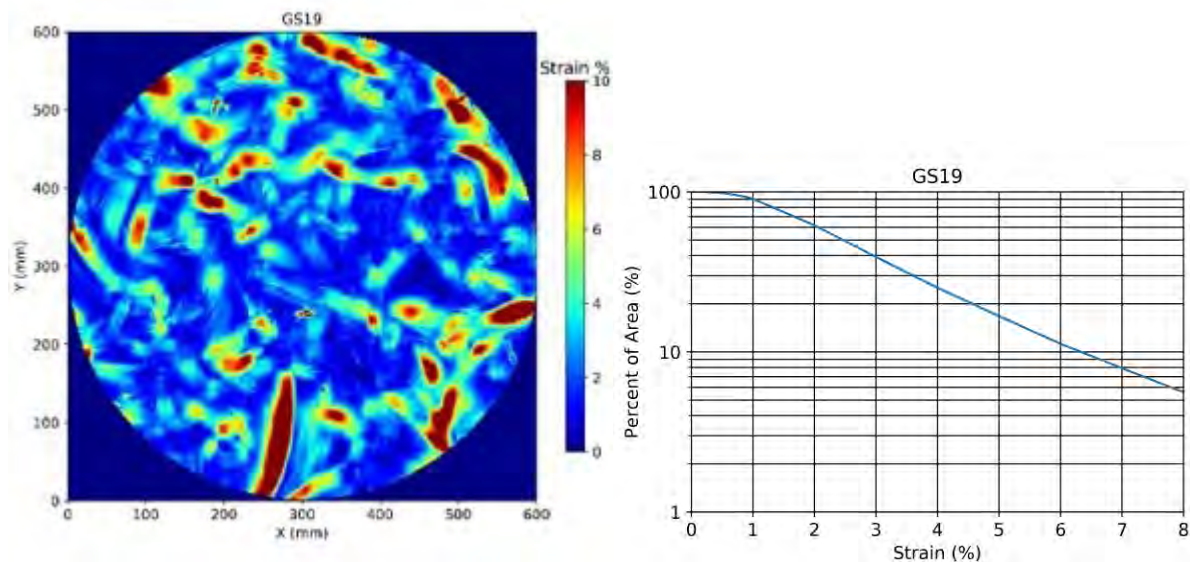


Test ID	GS17
Aggregate Above Geomembrane	TDA
Aggregate Description	ARMA
Soil Name	Floral Till
Water Content	26%
Percent wet of Proctor optimum	4.3%
Undrained Shear Strength (kPa)	61
% Standard Proctor Optimum	94%
Loading Rate	100 kPa every 10 min
Time Held at Load (hours)	24
Pressure (kPa)	350
Geomembrane Manufacturer	Solmax
Geomembrane Thickness (mm)	2
Geomembrane Type	HDPE
Protection Layer	None
Protection Layer MUA (g/m ²)	

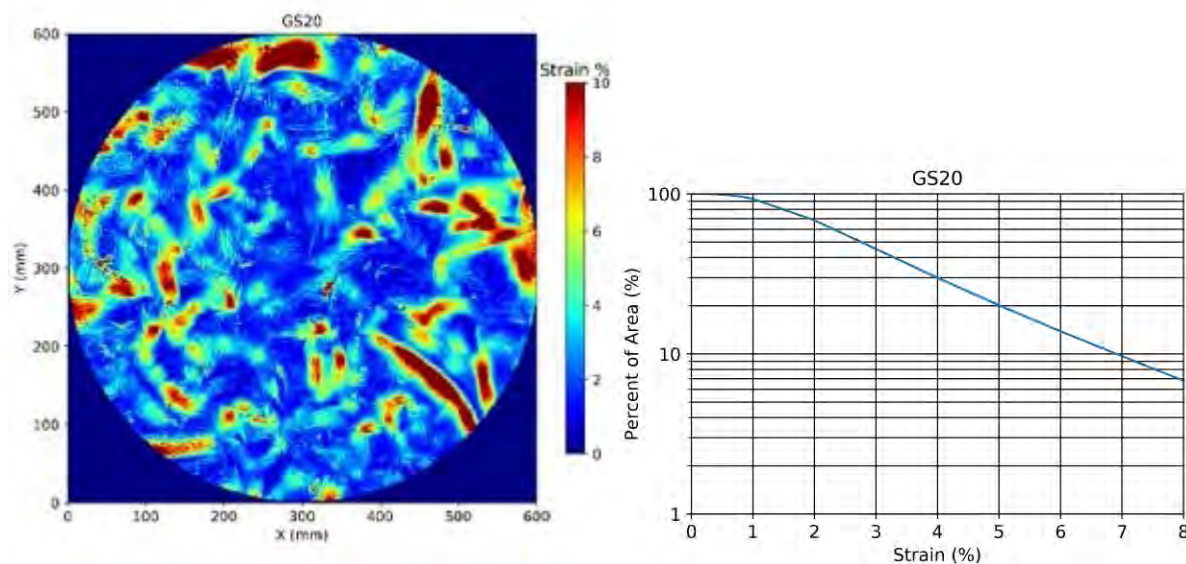
Test ID	GS18
Aggregate Above Geomembrane	TDA
Aggregate Description	ARMA
Soil Name	Floral Till
Water Content	25%
Percent wet of Proctor optimum	2.7%
Undrained Shear Strength (kPa)	63
% Standard Proctor Optimum	94%
Loading Rate	100 kPa every 10 min
Time Held at Load (hours)	24
Pressure (kPa)	350
Geomembrane Manufacturer	Solmax
Geomembrane Thickness (mm)	2
Geomembrane Type	HDPE
Protection Layer	PDG
Protection Layer MUA (g/m ²)	GS18



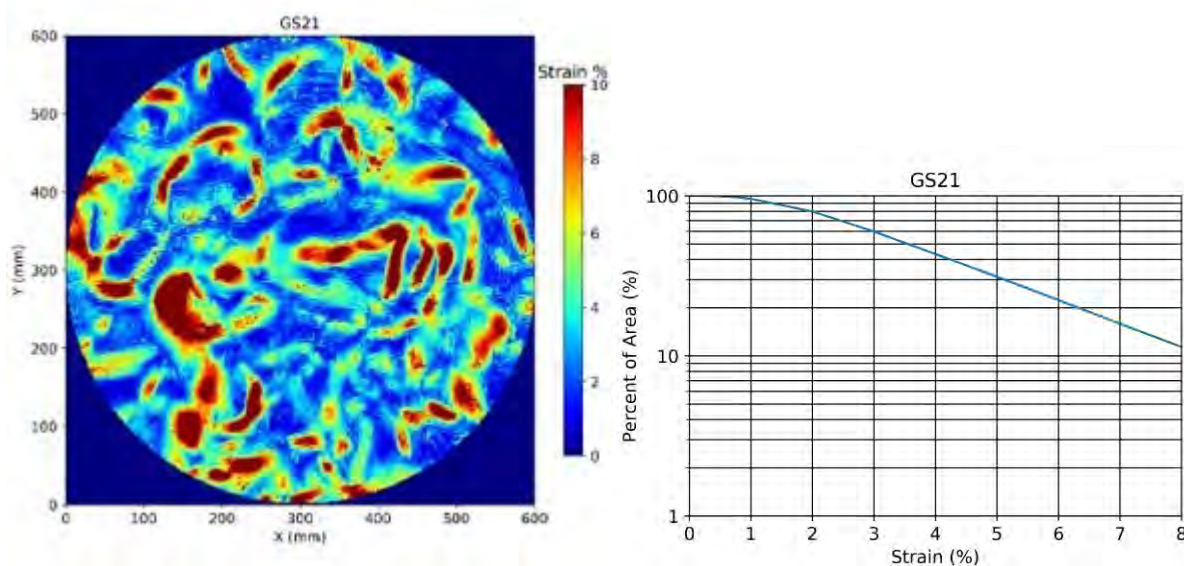
Test ID	GS19
Aggregate Above Geomembrane	TDA
Aggregate Description	ARMA
Soil Name	Floral Till
Water Content	25%
Percent wet of Proctor optimum	3.2%
Undrained Shear Strength (kPa)	65
% Standard Proctor Optimum	94%
Loading Rate	100 kPa every 10 min
Time Held at Load (hours)	24
Pressure (kPa)	500
Geomembrane Manufacturer	Solmax
Geomembrane Thickness (mm)	2
Geomembrane Type	HDPE
Protection Layer	PDG
Protection Layer MUA (g/m ²)	



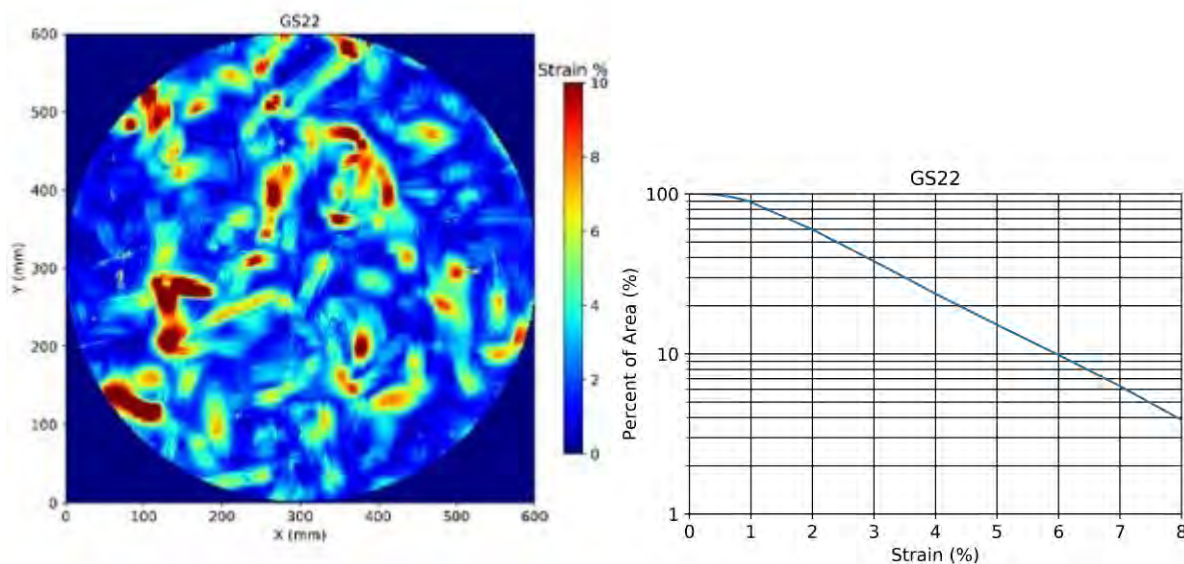
Test ID	GS20
Aggregate Above Geomembrane	TDA
Aggregate Description	ARMA
Soil Name	Floral Till
Water Content	25%
Percent wet of Proctor optimum	2.9%
Undrained Shear Strength (kPa)	66
% Standard Proctor Optimum	94%
Loading Rate	100 kPa every 10 min
Time Held at Load (hours)	24
Pressure (kPa)	350
Geomembrane Manufacturer	Solmax
Geomembrane Thickness (mm)	2
Geomembrane Type	HDPE
Protection Layer	Non-Woven
Protection Layer MUA (g/m ²)	340



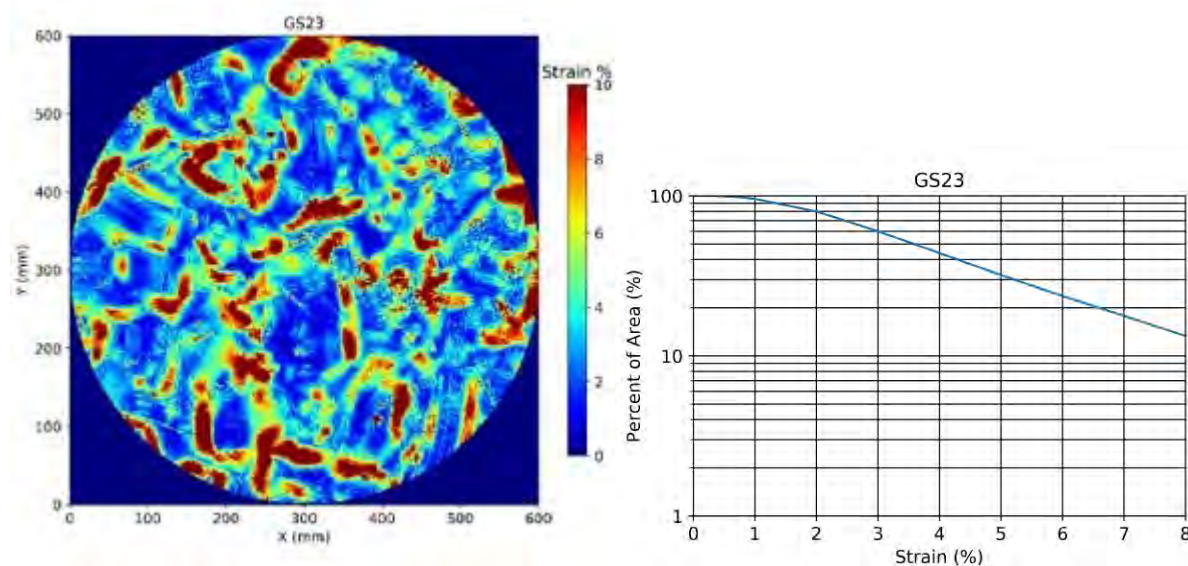
Test ID	GS21
Aggregate Above Geomembrane	TDA
Aggregate Description	ARMA
Soil Name	Floral Till
Water Content	26%
Percent wet of Proctor optimum	3.9%
Undrained Shear Strength (kPa)	68
% Standard Proctor Optimum	94%
Loading Rate	100 kPa every 10 min
Time Held at Load (hours)	24
Pressure (kPa)	500
Geomembrane Manufacturer	Solmax
Geomembrane Thickness (mm)	2
Geomembrane Type	HDPE
Protection Layer	Non-Woven
Protection Layer MUA (g/m ²)	408



Test ID	GS22
Aggregate Above Geomembrane	TDA
Aggregate Description	ARMA
Soil Name	Floral Till
Water Content	24%
Percent wet of Proctor optimum	2.2%
Undrained Shear Strength (kPa)	67
% Standard Proctor Optimum	94%
Loading Rate	100 kPa every 10 min
Time Held at Load (hours)	24
Pressure (kPa)	500
Geomembrane Manufacturer	Solmax
Geomembrane Thickness (mm)	3
Geomembrane Type	HDPE
Protection Layer	None
Protection Layer MUA (g/m ²)	

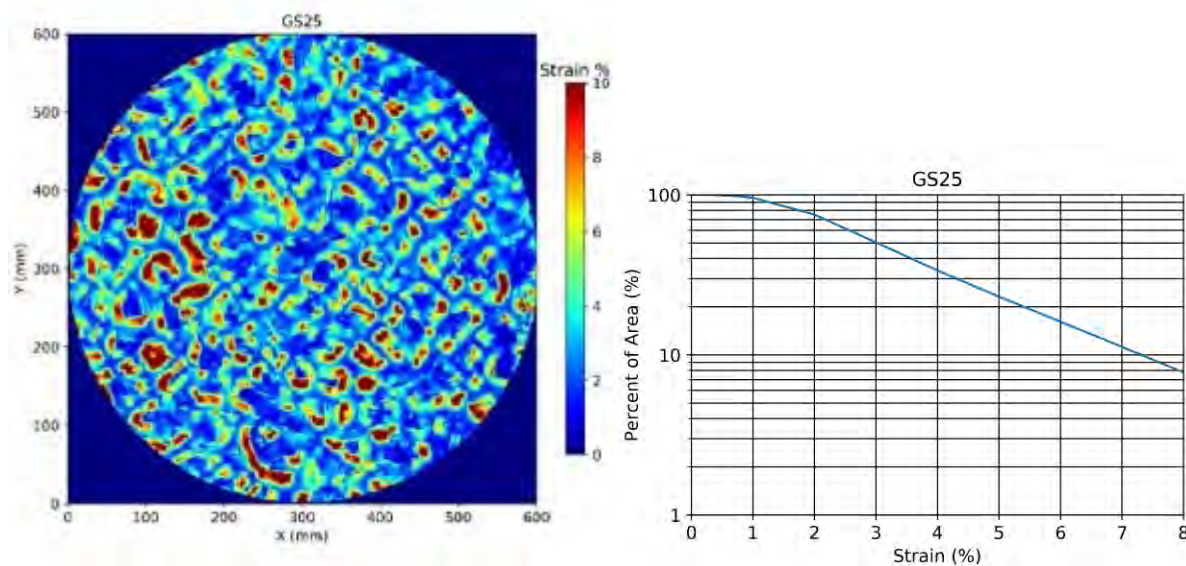


Test ID	GS23
Aggregate Above Geomembrane	TDA
Aggregate Description	ARMA
Soil Name	Floral Till
Water Content	24%
Percent wet of Proctor optimum	2.2%
Undrained Shear Strength (kPa)	67
% Standard Proctor Optimum	94%
Loading Rate	100 kPa every 10 min
Time Held at Load (hours)	24
Pressure (kPa)	350
Geomembrane Manufacturer	Solmax
Geomembrane Thickness (mm)	2
Geomembrane Type	LLDPE
Protection Layer	None
Protection Layer MUA (g/m ²)	

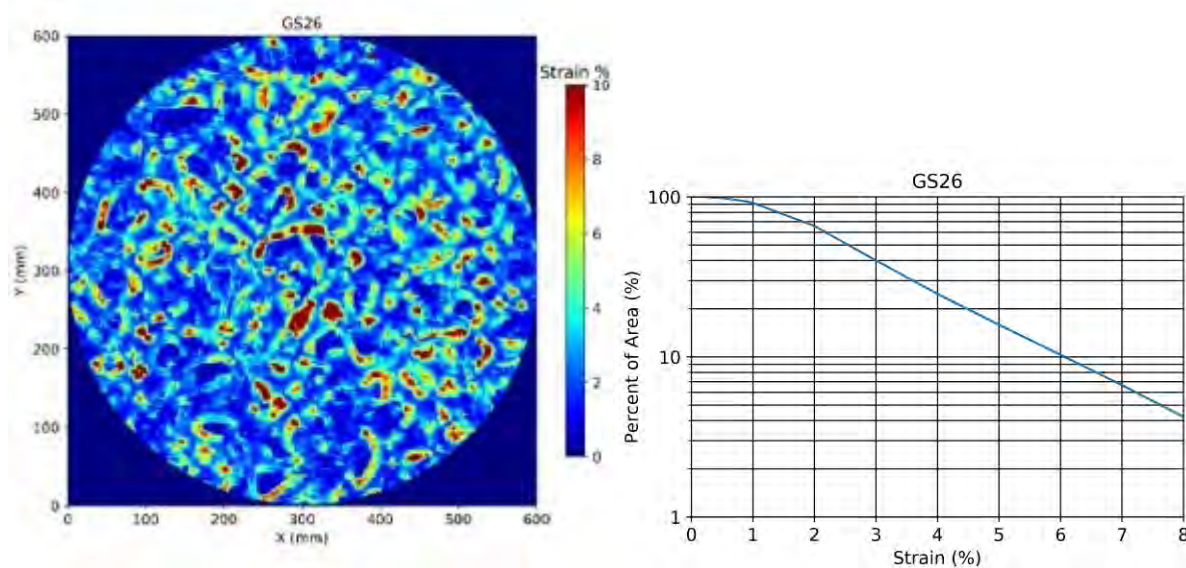


Test ID	GS24
Aggregate Above Geomembrane	TDA
Aggregate Description	ARMA
Soil Name	Floral Till
Water Content	24%
Percent wet of Proctor optimum	1.6%
Undrained Shear Strength (kPa)	78
% Standard Proctor Optimum	94%
Loading Rate	100 kPa every 10 min
Time Held at Load (hours)	24
Pressure (kPa)	550
Geomembrane Manufacturer	Solmax
Geomembrane Thickness (mm)	2
Geomembrane Type	HDPE
Protection Layer	Non-Woven
Protection Layer MUA (g/m ²)	680

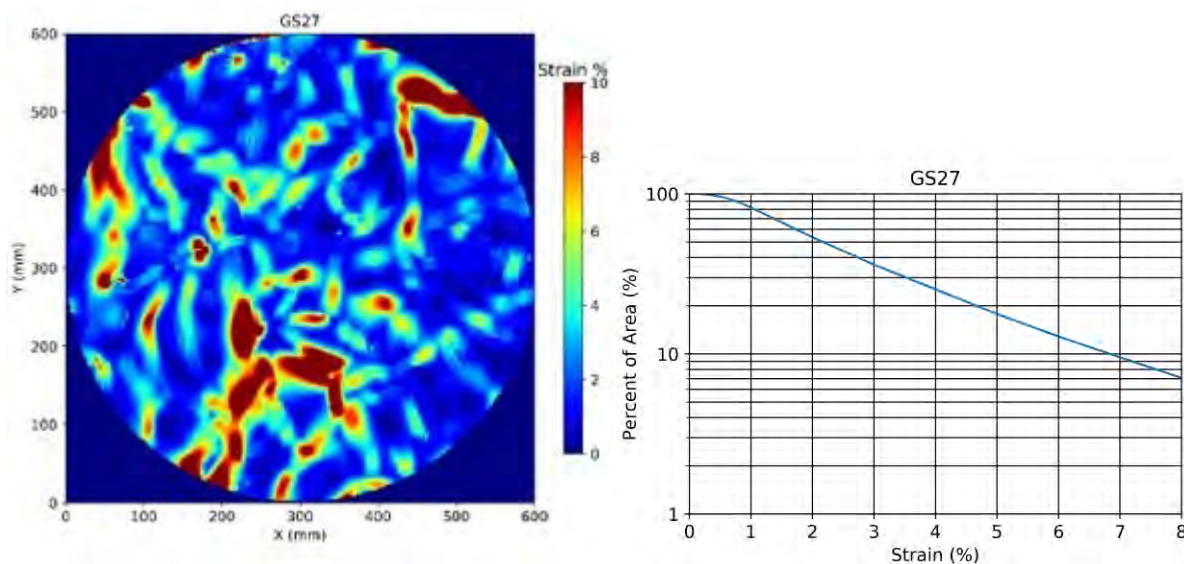
Test ID	GS25
Aggregate Above Geomembrane	Gravel
Aggregate Description	Angular White
Soil Name	Floral Till
Water Content	23%
Percent wet of Proctor optimum	1.0%
Undrained Shear Strength (kPa)	115
% Standard Proctor Optimum	98%
Loading Rate	45 kPa / Hour
Time Held at Load (hours)	1 Week
Pressure (kPa)	550
Geomembrane Manufacturer	Solmax
Geomembrane Thickness (mm)	1.5
Geomembrane Type	HDPE (Goliath)
Protection Layer	None
Protection Layer MUA (g/m ²)	



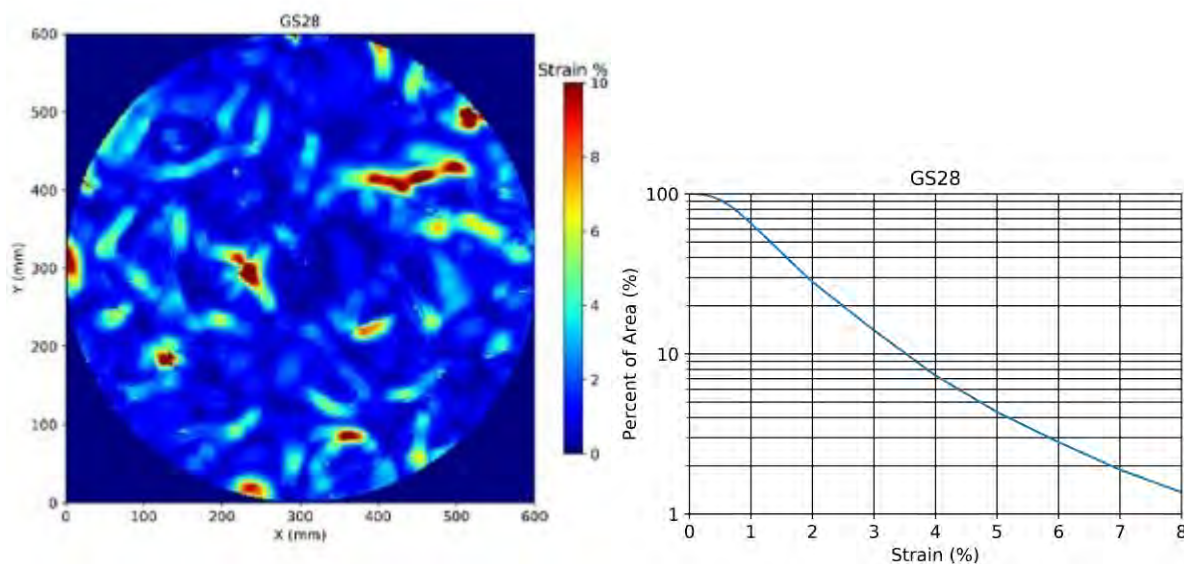
Test ID	GS26
Aggregate Above Geomembrane	Gravel
Aggregate Description	Angular White
Soil Name	Floral Till
Water Content	22%
Percent wet of Proctor optimum	0.0%
Undrained Shear Strength (kPa)	115
% Standard Proctor Optimum	98%
Loading Rate	46 kPa / Hour
Time Held at Load (hours)	1 Week
Pressure (kPa)	559
Geomembrane Manufacturer	Solmax
Geomembrane Thickness (mm)	1.5
Geomembrane Type	HDPE (Regular)
Protection Layer	None
Protection Layer MUA (g/m ²)	



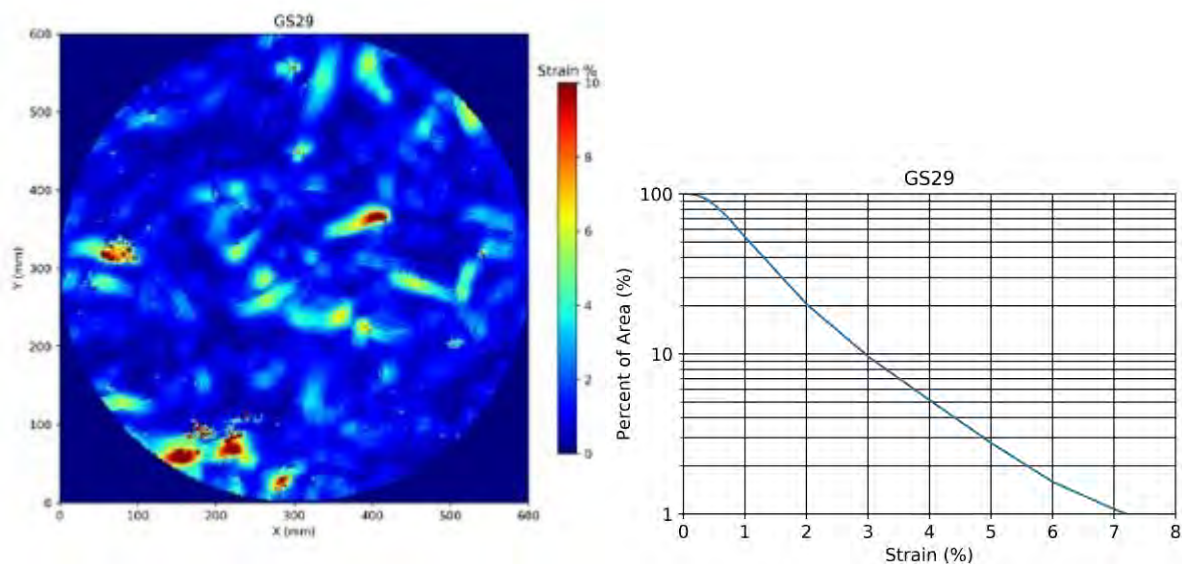
Test ID	GS27
Aggregate Above Geomembrane	TDA
Aggregate Description	ARMA
Soil Name	Battleford Till
Water Content	13%
Percent wet of Proctor optimum	2.2%
Undrained Shear Strength (kPa)	93
% Standard Proctor Optimum	101%
Loading Rate	100 kPa every 10 min
Time Held at Load (hours)	24
Pressure (kPa)	500
Geomembrane Manufacturer	Solmax
Geomembrane Thickness (mm)	1.5
Geomembrane Type	HDPE
Protection Layer	Non-Woven
Protection Layer MUA (g/m ²)	542



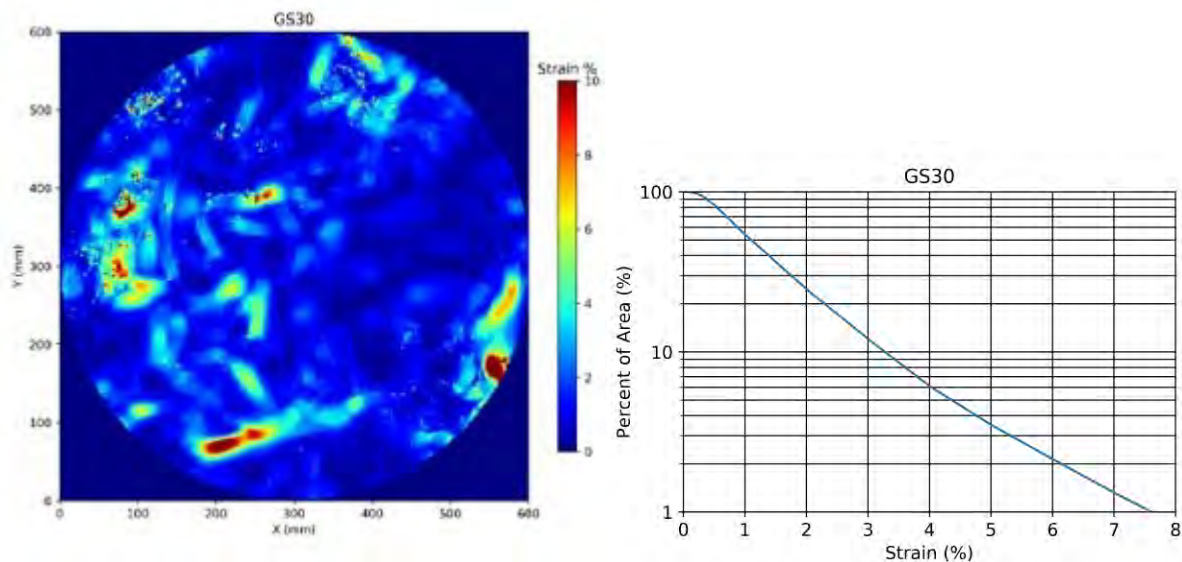
Test ID	GS28
Aggregate Above Geomembrane	TDA
Aggregate Description	ARMA
Soil Name	Battleford Till
Water Content	12%
Percent wet of Proctor optimum	1.7%
Undrained Shear Strength (kPa)	109
% Standard Proctor Optimum	101%
Loading Rate	100 kPa every 10 min
Time Held at Load (hours)	24
Pressure (kPa)	500
Geomembrane Manufacturer	Solmax
Geomembrane Thickness (mm)	1.5
Geomembrane Type	HDPE
Protection Layer	Non-Woven
Protection Layer MUA (g/m ²)	812



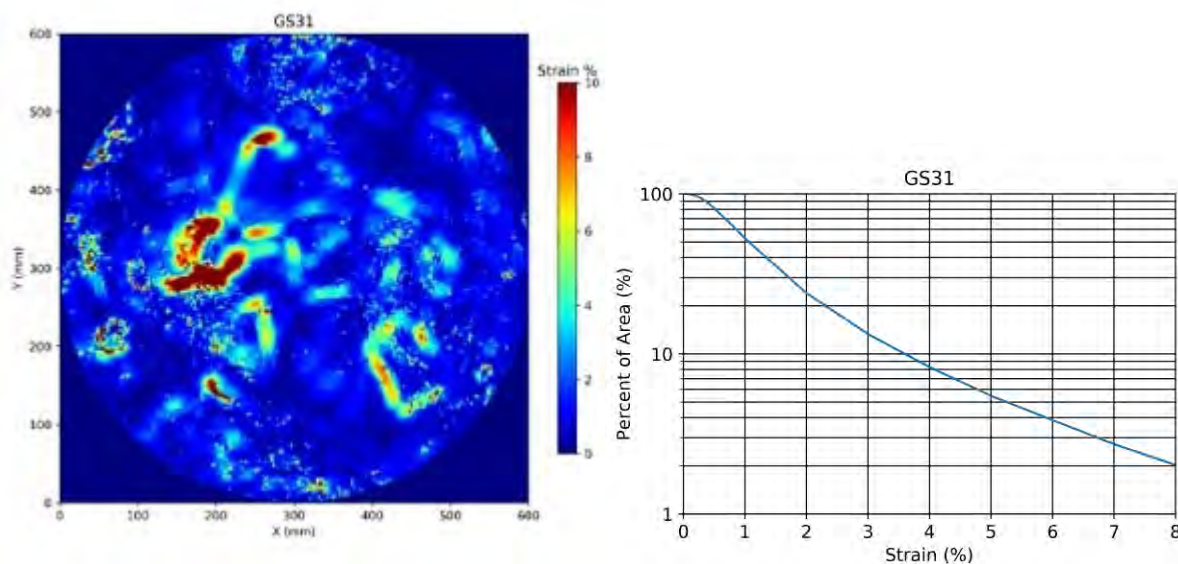
Test ID	GS29
Aggregate Above Geomembrane	TDA
Aggregate Description	ARMA
Soil Name	Battleford Till
Water Content	12%
Percent wet of Proctor optimum	1.7%
Undrained Shear Strength (kPa)	113
% Standard Proctor Optimum	101%
Loading Rate	100 kPa every 10 min
Time Held at Load (hours)	24
Pressure (kPa)	500
Geomembrane Manufacturer	Solmax
Geomembrane Thickness (mm)	1.5
Geomembrane Type	HDPE
Protection Layer	Non-Woven
Protection Layer MUA (g/m ²)	1360



Test ID	GS30
Aggregate Above Geomembrane	TDA
Aggregate Description	ARMA
Soil Name	Battleford Till
Water Content	12%
Percent wet of Proctor optimum	1.3%
Undrained Shear Strength (kPa)	110
% Standard Proctor Optimum	101%
Loading Rate	100 kPa every 10 min
Time Held at Load (hours)	24
Pressure (kPa)	500
Geomembrane Manufacturer	Solmax
Geomembrane Thickness (mm)	1.5
Geomembrane Type	HDPE
Protection Layer	Non-Woven
Protection Layer MUA (g/m ²)	1624



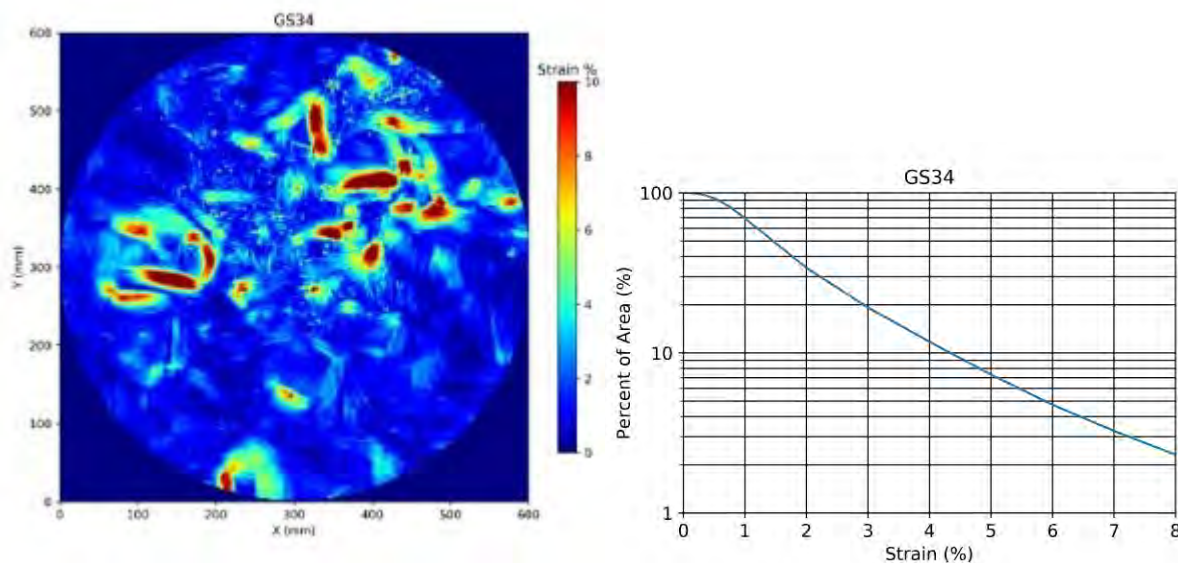
Test ID	GS31
Aggregate Above Geomembrane	TDA
Aggregate Description	ARMA
Soil Name	Battleford Till
Water Content	12%
Percent wet of Proctor optimum	1.2%
Undrained Shear Strength (kPa)	115
% Standard Proctor Optimum	101%
Loading Rate	100 kPa every 10 min
Time Held at Load (hours)	24
Pressure (kPa)	500
Geomembrane Manufacturer	Solmax
Geomembrane Thickness (mm)	1.5
Geomembrane Type	HDPE
Protection Layer	Non-Woven
Protection Layer MUA (g/m ²)	1080



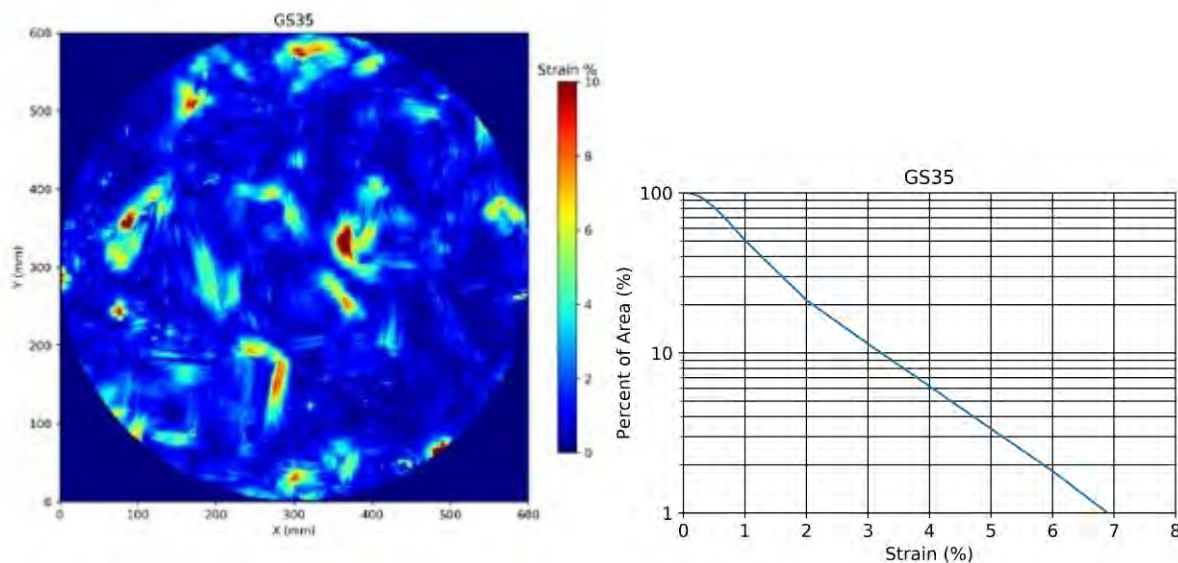
Test ID	GS32
Aggregate Above Geomembrane	TDA
Aggregate Description	ARMA
Soil Name	12%
Water Content	11%
Percent wet of Proctor optimum	0.7%
Undrained Shear Strength (kPa)	132
% Standard Proctor Optimum	102%
Loading Rate	100 kPa every 10 min
Time Held at Load (hours)	24
Pressure (kPa)	500
Geomembrane Manufacturer	Solmax
Geomembrane Thickness (mm)	2
Geomembrane Type	HDPE
Protection Layer	Non-Woven
Protection Layer MUA (g/m ²)	1080

Test ID	GS33
Aggregate Above Geomembrane	TDA
Aggregate Description	ARMA
Soil Name	Battleford Till
Water Content	12%
Percent wet of Proctor optimum	1.1%
Undrained Shear Strength (kPa)	127
% Standard Proctor Optimum	102%
Loading Rate	100 kPa every 10 min
Time Held at Load (hours)	24
Pressure (kPa)	500
Geomembrane Manufacturer	Solmax
Geomembrane Thickness (mm)	2
Geomembrane Type	HDPE
Protection Layer	Non-Woven
Protection Layer MUA (g/m ²)	1080

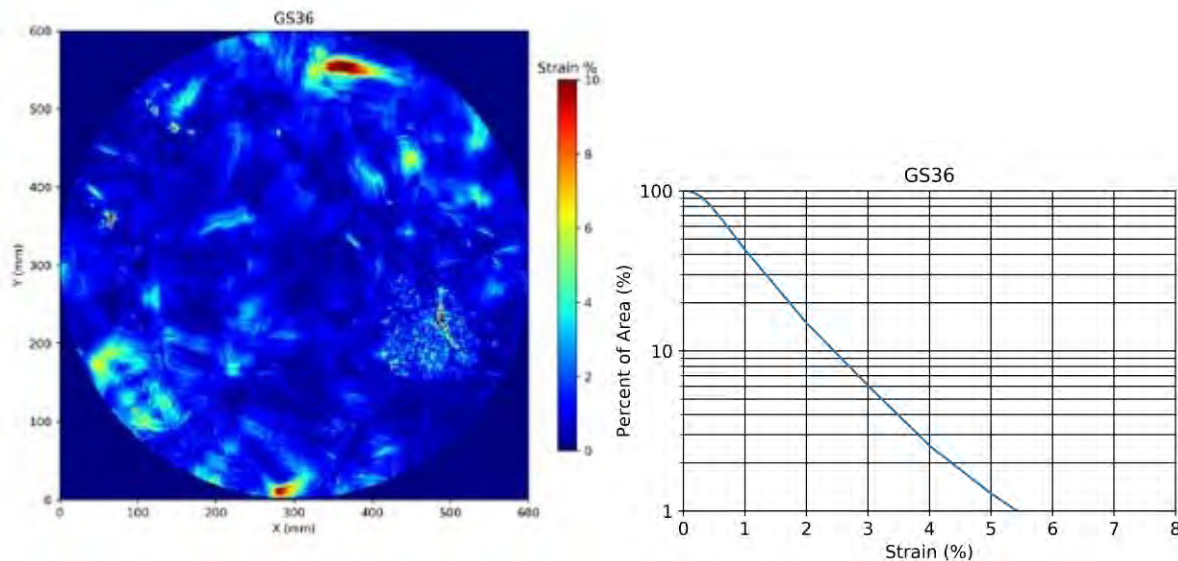
Test ID	GS34
Aggregate Above Geomembrane	TDA
Aggregate Description	ARMA
Soil Name	Battleford Till
Water Content	11%
Percent wet of Proctor optimum	0.9%
Undrained Shear Strength (kPa)	128
% Standard Proctor Optimum	102%
Loading Rate	100 kPa every 10 min
Time Held at Load (hours)	24
Pressure (kPa)	500
Geomembrane Manufacturer	Solmax
Geomembrane Thickness (mm)	2
Geomembrane Type	HDPE
Protection Layer	Non-Woven
Protection Layer MUA (g/m ²)	1080



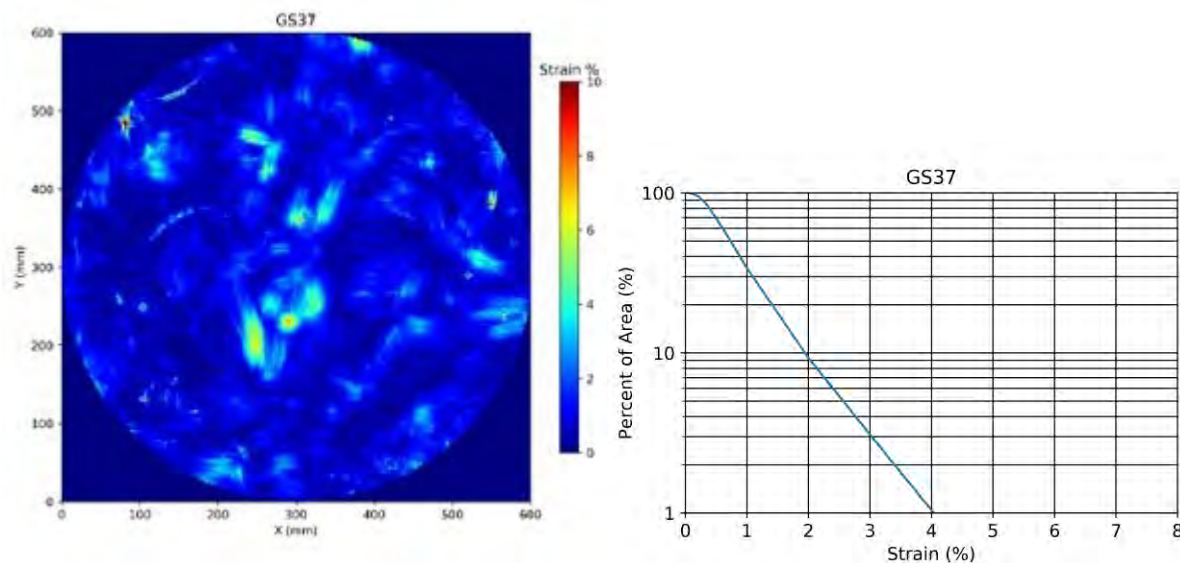
Test ID	GS35
Aggregate Above Geomembrane	TDA
Aggregate Description	ARMA
Soil Name	Battleford Till
Water Content	12%
Percent wet of Proctor optimum	1.2%
Undrained Shear Strength (kPa)	125
% Standard Proctor Optimum	102%
Loading Rate	100 kPa every 10 min
Time Held at Load (hours)	24
Pressure (kPa)	500
Geomembrane Manufacturer	Solmax
Geomembrane Thickness (mm)	2
Geomembrane Type	HDPE
Protection Layer	Non-Woven
Protection Layer MUA (g/m ²)	1360



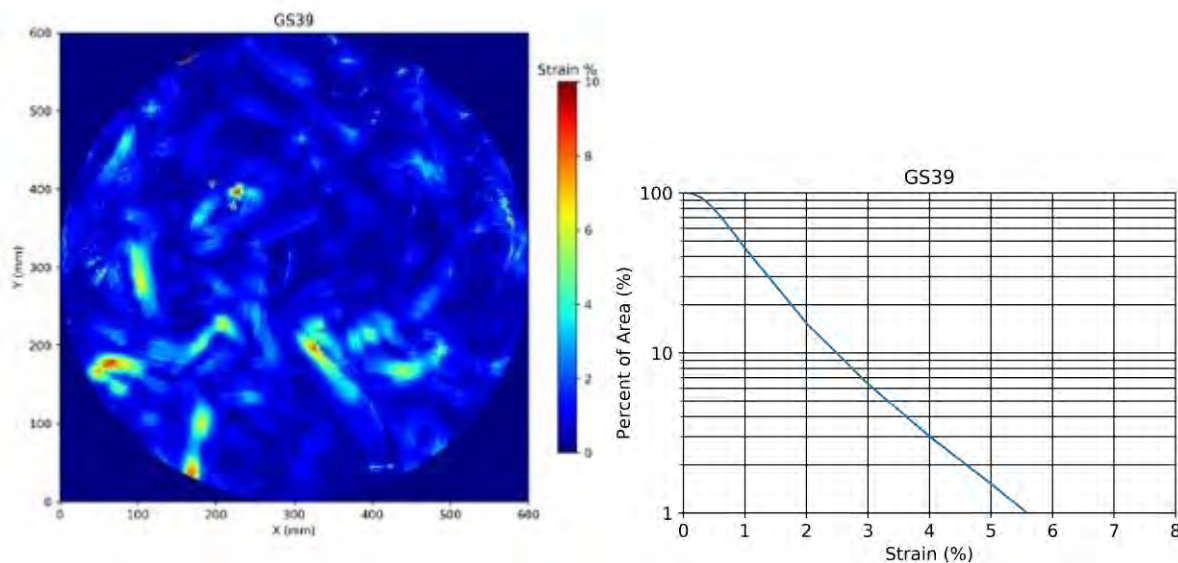
Test ID	GS36
Aggregate Above Geomembrane	TDA
Aggregate Description	ARMA
Soil Name	Battleford Till
Water Content	12%
Percent wet of Proctor optimum	1.2%
Undrained Shear Strength (kPa)	120
% Standard Proctor Optimum	102%
Loading Rate	100 kPa every 10 min
Time Held at Load (hours)	24
Pressure (kPa)	500
Geomembrane Manufacturer	Solmax
Geomembrane Thickness (mm)	2
Geomembrane Type	HDPE
Protection Layer	Non-Woven
Protection Layer MUA (g/m ²)	1624



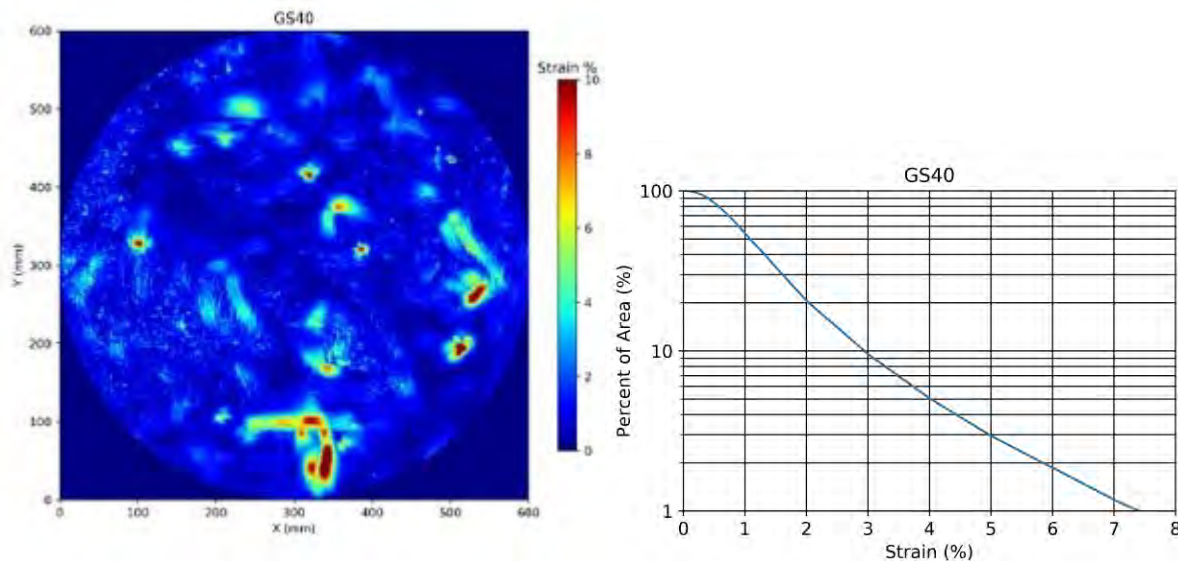
Test ID	GS37
Aggregate Above Geomembrane	TDA
Aggregate Description	ARMA
Soil Name	Battleford Till
Water Content	12%
Percent wet of Proctor optimum	1.2%
Undrained Shear Strength (kPa)	135
% Standard Proctor Optimum	102%
Loading Rate	100 kPa every 10 min
Time Held at Load (hours)	24
Pressure (kPa)	500
Geomembrane Manufacturer	Solmax
Geomembrane Thickness (mm)	2
Geomembrane Type	HDPE
Protection Layer	Non-Woven
Protection Layer MUA (g/m ²)	2450



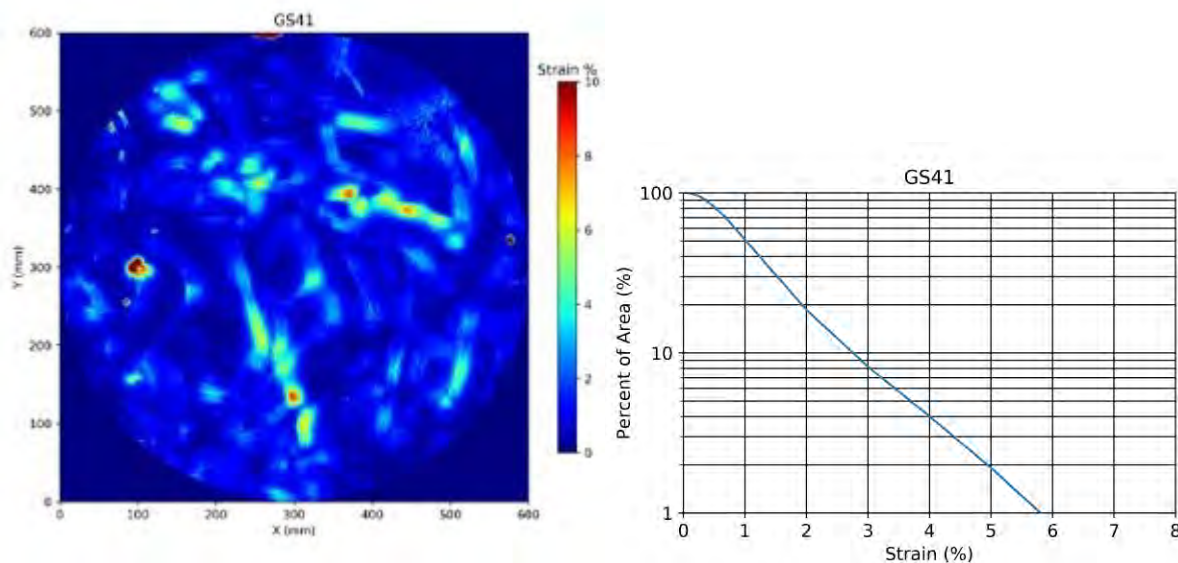
Test ID	GS39
Aggregate Above Geomembrane	TDA
Aggregate Description	ARMA
Soil Name	Battleford Till
Water Content	12%
Percent wet of Proctor optimum	1.1%
Undrained Shear Strength (kPa)	133
% Standard Proctor Optimum	102%
Loading Rate	100 kPa every 10 min
Time Held at Load (hours)	24
Pressure (kPa)	500
Geomembrane Manufacturer	Solmax
Geomembrane Thickness (mm)	2
Geomembrane Type	HDPE
Protection Layer	Non-Woven
Protection Layer MUA (g/m ²)	1624



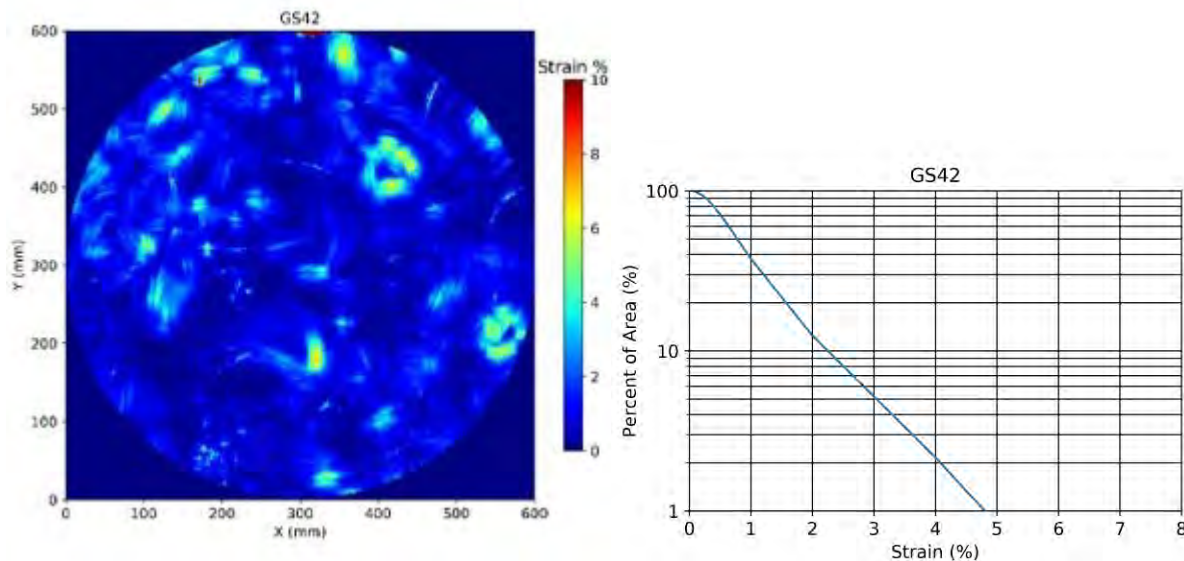
Test ID	GS40
Aggregate Above Geomembrane	TDA
Aggregate Description	ARMA
Soil Name	Battleford Till
Water Content	11%
Percent wet of Proctor optimum	0.9%
Undrained Shear Strength (kPa)	129
% Standard Proctor Optimum	102%
Loading Rate	100 kPa every 10 min
Time Held at Load (hours)	24
Pressure (kPa)	500
Geomembrane Manufacturer	Solmax
Geomembrane Thickness (mm)	2
Geomembrane Type	HDPE
Protection Layer	Non-Woven
Protection Layer MUA (g/m ²)	1360



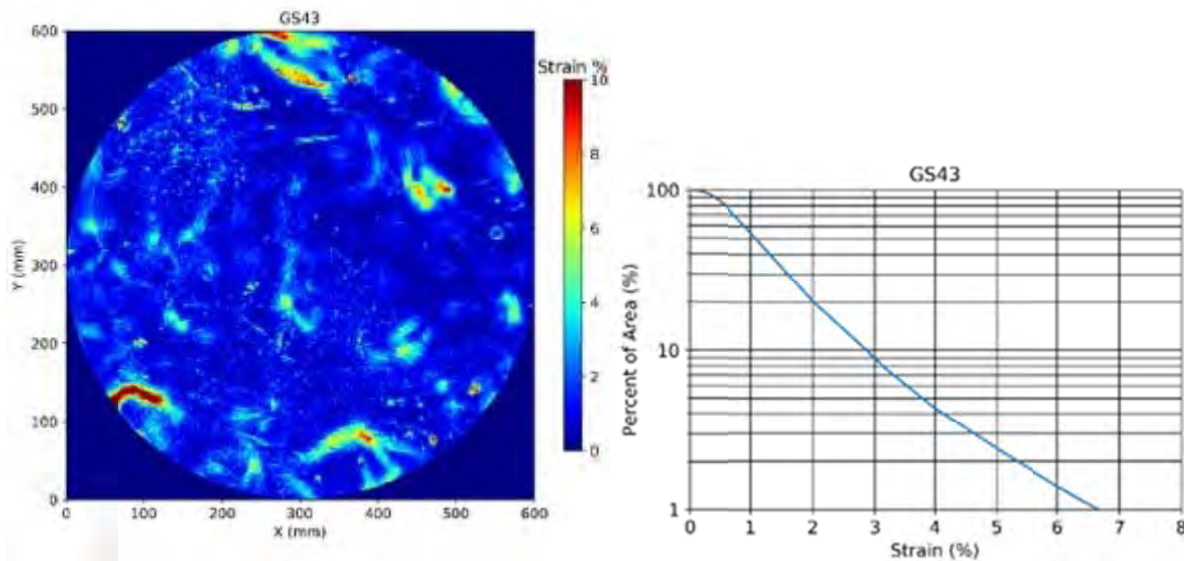
Test ID	GS41
Aggregate Above Geomembrane	TDA
Aggregate Description	ARMA
Soil Name	Battleford Till
Water Content	12%
Percent wet of Proctor optimum	1.2%
Undrained Shear Strength (kPa)	132
% Standard Proctor Optimum	102%
Loading Rate	100 kPa every 10 min
Time Held at Load (hours)	24
Pressure (kPa)	500
Geomembrane Manufacturer	Solmax
Geomembrane Thickness (mm)	2
Geomembrane Type	HDPE
Protection Layer	Non-Woven
Protection Layer MUA (g/m ²)	1624



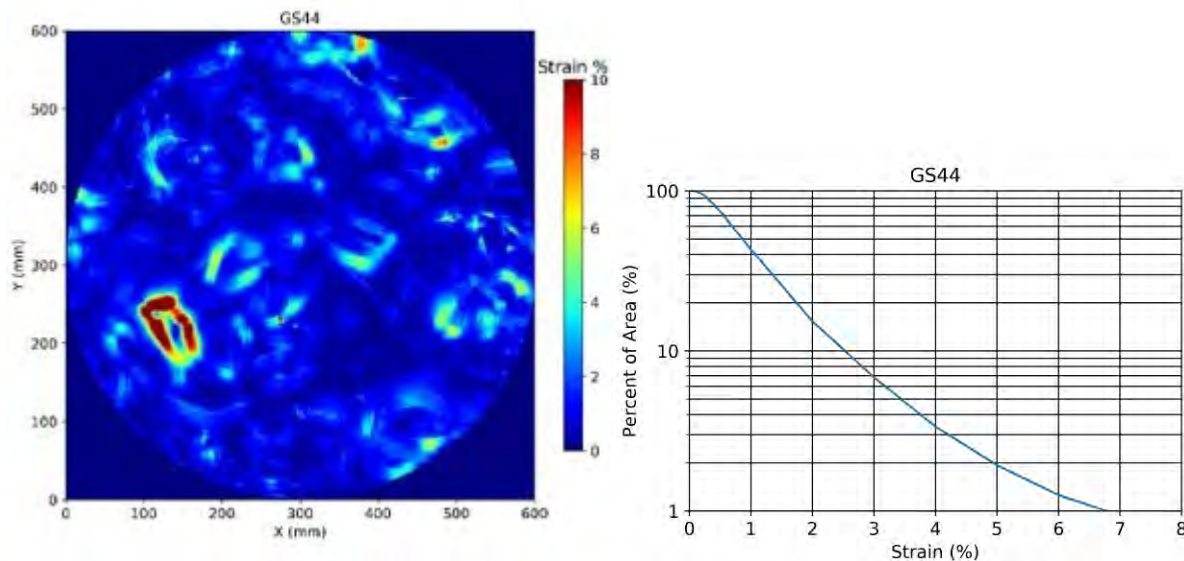
Test ID	GS42
Aggregate Above Geomembrane	TDA
Aggregate Description	ARMA
Soil Name	Battleford Till
Water Content	11%
Percent wet of Proctor optimum	0.9%
Undrained Shear Strength (kPa)	131
% Standard Proctor Optimum	102%
Loading Rate	100 kPa every 10 min
Time Held at Load (hours)	24
Pressure (kPa)	500
Geomembrane Manufacturer	Solmax
Geomembrane Thickness (mm)	2
Geomembrane Type	HDPE
Protection Layer	Non-Woven
Protection Layer MUA (g/m ²)	1360



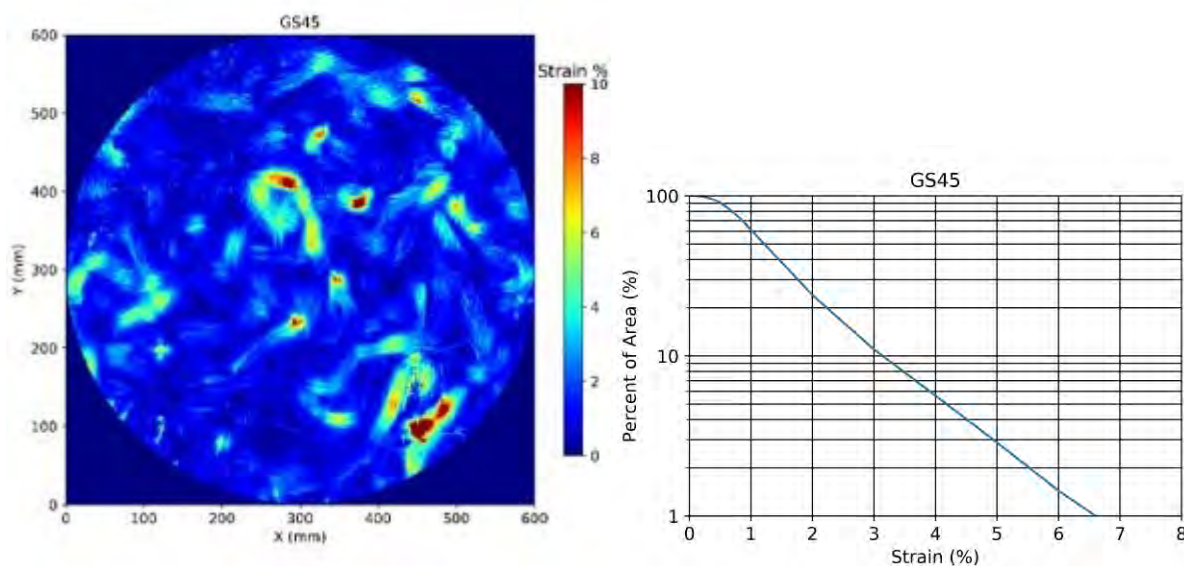
Test ID	GS43
Aggregate Above Geomembrane	TDA
Aggregate Description	ARMA
Soil Name	Battleford Till
Water Content	11%
Percent wet of Proctor optimum	0.8%
Undrained Shear Strength (kPa)	130
% Standard Proctor Optimum	101%
Loading Rate	100 kPa every 10 min
Time Held at Load (hours)	24
Pressure (kPa)	500
Geomembrane Manufacturer	Solmax
Geomembrane Thickness (mm)	1.5
Geomembrane Type	HDPE
Protection Layer	Non-Woven
Protection Layer MUA (g/m ²)	1624



Test ID	GS44
Aggregate Above Geomembrane	TDA
Aggregate Description	ARMA
Soil Name	Battleford Till
Water Content	12%
Percent wet of Proctor optimum	1.2%
Undrained Shear Strength (kPa)	127
% Standard Proctor Optimum	101%
Loading Rate	100 kPa every 10 min
Time Held at Load (hours)	24
Pressure (kPa)	500
Geomembrane Manufacturer	Solmax
Geomembrane Thickness (mm)	1.5
Geomembrane Type	HDPE
Protection Layer	Non-Woven
Protection Layer MUA (g/m ²)	1360

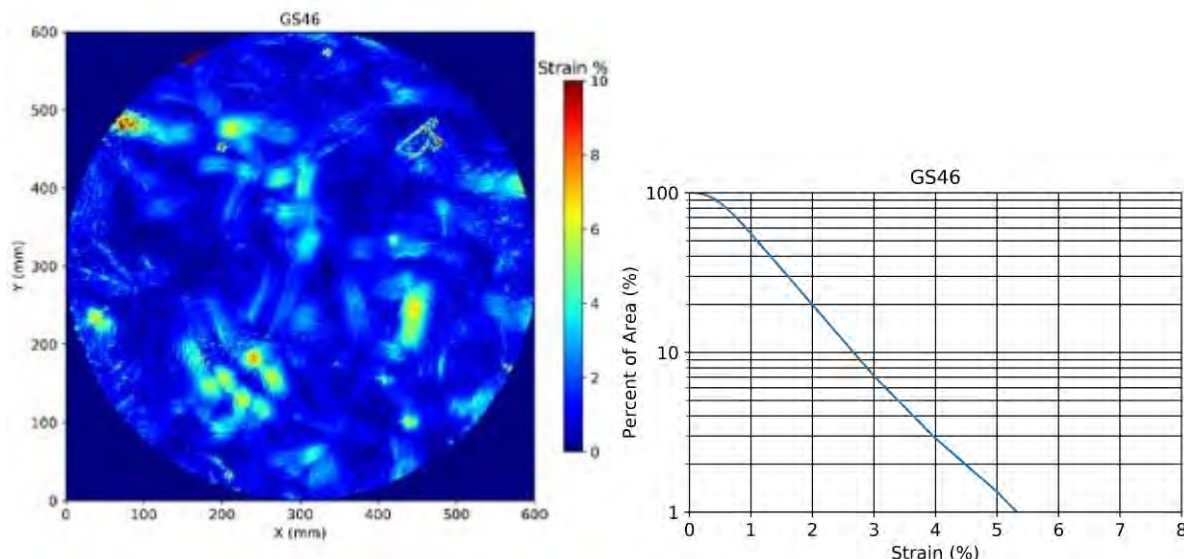


Test ID	GS45
Aggregate Above Geomembrane	TDA
Aggregate Description	ARMA
Soil Name	Battleford Till
Water Content	12%
Percent wet of Proctor optimum	1.5%
Undrained Shear Strength (kPa)	126
% Standard Proctor Optimum	101%
Loading Rate	100 kPa every 10 min
Time Held at Load (hours)	24
Pressure (kPa)	500
Geomembrane Manufacturer	Solmax
Geomembrane Thickness (mm)	2
Geomembrane Type	HDPE
Protection Layer	Non-Woven and Woven
Protection Layer MUA (g/m ²)	812 +Woven



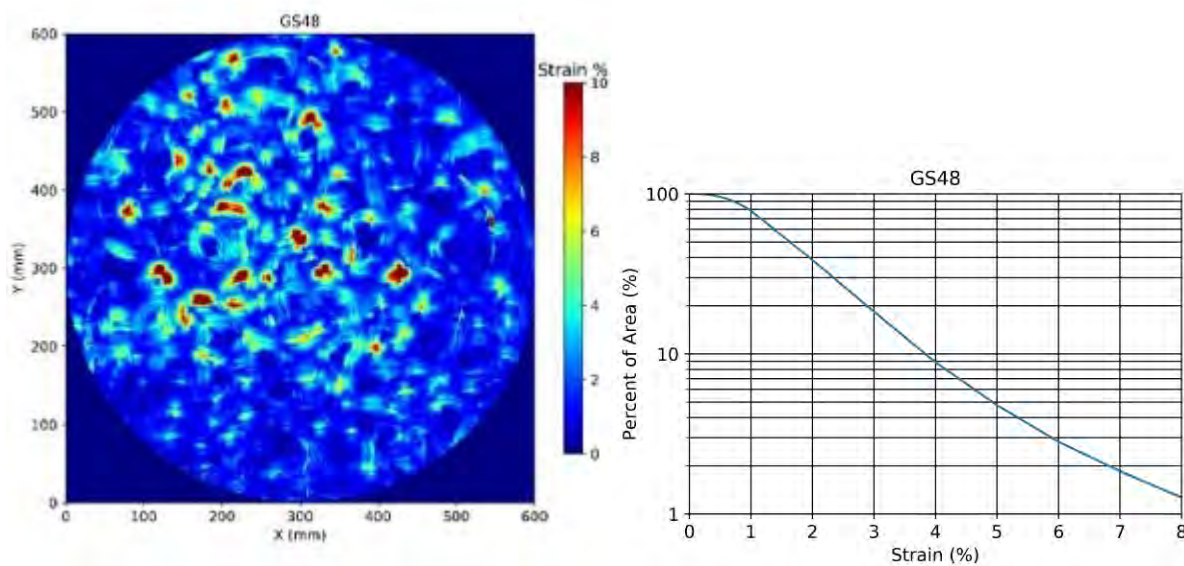
Test ID	GS46
---------	------

Aggregate Above Geomembrane	TDA
Aggregate Description	ARMA
Soil Name	Battleford Till
Water Content	12%
Percent wet of Proctor optimum	1.2%
Undrained Shear Strength (kPa)	128
% Standard Proctor Optimum	101%
Loading Rate	100 kPa every 10 min
Time Held at Load (hours)	24
Pressure (kPa)	500
Geomembrane Manufacturer	Solmax
Geomembrane Thickness (mm)	2
Geomembrane Type	HDPE
Protection Layer	Non-Woven and Woven
Protection Layer MUA (g/m ²)	1360 +Woven



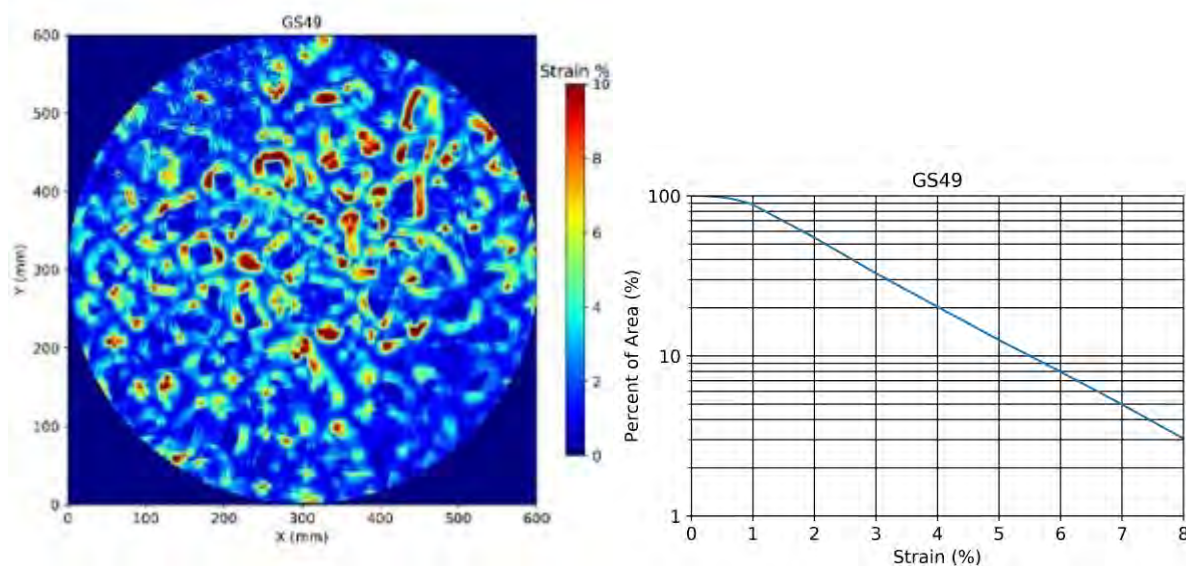
Test ID	GS47
Aggregate Above Geomembrane	TDA

Soil Name	Battleford Till
Water Content	12%
Percent wet of Proctor optimum	1.7%
Undrained Shear Strength (kPa)	126
% Standard Proctor Optimum	101%
Loading Rate	100 kPa every 10 min
Time Held at Load (hours)	24
Pressure (kPa)	500
Geomembrane Manufacturer	Solmax
Geomembrane Thickness (mm)	2
Geomembrane Type	HDPE
Protection Layer	Non-Woven
Protection Layer MUA (g/m ²)	1080



Test ID	GS49
Aggregate Above Geomembrane	Gravel

Aggregate Description	
Soil Name	Battleford Till
Water Content	12%
Percent wet of Proctor optimum	1.6%
Undrained Shear Strength (kPa)	123
% Standard Proctor Optimum	101%
Loading Rate	100 kPa every 10 min
Time Held at Load (hours)	24
Pressure (kPa)	500
Geomembrane Manufacturer	Solmax
Geomembrane Thickness (mm)	1.5
Geomembrane Type	HDPE
Protection Layer	Non-Woven
Protection Layer MUA (g/m ²)	540



Attachments: Volume 2



The role of undrained clay soil subgrade properties in controlling deformations in geomembranes



B.A. Marcotte*, I.R. Fleming

University of Saskatchewan, Saskatoon, SK S7N 5B4, Canada

ARTICLE INFO

Keywords:
 Geosynthetics
 Geomembrane
 Clay liner
 Protection layer
 Strain
 Stress cracking

ABSTRACT

Strains were evaluated in a 1.5 mm HDPE geomembrane from overlying coarse uniform drainage gravel when placed above six different compacted clayey soils while keeping pressure, protection, loading rate equal. In each case, a protection layer consisting of 400 g/m² nonwoven geotextile was placed over the geomembrane. Vertical load of 300 kPa was applied in a relatively short duration. A photogrammetry procedure was used to develop a digital elevation model for each deformed geomembrane surface and the distribution of resulting strain in the geomembrane was evaluated on a percent area basis. The proportion of the overall geomembrane area in which the localised strain exceeded 3% was related to the compacted water content, index soil properties, and undrained shear strength of the six different clayey soils. It was found that an increase in moulding moisture content resulted in increased geomembrane strain in all cases, but the magnitude of the increase in strain varied considerably, depending on the plasticity and silt content of the soil used.

1. Introduction

Geomembranes are manufactured from synthetic polymers used to control fluid migration between two materials. Composite liners are a system where a geomembrane is placed directly over a compacted clay liner (CCL) or geosynthetic clay liner. The geomembrane acts as an advection barrier when intact. The geomembrane is usually placed directly on clay liner to control transmissive flow along the interface (Nosko and Touze-Foltz, 2000). This combination of synthetic and a natural barrier acting together works effectively to impede the movement of contaminants between solid waste landfills and the environment (Rowe, 2005).

The construction of clay beneath a waste containment facility to provide a hydraulic barrier against contaminant movement predates the use of geomembranes and has been well documented over the years (Benson et al., 1999; Benson and Daniel, 1990, 1994; Boynton and Daniel, 1985; Daniel, 1984, 1987). Current practice is to ensure that the CCL is compacted at a water content higher than the Standard Proctor optimum moisture content (W_{opt}), as this has been shown to reduce the hydraulic conductivity due to the reduction in macropores as the soil becomes homogenous but is accompanied by decreased strength characteristics (Benson and Daniel, 1990; Benson et al., 1999).

In solid waste management facilities, a drainage layer is placed over the geomembrane to control hydraulic head caused by leachate. Coarse

uniform gravel is recommended as it has been shown that a larger particle size reduces the rate of biologically induced clogging (Fleming et al., 1999; Fleming and Rowe, 2004). A major disadvantage of the large, uniform aggregate is the high contact pressures on the geomembrane, which have been shown to be approximately 100 times larger than the average applied pressure of the waste above, when 50 mm gravel is used (Brachman and Gudina, 2008).

The placement of a geomembrane between a deformable subgrade and drainage layer results in localised deformations of the geomembrane. The deformations result in small areas of high tensile strain in the geomembrane which accelerate stress-cracking. Mechanical properties are reduced by the presence of elevated temperatures and chemical leachates (Ewais et al., 2018). Seeger and Muller (2003) suggest that strains be limited to 3% to be conservative in allowing for 100 years of service life. A 6% strain limit has been proposed by Peggs et al. (2005) for smooth HDPE geomembranes. A study by Abdelaal et al. (2014) evaluated strains under simulated field conditions. The geomembranes were first aged in synthetic leachate (Rowe et al., 2014), and testing occurred under a 250 kPa load until puncture was detected. The study was performed with 1.5 mm HDPE geomembrane placed over a geosynthetic clay liner. Cracking occurred at strains as low as 6% strain (Abdelaal et al., 2014) when strains were calculated using the method developed by Tognon et al. (2000).

Generally, a geomembrane strain study consists of large scale

* Corresponding author.

E-mail addresses: bryce.marcotte@usask.ca (B.A. Marcotte), ian.fleming@usask.ca (I.R. Fleming).

testing at known pressures corresponding to a reasonable height of waste. Early geomembrane strain testing consisted of gravel on a geomembrane above an elastomer pad (Brummermann et al., 1994; Zanzinger, 1999). Recent testing with a hard elastomer pad, a hydrated GCL, and no foundation layer highlighted the importance of the sub-grade stiffness. Repeat testing indicated that testing with a hard foundation layer resulted in the least strain, whereas testing with no foundation layer present gave a conservative estimate of maximum strain (Austin et al., 2014).

Tognon (1999) questioned whether strain testing on rubber mats was representative of field conditions as compacted clay behaves differently than a rubber mat. Instead of a rubber mat, Tognon (1999) compacted a clay barrier at conditions reasonably representative of the field. The clay consisted of a low plasticity Halton Till, with a plasticity index of 10, and was compacted at 4% wet of proctor optimum to 90% of maximum proctor dry density with an undrained shear strength of 34 kPa, representing the upper range of water contents and lower range of densities as proposed by Benson et al. (1999).

Strain in the geomembrane has been measured through scanning the surface of a lead sheet placed between the geomembrane and the underlying clay to acquire a profile (i.e. Brachman and Gudina, 2008; Brachman and Sabir, 2013; Hornsey and Wishaw, 2012; Tognon et al., 2000). Working from the method developed by Brummermann et al. (1994), Tognon et al. (2000) developed a more adaptable grid scanning method. Basic kinematic deformations were used to assess the geomembrane strain. The method developed by Tognon et al. (2000) considers the membrane and bending components of strain through numerical approximates. The membrane strain assumes zero shear strain and that every point is displaced solely in the vertical direction. Using a uniform horizontal spacing (Δx) of the vertical locations (z), the membrane strain can be approximated by:

$$\varepsilon_M = \sqrt{\left[1 + \left(\frac{1}{2\Delta x}[z_{i+\Delta x} - z_{i-\Delta x}]\right)\right]} - 1 \quad (1)$$

Where $z_{i+\Delta x}$ and $z_{i-\Delta x}$ are the vertical displacements at point $i + \Delta x$ and $i - \Delta x$, and Δx is the horizontal spacing. The bending strain considers differences in strain through the thickness of the geomembrane (Brachman and Eastman, 2013). The bending strain will be the greatest at the geomembrane surface and zero at the middle. It is considered by a second-order finite difference approximation:

$$\varepsilon_B = \frac{m}{(\Delta x)^2}[z_{i+\Delta x} - 2z_i + z_{i-\Delta x}] \quad (2)$$

Where m is the distance from the middle of the geomembrane. The resulting strain is the sum of the membrane and bending strain:

$$\varepsilon_T = \varepsilon_M + \varepsilon_B \quad (3)$$

This method (Tognon et al., 2000) was applied to deformations selected manually, and only applied to measurements made along a single line. Hornsey and Wishaw (2012) identified that manual selection of dimples may not properly assess damage to geomembranes and suggested a grid scanning method which reproduces the geomembrane surface into a uniform grid in both x and y directions. For each grid point, the maximum strain is then calculated by considering membrane strain only for each of the eight neighboring points. Each point has four orthogonal neighbors and four diagonal neighbors, and the highest calculated strain was then assigned to the cell (Hornsey and Wishaw, 2012). Strain of the geomembrane was then assessed on a percentage of the total area above a given strain as opposed to simply the maximum strain from manual selection of dimples.

Numerous studies on geomembrane strains have evaluated behavior when placed above compacted clay with a plasticity index between 10 and 12% (Brachman and Gudina, 2008; Brachman and Sabir, 2013; Gudina and Brachman, 2006; Rowe et al., 2013; Tognon et al., 2000). A significant increase in strain was calculated when the moulding water content at which the clay was compacted was higher than the standard

proctor optimum water content, hereafter referred to as “wet of optimum” (Rowe et al., 2013). This increase in strain with increasing water content indicates that a more deformable foundation layer may result in greater geomembrane strains.

Brachman et al. (2018) evaluated geomembrane strains using a machined probe with compacted Halton Till below. The till was compacted to different densities and moisture contents. It was concluded that more strain was developed at a higher degree of saturation due to a reduction in soil suction (which would reduce the effective stress and strength). Tests completed using soil at the same water content but different dry densities (and therefore different degrees of saturation) resulted in almost identical strains – which was attributed to initial suction and dry densities offsetting one another between each soil, although suctions were not measured (Brachman et al., 2018).

As noted by Benson et al. (1999), compacting CCL's wet of W_{opt} will result in decreased bearing capacity, shear strength, and increased compressibility. Numerous studies have evaluated geomembrane strains above different compressible medium such as geosynthetic clay liners, sand layers, rubber mats, and CCL's (Brachman and Gudina, 2008; Brachman and Sabir, 2013; Brummermann et al., 1994; Dickinson & Brachman 2008; Gudina and Brachman, 2006; Tognon, 1999; Tognon et al., 2000). However, there has been relatively little focus on the compacted clayey soil subgrade and the interaction between variations in clayey soil properties, compacted moisture content and the geomembrane in terms of the resulting strain in the geomembrane.

The objective of this research is to evaluate the influence of varying the type of clayey soil and its moulding water content on the strains induced in the overlying geomembrane. A testing procedure based on digital photography was developed to allow for in-place surface scanning of the deformed clay. Six different clayey soils at differing water contents were compared and evaluated using the method developed by Tognon (1999) at the same applied pressure, duration, and with equal geotextile protection.

2. Materials and methods

2.1. Test apparatus

Each test was performed using a 300 mm × 300 mm box. It consisted of (from bottom to top) compacted clay, a thin layer of plastic wrap, a 1.5 mm HDPE geomembrane, 400 g/m² nonwoven geotextile, drainage gravel, separator geotextile, sand and load plate. A diagram of the test set up is given in Fig. 3. A layer of plastic wrap was added to prevent adherence of the clay to the geomembrane and allowed for direct scanning of the resulting clay surface. Others have used lead sheets to capture the deformation (Tognon et al., 2000; Rowe et al., 2013). A sand layer was added to aid in distributing the applied load evenly to the gravel. The load was applied through a hydraulic loading ram.

2.2. Materials

Six clayey soils from across Canada were used: Regina clay from southern Saskatchewan; Battleford till and Floral till from central Saskatchewan; a glacial till from east-central Alberta herein referred to as “Edmonton Till”; commercial pottery clay from southern Alberta; and Halton till from southern Ontario. Each of these soils (with the exception of the pottery clay) is typically used for CCL construction in their respective localities, and this group of soils exhibit a reasonable range of index properties as tested and given in Table 1 and by the grain size distribution in Fig. 1. Gravel larger than 10 mm was removed prior to testing.

The samples of Regina clay were taken at a site near Regina, Saskatchewan. The index results of the lacustrine Regina clay are consistent with Fredlund (1975). The Battleford and Floral till samples

Table 1

Index properties of soil subgrades used in testing.

Soil	USCS	Gs	LL (%)	PI (%)	Activity	w_{opt} (%)	ρ_{Dmax} (kg/m^3)	Sand & Gravel (%)	Silt (%)	Clay (%)
Regina Clay (southern Sask.)	CH	2.83	74.7	47.7	0.8	26.0	1460	21.0	21.0	58.0
Battleford Till (central Sask.)	CL	2.73	23.3	9.7	0.65	10.0	2030	49.5	35.6	14.9
Floral Till (central Sask.)	CL	2.78	42.9	20.9	0.54	21.0	1620	9.2	51.7	39.0
Halton Till (southern Ont.)	CL	2.79	31.5	13.5	0.75	13.0	1960	33.8	48.3	17.9
Edmonton Till (Alberta)	CL	2.72	32.8	17.8	0.87	13.5	1875	36.7	43.0	20.4
Pottery Clay	CL	2.63	46.0	27.2	0.64	18.0	1680	5.5	52.3	42.2

LL –liquid limit; PI – plasticity index; w_{opt} – optimum moisture content using standard compaction; ρ_{Dmax} – maximum dry density using standard compaction; Gs – Specific Gravity.

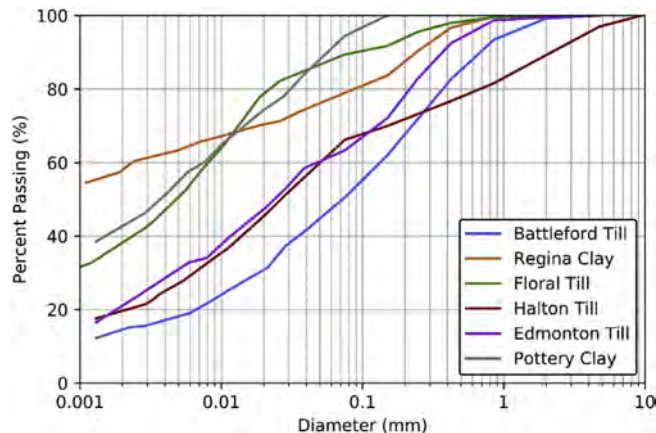


Fig. 1. Grain size distribution of soils used in testing.

were taken from a site 20 km north of Saskatoon, Saskatchewan. The index results are consistent of a lower deposit of Battleford till, and an upper deposit of Floral till (Sauer et al., 1992). The Halton till was obtained from Ontario. The index results are similar to the findings by Rowe et al. (1993) for the weathered upper Halton till deposit. The Edmonton till sample was taken from the construction of a compacted liner in Alberta, and index properties are similar to those reported by Elwood and Martin (2016).

Standard proctor compaction curves for each soil are presented in Fig. 2. To ensure a uniform soil, each soil was dried, crushed, sieved to remove gravel larger than 10 mm, mixed, and then the required amount of distilled water was added. Samples were then placed in a humidity controlled room for a period of at least 48 h to ensure a uniform distribution of water.

A 1.5 mm non-textured high-density polyethylene (HDPE) geomembrane was used in all tests. All samples of geomembrane were cut from the same roll. A $400 \text{ g}/\text{m}^2$ (12 oz/yd) non-woven needle-punched

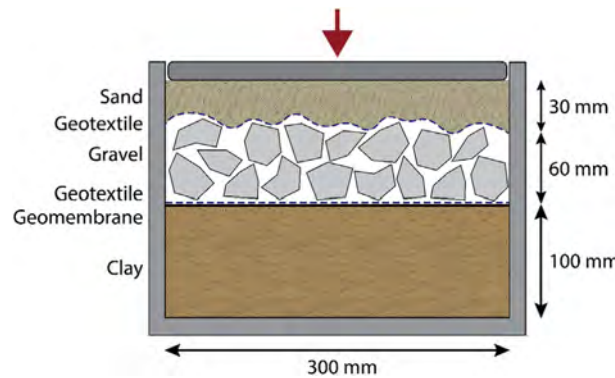


Fig. 3. Diagram of testing device used in current study.

geomembrane was placed over the geomembrane. It should be noted that there are published recommendations that even much heavier non-woven geotextiles may provide inadequate protection (Brachman et al., 2014; Rowe et al., 2013). The relatively light protection layer was used to amplify the differences in induced geomembrane strain placed over different clayey soils compacted to varying density at different moulding water content.

2.3. Test procedure

2.3.1. Test set-up

The clays were compacted into the testing apparatus using a standard Proctor hammer in three lifts at 240 Proctor hammer drops per lift, which corresponds to standard proctor energy for the larger volume of the device. Each lift of soil was weighed prior to compaction to determine bulk density, and allow for calculation of as compacted dry density. Moisture contents were acquired on the mixed soil prior to testing. A steel rolling pin was used to smooth the surface, significant irregularities in the smoothed surface could lead to inaccurate estimation of strain as described in section 2.3.3. Undrained shear strength measurements were performed using a hand shear vane after placement of the second lift of soil as to not disturb the final surface. Five measurements of undrained shear strength were conducted for each soil. The average standard deviation of shear strength measurements for all soils was 6 kPa.

A single sheet of polyethylene plastic wrap of 0.02 mm thickness was placed on top of the clay. The polyethylene plastic wrap was used to prevent the clay from adhering to the geomembrane upon removal. Others have used a thin (0.3 mm–0.5 mm) lead sheet to capture the deformations (Rowe et al., 2013; Tognon et al., 2000) or suggested an aluminum sheet (Hornsey and Wishaw, 2012). The lead sheet is advantageous when laser scanning, as a plaster mold can be created, and the surface can be transported for analysis (Gudina, 2007). Rowe et al. (2013) observed fewer punctures from gravel in areas where a lead sheet was present, however no conclusion about the observer effect of the lead sheet could be made. Since a photogrammetric procedure was used in this study, the lead sheet could be replaced by the very thin

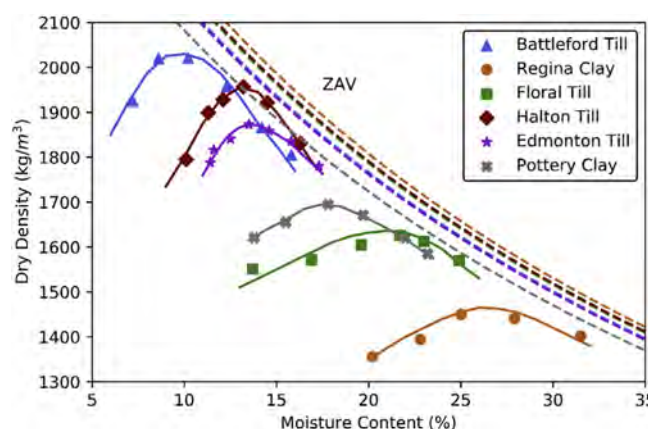


Fig. 2. Standard Proctor curves of soils used in testing (ZAV = zero air voids).



Fig. 4. Screened and crushed gravel used in testing.

polyethylene film to reduce the potential observer effect, and the clay surface was photographed directly in place.

The geomembrane and geotextile cushion were placed over the polyethylene sheet. Screened crushed angular gravel, shown in Fig. 4, was dropped loosely from a height of 300 mm onto the geotextile. The gravel was between 50.8 mm and 31.5 mm with 65% passing the 37.5 mm screen and was routinely sieved between tests to ensure it was as identical as possible. The gravel was placed at a bulk density of 1600 kg/m³. No friction treatment was used as the layer of gravel was thin relative to the dimensions of the device. Furthermore, as only a single pressure was used in the experiment, any loss due to friction would be constant throughout each test. Uniform pressure was applied to the gravel through placement of a geotextile covered in sand. A steel plate of 25 mm thickness applied pressure to the sand. Load was applied using a hydraulic loading system. The applied pressure was increased to 300 kPa in 50 kPa increments every 0.5 h. The final pressure of 300 kPa was held for a duration of 21 h. This would correspond to a landfill height of approximately 20–25 m if the unit weight of waste is taken between 12 and 15 kN/m³. All tests were conducted at 23 °C ± 2 °C.

Testing in the same apparatus at a lower applied vertical stress of 75 kPa with tensiometers indicated the buildup of excess pore water pressures greater than 30 kPa at similar loading rates. The development of excess pore pressures in the unsaturated soil would result in a different response when compared to drained conditions (Fredlund et al., 1978; Jennings and Burland, 1962). The loading applied during this testing can therefore be taken to be essentially undrained. While many municipal landfills are slowly filled over many years or decades, this is usually not the case for industrial or mining wastes. In the authors' experience, many industrial waste disposal sites are filled to several tens of metres height in two years or less. Given the consolidation rate of compacted clay liners, this rapid filling rate would result in excess pore pressure within the clay liner.

It should be noted that others have demonstrated that the long-term geomembrane stress-strain behavior results in larger strains over time, and this can be accelerated with temperature and/or longer test durations (Brachman and Sabir, 2013; Sabir and Brachman, 2012). However, short term tests have been used to evaluate specific interactions such as gravel contacts and spacings (Brachman and Gudina, 2008). Therefore, this paper intends to evaluate the role the clay has on the deformation of the geomembrane as a means of predicting performance, rather than the long term assessment in geomembrane strains. This is further amplified through the use of a unreasonably light geotextile protection layer.

2.3.2. Photogrammetry procedure

The gravel, geotextile, geomembrane and polyethylene wrap were

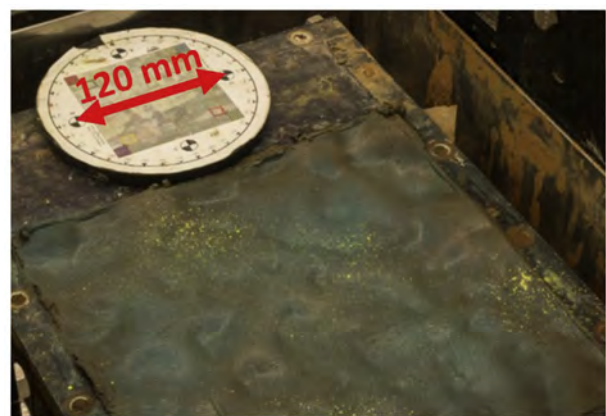


Fig. 5. Photograph of spray painted clay surface and scale bar.

taken off to reveal the deformed clay surface. A light coat of three different coloured matte spray paints were applied to the clay surface in a random fashion, as shown in Fig. 5. The spray paint removed any shine from the surface and provided random coloured pixels for the photogrammetry software to match. Photogrammetry methods involve triangulation in which common points from at least two different images are mathematically evaluated to determine the location of the point and the camera positions (Mikhail et al., 2001).

A scale bar (Porter et al., 2016) was placed near the clay, as shown in Fig. 5, to provide a reference distance to calculate elevations and locations. Approximately 35 photographs were taken from different angles and heights around the clay surface and scale bar. Each photograph was taken using a Canon 70D (APS-C 20.2 megapixels) with a 50 mm fixed lens mounted on a tripod. The aperture, shutter speed, and ISO setting remained constant for all pictures (f22, 1", ISO 100). The photographs were then processed and analyzed using photogrammetry software to create a digital elevation model (Agisoft, 2016; Cignoni et al., 2008).

The photogrammetry procedure resulted in a dense point cloud distribution with an average point density of 107 points per square millimeter (standard deviation of 15 points per square millimeter). The check scale bars were accurate within an average of 0.14% (standard deviation of 0.05%) across an 84.85 mm length scale bar. The point cloud was then developed into a high-quality digital elevation mesh model. The model was then refined into a defined grid, as described below.

2.3.3. Strain calculation

The areal distribution of strain was calculated using Tognon's combined bending and membrane strain (Tognon et al., 2000) with the grid scanning method developed by Horsey and Wishaw (2012) as described in the introduction. A uniform 1.5 mm by 1.5 mm grid was developed and elevation values from the digital elevation model were interpolated onto each grid "cell". For each cell, the membrane strain for the geomembrane was computed using Eq. (1) for the eight surrounding neighbor cells – two orthogonal and two diagonal calculations.

Similarly, bending strain was calculated using Eq. (2) for the surrounding orthogonal and diagonal cells. The bending strain was calculated for both the bottom and top of the geomembrane. The total maximum calculated strain was then the sum of the maximum bending and maximum membrane strain for each grid point. The total maximum strain was then assigned to the strain array. The procedure continued iterating until all strains were calculated across the grid.

It should be noted that the method developed by Tognon et al. (2000) does not properly assess geomembrane strain as it assumes only vertical deformation in the calculation of membrane strain (Eq. (1)). Brachman and Eastman (2013) found that under perfect axisymmetric

Table 2

Summary of compacted clay soil properties.

Test Name	Compacted Water Content (%)	Water Content Relative to W_{opt} (%)	% Relative compaction (ρ_D/ρ_{Dmax})	Undrained Shear Strength (kPa)	% Area Greater than 3% Strain
BT1	10.3	+0.3	98	138	8.5
BT2	11.9	+1.9	96	78	16.9
BT3	11.9	+1.9	96	82	21.5
BT4	11.9	+1.9	96	94	18.4
BT5	11.9	+1.9	96	100	17.0
BT6	11.8	+1.8	96	100	18.9
BT7	11.8	+1.8	96	100	16.2
BT8	13.6	+3.6	94	48	32.1
BT9	14.0	+4.0	91	36	32.7
RC1	25.5	-0.5	97	146	2.7
RC2	26.3	+0.3	98	144	7.1
RC3	28.0	+2.0	96	101	15.8
RC4	30.6	+4.6	93	67	27.7
FT1	19.6	-1.5	95	174	11.8
FT2	20.5	-0.5	97	164	11.6
FT3	22.7	+1.7	97	70	31.8
FT4	23.9	+2.9	92	63	32.4
HT1	12.6	-0.4	97	138	6.0
HT2	13.6	+0.6	96	121	11.9
HT3	15.9	+2.9	91	46	30.4
HT4	17.3	+3.8	89	29	31.5
ET1	13.0	-0.5	99	155	6.9
ET2	14.0	+0.5	97	141	8.5
ET3	16.2	+2.7	94	67	24.8
ET4	17.1	+3.6	92	57	32.7
PC1	18.2	+0.2	98	164	13.4
PC2	22.5	+4.5	91	53	37.6

BT – Battleford Till; RC – Regina Clay; FT – Floral Till; HT – Halton Till; ET – Edmonton Till; PC – Pottery Clay.

conditions, neglecting radial displacements underestimated the true strain. The laboratory data collected by Brachman and Eastman (2013) was used to compare axisymmetric thin plate theory to a finite element solution, further confirming the underestimation of maximum strain (Eldesouky and Brachman, 2018). However, it was recognized that Tognon's method is the most appropriate for non-axisymmetric conditions (Eldesouky and Brachman, 2018) and therefore is used for this study.

3. Results

3.1. Summary of test results

Strain measurements were completed on the geomembrane over each subgrade soil listed in Table 1. A summary of the compacted clay water content and shear strength results are given in Table 2 and strain distributions in Fig. 7. Undrained shear strength was measured with a hand vane and measured values were corrected for plasticity (Bjerrum, 1972).

3.2. Deformed surfaces and strain maps

An example of the deformed surface and contour maps showing the distribution of strain are given in Fig. 6 for the Halton Till compacted at the lower and upper water contents. Less vertical deformations are observed in the soils compacted at lower moisture contents (relative to their respective optimums), which result in lower average strains.

3.3. Strain area distributions

Strain area distributions, as proposed by Hornsey and Wishaw (2012), are shown in Fig. 7 as a method of comparing the response of the different clay/geomembrane systems in terms of the induced

geomembrane strains. The amount of strain in the geomembrane may be represented as the percent of the overall geomembrane area in which the allowable maximum threshold strain was exceeded. The distribution allows for a visual comparison between tests of geomembrane strains at any level relative to the total area. For example, in Fig. 7, the area of the geomembrane surface exceeding 3% strain was lower for the Battleford till compacted at $W_{opt} + 0.3\%$ (8.5% of the area) compared to the same Battleford till compacted at $W_{opt} + 4\%$ (32.7% of the area).

As shown in Fig. 7, all soils exhibited an increase in strain at higher water contents. The shaded region represents the increased strain when moving from lower to higher compacted water content (relative to optimum).

For the purpose of the discussion of test results, a minimum calculated strain (Tognon method) of 3% is assumed to be a reasonable allowable threshold maximum strain value above which stress cracking may occur based on the recommendations by Seeger and Muller (2003) for strain calculations that consider bending and membrane strain. However, proper threshold strain should be assessed and assigned based on design constraints and further research. Furthermore, this study is not intended to suggest what should be the acceptable proportion of the overall geomembrane area in which localised strain exceeds such a threshold. All the geomembrane tests in this study have some portion exceeding this 3% threshold strain, however, a different percentage of the total area exceeds this threshold depending upon the soil type, compacted moisture content and dry density. The same conclusions would have been reached regardless of the particular value selected for the threshold strain.

3.4. Undrained shear strength

The percent area greater than threshold strain can also be plotted against the undrained shear strengths as shown in Fig. 8. Undrained shear strength appears to provide a relatively quick indication of geomembrane strains which might be expected. For some of the tests, the compacted density would have failed to meet 95% standard proctor compaction, a typical field specification, and results for these tests are shown as non-filled symbols in Figs. 8, 9 and 13.

As demonstrated in Fig. 8, there is relationship between the undrained shear strength of the clay and the area of the geomembrane subject to the threshold strain. Soils compacted at high moisture content, low dry density and weak undrained shear strengths do correspond to large areas of the geomembrane exceeding the threshold strain. Undrained shear strength is a relatively poor correlation as the silty Floral Till and Pottery clay, while having similar undrained shear strength to other soils, were associated with increased geomembrane strains.

3.5. Influence of moulding water content

Each soil increased in the percent area greater than 3 percent strain by 5–6 times when the moisture content increased from near optimum to wet of standard proctor optimum. Daniel and Benson (1990) indicate the importance of compacting wet of standard optimum moisture content, but also recommend considering the resulting effect of reduction in shear strength and interactions with the overlying geomembrane. In Fig. 9, a direct comparison is made between moulding water content (expressed as a difference from optimum) and the percentage of the area with strain exceeding 3%. It is evident that there is a similar trend for all six soils. The increase in strain with higher compacted water content is consistent with the findings of others (Brachman and Sabir, 2010; Rowe et al., 2013).

As shown in Fig. 9, not all soils tend to fall on the same trend line. The highly plastic Regina Clay falls below the line of best fit, which may be attributed to the higher matric suction developed in the clay increasing strength and reducing geomembrane deformation. In contrast, the medium plasticity Floral Till and pottery clay both fall above the

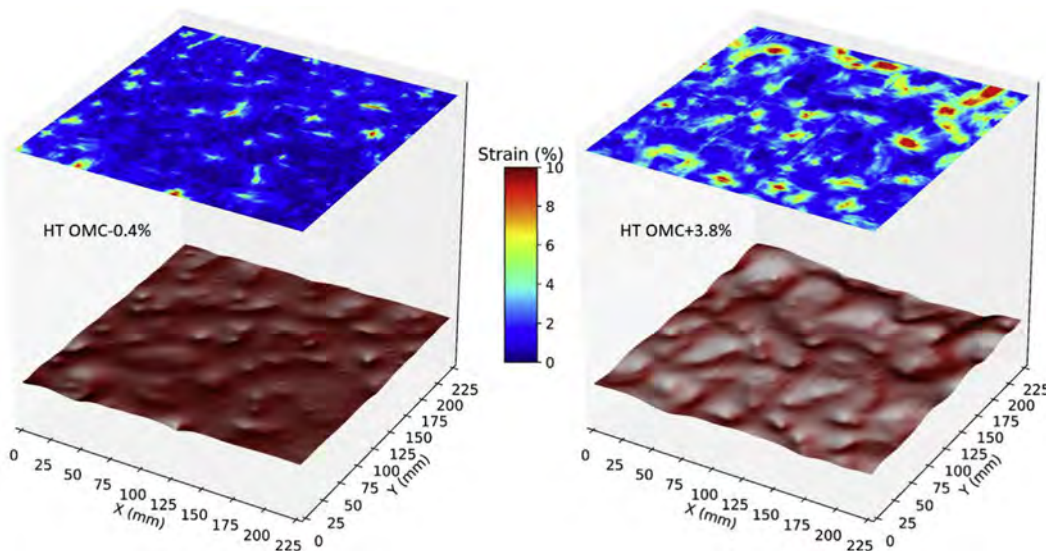


Fig. 6. Strain maps and deformed surfaces for geomembrane above Halton Till.

line of best fit, which may be caused by differences in grain size distributions, such as the absence of coarse grained fraction as well as high silt content (see Fig. 1).

A series of repeat tests were performed at BT $W_{opt} + 2\%$ to evaluate repeatability. The area greater than 3% strain varied from 16.2% to 21.5% indicating a test precision of approximately 2.7%. Differences between tests reflect the random distribution and orientation of the contact points between the gravel as placed on the geomembrane surface. Varying the contact pressure has been shown to result in different geomembrane strains (Brachman and Gudina, 2008).

3.6. Geomembrane strain related to clay index properties

Taking the slope of each soil in Fig. 9, results in a different relationship between compacted water content and geomembrane strain depending on the soil used. As an example, the Battleford Till, Floral Till and Regina Clay soils and their respective slopes are given in Fig. 10.

The slope, denoted by $\Delta SA_{3\%}/\Delta w$ in Fig. 10, represents the amount of change in geomembrane strain with unit change in moisture content for cases with equal compactive energy. This value might be considered an indication of how carefully moisture content might have to be controlled during CCL construction. For the low plasticity Battleford till, smaller changes in moisture content result in greater increase in strain compared with the more plastic Regina Clay soil. The Floral till had a $\Delta SA_{3\%}/\Delta w$ value higher than the Regina Clay, but less than the Battleford Till. Values of $\Delta SA_{3\%}/\Delta w$ for the other clayey soils were determined and are presented in Fig. 11.

A decrease in plasticity index is associated with increased vulnerability of the soil geomembrane system to increased moulding water content – and thus a greater difference in geomembrane strain across a narrower acceptable range of water content. A geomembrane placed above the highly plastic Regina Clay should be less affected by changes in moisture content during construction compared to the low plasticity Battleford and Halton Tills. Therefore, more rigorous quality control may be recommended for low plasticity soils to ensure that the soil falls within the prescribed dry density and moisture content design criteria, as small changes may result in loss of geomembrane performance.

Caution should also be taken from this graph, as the more plastic soils did not necessarily result in lower overall geomembrane strains. It is evident in Fig. 10 that although the geomembrane above the Floral Till is less vulnerable to changes in moisture, the absolute magnitude of geomembrane strains are higher when compared to soils at similar

water contents (indicated by a higher intercept of the line of best fit).

Silt content of the soil was found to influence the geomembrane strain. Soils with higher silt content were associated with larger area exceeding 3% strain, as demonstrated in Fig. 12. This relationship with silt could be plotted by interpolating the percent area at optimum moisture content from Fig. 9 for each soil (the zero intercept of the best fit line).

In an effort to show the interaction of water content, plasticity index and silt content, a correction factor was applied to the compacted water content, as given in Fig. 13, to account for different index properties of the various soils.

The correction factor is a function of the silt as well as the activity of the clayey soil being used. The fine grained Floral and Pottery clay are shifted to the right (relative to Fig. 8) given their higher percentage of silt material. The Regina Clay, having high activity, is shifted to the left with the application of the correction factor. The high activity/clay fraction would likely lead to the high matric suction which would develop in the unsaturated soil and increase strength.

The correction factor demonstrates that the strains developed in the geomembrane follow a predictable pattern that can be inferred from different soil properties. Moisture content, silt fraction, and activity were found to influence geomembrane strain under the specific conditions of this test. It should be emphasized that these tests were completed using similar compactive effort for each test, which may not be equivalent to field specifications or conditions.

3.7. Comparisons with other studies

Strain within the geomembrane has been demonstrated to be influenced by the underlying subgrade. With very soft subgrades, or no subgrade (see Austin et al., 2014), there is a maximum strain developed in the geomembrane based on the tensile properties of the geomembrane itself. Increasing the protection layer or stiffness of the underlying subgrade reduces the average geomembrane strain (Austin et al., 2014). Brachman and Sabir (2010) recommended placing the upper lift near optimum water content, which would result in lower geomembrane strains provided adequate compaction of the upper lift can be achieved over the softer underlying lifts of wetter soil. When using a very weak subgrade ($s_u = 40 \text{ kPa}$, $w = w_{opt} + 4\%$, to 90% standard Proctor maximum dry density) Brachman and Sabir (2013) concluded that geotextiles alone were insufficient in limiting geomembrane strains. Similarly, Tognon et al. (2000) determined that geotextile protection layers resulted in high geomembrane strains when compared

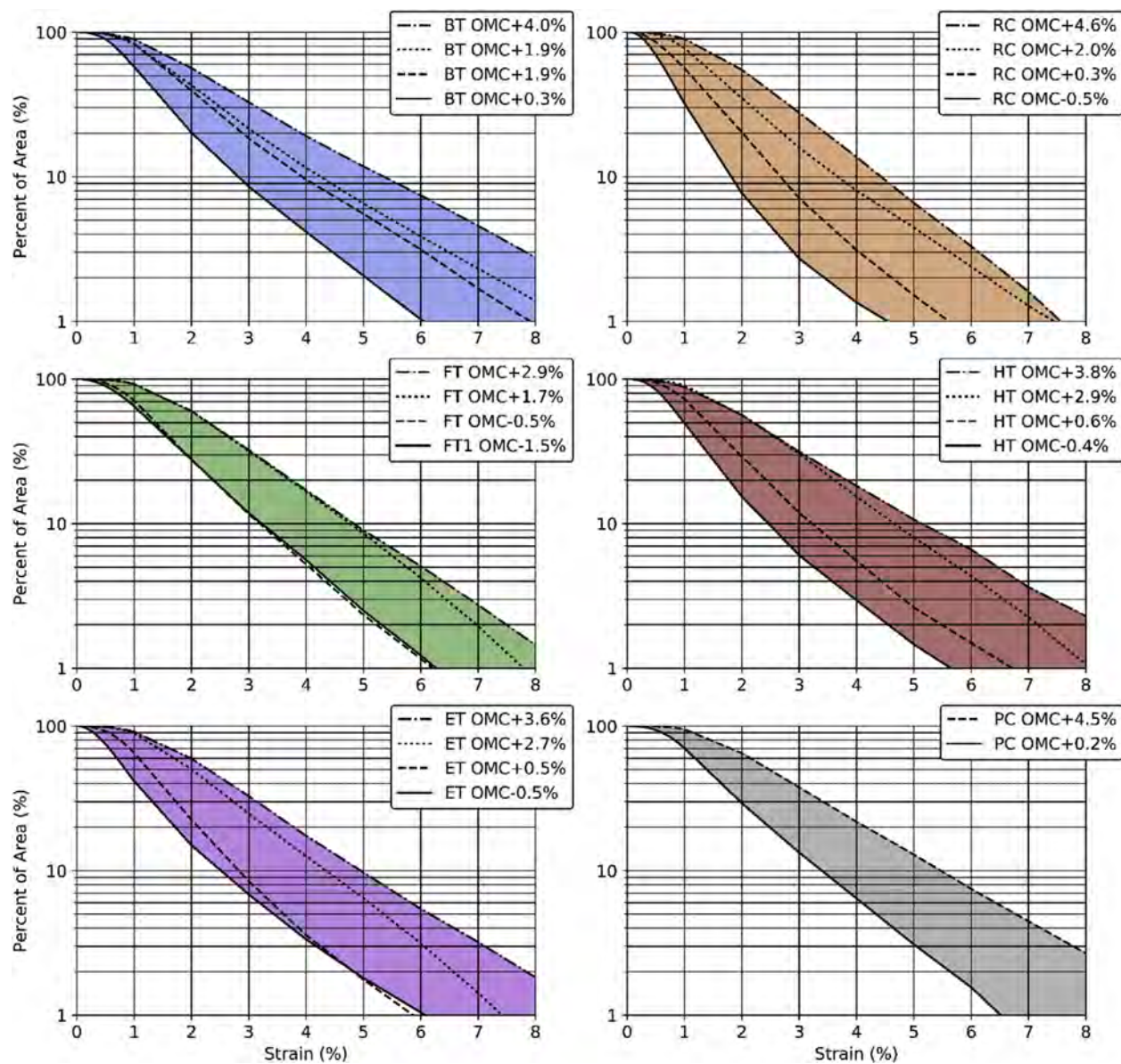


Fig. 7. Distribution of geomembrane strains for different compacted clay subgrades.

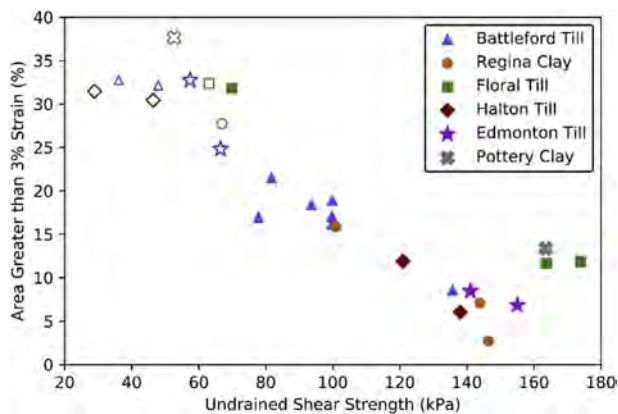


Fig. 8. Undrained shear strength and percent of total area of geomembrane exceeding 3% strain with points failing to meet 95% standard Proctor dry density shown as non-filled symbols.

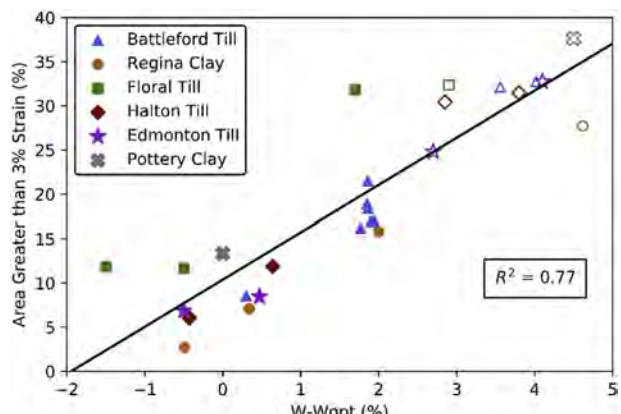


Fig. 9. Geomembrane area greater than 3% strain with increases in compacted water content with points failing to meet 95% std Proctor dry density shown as non-filled symbols.

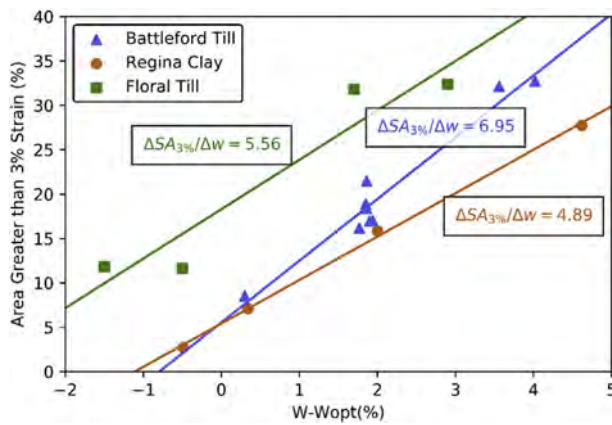


Fig. 10. Slope of area greater than 3% geomembrane strain and moulding water content for different soils.

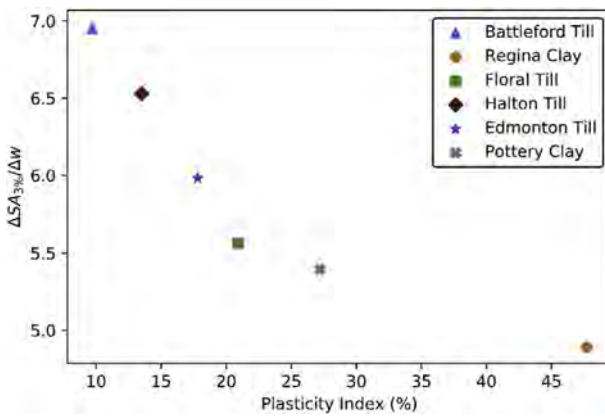


Fig. 11. Sensitivity of geomembrane strain above clayey soils to changes in moulding water content related to the plasticity of the clayey soil.

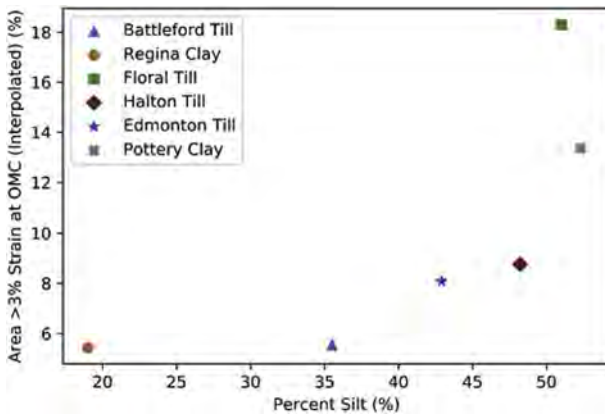


Fig. 12. Influence of silt on the magnitude of geomembrane strains.

with alternative protection layers such as sand filled geocushions or rubber geomats; however the compacted clayey soil that was used exhibited undrained shear strength of only 34 kPa.

Setting aside the question of adequate protection, it is evident that the role of the clayey soil is important in the deformation of a geomembrane overlying compacted clayey soil. The current study evaluated the role of the soil in controlling development of geomembrane strain during undrained loading with a pressure increase of 0–300 kPa occurring over 3 h. All testing was carried out using a single thickness (1.5 mm) of geomembrane placed below a 400 g/m² geotextile cushion. The decrease in subgrade rigidity in this study was evaluated through

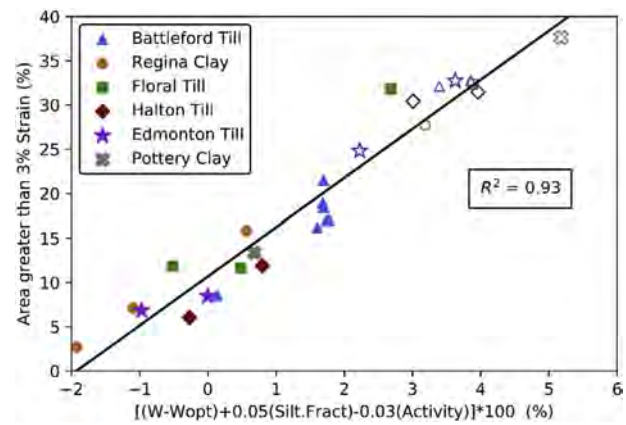


Fig. 13. Correction factor to moulding water content to account for differences in soil index properties with points failing to meet 95% std Proctor dry density shown as non-filled symbols.

increasing the compacted water content relative to optimum while maintaining constant standard proctor compactive energy for different clayey soils.

Higher plasticity clay soils may require less stringent moisture control during field compaction. For example, compacting the Regina Clay within a range of 0–3% wet of optimum would result in a less dramatic change in geomembrane strain when compared to the Battleford Till over the same 0–3% range. However, plasticity in itself is not a good performance indicator. The silty Floral till, while having a higher plasticity index, would be associated with more geomembrane strain than the Battleford Till or Regina Clay at similar moisture contents. For soils such as the Floral Till therefore, it may be more practical to focus efforts on sufficient geomembrane protection rather than imposing stricter moisture content requirements during placement and compaction.

However, as the geomembrane acts as a single component in a composite system, the findings presented herein must be considered in the context of increased hydraulic conductivity for clayey soils compacted at lower water content (Benson and Daniel, 1990). The results presented in this paper reflect only the test conditions used, and similar tests should be carried out at slower loading rates representative of field conditions.

4. Conclusion

Geomembrane strain tests were carried out using uniform coarse gravel, a 400 g/m² nonwoven geotextile protection layer and 1.5 mm HDPE geomembrane placed over clayey soils compacted with standard proctor compactive energy at varying moulding water contents. A total of six clayey soils from across Canada, with varying index properties, were used in this study. The resulting deformed clay surfaces were analyzed using digital images to generate successive computer elevation models. Using the deformed location of a dense grid of points, a map of the distribution of localised tensile strain in the geomembrane may be determined with strain calculated using the method of Tognon et al. (2000). Setting a threshold value for maximum allowable strain (e.g. 3% as per Seeger and Muller (2003)), the proportion of the overall geomembrane area exceeding this strain may be determined from each strain map. The role of the properties of the different clayey soils at varying water content may then be related to the area of the geomembrane surface over which this threshold strain is exceeded.

The results of the strain testing indicate that clays compacted wet of standard proctor optimum result in larger strains, which is consistent with findings published in the literature. At optimum water content for the Battleford Till, the geomembrane had very low strains. However, when the same soil was compacted at four percent wet of proctor

optimum, the proportion of the geomembrane area exhibiting strain > 3% increased by a factor of 6. This large shift with a 4% increase in moisture content was the greatest increase among the soils tested, demonstrating that the role of moisture content may be more pronounced in lower plasticity soils. When placed over higher plasticity soils, the induced strains in the geomembrane were found to be less sensitive to moisture content changes.

However, higher plasticity soils did not result in lower geomembrane strains in all cases. The Floral Till studied, although having a high plasticity index, resulted in the highest magnitude of strain when compared to other soils at similar water contents. Soils with lower silt fractions and higher activities were associated with decreases in geomembrane area exceeding the threshold strain.

The role of the clay has been shown to exhibit a significant influence on deformation of the overlying geomembrane. However, in this study the clay was loaded rather quickly and excess pore pressure would have developed. Future testing should attempt to quantify the difference in geomembrane strain under loading conditions where load is increased sufficiently slowly as to limit the role of excess pore pressure which would be more representative of field conditions for slowly-filled waste containment facilities.

Acknowledgements

The authors would like to acknowledge the contributions of Alberta Recycling, Adelantar Consulting, Loraas Disposal, Engineered Pipe Group (Saskatoon), Solmax International, Agru, and Nilex for their roles in funding this work and providing material. We acknowledge the support of the Natural Sciences and Engineering Research Council of Canada (NSERC).

References

- Abdelaal, F.B., Rowe, R.K., Brachman, R.W.I., 2014. Brittle rupture of an aged HDPE geomembrane at local gravel indentations under simulated field conditions. *Geosynth. Int.* 21 (1), 1–23.
- Agisoft, L.L.C. Agisoft PhotoScan User Manual: Professional Edition, Version 1.2. http://www.agisoft.com/pdf/photoscan-pro_1.2_en.pdf.
- Austin, R.A., Gibbs, D.T., Kendall, P.K., 2014. Geomembrane protection using cushioning geotextiles. In: 7th International Congress on Environmental Geotechnics: iceg2014. Engineers Australia, pp. 762.
- Benson, C.H., Daniel, D.E., 1990. Influence of Clods on the Hydraulic Conductivity of Compacted Clay. *J. Geotech. Eng.* 116 (8), 1231–1248.
- Benson, C.H., Daniel, D.E., 1994. Minimum Thickness of Compacted Soil Liners: II. Analysis and Case Histories. *J. Geotech. Eng.* 120 (1), 153–172.
- Benson, C.H., Daniel, D.E., Boutwell, G.P., 1999. Field Performance of Compacted Clay Liners. *J. Geotech. Geoenvir. Eng.* 125 (5), 390–403.
- Bjerrum, L., 1972. Embankments on soft ground. In: Proceedings of Specialty Conference on Performance of Earth and Earth-Supported Structures, pp. 1–54.
- Boynton, S.S., Daniel, D.E., 1985. Hydraulic Conductivity Tests on Compacted Clay. *J. Geotech. Eng.* 111 (4), 465–478.
- Brachman, R.W.I., Eastman, M.K., 2013. Calculating local geomembrane indentation strains from measured radial and vertical displacements. *Geotext. Geomembranes* 40, 58–68.
- Brachman, R.W.I., Eastman, M.K., Eldesouky, H.M.G., 2018. Screening Tests to Limit Geomembrane Strain from Gravel Indentations. *J. Geotech. Geoenvir. Eng.* 144 (6), 04018031.
- Brachman, R.W.I., Gudina, S., 2008. Gravel contacts and geomembrane strains for a GM/GCL composite liner. *Geotext. Geomembranes* 26 (6), 448–459.
- Brachman, R.W.I., Rowe, R.K., Irfan, H., 2014. Short-Term Local Tensile Strains in HDPE Heap Leach Geomembranes from Coarse Overliner Materials. *J. Geotech. Geoenvir. Eng.* 140 (5), 1–7.
- Brachman, R.W.I., Sabir, A., 2010. Geomembrane puncture and strains from stones in an underlying clay layer. *Geotext. Geomembranes* 28 (4), 335–343.
- Brachman, R.W.I., Sabir, A., 2013. Long-Term Assessment of a Layered-Geotextile Protection Layer for Geomembranes. *J. Geotech. Geoenvir. Eng.* 139 (5), 752–764.
- Brummermann, K., Blumerl, W., Stoewahse, C., 1994. Protection layers for geomembranes: Effectiveness and testing procedures. In: Proc. 5th International Conference on Geosynthetics, pp. 1003–1006.
- Cignoni, P., Callieri, M., Corsini, M., Dellepiane, M., Ganovelli, F., Ranzuglia, G., 2008. MeshLab: an Open-Source Mesh Processing Tool.
- Daniel, D.E., 1984. Predicting Hydraulic Conductivity of Clay Liners. *J. Geotech. Eng.* 110 (2), 285–300.
- Daniel, D.E., 1987. Earthen liners for land disposal facilities. In: Woods, R.D. (Ed.), *Geotechnical practice for waste disposal '87*. ASCE, New York, N.Y, pp. 21–39.
- Daniel, D.E., Benson, C.H., 1990. Water content-density criteria for compacted soil liners. *J. Geotech. Eng.* 116 (12), 1811–1830.
- Dickinson, S., Brachman, R.W.I., 2008. Assessment of alternative protection layers for a geomembrane – geosynthetic clay liner (GM-GCL) composite liner. *Can. Geotech. J.* 45, 1594–1610.
- Eldesouky, H.M.G., Brachman, R.W.I., 2018. Calculating local geomembrane strains from a single gravel particle with thin plate theory. *Geotext. Geomembranes* 46 (1), 101–110.
- Elwood, E.Y., Martin, C.D., 2016. Ground response of closely spaced twin tunnels constructed in heavily overconsolidated soils. *Tunn. Undergr. Space Technol.* 51, 226–237.
- Ewais, A.M.R., Rowe, R.K., Rimal, S., Sangam, H.P., 2018. 17-year elevated temperature study of HDPE geomembrane longevity in air, water and leachate. *Geosynth. Int.* 25 (5), 525–544.
- Fleming, I.R., Rowe, R.K., 2004. Laboratory studies of clogging of landfill leachate collection and drainage systems. *Can. Geotech. J.* 41 (1), 134–153.
- Fleming, I.R., Rowe, R.K., Cullimore, D.R., 1999. Field observations of clogging in a landfill leachate collection system. *Can. Geotech. J.* 36 (4), 685–707.
- Fredlund, D.G., 1975. Engineering Properties of Expansive Clays. In: Seminar on Shallow Foundations on Expansive Clays. Regina, Saskatchewan, pp. 1–58.
- Fredlund, D.G., Morgenstern, N.R., Widger, R.A., 1978. Shear strength of unsaturated soils. *Can. Geotech. J.* 15, 313–321.
- Gudina, S., Brachman, R.W.I., 2006. Physical Response of Geomembrane Wrinkles Overlying Compacted Clay. *J. Geotech. Geoenvir. Eng.* 132 (10), 1346–1353.
- Gudina, S.K., 2007. Short-term physical response of HDPE geomembranes from gravel indentations and wrinkles. PhD thesis. Department of Civil Engineering, Queen's University, Kingston, Ontario.
- Hornsey, W.P., Wishaw, D.M., 2012. Development of a methodology for the evaluation of geomembrane strain and relative performance of cushion geotextiles. *Geotext. Geomembranes* 35, 87–99.
- Jennings, J.E.B., Burland, J.B., 1962. Limitations to the Use of Effective Stresses in Partly Saturated Soils. *Geotechnique* 12 (2), 125–144.
- Mikhail, E.M., Bethel, J.S., MacGloin, J.C., 2001. Introduction to modern photogrammetry. Wiley, New York.
- Nosko, V., Touze-Foltz, N., 2000. Geomembrane liner failure: modelling of its influence on contaminant transfer. In: Proceedings of 2nd European Geosynthetics Conference, vol. 2. EUROGEO, pp. 557–560 2000.
- Peggs, I.D., Schmucker, B., Carey, P., 2005. Assessment of Maximum Allowable Strains in Polyethylene and Polypropylene Geomembranes. In: Proc. Geo-frontiers 2005, Austin, Texas, . [https://doi.org/10.1061/40789\(168\)23](https://doi.org/10.1061/40789(168)23).
- Porter, S.T., Roussel, M., Soressi, M., 2016. A Simple Photogrammetry Rig for the Reliable Creation of 3D Artifact Models in the Field: Lithic Examples from the Early Upper Paleolithic Sequence of Les Cottés (France). *Adv. Archaeol. Pract.* 4 (1), 71–86.
- Rowe, R.K., 2005. Long-term performance of contaminant barrier systems. *Geotechnique* 55 (9), 631–678.
- Rowe, R.K., Brachman, R.W.I., Irfan, H., Smith, M.E., Thiel, R., 2013. Effect of underliner on geomembrane strains in heap leach applications. *Geotext. Geomembranes* 40, 37–47.
- Rowe, R.K., Abdelaal, F.B., Islam, M.Z., 2014. Aging of high-density polyethylene geomembranes of three different thicknesses. *J. Geotech. Geoenvir. Eng.* 140 (5), 04014005.
- Rowe, R.K., Caers, C.J., Chan, C., 1993. Evaluation of a compacted till liner test pad constructed over a granular subliner contingency layer. *Can. Geotech. J.* 31 144–144.
- Sabir, A., Brachman, R.W.I., 2012. Time and temperature effects on geomembrane strain from a gravel particle subject to a sustained vertical force. *Can. Geotech. J.* 49, 249–263.
- Sauer, E.K., Egeland, A.K., Christiansen, E.A., 1992. Compression characteristics and index properties of tills and intertill clays in southern Saskatchewan, Canada. *Can. Geotech. J.* 30 (2), 257–275.
- Seeger, S., Muller, W., 2003. Theoretical approach to designing protection: selecting a geomembrane strain criterion. In: Dixon, N., Smith, D.M., Greenwood, J.H., Jones, D.R.V. (Eds.), *Geosynthetics: Protecting the Environment*. Thomas Telford, London.
- Tognon, A.R.M., 1999. Laboratory testing of geosynthetics used in landfill barrier systems. M.E.Sc. thesis. ProQuest Dissertations Publishing, London, Ont, Canada Faculty of Engineering, University of Western Ontario.
- Tognon, A.R., Kerry Rowe, R., Moore, I.D., 2000. Geomembrane Strain Observed in Large-Scale Testing of Protection Layers. *J. Geotech. Geoenvir. Eng.* 126 (12), 1194–1208.
- Zanzinger, H., 1999. Efficiency of Geosynthetic Protection Layers for Geomembrane Liners: Performance in a Large-Scale Model Test. *Geosynth. Int.* 6 (4), 303–317.